

DOKUZ EYLÜL UNIVERSITY
GRADUATE SCHOOL OF NATURAL AND APPLIED SCIENCES

INVESTIGATION OF ACTIVE MICROSTRIP
ANTENNAS AND IMPROVED PERFORMANCE
TECHNIQUES

by
Adnan KAYA

May, 2006
İZMİR

**INVESTIGATION OF ACTIVE MICROSTRIP
ANTENNAS AND IMPROVED PERFORMANCE
TECHNIQUES**

**A Thesis Submitted to the
Graduate School of Natural and Applied Sciences of Dokuz Eylül University
In Partial Fulfillment of the Requirements for the Degree of Doctor of
Philosophy in Electrical and Electronics Engineering,
Applied Electrical and Electronics Program**

by
Adnan KAYA

**May, 2006
İZMİR**

Ph.D. THESIS EXAMINATION RESULT FORM

We have read the thesis entitled “**INVESTIGATION OF ACTIVE MICROSTRIP ANTENNAS AND IMPROVED PERFORMANCE TECHNIQUES**” completed by **ADNAN KAYA** under supervision of **Assist. Prof. Dr. E. YEŞİM YÜKSEL** and we certify that in our opinion it is fully adequate, in scope and in quality, as a thesis for the degree of Doctor of Philosophy.

.....

Supervisor

.....

Committee Member

.....

Committee Member

.....

Jury Member

.....

Jury Member

Prof.Dr. Cahit HELVACI
Director
Graduate School of Natural and Applied Sciences

ACKNOWLEDGMENTS

I express my deepest gratitude to my advisor Assist. Prof. Dr. E. Yeřim YÜKSEL for her guidance and support in every stage of my research. The research experience I have gained under her care will be valuable asset to me in the future.

I also would like to thank colleague Adem ÇELEBİ for his valuable guidance during preparation of this thesis.

I would like to thank my parents, brothers, for their trust and patience.

Finally, I would like to thank my dear wife, for her trust. Her kindness and supportiveness mean a lot to me. Without her continuous encouragement; I could not start and finish this work. Thank you for believing in me.

Adnan KAYA

INVESTIGATION OF ACTIVE MICROSTRIP ANTENNAS AND IMPROVED PERFORMANCE TECHNIQUES

ABSTRACT

The microstrip antenna (MSA) is one of the most widely used microwave antennas possessing several advantages. However, it presents a low impedance bandwidth, low gain, and tolerance problems. Probably the most direct way of improving the impedance bandwidth of a microstrip antenna is to attach a separate lossless matching network. The aim of this study is to develop a new wide band matching systems for improving the electrical characteristics such as, low efficiency, low antenna gain and narrow band. In the research stage of this thesis, different microstrip antenna geometries, matching networks and theoretical models for analysis and design of microstrip antennas were investigated. Three different types of the matching circuits which are realized as the negative capacitance, the negative inductance and the Pi-matching circuit with RC mutator, have been proposed. The impedance bandwidth and the return loss level were improved by using the proposed new compensation networks. The theoretical solutions of the developed matching networks by using the active circuit components were investigated and the mathematical models were developed. A parametric study of the components in the active compensation networks on both radiation and input characteristics of the microstrip antennas were carried out. The performance parameters of the designed microstrip antennas with and without compensation networks and classical techniques have been compared. The matched antenna prototypes for some of the configurations have been fabricated and tested in order to verify the simulated and the theoretical results. Within the tolerances, the agreement with the results has been satisfactory.

Key Words: Microstrip antenna, matching network, impedance bandwidth, RMSA, active antenna

AKTİF MİKROŞERİT ANTENLERİN ARAŞTIRILMASI VE PERFORMANS GELİŞTİRME TEKNİKLERİ

ÖZ

Mikroşerit anten birçok avantaja sahip, yaygın olarak kullanılan bir mikrodalga antenidir. Bununla birlikte düşük empedans bant genişliği, düşük anten kazancı ve tolerans problemlerine sahiptir. Bu çalışmanın amacı, mikroşerit antenlerde dar bant, düşük verimlilik, düşük anten kazancı gibi elektriksel özelliklerin iyileştirilmesi için yeni geniş bant uyumlandırma sistemlerinin geliştirilmesidir.

Mikroşerit anten analiz ve tasarımı için teorik modeller incelenmiş ve farklı tipte mikroşerit anten yapıları araştırılmıştır. Negatif bobin, negatif kapasite ve RC dönüştürücülü Π uyumlandırma devreleri kullanılarak gerçekleştirilen üç farklı tip uyumlandırma devresi sunulmuştur. Geliştirilen bu yeni uyumlandırma sistemleri ile özellikle anten empedans bant genişliği ve geri dönüş kaybı iyileştirilmiştir. Aktif devre elemanları kullanılarak geliştirilen uyumlandırma sistemlerinin teorik çözümleri incelenmiş ve matematik modelleri geliştirilmiştir. Aktif uyumlandırma sistemindeki bileşenlerin mikroşerit antenin ışınma örüntüsü ve giriş karakteristikleri üzerine etkileri incelenmiştir. Tasarlanan mikroşerit antenlerin uyumlandırma varken ve yokken ki durumları karşılaştırılmıştır. Buna ek olarak önerilen yeni uyumlandırma teknikleri, klasik uyumlandırma teknikleri ile karşılaştırılarak benzetim sonuçları verilmiştir. Bazı uyumlandırılmış antenlerin laboratuvar testleri yapılarak teorik ve benzetim sonuçları doğrulanmıştır. Tolerans sınırları içerisinde tatmin edici sonuçlar elde edilmiştir.

Anahtar Kelimeler: Mikroşerit anten, uyumlandırma sistemi, bant genişliği, RMSA, aktif anten

CONTENTS

| | Page |
|---|-------------|
| THESIS EXAMINATION RESULT FORM | ii |
| ACKNOWLEDGEMENTS | iii |
| ABSTRACT..... | iv |
| ÖZ | v |
| CONTENTS..... | vi |
| | |
| CHAPTER ONE – INTRODUCTION | 1 |
| | |
| 1.1. Introduction | 1 |
| 1.2. Research Objective and Aim of Thesis | 3 |
| 1.3. Thesis Outline..... | 4 |
| | |
| CHAPTER TWO – THEORETICAL BACKGROUND OF THE ACTIVE MICROSTRIP ANTENNAS | 6 |
| | |
| 2.1 Active Microstrip Antenna..... | 6 |
| 2.1.1 Early Active Integrated Antenna | 7 |
| 2.2 Microstrip Antennas Used in AIA..... | 8 |
| 2.2.1 Microstrip Patch Antenna..... | 9 |
| 2.2.1.1 Microstrip Antenna Design Formulas..... | 11 |
| 2.2.1.2 Resonant Input Impedance..... | 14 |
| 2.2.1.3 Microstrip Antenna Bandwidth..... | 16 |
| 2.2.1.4 Radiation Pattern of the Microstrip Antenna..... | 19 |
| 2.3 Microstrip Antenna Array | 22 |
| 2.3.1 Circularly Polarized Planar Microstrip Antenna Array..... | 22 |
| 2.4 Analytical Techniques for Microstrip Antennas | 26 |
| 2.4.1 Cavity Model Analysis for the Microstrip Antenna | 28 |
| 2.4.2 Multiport Network Model (MNM) for the Microstrip Antenna | 33 |
| 2.4.3 Method of Moment (MoM) Model..... | 34 |

CHAPTER THREE – BANDWIDTH ENHANCEMENT TECHNIQUES IN MICROSTRIP ANTENNAS..... 36

3.1 Early Bandwidth Enhancement Techniques 36

3.2 Reactive Matching Technique for Increasing the Impedance Bandwidth of Rectangular Microstrip Antennas (RMSA)..... 38

 3.2.1 Bandwidth Improvement Theory 40

 3.2.2 Impedance Characteristics of RMSA 44

 3.2.3 Bandwidth Enhancement of RMSA Using Negative Inductance as Matching Device..... 46

 3.2.3.1 Active Floating Negative Inductors with Two and Three FETs 46

 3.2.4 Simulation Results of the Active Compensated Antenna and Reference Antenna..... 51

3.3 Loaded Rectangular Microstrip Antennas..... 58

 3.3.1 Multiport Network Model for Loaded RMSA..... 58

 3.3.2 Bandwidth Enhancement of a Rectangular Microstrip Antenna by Integrated Reactive Loading..... 61

 3.3.2.1 Negative Capacitance Circuit with Two FET 61

 3.3.3 Simulation and Theoretical Results of the Reactive Loaded Antenna 63

 3.3.3.1 Negative-capacitor and Chip-Resistor-Loaded RMSA 67

3.4 Comparison with other Techniques..... 73

CHAPTER FOUR – ELECTRONICALLY CONTROLLED IMPEDANCE TUNING NETWORKS 87

4.1 Impedance Matching Networks 87

4.2 Design of Pi-Matching Network for Compensated Antenna 90

 4.2.1 Theory..... 91

 4.2.2 Analytical Solution of Compensation Network under Load Condition .. 95

4.3 Mutators and Generalized Mutators 104

 4.3.1 Single Capacitor RC Mutators..... 107

| | |
|--|------------|
| 4.4 Input Impedance Analysis of Rectangular Microstrip Antenna with Pi Matching Network using RC Mutator | 108 |
| 4.5 Analysis of Radiation Pattern from Compensated RMSA | 111 |
| 4.6 Evaluation of Sensitivities..... | 115 |
| 4.7 Design Example and Simulation, Measurement Results | 118 |
| | |
| CHAPTER FIVE – DESIGN, FABRICATION AND MEASUREMENT RESULTS OF DIFFERENT MICROSTRIP PATCH ANTENNAS | 127 |
| | |
| 5.1 Design Concept of Compensated Microstrip Patch Antennas (MPA)..... | 127 |
| 5.2 Experimental and Theoretical Analysis for Different MPA | 130 |
| 5.3 Amplifying Active Integrated Microstrip Patch Antennas | 146 |
| | |
| CHAPTER SIX – CONCLUSION | 150 |
| | |
| 6.1 Conclusion..... | 150 |
| 6.2 Suggestion for Future Research | 152 |
| | |
| REFERENCES | 154 |
| | |
| APPENDIX A Manufacturer Data..... | 162 |
| | |
| APPENDIX B Receiver Antenna and Algorithm..... | 166 |

CHAPTER ONE

INTRODUCTION

1.1 Introduction

The idea of the microstrip antenna dates back to the 1950's (Deschams, 1953). Originally, the element was fed with either a coaxial line through the bottom of the substrate, or by a coplanar microstrip line. The microstrip antenna radiates a relatively broad beam broadside to the plane of the substrate. Thus the microstrip antenna has a very low profile, compact, lightweight, low cost and can be fabricated using printed circuit (photolithographic) techniques. Other advantages include easy fabrication into linear or planar arrays, and easy integration with microwave integrated circuits. To a large extent, the development of microstrip antennas has been driven by system requirements for antennas, with microwave integrated circuits or polarization diversity (Garg, Bhartia, Bahl & Ittipiboon, 2001). Thus microstrip antennas have found application in both the military and civil sectors.

Disadvantages of the original microstrip antenna configurations include narrow bandwidth, spurious feed radiation, poor polarization purity, limited power capacity, and tolerance problems. Much of the development work in microstrip antennas has thus gone into trying to overcome these problems, in order to satisfy increasingly stringent system requirements.

Applications in present-day mobile communication systems usually require smaller antenna size in order to meet the miniaturization requirements of mobile units. Thus, size reduction and bandwidth enhancement are becoming major design considerations for practical applications of microstrip antennas. For this reason, studies to achieve compact and broadband operations of microstrip antennas have greatly increased. Much significant progress in the design of compact microstrip antennas with broadband, bandwidth - enhanced (Poes & Van De Capelle, 1989) ,

dual frequency (Maci & Gentili, 1997), dual-polarized, circularly-polarized (Kaya, Çelebi & Yüksel, 2003), and gain-enhanced (Shin & Kim, 2002) operations have been reported over the past several years.

The bandwidth of an antenna specifies the operational range over which the properties of the antenna are within the designed specifications. Each antenna parameter is examined over the frequency range of interest. Most of the work in the area of bandwidth enhancement has been done to increase the impedance bandwidth of the microstrip patch element. For single microstrip elements, the impedance bandwidth is a few percent, generally the limiting factor; the pattern and directivity of a microstrip element generally vary a little with respect to frequency. However, various techniques have been proposed for bandwidth enhancement; e.g., stack multilayer patched, multilayer elements (Chen, Tulintseff & Sorbello, 1986), and multiresonator impedance-matching network (Pozar & Van De Capelle, 1989). The straightforward approach to improving bandwidth is increasing the thickness of the substrate supporting the microstrip patch. However, limitations still exist on the ability to effectively feed the patch on a thick substrate and radiation efficiency can degrade with increasing substrate thickness. All these techniques suffer from poorer radiation attributes, complexity and enlarged element size. Radiating efficiency is decreased at the end because of the geometry. Techniques of overcoming these problems include using the parasitic tuning elements, external matching and separating the feed and antenna. Generally, impedance matching method is used as a classical method with success. It seems that impedance variations are dominant bandwidth limiting factors. Impedance matching at the feed point of the microstrip antenna element using active components has been also proposed to improve the bandwidth in the literature (Lin & Itoh, 1994).

The implementation of active devices in passive radiating elements showed several advantages, e.g. improving the noise factor and impedance bandwidth, increasing the mutual coupling between array elements (Deal, Kaneda, Sor, Qian & Itoh, 2000). These advantages helped to improve the antenna performance and made the research of active antennas popular.

The other method is reactive loading technique for the matching and there are many studies in literature. The capacitor loading (Lu, Tang & Wong, 1998), shorting pin loading or resistors loading (Wong & Lin, 1997) are example of this method presented in the literature. The good antenna performances can be obtained with reactive loading. Dual band or a few resonance points can be obtained in according to *TM* modes with these types of antennas. Better results can be obtained via development of this dynamical model. However, it is noted that there is a trade-off between the antenna bandwidth and the performance on gain variation for broadband microstrip antenna with an embedded reactive loading (Wong & Kou, 1999). In addition, the impedance matching for the antenna's feed and loading position is very sensitive.

Microstrip antennas are limited in that they tend to radiate efficiently only over a narrow band of frequencies. In this project, broadband impedance inserting method is proposed for improving the bandwidth and the radiation pattern of the microstrip antennas. When the active components are used with passive microstrip antenna structures, antenna performances are increased. Active integrated antenna can be regarded as an active microwave circuit in which the output and input port is free space instead of a conventional 50 ohm interface. In this case, the antenna can provide certain circuit functions such as resonating, filtering, in addition the radiating.

1.2 Research Objective and Aim of Thesis

The key objectives of this research may be defined as follows:

- First, to fuse antenna design and microwave circuit technology;
- To investigate types of elements that can be used for increasing the bandwidth, improving the radiating pattern and reducing the return loss parameter;
- Design and build a reactive loading antenna with new configurations;
- Evaluate the ability of the new matching techniques by using the new circuits such as negative floating inductor;

- Furthermore, optimize the active antenna characteristics such as radiation, efficiency, bandwidth, input impedance, and radiation pattern by using active negative capacitance, inductance, Pi type matching (with RC mutator) as a compensation network;
- Performance of the proposed methods on the other microstrip geometries;
- Evaluate the advantages and disadvantages between the classical matching techniques and new proposed techniques.

In this thesis, negative capacitance and inductance has been used as a *MMIC* (Monolithic Microwave Integrated Circuit) device. In this design presented of active microstrip antennas by combination of the negative capacitance and inductance with radiating patches to obtain broad bandwidth. The results are very attractive for broadband *MMIC* active *RMSA* (Rectangular Microstrip Antenna) design and this design will be illustrated with an active transmit or receive antenna.

1.3 Thesis Outline

Thesis is organized into six chapters. The topical organization of the thesis starts with an initial discussion of the rectangular microstrip antenna design. In this thesis, some new techniques will be proposed to overcome narrow bandwidth, radiation pattern and gain problem. Chapter 2 introduces concept of the theoretical model of the microstrip antenna analysis and design. Many techniques have been proposed and used to determine microstrip antenna characteristics. The analytical techniques include the transmission line model, cavity model, and multiport network model (*MNM*). These techniques maintain simplicity at the expense of accuracy. Cavity model was advances by Lo et al. The *MNM* can be considered an extension of the cavity model in which the impedance boundary condition at the periphery is enforced. Cavity model and *MNM* is summarized in Chapter 2. In Chapter 3 improvement of bandwidth by utilizing floating negative inductor circuit as compensation network is presented. Extensive details of *MNM* are mentioned in this Chapter. The inductive compensation circuit is realized using the FETs. Simulation

results for both compensated and non-compensated antenna are presented. It is observed that utilization of this technique is a promising solution to increase the bandwidth. Chapter 4 provides a literature review relating to the design of matching network. After giving an explanation of the synthesis equations about impedance area of the matching network, the real and imaginary impedance plots for the compensated system are given. Sensitivity analysis of the compensated system with respect to matching components is shown. This chapter ends with an analysis of input impedance control on compensated rectangular microstrip antenna with Pi matching network using *RC* Mutator (Goras, 1981). Chapter 5 provides almost all the simulation, the measurement and the theoretical results related to the compensated network. The effects of the parameters on antennas operational frequency and impedance bandwidth are investigated and the parameters most affecting the performance of the antenna are identified. Additionally, the radiation patterns and parameters generated by the antennas are shown. Chapter 6 concludes this thesis with a summary of the work carried out through this study and the future prospects for the active compensated antenna systems. These chapters are followed by an extensive list of references and some important appendices. Properties of the circuit components employed in the measurements are combined in Appendix A using manufacturer data. Appendix B presents cavity model algorithm and expressions for the quasi yagi antenna.

CHAPTER TWO

THEORETICAL BACKGROUND OF THE ACTIVE MICROSTRIP ANTENNAS

2.1 Active Microstrip Antennas

The terminology of “active microstrip antenna” means that the active devices are employed in passive microstrip antenna elements to improve antenna performance. The terminology of “active integrated microstrip antenna” indicates more specifically that the passive antenna elements and the active circuitry are integrated on the same substrate.

Active microstrip antenna provides a new model for designing modern microwave and millimeter-wave wireless systems. A benefit of this technique includes compactness, reduced losses and weight, low profile and multiple functions. An active antenna is essentially a direct integration of the antenna and microwave circuit platform. This allows new functionality of the antenna (such as mixing, amplification, impedance matching and even signal generation), as well as for new active circuit topologies where the antenna is included as a circuit component (Lin & Itoh, 1994). Active circuits can be used as only matching system on planar microstrip antenna geometries. Some advantages are obtained in related to matching level. Active compensated circuits which include three or two terminal components have adjustable characteristic, therefore the impedance matching level is high in variable environmental condition.

Active integrated antennas (AIA), in which solid-state devices and antennas are integrated together on a single substrate, offer significant advantages in performance, size and cost for microwave wireless systems. Recent developments include elements for integrated transmitters, receivers, transceivers and transponders operating at frequencies from UHF through millimeter-wave. The potential of such technology is vary large.

Single integrated antenna elements offer small size and high capability with the potential low cost. This opens up a range of applications such as personal communications and sensors. It is also used in broadcast receive antenna system, vehicle radio antenna, satellite radar and satellite communications antennas system.

2.1.1 Early Active Integrated Antennas

Looking back in history, the idea using active antennas can be traced back to as early as 1928 that a small antenna with an electron tube was commonly used in radio broadcast receivers around 1MHz. After the invention of high- frequency transistors, the study of active antennas received much more attention and several works were reported in the 1960s and 1970s (Copeland, Roberston & Verstraete, 1964; Anderson, Davies, Dawoud & Galanakis, 1971; Daniel & Terret, 1975).

The active integrated antenna has been a growing area of research in recent years, as the microwave integrated circuit (MIC) and monolithic microwave integrated circuit (MMIC) technologies became more mature allowing for high-level integration. AIA can be regarded as an active microwave circuit in which the output or input port is free space instead of a conventional 50Ω interface. In this case, the antenna can provide certain circuit functions for example resonating, filtering, coupling, matching and transforming in addition to its original role as a radiating element (Chang at al, 2002). A typical AIA consists of active devices such as two-terminal devices (Varicap diode), or three-terminal devices (GaAs FET) to form active circuits and planar antennas such as microstrip patches, dipoles, bowties, or slot antennas

The concept of microstrip antennas was first proposed by Deschamps as early as 1953 (Descamps, 1953), Gutton and Bassinot in 1955. However, not much carry-on researches have been carried out until 1972. Since then, it took about twenty years before the first practical microstrip antennas were fabricated in the early 1970's by Munson and Howell (Munson, 1974; Howell, 1975). Howell first presented the design procedures for microstrip antennas whereas Munson tried to develop microstrip antennas as low-profile flushed-mounted antennas on rockets and missiles.

In addition, research publications regarding the development of microstrip antennas were also published by Bahl and Bhartia, James, Hall and Wood (Garg, Bhartia, Bahl & Ittipiboon, 2001). Dubost had also published a research monograph which covers more specialized and innovative microstrip developments (Dubost & Rabbaa, 1986). In fact, all these publications are still in use today.

Several works were reported about the active microstrip antennas, after invention high frequency transistor (Daniel & Terret, 1975). These works focused on increasing the antenna impedance bandwidth, decreasing the mutual coupling effect, improving the radiation pattern and noise factor. To enhance the impedance bandwidth of the microstrip patch antennas is still popular research area in recent years.

Due to the variation technology of microwave integrated circuit (MIC) and monolithic microwave integrated circuit (MMIC), the active integrated antenna became an area of growing interest in recent years (An, Nauwelaers & Capelle, 1991). The implementation of active devices in passive radiating elements showed improving the noise factor. The active integrated antennas may be classified by their different applications. Two basic categories are transmitting and receiving type's active antennas. The other types with both functions of transmitting and receiving are transceivers, transponders, repeaters, and so on. A matching network may be integrated with antenna elements at its input port or output port to become transmitter or receiver. All these configurations have a common feature: the integration of a compensated network and antenna elements.

2.2 Microstrip Antennas Used in AIA

Microstrip antennas are an extension of microstrip circuits. This feature has given rise to microstrip integrated active antennas in which circuit functions are integrated with the antenna function to produce compact transceivers. The attractiveness of the microstrip antenna method stems from the idea of making use of printed circuit technology. Many of the microstrip antenna applications for satellite links, mobile

communications, wireless local-area networks, and so on, impose constraints on compactness, dual-frequency operation, polarization control, radiation pattern control, and so on. These functions can be achieved by suitably loading simple microstrip antennas, and hence those antennas are becoming more commonly used.

2.2.1 Microstrip Patch Antenna

Microstrip antennas consist of a patch of metallization on a grounded substrate. Due to the fact that the microstrip antenna's structure is planar in its configurations, it is able to enjoy all the advantages of a printed circuit board with all of the power dividers, matching networks, phasing circuits and radiators. In addition, as the backside of the microstrip antenna is a metal ground plane, the antenna can be directly placed onto a metallic surface of an aircraft or missile. Moreover, microstrip antennas have several advantages compared to conventional microwave antennas and therefore, it can accommodate many applications over the broad frequency range from 100 MHz to 50 GHz. Some of the outstanding advantages of the microstrip antennas compared to conventional microwave antennas are (Balanis, 1989; Pozar, 1992):

- Light in weight, small in size, low profile planar configurations which can be made conformal. Low fabrication cost, suitable for mass production can be made thin so that the aerodynamics of any aerospace vehicles would not be affected.
- Possible to achieve linear, circular (left hand or right hand) polarizations with simple changes in feed position. Easy to obtain dual frequency operations requires no cavity backing. Compatible with modular designs (solid state devices such as oscillators, amplifiers, variable attenuators, switches, modulators, mixers, phase shifters, etc. can be added directly to the antenna substrate board). Feed line and matching networks are fabricated all together with antenna structure.

There are many techniques used to feed or excite microstrip antennas (Pozar, 1986). Early microstrip antennas used either a microstrip feed lines or a coaxial probe feed (Carver & Mink, 1981). As most microstrip antennas have radiating elements on one side of a dielectric substrate, it is therefore necessary to be fed by either a microstrip or coaxial line. Classical coaxial-fed microstrip patch antenna geometry is shown in Figure 2.1. Matching is normally required between the feed line and the antenna. Since the antenna input impedance is different from the normal 50Ω line impedance. In addition, real and imaginary value of the input antenna impedance can be very high. Matching can be achieved by correctly choosing the position of the feed line. On the other hand, the position of the feed may also affect the radiation characteristics.

When operating in the transmitting mode, the antenna is driven with a voltage between the feed probe and the ground plane. This excites current on the patch, and a vertical electric field between the patch and ground plane.

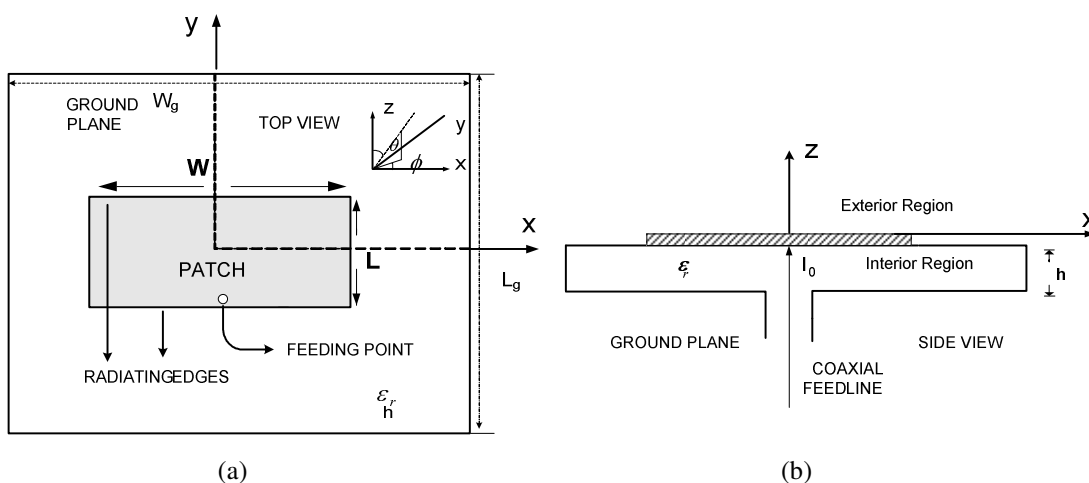


Figure 2.1 Coaxial-fed microstrip patch antenna (a) Top view (b) Side view

For a feed point at radiating edge ($x=0$ or $x=W$), the voltage is maximum and the current is a minimum, so the input impedance is maximum. For a feed point at the centre of the patch ($x=W/2$), the voltage is zero and the current is maximum, so the impedance is zero. Thus the input impedance can be controlled by adjusting the position of the feed point; typical input impedance at an edge of a resonant patch ranges from 150Ω to 300Ω . The impedance locus is that of a half wave

open-ended transmission line resonator, which can be modeled as a parallel *RLC* network.

2.2.1.1 Microstrip Antenna Design Formulas

The first design step is to choose a suitable dielectric substrate of appropriate thickness h and loss tangent. A thicker substrate, besides being mechanically strong, will increase the radiated power, reduce conductor loss, and improve the impedance bandwidth (Pozar, 1992). However, it will also increase the weight, dielectric loss, surface wave loss, and extraneous radiations from the probe feed. A rectangular patch antenna stops resonating for substrate thickness greater than $0.11 \lambda_0$ due to inductive reactance of probe feed (Pozar, 1983). A low value of ϵ_r for the substrate will increase the fringing field at the patch periphery, and thus the radiated power.

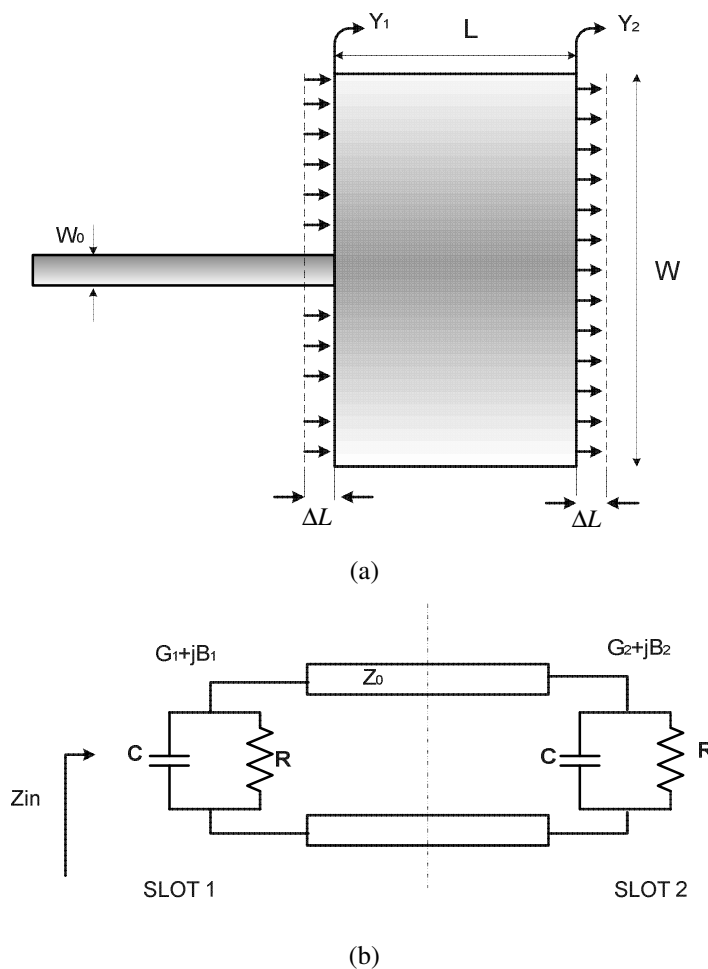


Figure 2.2 (a) Microstrip antenna (b) Transmission line model

In terms of the transmission line model, the antenna is viewed as a length of open-circuited transmission line. This model of rectangular microstrip antenna is shown in Figure 2.2.

Transmission line model is a good method for initial microstrip antenna design. Given the operating frequency f_r , thickness h of the substrate, and relative permittivity ϵ_r of the substrate, following is a procedure to design the microstrip patch antenna. The dielectric substrate is usually electrically thin ($h < 0.05\lambda_0$), so electric field components parallel to the ground plane must be very throughout the substrate. The patch element resonate when their length are near $\lambda_g/2$, leading to relatively large current and field amplitudes.

The width of the patch is given as (Garg, Bhartia, Bahl & Ittipiboon, 2001)

$$W = \frac{c}{2f_0 \sqrt{\frac{(\epsilon_r + 1)}{2}}} \quad \text{Eq. (2.1)}$$

Patch width has minor effect on the resonant frequency and radiation pattern of the antenna. It affects the input resistance and bandwidth to a large extent. A larger patch width increases the power radiated and thus gives decreased resonant resistance, increased bandwidth, and increased radiation efficiency. With proper excitation one may choose a patch width W greater than the patch length L without exciting undesired modes. A constraint against a larger patch width is the generation of grating lobes in antenna arrays. The patch width also affects cross-polarization characteristics. It has been suggested that $1 < W/L < 2$ (Richards, et al., 1981).

The effective dielectric constant ϵ_{eff} is usually not equal to the dielectric constant ϵ_r for a non-uniform structure. For a uniformly filled structure such a strip line, coaxial line, or parallel plate, the effective dielectric constant is equal to the dielectric constant of the material ($\epsilon_{eff} = \epsilon_r$). However, for microstrip structures, it is necessary to calculate the effective dielectric constant of the structure. Firstly, assume two extreme cases for the effective dielectric constant. Shown above in Figure 2.2 are two cases whereby

the width of the microstrip W is much greater than the thickness of the substrate ($W \gg h$) in the top diagram and in the bottom diagram, width W is much smaller the thickness of the substrate ($W \ll h$). Effective dielectric constant ϵ_{eff} of the microstrip feed line is calculated with (Balanis, 1989)

$$\epsilon_{eff} = \frac{\epsilon_r + 1}{2} + \frac{\epsilon_r - 1}{2} \left[1 + 12 \frac{h}{W} \right]^{-1/2} \quad \frac{W}{h} > 1. \quad \text{Eq. (2.2)}$$

For a substrate material, the effective dielectric constant has values in the range of $1 < \epsilon_{eff} < \epsilon_r$. The effective dielectric constant is also a function of frequency. As the frequency of operation increases, most of the electric fields lines concentrate in the substrate. When ϵ_r is decreased, W is increased and the impedance bandwidth (BW) is decreased.

Equation (2.2) gives the effective length as (Balanis, 1997):

$$L_{eff} = \frac{c}{2f_0 \sqrt{\epsilon_{eff}}} = \frac{\lambda_g}{2} \quad \text{Eq. (2.3)}$$

where λ_g is the guide wavelength. The λ_g is depended the effective dielectric constant and is given $\lambda_g = \lambda / \sqrt{\epsilon_{eff}}$.

The fringing fields is calculated with (Hammerstad, 1975)

$$\frac{\Delta L}{h} = 0.412 \frac{(\epsilon_{eff} + 0.3) \left(\frac{W}{h} + 0.264 \right)}{(\epsilon_{eff} - 0.258) \left(\frac{W}{h} + 0.8 \right)}. \quad \text{Eq. (2.4)}$$

The actual length of the patch that takes into account of the fringing effect can be solved by (Balanis, 1997)

$$L = L_{eff} - 2\Delta L. \quad \text{Eq. (2.5)}$$

The ground plane dimensions would be given as:

$$L_g = L + 6h \quad W_g = W + 6h \quad \text{Eq. (2.6)}$$

The actual separation of the two slots defining patch length is slightly less than $\lambda_g/2$ for the TM_{10} .

Finally, these behaviors lead us to conclude that microstrip antennas operate best when the substrate is electrically thick with a low dielectric constant.

2.2.1.2 Resonant Input Impedance

For the impedance evaluation, a patch antenna can be modeled as two parallel radiation slots. Each slot is modeled as parallel resonator that is shown in Figure 2.2.b with an equivalent admittance of Y_1 and Y_2 , respectively (Harrington, 1961).

$$Y_1 = Y_2 = G_1 + jB_1 = G_1 + jB_1 \quad \text{Eq. (2.7)}$$

where

$$G_1 = \frac{I_1}{120\pi^2}, I_1 = \int_0^\pi \frac{\text{Sin}\left(\frac{k_0 W}{2} \text{Cos}(\theta)\right)}{\text{Cos}(\theta)} \text{Sin}^3(\theta) d\theta. \quad \text{Eq. (2.8)}$$

If the reduction of the length is properly chosen using Eq 2.4 (typically $0.48\lambda_g < L < 0.49\lambda_g$), the transformed admittance of slot 2 becomes

$$\tilde{Y}_2 = \tilde{G}_2 + j\tilde{B}_2 = G_1 - jB_1 \quad \text{Eq. (2.8)}$$

Therefore the total resonant input admittance is real and is given by

$$Y_{in} = Y_1 + \tilde{Y}_2 = 2G_1 - jB_1 + jB_1 = 2G_1 = \frac{1}{Z_{in}} \quad \text{Eq. (2.9)}$$

The characteristic impedance, although real and looking like a resistance, is actually lossless, non-dissipative impedance. In fact, nothing gets hot as a result of supplying energy to this resistance. The reason behind that is because the energy transferred from the generator is stored temporarily in the transmission line. At some later time, possibly a great many transit times later, it can be extracted and returned to the generator, or used to make a real resistive dissipative load become hot. The characteristic impedance is given by

$$Z_0 = \frac{\frac{120\pi}{\sqrt{\epsilon_{re}}}}{\frac{W}{h} + 1.393 + 0.667 \ln\left(\frac{W}{h} + 1.444\right)} \quad \frac{W}{h} \geq 1 \quad \text{Eq. (2.10)}$$

A combination of parallel-plate radiation conductance and capacitive susceptance loads both radiating edges of the patch. Harrington gives the radiation conductance for a parallel plate radiator as (Harrington, 1961).

$$G = \frac{\pi W}{\eta \lambda_0} \left[1 - \frac{(kh)^2}{24} \right] \quad \text{Eq. (2.11)}$$

where λ_0 is free-space wavelength and η is the free- space impedance characteristic. The capacitive susceptance relates to the effective strip extension

$$B = 0.01668 \frac{\Delta}{h} \left(\frac{W}{\lambda_0} \right) \epsilon_{eff} \quad \text{Eq. (2.12)}$$

This G and B equations can be used in Multiport Network Model (MNM) and obtained good results in regular geometries. In the vicinity of its fundamental resonant frequency, the input impedance of a microstrip antenna can be modeled by either a series-resonant or a parallel-resonant RLC circuit. The input impedance of an antenna is a complicated function of frequency, which cannot be described in any simple analytical form. Nevertheless, at a single frequency, the antenna terminal impedance may be accurately represented by a resistance series with a reactance. If, as is often case, the band of frequencies is centered about the “resonant frequency” of the antenna, a better approximation is obtained by representing the antenna as a series RLC circuit. If the range of operation extends over wider band frequencies, this representation is no longer adequate. It can be improved by adding elements to the “equivalent” network, but the number of elements required for reasonably good representation becomes very large as the frequency range is extended.

For both transmitting and receiving, an antenna is often operated at its resonant frequency, that is, at the center frequency of the narrow band of operation where the antenna input impedance pure resistance. Below this center frequency the antenna reactance is capacitive, and above this frequency the reactance is inductive. The

input impedance can then be represented approximately by a RLC circuit. General expression for impedance is (Ludwig & Bretchko, 2000)

$$Z_a = R_a + j \left(\omega L_a - \frac{1}{\omega C_a} \right) \quad \text{Eq. (2.13)}$$

and at the resonant frequency $f = f_r$,

$$\omega_r L_a = \frac{1}{\omega_r C_a} \quad Z_a = Z_r = R_a \quad \text{Eq. (2.14)}$$

For a small angular frequency increment, $\delta\omega$, from the resonant frequency, the impedance increment is

$$\delta Z_a = j \left(\delta\omega L_a + \frac{\delta\omega}{\omega^2 C_a} \right) \quad \text{Eq. (2.15)}$$

When the microstrip patch antenna fed by a transmission line, it behaves as a complex impedance ($Z_{in}=R+jX$), which depends mainly on the geometry of the coupling between transmission line and the patch antenna. At the same time, the input impedance determined to the return loss level.

2.2.1.3 Microstrip Antenna Bandwidth

For an antenna, the bandwidth (BW) can be defined in a number of ways depending on the characteristics selected. The bandwidth term refers “the range of frequencies within which the performance of the antenna, with respect to some characteristic, conforms to a specified standard”. It can be considered to be range of frequencies, on either side of a center frequency. For a microstrip antenna, the bandwidth is expressed as a percentage of the frequency difference (upper minus lower) over the center frequency of the bandwidth. The BW could be defined in terms of its voltage standing-wave ratio ($VSWR$) or input impedance variation with frequency. The most widely used impedance BW is presented in Figure 2.3.

Return Loss (RL) which is the ratio of reflected power, to incident power, expressed as

$$RL = -10 \text{Log} \left(\frac{P_r}{P_i} \right) = -20 \log |\Gamma_{in}| \quad \text{Eq. (2.16)}$$

where Γ_{in} is a measure of reflected signal at the feed-point of the antenna. Return Loss is useful in describing the amount of power that a device does not utilize, typically due to a mismatch between the input impedance of the device and output impedance of the signal source. The return loss is used in this thesis to measure the amount of energy that is reflected by the antenna element. For this study, -10 dB return loss is established as a minimum requirement, which represents 90% of the incident power entering the device and 10% of the power being reflected.

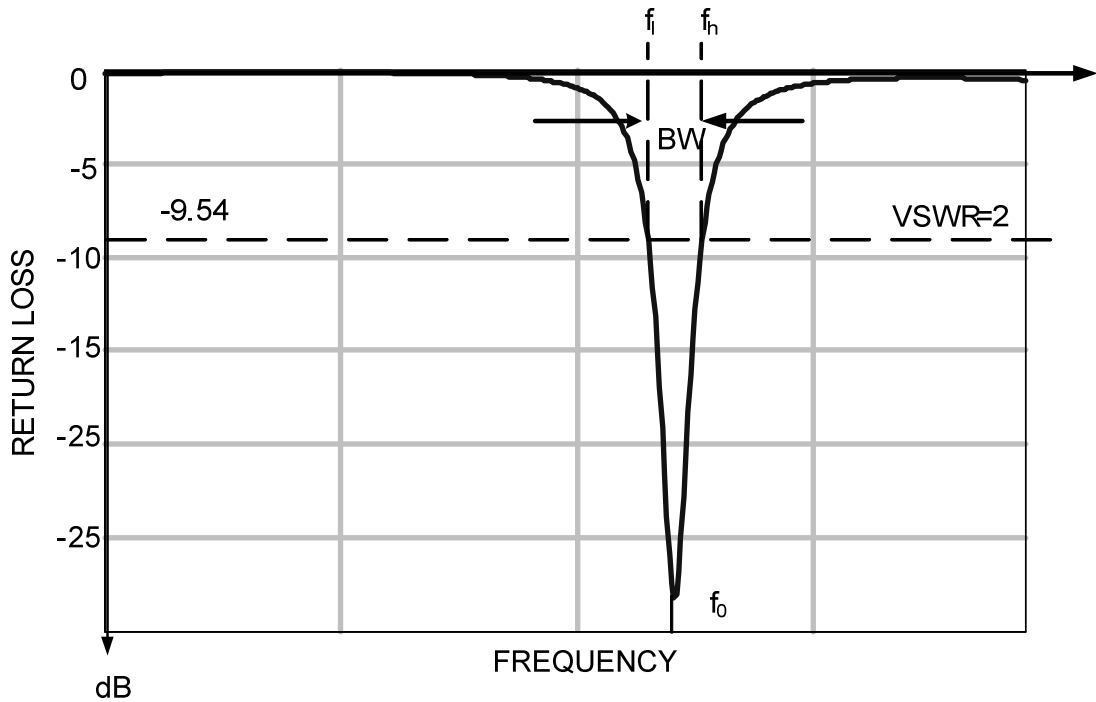


Figure 2.3 Impedance bandwidth

The percent bandwidth of the antennas was determined from impedance data. The bandwidth is normally defined as

$$\%BW = \frac{(f_h - f_l)}{f_0} \times 100 \quad \text{Eq. (2.17)}$$

where f_o is the resonant frequency, while f_h and f_l are the frequencies between which the magnitude of the reflection coefficient of the antenna is less than or equal to $1/3$ (which corresponds to $VSWR \leq 2.0$ and $S_{11} < -10\text{dB}$).

The bandwidth of the microstrip antenna (MSA) is inversely proportional to its quality factor and is given by (Pues & Capelle, 1989)

$$BW = \frac{VSWR - 1}{Q\sqrt{VSWR}} \quad \text{Eq. (2.18)}$$

where Q is the quality factor.

However Q of the patch antenna on a thin substrate is large, therefore the bandwidth is small. The impedance bandwidth increases with substrate thickness (h), and decreases with an increase in substrate permittivity (ϵ_r). This behavior concludes that microstrip antennas operate best when the substrate is electrically thick with a low dielectric constant. On the other hand, a thin substrate with a high dielectric constant is preferred for microstrip transmission lines and microwave circuitry.

Sometimes for stringent applications, the VSWR requirement is specified to be less than 1.5 (which corresponds to a return loss of 14 dB or 4% reflected power). A one simplified relation for quick calculation of BW (in megahertz) for $VSWR=2$ of the microstrip antenna operating at frequency f in gigahertz, with h expressed in centimeters, is given by (Johnson, 1993).

$$BW \cong 50hf^2 \quad \text{Eq. (2.19)}$$

Variation of bandwidth with h , ϵ_r , W and L is clearly brought out by the approximate expression given below (Jackson & Alexopoulos, 1991).

$$BW \cong \frac{16}{3\sqrt{2}} \frac{p}{e_r} \frac{1}{\epsilon_r} \frac{h}{\lambda_0} \frac{W}{L} q \quad \text{Eq. (2.20)}$$

where

$$p = 1 - \frac{0.16605}{20} (k_0 W)^2 + \frac{0.02283}{560} (k_0 W)^4 - 0.009142 (k_0 L)^2 \quad \text{Eq. (2.21)}$$

$$q = 1 - \frac{1}{\epsilon_r} + \frac{2}{5\epsilon_r^2} \quad \text{Eq. (2.22)}$$

and e_r is the radiation efficiency and k_0 is the free space wave number.

The bandwidth of the RMSA can also be increased by increasing the inductance of the radiators by cutting holes or slots in it or by adding reactive components to improve the match of the radiator to the feed line.

2.2.1.3 Radiation Pattern of Microstrip Antenna

The radiation patterns of an antenna as shown in Figure 2.4 are of prime importance in determining most of its radiation characteristics, which include beamwidth, beamshape, sidelobe level, directivity, polarization, and radiated power.

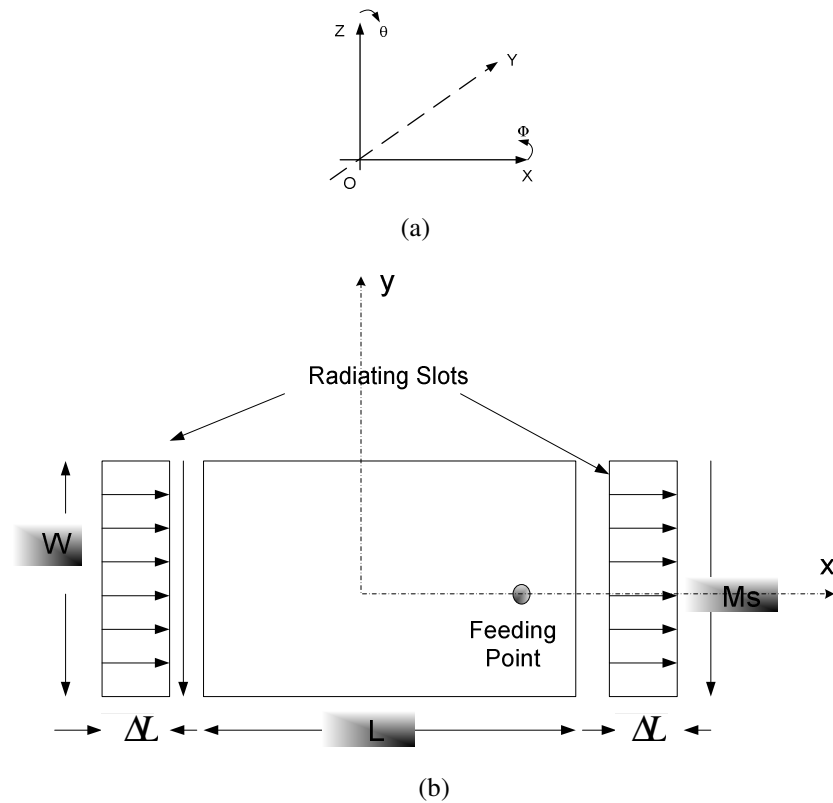


Figure 2.4 (a) Pattern coordinate system (b) Two radiating slots

The rectangular microstrip patch antenna can be operated in several different modes. However, the most common modes of operation for the antenna are the TM_{10} and TM_{01} modes (Lo, et al, 1979), Since they produce principal plane radiation patterns with maxima in the broadside direction. Higher order modes tend to produce maxima off broadside. If W is too large, then the higher order modes could get excited.

In order to calculate the radiation pattern from rectangular microstrip antenna (RMSA), first the radiation field from one of the approximating slots is calculated, after that, array theory can be used to calculate radiation pattern from both slots. The radiation from the patch can be derived from the E_z field across the aperture between the patch and the ground plane (using electric vector potentials) or from currents on the surface of the patch conductor (employing the vector magnetic potentials).

The radiation pattern of rectangular microstrip antenna (RMSA) for the TM_{10} mode could be calculated by combining the radiation pattern of the two slots of length W_e (effective dimension) and width ΔL on the infinite ground plane, which are spaced at a distance $L + \Delta L$. The normalized pattern in the E-plane (E_θ in $\phi = 0^\circ$ plane) and the H-plane (E_ϕ in $\phi = 90^\circ$ plane) are given by (Balanis, 1997)

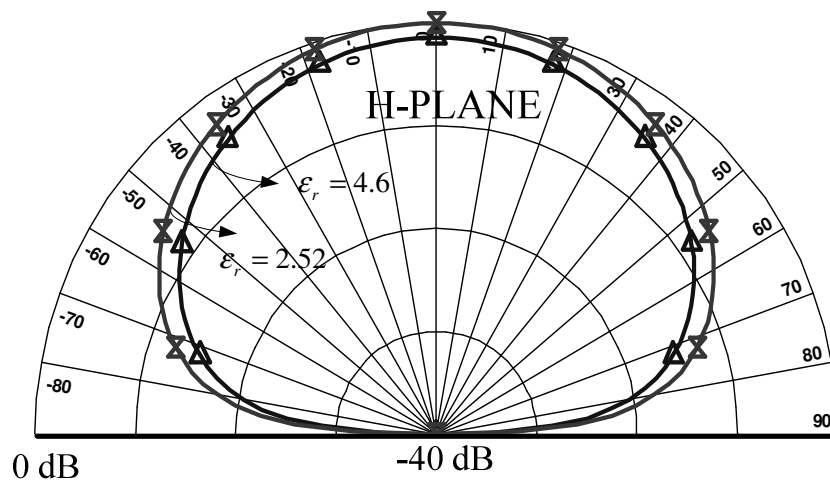
$$E_\theta = \frac{\sin\left(\frac{k_0 \Delta L \sin(\theta)}{2}\right)}{\frac{k_0 \Delta L \sin(\theta)}{2}} \cos\left(\frac{k_0 (L + \Delta L) \sin(\theta)}{2}\right) \quad \text{Eq. (2.22)}$$

$$E_\phi = \frac{\sin\left(\frac{k_0 W_e \sin(\theta)}{2}\right)}{\frac{k_0 W_e \sin(\theta)}{2}} \cos(\theta) \quad \text{Eq. (2.23)}$$

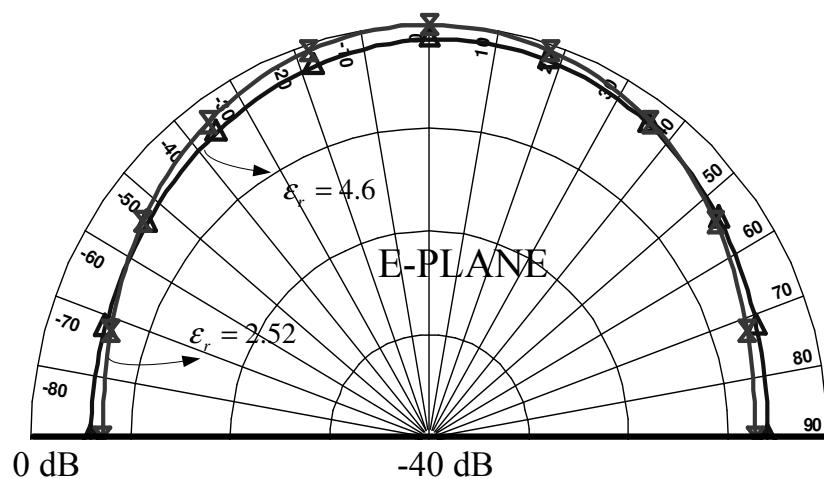
where θ is angle measured from the broadside as shown in Figure 2.4.

The radiation pattern for two different values of ϵ_r (2.52 – Taconic: TLY_5 CH-200 and 4.6) are shown in Figure 2.5. To illustrate the modeling of the microstrip

antenna, the principal E- plane and H-plane patterns have been simulated at $f_0=2.5$ GHz for the square microstrip antenna.



(a)



(b)

Figure 2.5 Radiation pattern of square patch microstrip antenna (a) H-Plane (b) E-Plane ($W \times L = 40 \times 40$ mm, $f_0 = 2.5$ GHz)

Figure 2.5 shows the computed principal plane radiation patterns for the TM_{10} mode of two antennas. As a substrate material TLYA-5-CH-200 which has a relative permittivity of 2.2 and a thickness of 0.52 mm defined by the manufacture firm Taconic is utilized. The shape of the H- plane patterns are not affected by the dielectric cover or the edges (Balanis, 1997).

2.3 Microstrip Antenna Array

Microstrip broadband planar antennas have been of interest to antenna designers for many years in microwave and millimeter-wave integrated systems. A planar configuration implies that the characteristics of the element can be determined by the dimensions in a single plane. Despite their planar geometry, the antennas can produce a symmetric beam, often over a wide band of frequencies. While both the Tapered Slot antenna and the Quasi-Yagi antenna possess wide bandwidth and end-fire radiation pattern, the microstrip patch antenna produces broadside radiation.

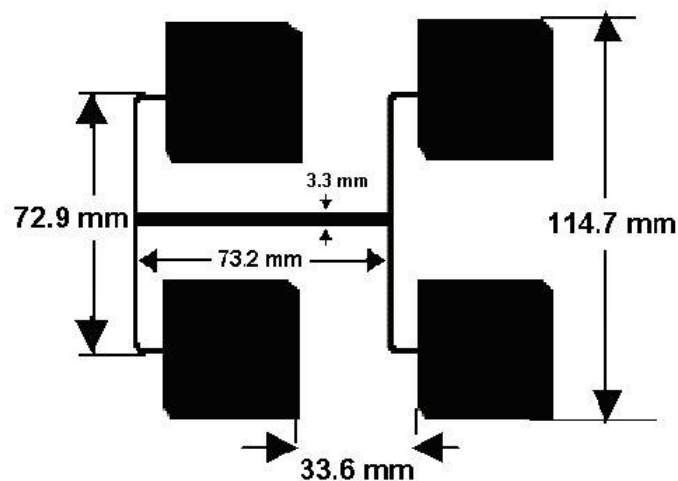
Microstrip patch antennas are also often used in arrays because of its low gain and wide beamwidth. Due to the fact that the array consists of many patch antennas, the feeding structure of the array is definitely more complicated than that of a single element. In addition, coupling will also occur between the microstrip single elements, the feeding structure and the substrates in the array. As a result, when considering the bandwidth of the array, it is necessary to consider the effects of coupling. And in large arrays of microstrip antennas, destructive interference of surface wave power can occur, raising the radiating efficiency.

2.3.1 Circularly Polarized Planar Microstrip Antenna Array

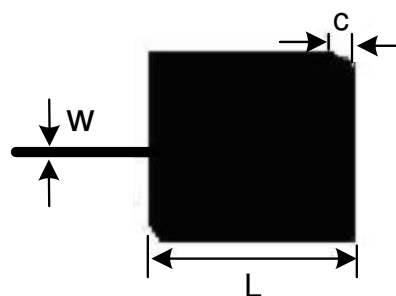
Linearly polarized transmit – receive antenna systems can cause energy loss. Against the energy-loss problem with linearly polarized antennas, circularly polarized antenna system is aimed to design. High-frequency systems (e.g. 2.4 GHz and higher) that use linear polarization typically require a clear line-of-sight path between the two points in order to operate. Such systems have difficulty in penetrating obstructions due to reflected signals, which weaken the propagating signal. Reflected linear signals return to the propagating antenna in the opposite phase, consequently weakening the propagating signal. Conversely, circularly polarized systems also incur reflected signals, but the reflected signal is returned in

the opposite sense, largely avoiding conflict with the propagating signal. The result is that circularly polarized signals are much better for penetrating and bending around obstructions. Thus, when a line-of-sight path is impaired by light obstructions (e.g. small buildings), circular polarization is much more effective than linear polarization for establishing communication links. In addition, circular polarization is more resistant to signal fading due to bad weather conditions.

This type of planar antenna arrays can be realized using microstrip antennas since they can offer small dimensions, conformality, cheapness, ease of manufacturing, obtaining either linear or circular polarization with small perturbations in geometry and feeding, modularity in design (Kaya, Özmehmet, Yüksel, Tamer, 2005).



(a)



(b)

Figure 2.6 (a) Microstrip antenna array configuration (b) An element of the array ($L=39.705\text{mm}$, $c=3\text{ mm}$, $W=0.6\text{ mm}$)

An example of an array made up of microstrip patch antennas is shown in Figure 2.6. Microstrip design formulas mentioned before were used for this example. The material used in this work is one of the special materials designed for antenna design applications by Taconic, TLY-5A-CH 200. Thickness of the dielectric substrate is 0.52 mm that is covered by copper sheets with a thickness of 18 μm . It has a dielectric constant of 2.17 and a loss tangent (δ) of 0.0009. Copper faces are covered by tin, which is a good conductor to prevent the oxidations on the copper layer, namely the lifetime and stability of the antenna is increased.

The array is designed as a four-element structure in Figure 2.6. Spacing between elements is chosen as $\lambda/2$. If it is chosen smaller than $\lambda/2$, then undesired side beams arise but also the main beam width will increase. Enlarging the spacing causes narrower main beam width, increasing the directivity of the structure. On the other hand the existing side beam amplitudes are also increased and extra side beams are arose.

For circular polarization occurrence from single feed patch, one can feed the patch on one of the sides and truncate corners of the square patch. If the corners were not truncated, one resonance mode will occur from the side that is fed to the opposite side. This would create a linear polarization. Since one of the diagonals is shorter than the other, the resonance frequencies differ slightly for the two modes. If the corners are truncated exactly at the right amount, the difference in frequencies will cause the 90° phase shift for the nearly square patch (Kaya, Çelebi & Yüksel, 2003).

The antenna in Figure 2.6 produces circular polarization by creating a small perturbation in antenna's geometric symmetry. The return loss graphic and E-H plane patterns are shown in Figure 2.7 and 2.8 for the circular array patch antenna.

In satellite communications, circularly polarized radiation patterns are required. Therefore, this type of antenna can be selected for a microstrip antenna design. In addition the beam shapes such as sector beam, multi beam can be produced using this configuration.

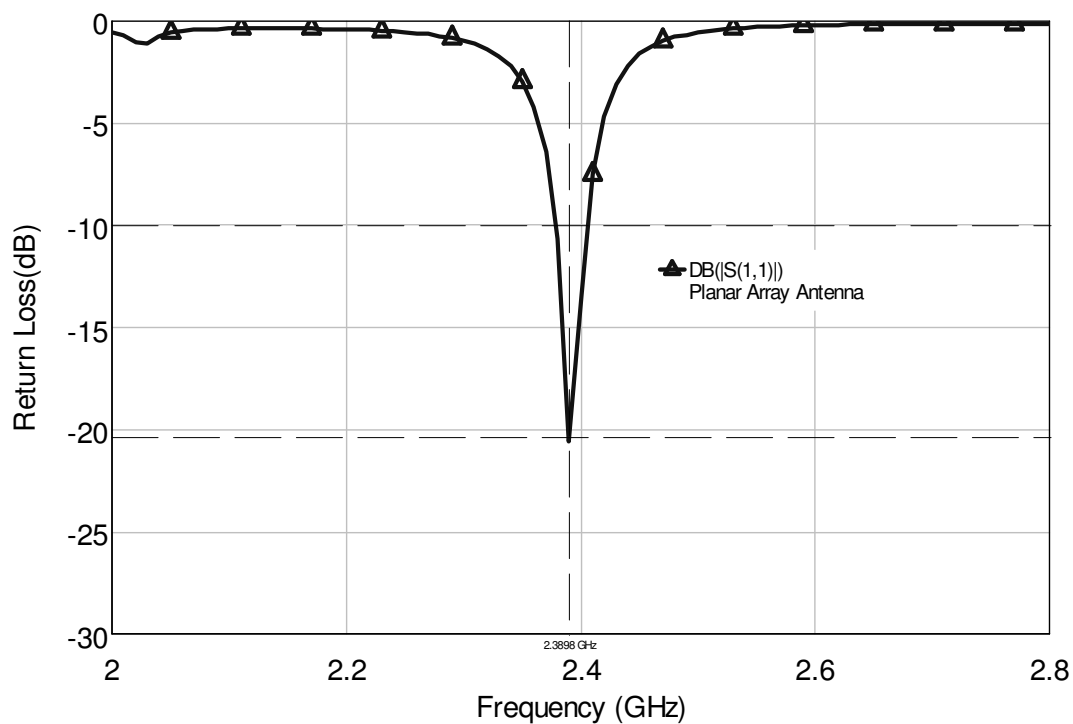


Figure 2.7 The simulated return loss parameter for circular array antenna

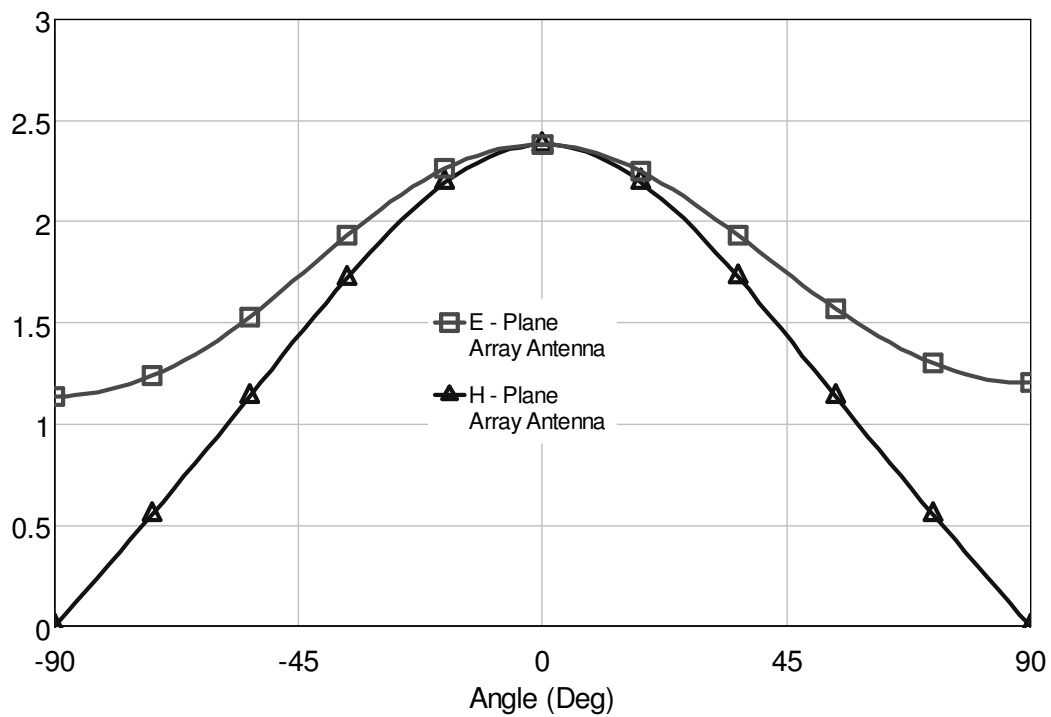


Figure 2.8 E and H plane pattern for 2.4 GHz frequency

2.4 Analytical Techniques for Microstrip Antennas

There are various methods used for the analysis of microstrip antenna elements. The methods are divided into the following three categories:

1. Empirical models,
2. Semi-empirical models,
3. Full-Wave analysis

Empirical models are generally based on some fundamental simplifying assumptions concerning the radiation mechanism of the antenna. The assumptions can be labeled “empirical” because they are mostly witnessed in practice rather than by theory. Phenomena such as surface wave propagation and dispersion are generally not included in these models. Most empirical models reported in literature are satisfactory accurate only at microwave frequencies. As frequencies increase, the accuracy of these models in predicting the performance of the antenna reduces and becomes almost completely unacceptable in the millimeter-wave band. There are three popular analytical techniques: transmission line model (TLM) and cavity model (CM), Multiport Network Model (MNM).

In the TLM model, each of the radiating edges of the antenna is simulated by a radiating slot having complex admittance (Garg, Bhartia, Bahl, & Ittipiboon, 2001). The radiated fields of each slot are then derived, assuming a trial function for the slot voltage as shown in Figure 2.2. Finally, the two radiated fields are superposed to obtain the complete radiation pattern of the antenna. The TLM can apply only rectangular or square patch.

The cavity model (Lo, Solomon & Richards, 1979) in principle, can handle any arbitrary shape. As indicated in the literature, the high-impedance condition at the patch periphery implies that the E-field parallel to the patch edge has a maximum at the edge, whereas the H-field has a minimum value there. The patch edge can thus be replaced by a magnetic wall, thereby reducing the antenna to an enclosed cavity

capable of supporting an infinite number of modes. The field expression inside the cavity thus can be easily written. The CM can handle almost regular patch shapes (including rectangular, circular, and triangular).

Semi-empirical models are a hybrid of empirical and full-wave analyses. The analytical and computational complexity involved is more than that of the empirical models and less than the full-wave analyses, and the effects of surface wave modes are taken into account in many models (Benalla & Gupta, 1988).

The various models included in this category are:

1. Variational approach,
2. Multiport Network Model (MNM)
3. Dual integral equation approach,
4. Electric surface current model,
5. Hankel transform technique,
6. Reciprocity method
7. Generalized edge boundary condition (GEBC) technique

In the full-wave analysis category, one finds formulations that are electromagnetically rigorous (no empirical or semi-empirical assumptions are made) as well as computationally extensive. These models, in general, require an extensive analytical and computational effort. The full-wave analyses, as applied to microstrip antennas, can be grouped into the following:

1. Moment method in space domain;
2. Moment method (MoM) in spectral domain;
3. Transform-domain analyses;
4. Mixed potential integral equation (MPIE) approach;
5. The finite-difference time domain (FDTD) method

In the MoM, the surface currents are used to model the microstrip patch, and volume polarization currents in the dielectric slab are used to model the fields in the dielectric slab. An integral equation is formulated for the unknown currents on the microstrip patches and the feed lines and their images in the ground plane (Newman & Tulyathan, 1981). The integral equations are transformed into algebraic equations that can be easily solved using a computer. This method takes into account the fringing fields outside the physical boundary of the two-dimensional patch, thus providing a more exact solution.

2.4.1 Cavity Model Analysis for the Microstrip Antenna

The simplicity of the cavity model is due to the assumption that the separation between the patch conductor and the ground plane is much less than the operation wavelength. Microstrip patch antennas can be termed lossy cavities. A cavity model was advanced by Lo et al (Lo, Solomon & Richards, 1979). In this model, the interior region of the patch is modeled as a cavity bounded by electric walls on the top and bottom, and a magnetic wall along the periphery (Michalski & Hsu, 1994). The bases for this assumption are the following observations for thin substrates $h \ll \lambda_0$.

For an arbitrary-shaped patch antenna excited by a current density J at a frequency ω on a substrate of thickness h , permeability μ and permittivity ϵ , Maxwell's equations are written as

$$\begin{aligned}
 \nabla \times \vec{E} &= -j\omega\mu\vec{H} \\
 \nabla \times \vec{H} &= j\omega\epsilon\vec{E} + \vec{J} \\
 \nabla \cdot \vec{E} &= \frac{\rho}{\epsilon} \\
 \nabla \cdot \vec{H} &= 0
 \end{aligned}
 \tag{2.24}$$

The exciting current J can be introduced with a microstrip line feed or a probe-feed. The fields in the interior region do not vary with z (that is, $\partial/\partial z \cong 0$) because the substrate is very thin, $h \ll \lambda_0$. The electric field is z directed only, and the magnetic field has only the transverse components in the region bounded by the

patch metallization and the ground plane. This observation provides for the electric walls at the top and bottom. The cavity model is shown in Figure 2.9.

The electric current in the patch has no component normal to the edge of patch metallization, which implies that the tangential component of \vec{H} along the edge is negligible, and a magnetic wall can be placed along periphery. Mathematically, $\partial E_z / \partial n = 0$.

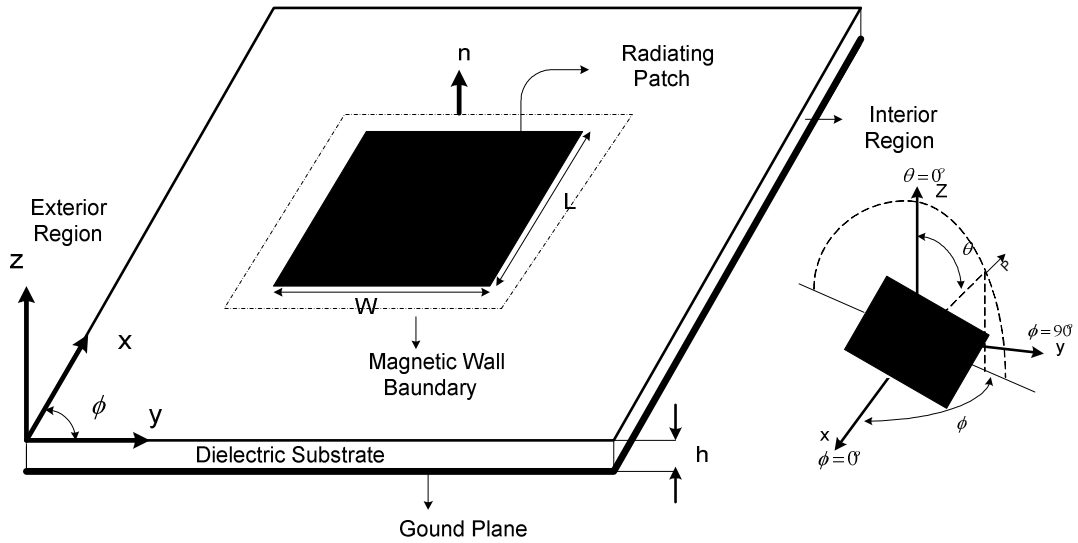


Figure 2.9 Magnetic wall model of a microstrip antenna

The interior electric field must satisfy the inhomogeneous wave equation

$$\nabla^2 E_z + k^2 E_z = j\omega\mu_0 \vec{z} \cdot \vec{J} \quad \text{Eq. (2.25)}$$

where $k^2 = \omega^2 \mu_0 \epsilon_0 \epsilon_r$, \vec{J} is the excitation electric current density either due to the coaxial feed or the microstrip feed, \vec{z} is a unit vector normal to the plane of patch, and ∇ is the transverse del operator with respect to the z axis. The interior electric field distribution is obtained in terms of eigenfunctions of the cavity and the electric field in the patch cavity can be written as

$$E_z(x, y) = \sum_m \sum_n A_{mn} \psi_{mn}(x, y) \quad \text{Eq. (2.26)}$$

where A_{mn} are the amplitude coefficients corresponding to the electric field mode vector or eigenfunctions Ψ_{mn} . The eigenfunctions are solutions of

$$(\nabla^2 + k_{mn}^2)\Psi_{mn} = 0, \quad \text{Eq. (2.27)}$$

with

$$\frac{\partial \Psi_{mn}}{\partial n} = 0 \quad (\text{on the magnetic walls}) \quad \text{Eq. (2.28)}$$

For rectangular patch, the eigenfunctions Ψ_{mn} must satisfy the homogeneous wave equation, boundary conditions, and normalization conditions, that is,

$$\left. \frac{\partial \Psi_{mn}}{\partial y} \right|_{y=0} = 0 = \left. \frac{\partial \Psi_{mn}}{\partial y} \right|_{y=W} \quad \text{Eq. (2.29.a)}$$

$$\left. \frac{\partial \Psi_{mn}}{\partial x} \right|_{x=0} = 0 = \left. \frac{\partial \Psi_{mn}}{\partial x} \right|_{x=L} \quad \text{Eq. (2.29.b)}$$

$$\iint_{x,y} \Psi_{mn} \Psi_{mn}^* dx dy = 1 \quad \text{Eq. (2.30)}$$

$$\left(\frac{\partial^2}{\partial x^2} + \frac{\partial^2}{\partial y^2} + k_{mn}^2 \right) \Psi_{mn} = 0 \quad \text{Eq. (2.31)}$$

The solutions of (2.29) to (2.30) are the orthonormalized eigenfunctions (Garg, et al., 2001)

$$\Psi_{mn}(x, y) = \sqrt{\frac{\delta_m \delta_n}{LW}} \cos(k_m x) \cos(k_n y) \quad m, n = 0, 1, 2, \dots, p \quad \text{Eq. (2.32)}$$

with

$$\delta_p = \begin{cases} 1 & \text{for } p = 0 \\ 2 & \text{for } p \neq 0 \end{cases} \quad \text{Eq. (2.33)}$$

$$k_m = \frac{m\pi}{L}, \quad k_n = \frac{n\pi}{W}, \quad k_{mn}^2 = k_m^2 + k_n^2 \quad \text{Eq. (2.34)}$$

The coefficients A_{mn} of (2.26) are determined by the excitation current

$$A_{mn} = \frac{j\omega\mu_0}{k^2 - k_{mn}^2} \frac{\iint J_z \psi_{mn}^* ds}{\iint \psi_{mn} \psi_{mn}^* ds} = \frac{j\omega\mu_0}{k^2 - k_{mn}^2} \iint J_z \psi_{mn}^* dx dy \quad \text{Eq. (2.35)}$$

Assume the coaxial feed as rectangular current source with cross-section $D_x D_y$ center at (x_0, y_0) e.g

$$J_z = \begin{cases} I_0 / D_x D_y \\ 0 \end{cases} \quad \text{Eq. (2.36)}$$

For a microstrip line feed connected along the width of the patch, $D_x = 0$ and D_y equal to the effective width of the feed line.

Use of (2.36) in (2.35) gives

$$\begin{aligned} A_{mn} &= \frac{1}{D_x D_y} \frac{j\omega\mu_0}{k^2 - k_{mn}^2} \iint I_0 \psi_{mn}^* dx dy \\ &= \frac{j\omega\mu_0}{k^2 - k_{mn}^2} \sqrt{\frac{\delta_m \delta_n}{LW}} \cos(k_m x_0) \cos(k_n y_0) G_{mn} \end{aligned} \quad \text{Eq. (2.37)}$$

where

$$G_{mn} = \text{Sinc}\left(\frac{n\pi D_x}{2L}\right) \text{Sinc}\left(\frac{m\pi D_y}{2W}\right) \quad \text{Eq. (2.38)}$$

Substituting (2.37) in (2.26) gives

$$E_z(x, y) = j\omega\mu_0 I_0 \sum_m \sum_{n=0}^{\infty} \frac{\psi_{mn}(x, y) \psi_{mn}(x_0, y_0)}{k^2 - k_{mn}^2} G_{mn} \quad \text{Eq. (2.39)}$$

The magnetic field components in the cavity region are determined from E_z and Maxwell's equations. Input impedance in this model is calculated as

$$Z_{in} = \frac{V_{in}}{I_0} \quad \text{Eq. (2.40)}$$

where V_{in} is the RF voltage at the feed point. It is computed from (2.39) as

$$V_{in} = -E_z(x_0, y_0)h = -j\omega\mu_0 I_0 h \sum_m \sum_{n=0}^{\infty} \frac{\psi_{mn}^2(x_0, y_0)}{k^2 - k_{mn}^2} G_{mn} \cdot \quad \text{Eq. (2.41)}$$

Therefore, (2.40) for the input impedance becomes (Richards & Harrison, 1981)

$$Z_{in} = -j\omega\mu_0 h \sum_m \sum_{n=0}^{\infty} \frac{\psi_{mn}^2(x_0, y_0)}{k^2 - k_{mn}^2} G_{mn}. \quad \text{Eq. (2.42)}$$

Equation (2.42) will yield the input impedance as reactive because all the quantities under the summation sign are real if the substrate is lossless. The effect of radiation and other losses on the input impedance has been included in the model. The substrate loss tangent is increased artificially to account for the power loss from the antenna (Richards, Lo & Harrison, 1981). The new loss tangent denoted as δ_{eff} is given by

$$\delta_{eff} = \tan \delta + \frac{\Delta}{h} + \frac{P_r}{\omega W_T} \quad \text{Eq. (2.43)}$$

Here $\tan \delta$ is loss tangent of substrate, Δ is skin depth for the patch conductor, P_r is the power radiated by the patch antenna, and W_T is the time-averaged total energy stored under the patch geometry. With the losses described in terms of δ_{eff} , the expression for k^2 in (2.42) is now modified as

$$k^2 = k_0^2 \epsilon_r (1 - j\delta_{eff}) \quad \text{Eq. (2.44)}$$

Thouroude et al (Thouroude, et al., 1990) have obtained such an expression having an accuracy of 2.5 % for $L/\lambda_0 = 0.3(\epsilon_r = 2.5)$ and $W/\lambda_0 \leq 0.6$; and 4% for $L/\lambda_0 = 0.15(\epsilon_r = 12)$ and $W/\lambda_0 \leq 0.3$; this expression is given

$$P_r = \frac{(E_0 h)^2 A \pi^4}{23040} \left[(1-B) \left(1 - \frac{A}{15} + \frac{A^2}{420} \right) + \frac{B^2}{5} \left(2 - \frac{A}{7} + \frac{A^2}{189} \right) \right] \quad \text{Eq. (2.45)}$$

where $A = (\pi W / \lambda_0)^2$, and the resonant length $B = (2L / \lambda_0)^2$

The energy stored is determined by the fields under the patch, and is expressed as

$$W_T = W_e + 2W_m = \frac{\epsilon_0 \epsilon_r}{2} \iiint |E_z|^2 dV \quad \text{Eq. (2.46)}$$

to yield the following expression for Z_{in} :

$$Z_{in} = -j\omega\mu_0 h \sum_m \sum_{n=0}^{\infty} \frac{\psi_{mn}^2(x_0, y_0)}{k_0^2 \epsilon_r (1 - j\delta_{eff}) - k_{mn}^2} G_{mn} \quad \text{Eq. (2.47)}$$

with

$$\psi_{mn}(x, y) = \sqrt{\frac{\delta_m \delta_n}{LW}} \cos(k_m x_0) \cos(k_n y_0) \quad \text{Eq. (2.48)}$$

The various terms in (4.47) and (4.48) can be identified at the contribution of various modes of patch cavity. The term $(m, n; 1, 0)$ represents the resonant mode of the antenna. It is identical the transmission line mode and impedance behavior for this mode can be expressed in the form of a parallel RLC network. The $(0, 1)$ mode can be represented similar the type of RLC network.

2.4.2 Multiport Network Model (MNM) for the Microstrip Antenna

The MNM (Gupta, & Sharma, 1981) for analyzing the MSA is an extension of the cavity model. In this model, the interior region and the exterior region are modeled separately. The interior region is modeled as a multiport planar circuit, with the ports located all along the periphery, as shown the Figure 2.10. The fields in the exterior region, which include the fringing fields, radiating fields, and the surface wave fields, are represented by the load admittances. The load admittance corresponding to the given edge is equally divided into a number of ports. These loads are then connected to the corresponding ports on the planar circuit.

The width W_i is chosen so small that the fields over this length may be assumed to be uniform. In the Figure 2.10, R-EAN stands for the radiating edge admittance network, and NR-EAN denoted the nonradiating edge admittance network. The multiport impedance matrix of the patch is obtained from its two-dimensional Green's function. The fringing fields along the periphery and the radiated fields are obtained from the voltage distribution around the periphery. The elements of the Z-matrix are derived from the Green functions as

$$Z_{ij} = \frac{1}{W_i W_j} \int_{W_i} \int_{W_j} G(x_i, y_i / x_j, y_j) ds_i ds_j \quad \text{Eq. (2.49)}$$

Where $(x_{i,j}, y_{i,j})$ denote the locations of the two ports of widths W_i, W_j , respectively. Green's function G is usually a doubly infinite summation with terms corresponding

to various modes of the planar resonator with magnetic walls (Benalla & Gupta, 1988). The segmentation method is then used to find the overall impedance matrix.

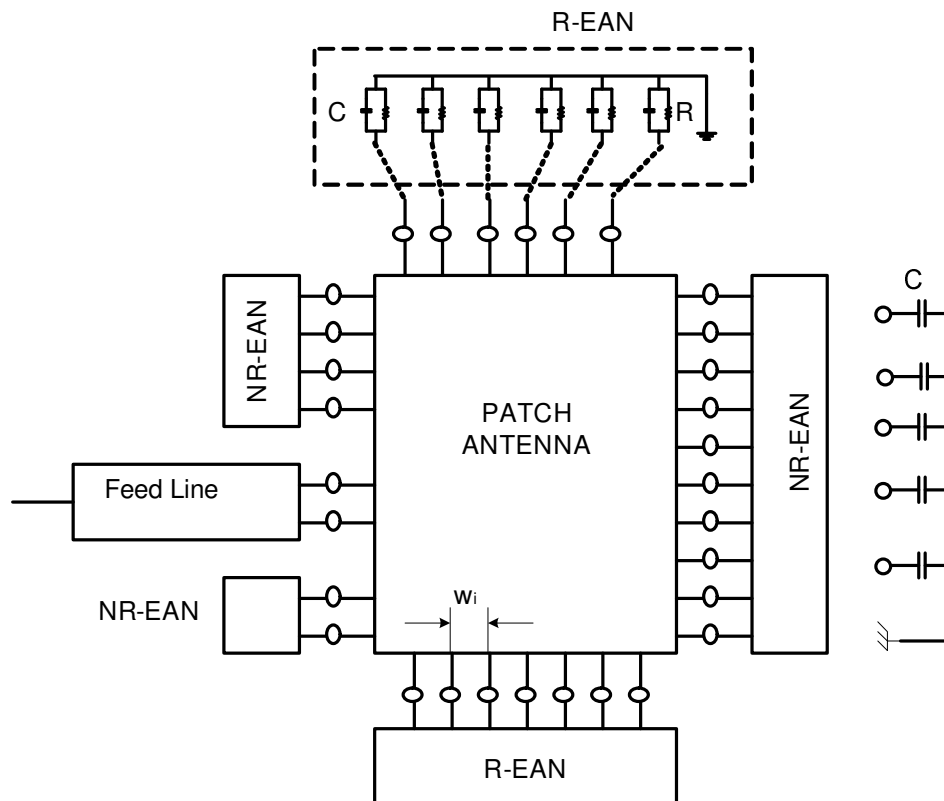


Figure 2.10 Multiport network model of a rectangular microstrip patch

The radiation from the RMSA is calculated from the equivalent magnetic current distribution around the periphery of radiating patch, which is obtained from the corresponding voltage distribution. This method is accurate for regular geometries but it isn't suited for arbitrary shaped patch geometries.

2.4.3 Method of Moment (MoM) Model

In the MoM model, the surface currents are used to model the microstrip patch, and volume polarization currents in the dielectric slab are used to model the fields in the dielectric slab. An integral equation is formulated for the unknown currents on the microstrip patches and the feed lines and their images in the ground plane

(Newman & Tulyathan, 1981). The integral equations are transformed into algebraic equations that can be easily solved using a computer. This method takes into account the fringing fields outside the physical boundary of the two-dimensional patch, thus providing a more exact solution.

CHAPTER THREE

BANDWIDTH ENHANCEMENT TECHNIQUES IN MICROSTRIP ANTENNAS

3.1 Early Bandwidth Enhancement Techniques

In many cases the narrow bandwidth (2%-5%) of the traditional microstrip antenna element is its most serious disadvantage, preventing its use in many practical microwave applications. Thus a large amount of effort has gone toward the development of creative designs and techniques for improving the bandwidth of microstrip patch antenna. A good review of many of these methods is given in (Henderson, et al. 1986). All these techniques basically work to overcome the fundamental bandwidth limitation and most can be classified as either using an impedance matching network, or parasitic elements.

The most direct method of increasing the bandwidth of the microstrip element is to use a thick, low dielectric constant substrate (Balanis, 1997). But as discussed Chapter 2, this inevitably leads to unacceptable spurious feed radiation, surface wave generation, or feed inductance. The antenna pattern and the polarization characteristics distort waves that travel within the substrate. Since the bandwidth of the element is usually dominated by the impedance variation (the radiation pattern bandwidth is generally much better than the impedance bandwidth), it is often possible to design a planar impedance matching network to increase bandwidth. Attachment of lossless matching network for impedance matching is also commonly utilized technique to improve the bandwidth. This type of bandwidth improvement can be conveniently realized using an on-board or off-board matching network and impedance bandwidth of about 10-30 % can be achieved. Pues and Van de Capelle obtained bandwidth of 10-12 % using passive coplanar matching network (Pues & Van De Capelle, 1989). Similar techniques have been applied by Paschen with a single microstrip element, for a bandwidth of more than 25 % (Paschen, 1986). Impedance matching at the feed point of the microstrip antenna element using

active components has been also proposed to improve the bandwidth in the literature (An et al, 1991). Another is the work by Svitak, et al., which contains a field effect transistor (FET) amplifier in the matching network, resulting a bandwidth of about 7 % (Svitak et al, 1991). An alternative widely employed broadening technique is to use multiple resonances introducing additional resonant patches. In this respect, stacking microstrip elements can be used (Iglesias et al, 2001) and bandwidth of 10-20 % can be obtained. A bandwidth of 13% was achieved for a proximity coupled patch element with a stub tuning network (Pojar & Kaufman, 1987). Spurious radiation from the matching network is coplanar with the antenna element. Bandwidths of 10%-20% have been achieved with probe-fed stacked patches (Lee, Lee & Bobinchak, 1987).

In this chapter the improvement of bandwidth by utilizing floating negative inductor circuit as a compensation network is presented. As an antenna, a simple microstrip patch operating at 10.55 GHz is designed. The active floating inductive compensation circuit (Khory, 1995) is realized using three FETs or two FETs. Simulation results for both compensated and non-compensated antenna are presented. It is observed that utilization of this technique is a promising solution to increase the bandwidth. Element bandwidth can also be affected by the shape of the element, as illustrated in Table 3.1 below, where it is seen that wide rectangular patch elements have slightly higher bandwidths as very narrow rectangular elements.

Table 3.1. Bandwidth of microstrip antennas with various dimensions ($\epsilon_r=2.32$, $h=0.159\text{cm}$)

| Element Shape | Element Size (mm) | Bandwidth (VSWR<2) |
|-------------------------------|--------------------|--------------------|
| Narrow Rectangular, f=2.0 GHz | L=49.24 W=20.00 | 0.7 % |
| Square, f=2.0 GHz | L=48.20 W=48.20 | 1.3 % |
| Wide Rectangular, f=2.0 GHz | L=47.90 W=72.00 | 1.6 % |
| Circular, f=2.0 GHz | R=27.80 | 1.3 % |

This table shows the approximate impedance bandwidths for three rectangular patches of varying aspect ratios, and a circular patch element, all on the same substrate with the same resonant frequency. The wider elements have better bandwidths essentially because their radiation resistances are lower.

3.2 Reactive Matching Technique for Increasing the Bandwidth of Rectangular Microstrip Antennas (RMSA)

In this section, broad-band impedance-matching is proposed as a method for bandwidth enhancement of microstrip antennas (Pues & Van De Capelle, 1989). Reactive matching network is added to compensate for the rapid frequency variations of the input impedance by using this technique. An experimental investigation of the frequency dependence of the operational characteristics of common RMSA clearly shows that the impedance variations are the dominant factor, whereas the gain and radiation pattern variations are almost negligible over a 10 – 20 percent bandwidth. This behavior can be explained easily using cavity analysis models. According to these models, the total input impedance can be written as a sum of modal impedances where each modal impedance behaves as a parallel or series resonant circuit. The configuration of the compensated rectangular patch antenna is shown in Figure 3.1.

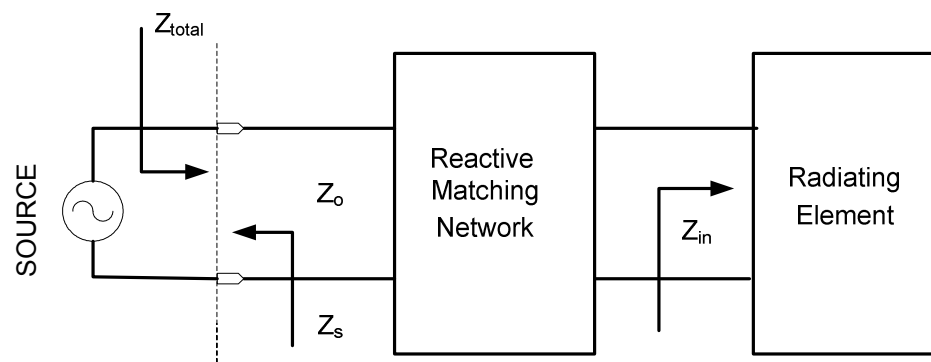


Figure 3.1 Broadband-matching system diagram

The modal indices term $(1, 0)$ represents the resonant mode of the patch. The impedance behavior for this mode can be expressed in the form of a parallel $R-L-C$ network, where R_{l0} represents the radiation, conductor, and losses. The $(0, 1)$ mode

can be represented by a similar R - L - C network (Derneryd, 1979). Parallel and series model of the antenna input impedance is shown in Figure 3.2.

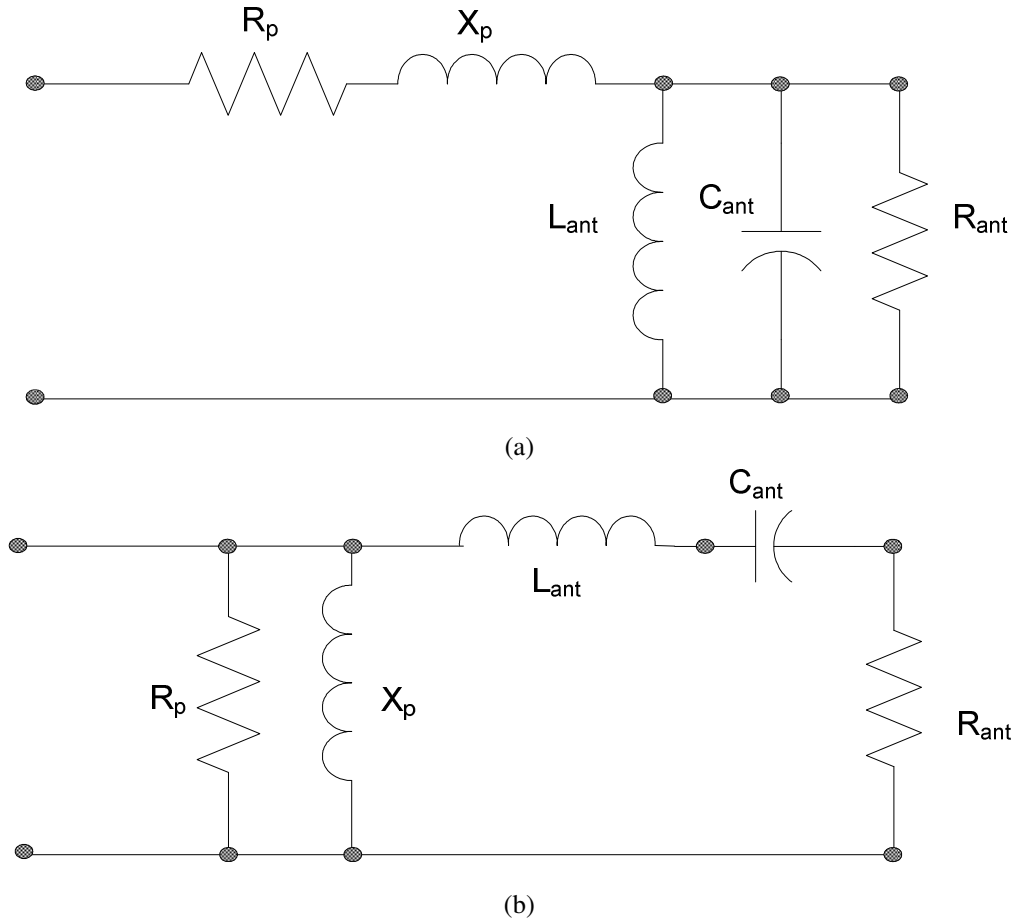


Figure 3.2 Parallel and series model of the antenna input impedance

Figure 3.2 (a) depicts the simplified equivalent microstrip antenna system for TM_{10} mode. The C_{ant} and L_{ant} component can be obtained from the (Eq. 2.42) and are given

$$C_{ant} = \frac{\epsilon_0 \epsilon_r L W}{2h} \cos^2 \left(\frac{\pi x_0}{L} \right) \quad \text{Eq. (3.1)}$$

$$L_{ant} = \frac{1}{(2\pi f_r)^2} \frac{2h}{\epsilon_0 \epsilon_r L W} \cos^2 \left(\frac{\pi x_0}{L} \right) \quad \text{Eq. (3.2)}$$

Evaluation of Z_{in} for the $(1,0)$ mode at $k_{10}^2 = k_0^2 \epsilon_r$ gives

$$R_{ant} = \frac{\omega\mu_0 h}{k_0^2 \epsilon_r \delta_{eff}} \frac{2}{LW} \cos^2\left(\frac{\pi x_0}{L}\right) = \frac{Q_T}{C_{ant} (2\pi f_r)^2} \quad \text{Eq. (3.3)}$$

where angular resonance frequency is $\omega_r = k_0 c$ and quality factor is $Q_T = 1/\delta_{eff}$. If f_r is the resonant frequency of the patch antenna, R is the resonant resistance and Q_T is the total quality factor of the resonator, all obtained from the impedance curve, as

$$f_r = \frac{1}{2\pi\sqrt{LC}} \quad \text{Eq. (3.4)}$$

The values L and C are given by

$$L = \frac{R}{2\pi f_r Q_T} \quad \text{Eq. (3.5.a)}$$

$$C = \frac{Q_T}{2\pi f_r R} \quad \text{Eq. (3.5.b)}$$

and the input impedance for a R - L - C parallel resonant circuit is found to be

$$Z_{in} = R_{in} + jX_{in} = \frac{1}{\frac{1}{R} + j\omega C + \frac{1}{j\omega L}} \quad \text{Eq. (3.6)}$$

This simple model can be used to obtain an approximate value of the input impedance as a function of the frequency. The peak input resistance can be used to define the resonant frequency.

3.2.1 Bandwidth Improvement Theory

A broad-band matching design procedure with external matching is presented to improve the bandwidth characteristics. The circuit model of input impedance of the antenna is modeled as an RLC tank circuit where resistance terms accounts both for the radiation and loss resistances, and the capacitor and inductor terms are the energy storage factors. Additional loss terms are accounted for by adding parasitic impedance R_p , X_p as shown in Figure 3.2. If ω is the shift, the input impedance Z_{in} is found to be

$$Z_{in} = R_{in} + jX_{in} = \frac{1}{\frac{1}{R} + j\omega C + \frac{1}{j\omega L}} \quad \omega = \omega_0 + \Delta\omega \quad \text{Eq. (3.7)}$$

$$Z_{in} = \left(\frac{1}{R} + \frac{1 - \Delta\omega/\omega_0}{j\omega_0 L} + j\omega_0 C + j\Delta\omega C \right)^{-1} \quad \frac{1}{1+x} \cong 1 - x + \dots \quad \text{Eq. (3.8)}$$

The quality factor is given by

$$Q = \omega_0 RC = \frac{R}{\omega_0 L} \quad \text{Eq. (3.9)}$$

The simplified new input impedance can be written as

$$Z_{in} = R_{in} + jX_{in} \cong \left(\frac{1}{R} + j \frac{\Delta\omega}{\omega_0^2 L} + j\Delta\omega C \right)^{-1} \quad \text{Eq. (3.10)}$$

The input impedance in terms of Q -factor and R may be written as

$$Z_{in} \cong \left(\frac{1}{R} + j \frac{\Delta\omega}{\omega_0 \frac{R}{Q}} + j \frac{\Delta\omega}{\omega_0 \frac{R}{Q}} \right)^{-1} \cong \left(\frac{1}{R} + 2j\Delta\omega C \right)^{-1} \quad \text{Eq. (3.10)}$$

$$Z_{in} = R_{in} + jX_{in} \cong \frac{R}{1 + 2jQ \frac{\Delta\omega}{\omega_0}} \quad \frac{(\omega^2 - \omega_0^2)}{\omega} \approx 2\Delta\omega \quad \text{Eq. (3.11)}$$

Finally, according to the parallel resonance situation (Pues & Van de Capelle, 1989)

$$Z_{in} = \frac{R_{\max}}{1 + jQv} \quad \text{Eq. (3.12)}$$

In this equation R_{\max} is the resonant resistance, Q is the quality factor and the normalized frequency deviation from the resonant point is given as (Ludwig & Bretchko, 2000)

$$v = \frac{f_r + f - f_r}{f_r} - \frac{f_r}{f_r + f - f_r} = \left(1 + \frac{\Delta f}{f_r} \right) - \left(1 + \frac{\Delta f}{f_r} \right)^{-1} \approx \frac{2\Delta f}{f_r} \quad \text{Eq. (3.13)}$$

$$v = \frac{f}{f_r} - \frac{f_r}{f} \approx \frac{2\Delta f}{f_r} \quad \text{Eq. (3.14)}$$

where f is the resonant variable and f_r is the resonant frequency. If the feed line has characteristic impedance Z_0 , the input $VSWR$ is given by

$$\left| \frac{Z_{in}(f) - Z_0}{Z_{in}(f) + Z_0} \right| = \frac{VSWR(f) - 1}{VSWR(f) + 1} \quad \text{Eq. (3.15)}$$

If $VSWR$ represents the voltage standing wave ratio and S represents the desired value of standing wave ratio, the bandwidth criterion is taken to be $VSWR \leq S$. For the lower and upper band edge frequencies f_1 and f_2 , respectively, $VSWR(f_1) = VSWR(f_2) = S$. Then the bandwidth (BW) can be written as

$$BW = \frac{f_2 - f_1}{f_r} \quad \text{Eq. (3.16)}$$

The quality factor can be written as below (Duffy, 2000)

$$Q = \frac{1}{BW} \sqrt{\frac{(SR_{norm} - 1)(S - R_{norm})}{S}} \quad \text{Eq. (3.17)}$$

where the R_{norm} is the normalized resistance with respect to the characteristic impedance Z_0

$$R_{norm} = \frac{R_{max}}{Z_0} \quad \text{Eq. (3.18)}$$

Equation (3.17) reduces to well-known expression for $R_{norm} = 1$

$$BW|_{R_{norm}=1} = \frac{1}{Q} \frac{S - 1}{\sqrt{S}} \quad \text{Eq. (3.19)}$$

An expression for the admittance of a parallel RLC resonance about a narrow band of frequencies can be approximated as

$$Y_{ant}(f_r + \Delta f) = G_{ant} - jB_{ant} \cong \frac{1 + 4Q^2 \left(\frac{\Delta f}{f_r} \right)^2}{R_{norm} - 2jR_{norm}Q \left(\frac{\Delta f}{f_r} \right)} \quad \text{Eq. (3.20)}$$

where the frequency shift from the resonance $\Delta f_{\max} = f - f_r$ and

$$\frac{\Delta f_{\max}}{f_r} = \frac{1}{2Q} \sqrt{2R_{\text{norm}} - 1} \quad \text{Eq. (3.21)}$$

At this band edge, the normalized admittance (Y_{active}) of a designed relative matching network can be represent by the conjugate reactance of the antenna admittance so that

$$Y_{\text{active}}(f_r + \Delta f_{\max}) = jB_{\text{ant}} \quad \text{Eq. (3.22)}$$

If the normalize admittance of a compensated active microstrip antenna denoted with Y_{system}

$$Y_{\text{system}}(f_r + \Delta f_{\max}) = Y_{\text{ant}} + Y_{\text{active}} = \frac{1}{S} \quad \text{Eq. (3.23)}$$

Then the new bandwidth (BW_{new}) of the compensated antenna can be written as

$$BW_{\text{new}} \cong 2 \frac{\Delta f_{\max}}{f_r} \geq BW \quad \text{Eq. (3.24)}$$

In practice patch antenna can be realized by a cascade connected compensation broad band network to an appropriate point of the patch. So, the new impedance bandwidth can be enhanced. The reactive part of the impedance is given by

$$X \cong \omega L - \frac{1}{\omega C} \quad \omega_0 = \frac{1}{\sqrt{LC}} \quad \text{Eq. (3.25)}$$

When taking derivative of the imaginary part, derivation gives

$$\left. \frac{dX}{d\omega} \right|_{\omega_0} = L + \frac{1}{\omega_0^2 C} = 2L = \frac{2QR}{\omega_0} \quad \text{Eq. (3.26)}$$

The Q can be obtained

$$Q = \frac{\omega_0}{2R} \left(\left. \frac{dX}{d\omega} \right|_{\omega_0} \right) \quad \text{Eq. (3.27)}$$

For a parallel-type resonance, the bandwidth is (Ludwig & Bretchko, 2000)

$$BW = \frac{2G}{\omega_0 \left. \frac{dB}{d\omega} \right|_{\omega_0}} \quad \text{Eq. (3.28)}$$

where $Y=G+jB$ is the input admittance at the resonance.

It is evident that the above calculated impedance bandwidth is increased by using reactive impedance matching network. Ideally, this compensation network could transform the frequency dependent complex antenna impedance Z_{in} to a pure real resistance Z_0 over a large bandwidth as required. Actually, it is not possible to realize a perfect match over a continuous band of frequencies by means of purely reactive (linear, passive losses) network. It is important that selected component for optimize the matching level and maximize the bandwidth.

3.2.2 Impedance Characteristics of RMSA

Impedance variation of the microstrip antennas is very important to investigate the bandwidth. In this study, the real and imaginary impedances of rectangular microstrip antennas have been investigated. TLY_5 substrate material manufactured by Taconic, which has a relative permittivity of 2.17 and a thickness of 0.52 mm, is used in the designs. For the feeding of the antenna coaxial feeding is utilized since it is easy to fabricate and match, and it has low spurious radiation. The patch dimensions of $W=12$ mm and $L=9.5$ mm, are selected along with the ground plane dimensions of 40 x 40 mm. For the chosen dimensions, the designed antenna operates at 10.37 GHz bandwidth (6.39 %), having $|S_{11}|$ of -14.68 dB at resonant frequency. Simulation (*MoM* in spectral domain) and theoretical (Cavity Model) results are shown in Figure 3.3 and 3.5. In Figure 3.3 and 3.4, variations of the real and imaginary parts of the rectangular microstrip antenna impedances are shown. The return loss parameter can be shown in Figure 3.5. Electrically thick antennas increased the bandwidth and it is simplest method as matching technique (Balanis, 1997). This technique has many of disadvantaged (radiation loss, surface waves, harness of connection etc.) mentioned in Chapter 2.

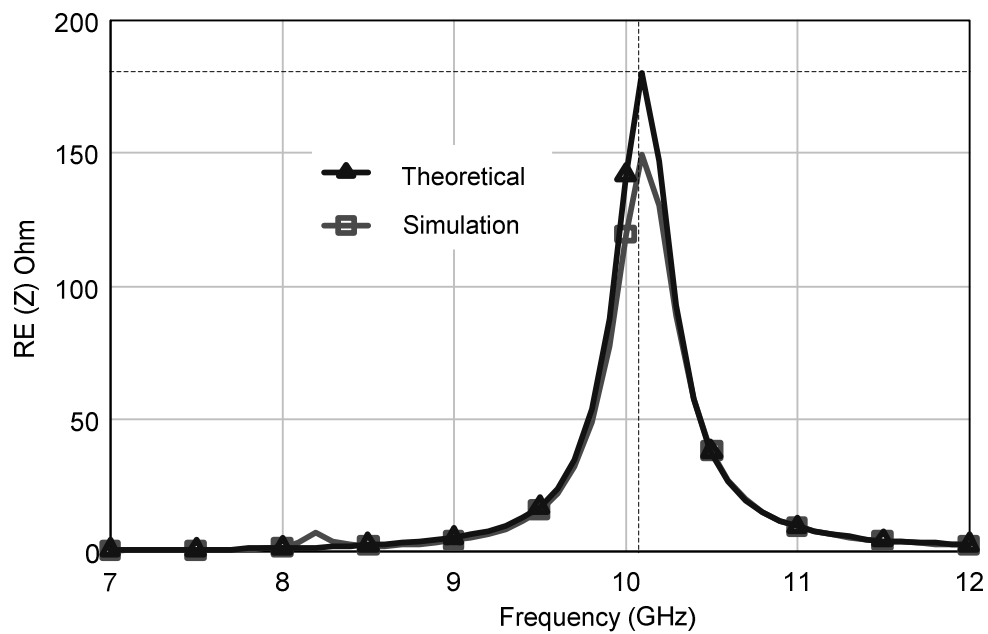


Figure 3.3 Variation of the real parts of the rectangular microstrip antenna impedances

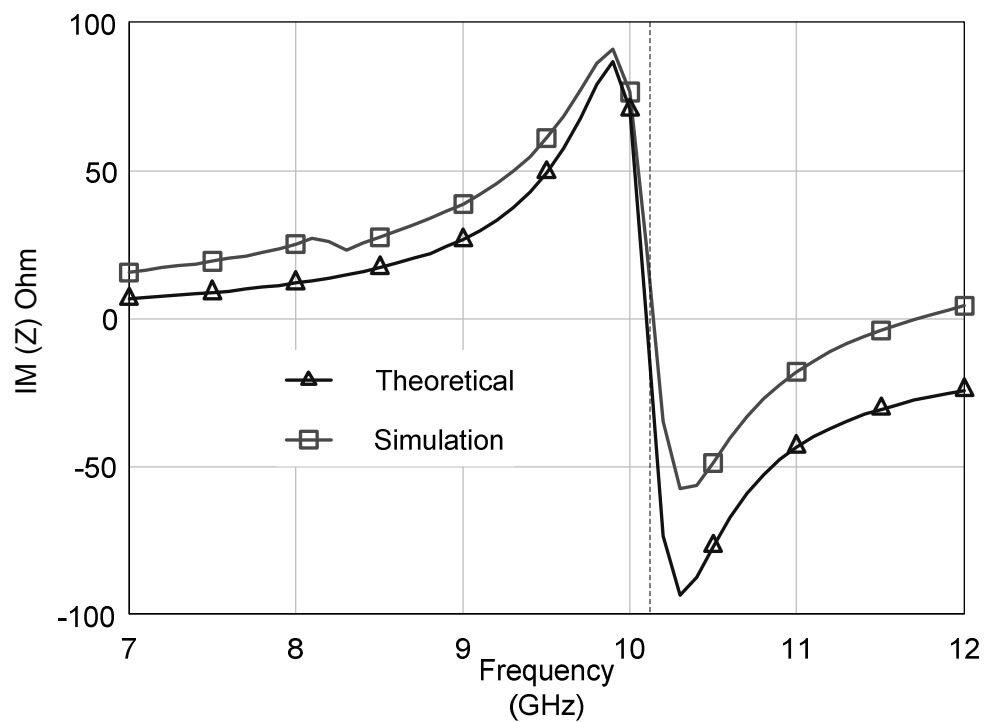


Figure 3.4 Variation of the imaginary parts of the rectangular microstrip antenna impedances

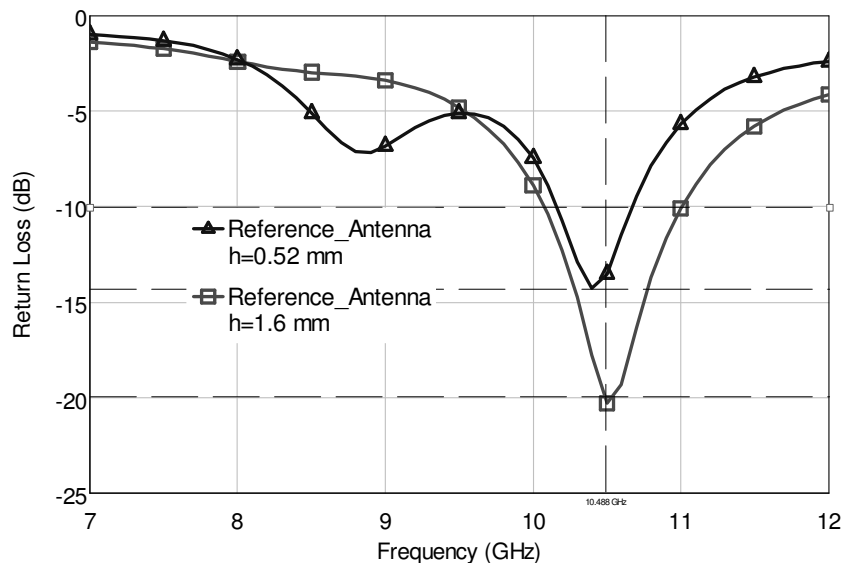


Figure 3.5 Return Loss versus frequency of the reference and thick antennas

3.2.3 Bandwidth Enhancement of RMSA Using Negative Inductance as Matching Device

Bandwidth enhancements studies are very important due to multipath effects and very wide use of modulated transmit and receive systems. Recently, active components having three or two port terminal have been used in matched-antenna systems. In this section, a new matching method that consists of a negative inductor circuit is employed. A broadband monolithic microwave floating active inductor is proposed (Kaya & Yüksel, 2004a, 2004b). This floating active inductor operates at a much higher frequency range than a spiral inductor and its size is independent of the inductance value. Circuits with large inductance, either positive or negative in value, can be obtained with a very low loss.

3.2.3.1 Active Floating Negative Inductors with Two and Three FET

One of the major limitations of the GaAs monolithic microwave integrated circuit (MMIC) is the difficulty of realizing the inductor. In MMIC design, spiral inductors are often used to reduce chip size. However, the area of a spiral inductor is still rather large compared to that of other lumped elements and the inductance values are

related to physical structure. It is also difficult to realize a broadband spiral inductor, especially one of high inductance value, because of intersegment fringing capacitance. A more serious problem is that of shunt capacitance to ground, especially in the case of microstrip format. This capacitance is important for determining the performance of inductor. Therefore, MMIC process usually preferred to realize inductor. Some circuits grounded and floating active inductors have been proposed in literature recent years (Khory, 1995). The floating inductor configuration with two FET is shown in Figure 3.6.

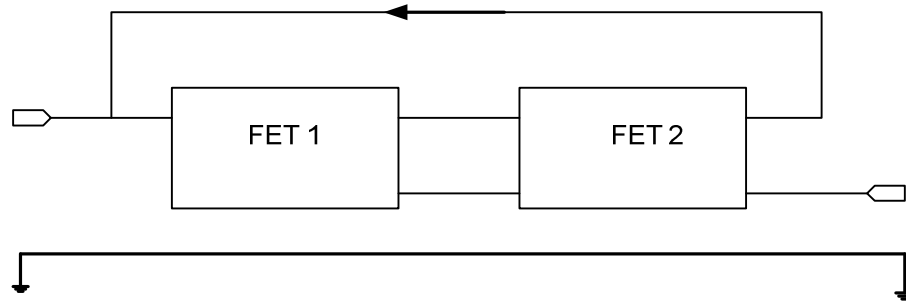


Figure 3.6 Configuration of the floating inductor containing two FET's

The small signal condition for a FET can be described as follows. A dc operating point is specified by a dc bias condition (i.e., V_{DC} and V_{GS}), and small-signals (ac signals) are superimposed to such a dc condition. Under the small signal condition, a field effect transistor can be described by a small-signal equivalent circuit with lump elements, as shown in Figure.3.6. The transconductance g_m describes the change of the drain current with respect to small variations of the gate-source voltage V_{GS} when V_{DS} is fixed (Ludwig & Bretchko, 2000):

$$g_m = \left. \frac{dI_D}{dV_{GS}} \right|_{V_{DS}=\text{const.}} \quad \text{Eq. (3.29)}$$

In the small-signal equivalent circuit, the gate-source capacitance C_{gs} is defined as

$$C_{gs} = \left. \frac{dQ_{gate}}{dV_{gs}} \right|_{V_{DS}=\text{const.}} \quad \text{Eq. (3.30)}$$

where Q_{gate} is the charge at the gate and in the space-charge region, respectively.

The cutoff frequency f_T is obtained as

$$f_T \approx \frac{g_m}{2\pi (C_{gs} + C_{gd})(1 + g_{ds}R_S) + C_{gd}g_mR_S} \quad \text{Eq. (3.31)}$$

Frequently, the cutoff frequency of MESFETs (and of GaAs FET, HEMTs and MOSFETs as well) is approximated by

$$f_T \approx \frac{g_m}{2\pi C_{gs}} \quad \text{Eq. (3.32)}$$

The simplified equivalent circuit of FET consists of only the gate-source capacitance C_{gs} and transconductance g_m as shown in Figure 3.7.

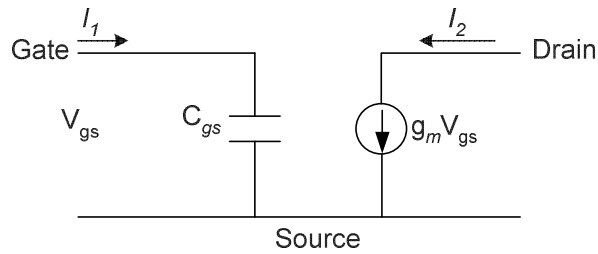


Figure 3.7 Simplified equivalent circuit

The diagram of the active floating negative inductor for the compensation circuit which is composed of two GaAs FET's is shown Figure 3.8 (Khory, 1996). Transistors denoted as T1 and T2 in Figure 3.8 (a) are cascade connected for realizing a transfer network. This circuit can operate in a very wide microwave frequency range. Basic principle in the design of match circuit is the ability of the circuit to operate near the resonant frequency. The compensation circuit shown in Figure 3.8 (b) can be represented with an equivalent parallel RLC circuit. When FET is assumed to be the combination of only the transconductance, g_m , and gate-source capacitance, C_{gs} , the admittance matrix, Y , of this active floating negative inductor can be represented by

$$Y = \left[sC_{gs} - \frac{g_m^2}{sC_{gs}} \right] \begin{bmatrix} 1 & -1 \\ -1 & 1 \end{bmatrix} \quad \text{Eq. (3.33)}$$

If two same type of FETs with identical transconductance ($g_{m1}=g_m$) and gate-

source capacitance parameters ($C_{gs1} = C_{gs2} = C_{gs}$) are chosen and, L_{eq} and C_{eq} can be written as (Kaya, Kılınc, Yüksel & Cam, 2004a).

$$L_{eq} = -\frac{C_{gs}}{g_m^2} \quad \text{Eq. (3.34)}$$

$$C_{eq} = C_{gs}$$

The negative inductance circuit is simulated using Fujitsu FHX35X GaAs FET model which has $C_{gs} = 0.27$ pF, $g_m = 60$ mS, $C_{gd} = 0.035$ pF, $C_{ds} = 0.069$ pF, $R_i = 1.9$ Ω , $R_s = 0.9$ Ω , $R_{ds} = 142$ Ω parameter values with operating conditions $V_{DS} = 3$ V, $I_{DS} = 10$ mA. Employing (3.34), the element values in the equivalent circuit are calculated as, $L_{eq} = -75$ pH, $C_{eq} = 0.27$ pF (Kaya, Kılınc, Yüksel & Cam, 2004b).

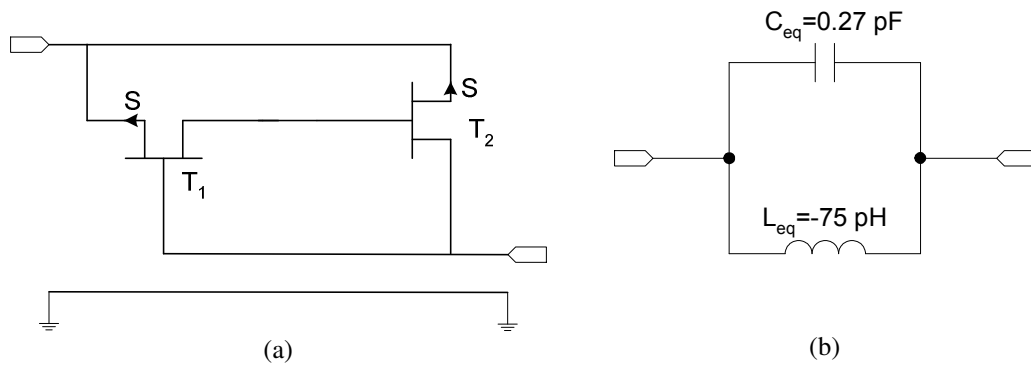


Figure 3.8 Floating active negative inductor with two FET: (a) Circuit configuration (b) RLC equivalent circuit

An alternative floating inductor circuits can also be realized by using three FETs (Khoury, 1996). The diagram of the proposed some active floating negative inductors circuits with three FET's are shown in Figure 3.9. and 3.10. The study of these floating inductors, with three GaAs FET's transistors, shows that in general their equivalent RLC circuit creates a larger inductor with a resistor.

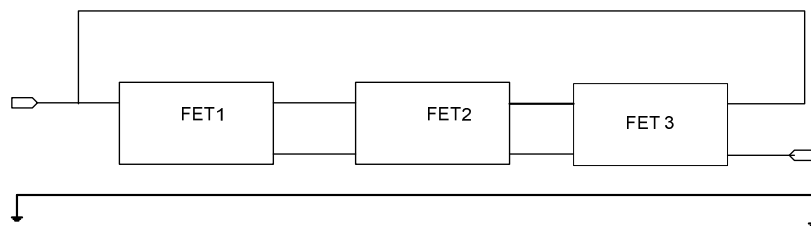


Figure 3.9 Configuration of the inductor containing with three FET's

These circuits can operate a very wide microwave frequency range. It has also the following features of the floating inductors i.e: (i) very wide-band frequency operation (ii) small size independent of the inductance value.

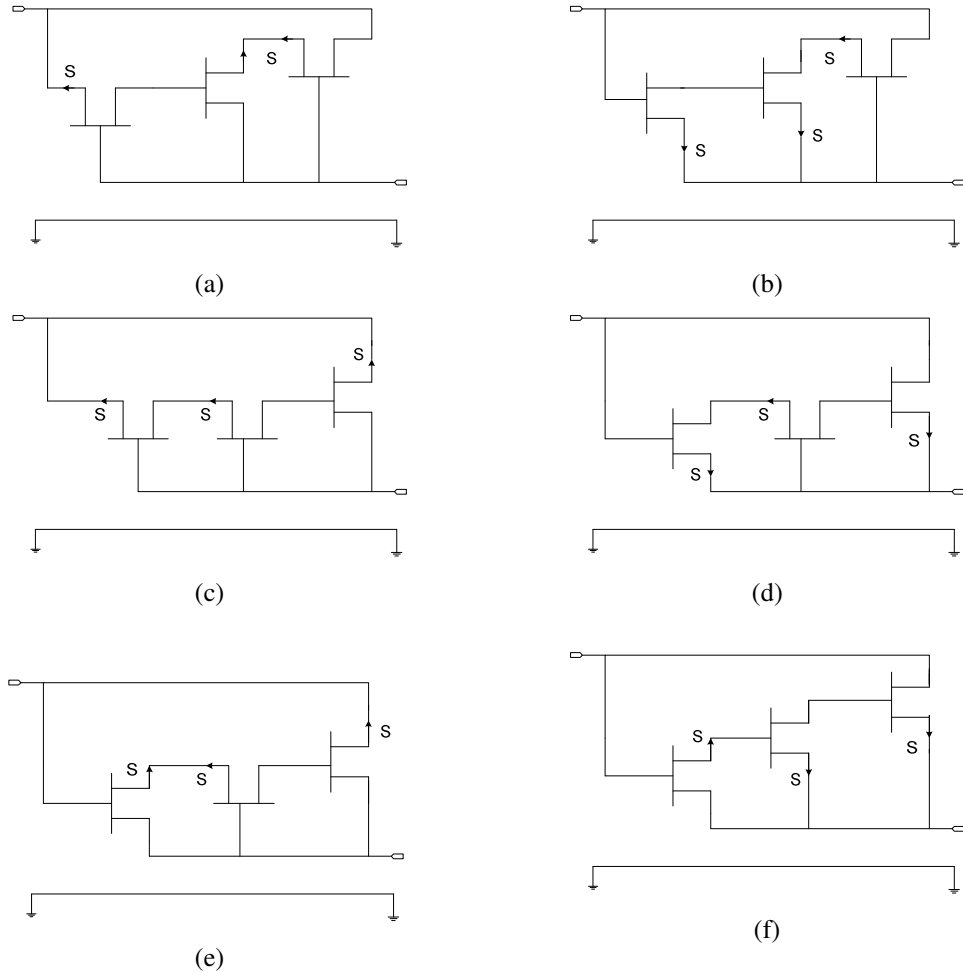


Figure 3.10 Circuit configurations of the floating active negative inductor with three FET's

When the negative active floating inductor with three FET is chosen as a Figure 3.10 (c), the admittance matrix, Y , of this active floating negative inductor can be represented by

$$Y = \begin{bmatrix} g_{m1} + sC_{gs1} & -\frac{g_{m1}g_{m2}(g_{m3} + sC_{gs3})}{sC_{gs3}(g_{m2} + sC_{gs2})} \\ -\frac{g_{m1}g_{m2}(g_{m3} + sC_{gs3})}{sC_{gs3}(g_{m2} + sC_{gs2})} & g_{m3} + sC_{gs3} \end{bmatrix} \begin{bmatrix} 1 & -1 \\ -1 & 1 \end{bmatrix} \quad \text{Eq. (3.35)}$$

If three same type of FET's with identical transconductance ($g_{m1} = g_{m2} = g_{m3} = g_m$) and gate-source capacitance parameters ($C_{gs1} = C_{gs2} = C_{gs3} = C_{gs}$) are chosen, (3.35) can be written as

$$Y = \begin{bmatrix} g_m + sC_{gs} & -\frac{g_m^2}{sC_{gs}} \\ -1 & 1 \end{bmatrix} \begin{bmatrix} 1 & -1 \\ -1 & 1 \end{bmatrix} \quad \text{Eq. (3.36)}$$

The diagram of the active floating negative inductor for the compensation circuit which is composed of three GaAs FETs and equivalent RLC model are shown in Figure 3.11.

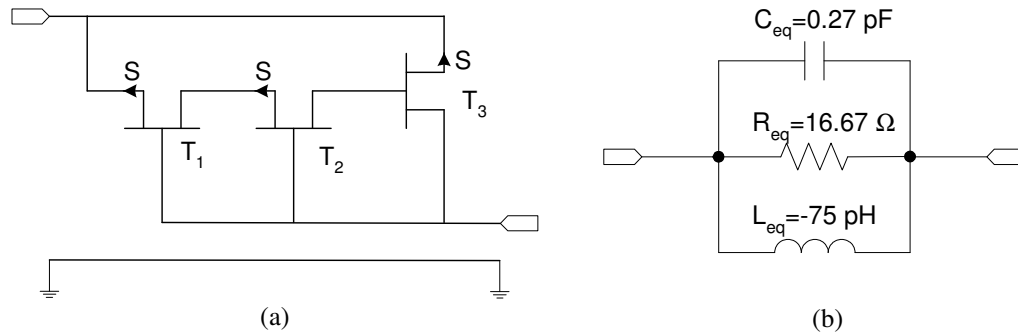


Figure 3.11 Floating active negative inductor with three FET: (a) Circuit configuration (b) RLC equivalent circuit

When the Fujitsu FHX35X GaAs FET is used, employing (3.34), the element values in the equivalent circuit are calculated as, $L_{eq}=-75$ pH, $C_{eq}=0.27$ pF and $R_{eq}=16.67$ Ohm (Kaya, Kılınc, Yüksel & Cam, 2004c).

3.2.4 Simulation Results of the Active Compensated Antenna and Reference Antenna

When the negative inductor having two FETs connected circuit to the antenna, equivalent circuit model is shown in Figure 3.12.

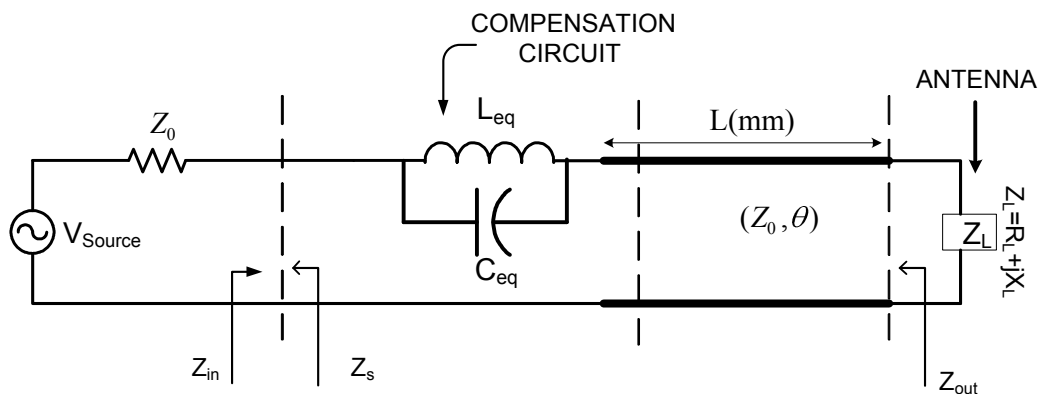


Figure 3.12 Equivalent circuit model of matching circuit and antenna section

It can easily shown that the input impedance Z_{in} seen from the left of the compensation circuit is given by (Kaya, et al., 2004b, 2004c)

$$Z_{in} = \frac{\left(\begin{array}{c} Z_0 (g_m^2 (X_L - jR_L) + \omega C_{gs} (-1 + \omega C_{gs} (X_L - jR_L))) \\ \cos\left(\frac{\omega \sqrt{\epsilon_{re}}}{c}\right) + (g_m^2 Z_0^2 + \omega C_{gs} (X_L - jR_L + \omega C_{gs} Z_0^2)) \\ \sin\left(\frac{\omega \sqrt{\epsilon_{re}}}{c}\right) \end{array} \right)}{\left(\begin{array}{c} (g_m^2 + \omega^2 C_{gs}^2) \left(-jZ_0 \cos\left(\frac{\omega \sqrt{\epsilon_{re}}}{c}\right) \right) \\ + (R_L + jX_L) \sin\left(\frac{\omega \sqrt{\epsilon_{re}}}{c}\right) \end{array} \right)} \quad \text{Eq. (3.37)}$$

For this condition, input reflection coefficient factor is given by

$$\Gamma_{in} = \frac{\left(-g_m^2 Z_0^2 + \omega C_{gs} (X_L - jR_L - Z_0 (j + \omega C_{gs} Z_0)) \right)}{\left(g_m^2 Z_0 (2R_L + 2jX_L + Z_0) + \omega C_{gs} \left(\begin{array}{c} X_L - jR_L - jZ_0 + \omega C_{gs} Z_0 \\ (2R_L + 2jX_L + Z_0) \end{array} \right) \right)} \quad \text{Eq. (3.38)}$$

where the reflection coefficient at the input side is expressed in terms of Γ_{in} under the transmission line length is zero for simplify the equation.

The terms of g_m and C_{gs} the two following equations are obtained:

$$g_m = \sqrt{\frac{\left(j\omega C_{gs} Z_0 - \omega^2 C_{gs}^2 (R_L Z_0 - jX_L Z_0 + Z_0^2) \right)}{2Z_0 (R_L + jX_L - Z_0)}} \quad \text{Eq. (3.39)}$$

$$C_{gs} = \frac{\left(\begin{array}{c} jZ_0 \omega + \sqrt{Z_0^2 \omega^2 + 4g_m^2 Z_0 (R_L - jX_L + Z_0)} \\ \sqrt{\omega^2 Z_0 (Z_0 - R_L - jX_L)} \end{array} \right)}{2Z_0 \omega^2 (R_L + jX_L - Z_0)} \quad \text{Eq. (3.40)}$$

It is interesting to note that for (3.39) and (3.40) to yield a valid solution,

$$Z_0 \omega (R_L + jX_L - Z_0) \neq 0 \quad \&$$

$$Z_0 \left(Z_0 \omega - j \sqrt{\begin{pmatrix} -Z_0^2 \omega^2 - 4g_m^2 Z_0 (-R_L - jX_L + Z_0) \\ (Z_0 \omega^2 (-R_L - jX_L + Z_0)) \end{pmatrix}} \right) \neq 0 \quad \text{Eq. (3.41)}$$

When the width of the RMSA 12 mm and the length of the RMSA 9.5 mm are selected by using the TLY_5A substrate manufacturing the Taconic firm, the return loss graphics are obtained as shown in Figure 3.13 for the compensated antenna systems. It is clearly seen that the impedance bandwidth straightly increased.

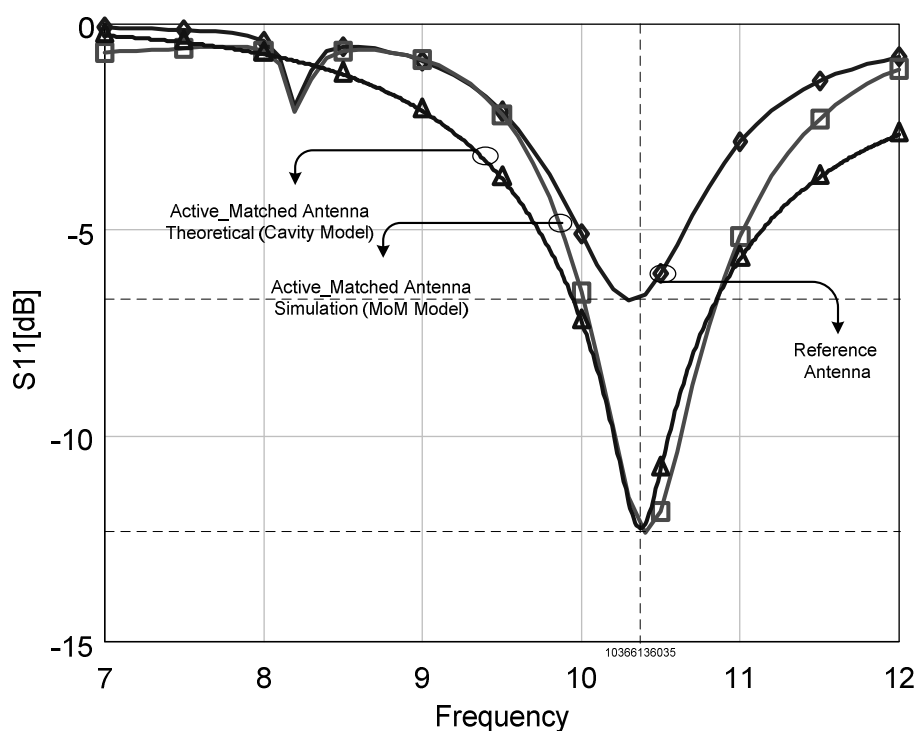


Figure 3.13 Return loss characteristics of the reference and active antennas versus frequency ($l=3.5$ mm, $\epsilon_r=2.17$, $h=0.52$ mm)

The impedance bandwidth is increased from 8.66% to 11.18%. The radiation pattern isn't distorted because of the antenna geometry isn't changed with in the defined impedance bandwidth. At the same time, impedance matching level is increased. These proposed new active floating inductors are very beneficial for compensated systems. The results can be investigated in terms of parametric study. Some theoretical results are shown in Figures 3.14-3.16.

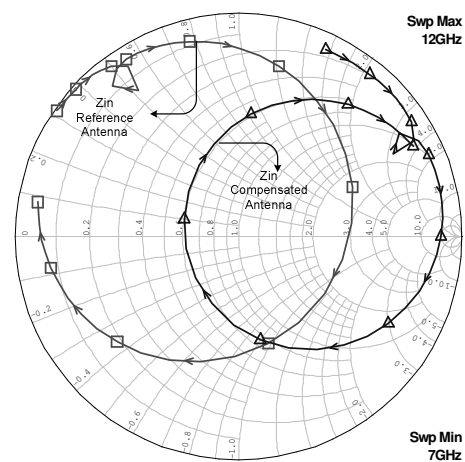


Figure 3.14 Input impedance

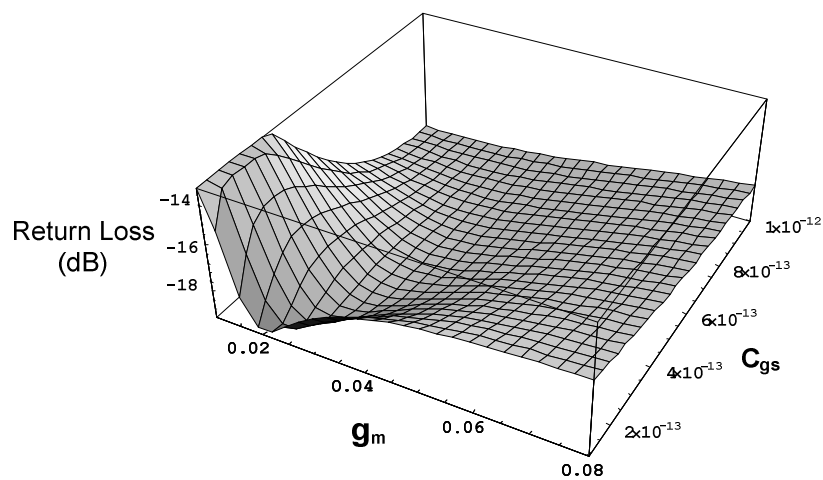


Figure 3.15 Return loss characteristics of the active antenna versus g_m and C_{gs} for frequency 10.3 GHz ($l=3.5$ mm)

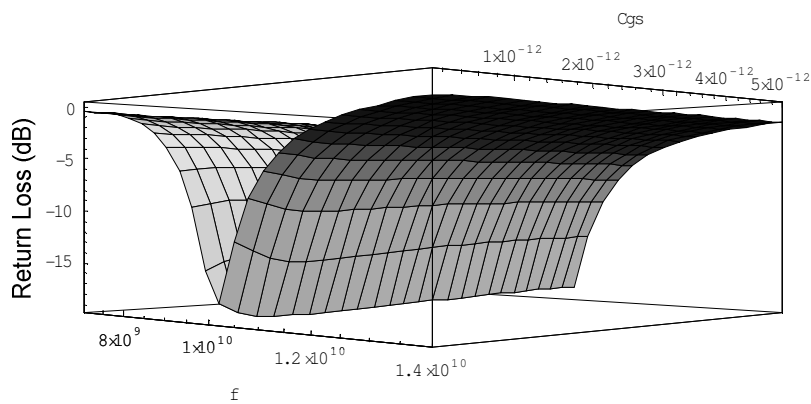


Figure 3.16 Return loss characteristics of the active antenna versus C_{gs} and frequency for $g_m = 60 \times 10^{-3}$ S ($l=3.5$ mm)

Table 3.1. Performance comparison for the reference and the active antenna

| Performance Parameter | Reference Antenna | Active Antenna | Active Antenna |
|-----------------------|-------------------|------------------|--------------------|
| | | <i>Simulated</i> | <i>Theoretical</i> |
| Bandwidth | 892.5 MHz | 1152 MHz | 1298 MHz |
| Percent bandwidth | 8.66% | 11.18% | 12.62% |
| $ S_{11} $ deep point | -6.77 dB | -12.35dB | -12.23dB |

Antenna performances are summarized in Table 3.1. According to table, it is seen that the antenna impedance bandwidth is increased. The matching level is increased from -6.77 dB to -12.35 dB at the resonant frequency.

When the negative inductor circuit having three FET is connected to the input of the antenna directly without transmission line, the resulting equivalent circuit of the compensated system can be obtained as shown in Figure 3.17 (Kaya, Kılınç, Yüksel & Cam, 2004c). The antenna impedance at the resonant frequency is a complex number having both real and imaginary parts. The imaginary part of the antenna impedance around the resonant frequency is minimized using the negative inductor circuit with equivalent element values.

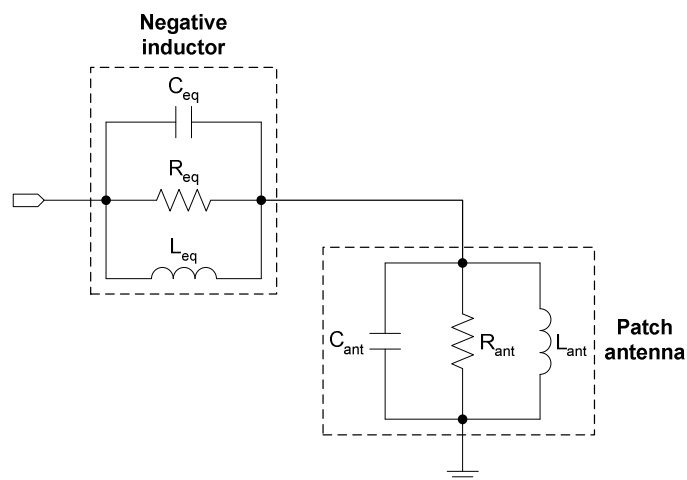


Figure 3.17 The equivalent circuit of the compensated antenna

Employing Eq. (3.36), the element values in the equivalent circuit are calculated as $R_{eq} = 16.67 \Omega$, $L_{eq} = -75 \text{ pH}$, $C_{eq} = 0.27 \text{ pF}$. The simulation results are shown in

Figures 3.17-3.19. Imaginary and real parts of the impedance for the reference and active antennas are presented in Figures 3.16 and 3.17, respectively. The patch dimensions of $W=16$ mm and $L=9$ mm, are selected along with the ground plane dimensions of 60×40 mm. For the chosen dimensions, the designed antenna operates at 10 GHz with 1.728 GHz bandwidth, having $|S_{11}|$ of -13.27 dB at resonant frequency.

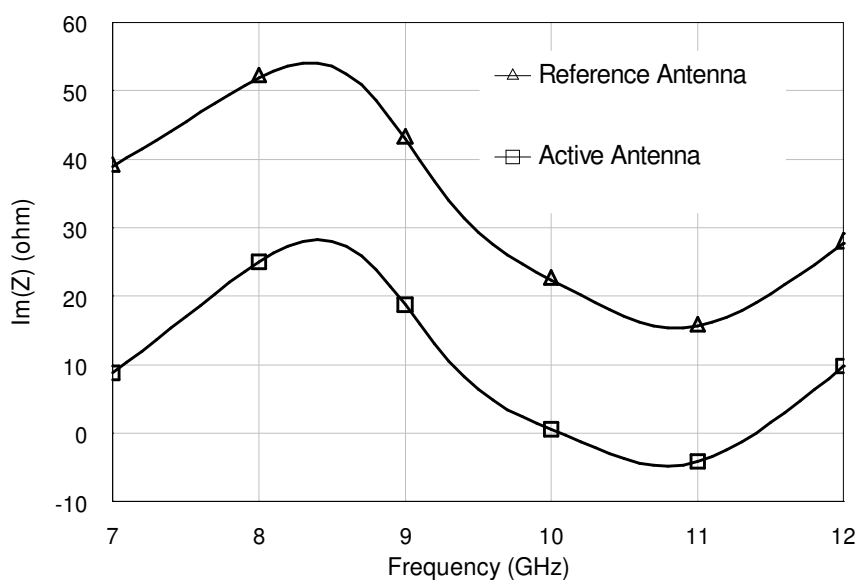


Figure 3.18 Variation of the imaginary parts of the reference and active antenna impedances ($\epsilon_r=3.2$, $h=0.78$ mm; TLC-32)

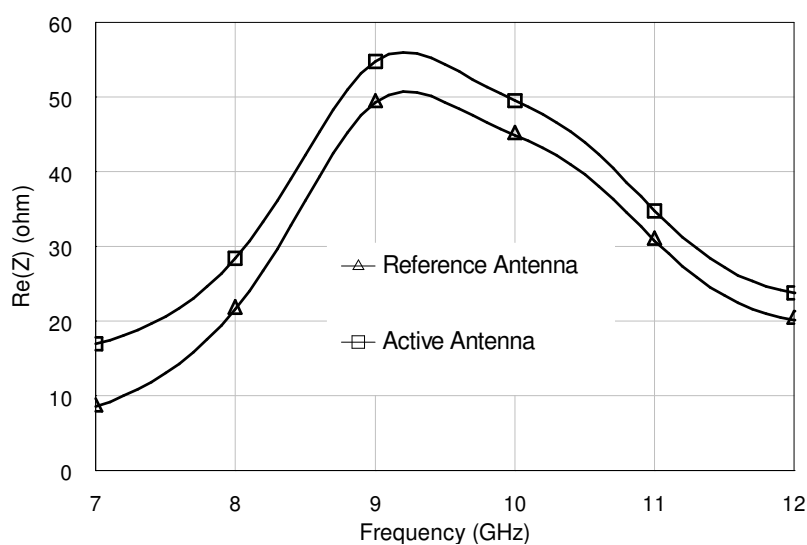


Figure 3.19 Variation of the real parts of the reference and active antenna impedances ($\epsilon_r=3.2$, $h=0.78$ mm; TLC-32)

As can be seen from these figures, the imaginary part of the active antenna impedance is zero, while the real part is approximately 50Ω , at the resonant frequency of 10 GHz.

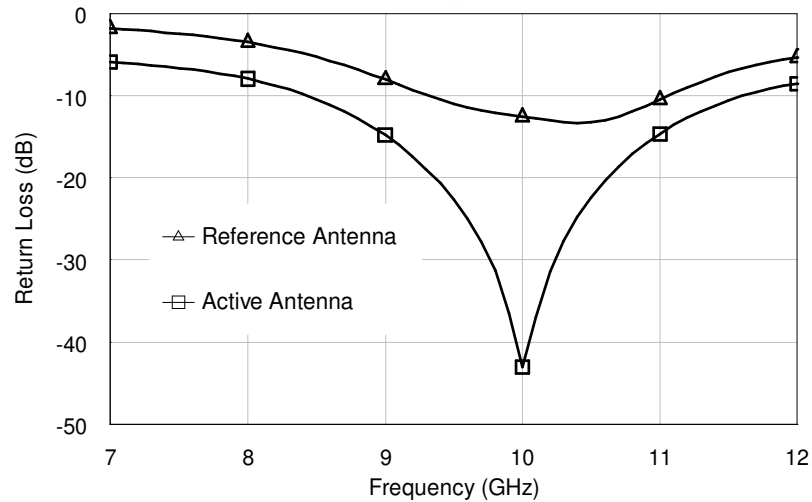


Figure 3.20 Return loss characteristics of the reference and active antennas versus frequency

The return loss characteristics $|S_{11}|$ for both reference and active antennas are shown in Figure 3.20. The reference antenna has a return loss better than -10 dB within a percent bandwidth of 17.21 %. This value is increased to 32.67 % by utilizing the negative inductor circuit together with the reference antenna, which is about two times the inherent bandwidth of the reference antenna. In the meantime, this improvement of the bandwidth does not cause a shift in the resonant frequency.

This technique not only improves the bandwidth but also lowers the deep point of the return loss characteristics at the resonant frequency. The simulation results are also summarized in Table 3.2 for the bandwidth and the return loss parameters. These results (Kaya, Kılınç, Yüksel & Cam, 2004c) are very attractive for broadband communications.

Table 3.2 Performance comparison for the reference and the active antenna

| Performance Parameter | Reference Antenna | Active Antenna |
|-----------------------|-------------------|----------------|
| Bandwidth | 1.728 GHz | 3.267 GHz |
| Percent bandwidth | 17.21% | 32.67% |
| $ S_{11} $ deep point | -13.27 dB | -41.61dB |

3.3 Loaded Rectangular Microstrip Antennas

This section deal with matching microstrip elements using reactive loads. A very simple theory which take advantage of the added flexibility that reactive loading provides is presented. The reactively loaded microstrip antenna is a simple antenna to which one or more, two-terminal lumped, lossless, linear load impedances are attached at one terminal to the patch and other to the ground plane (Srinivasan, Malhotra & Kumar, 2000). The loading can take various forms such as stub loading, slot or notch loading, short circuits or vias, parasitic coupling substrate loading, resistors, capacitors and diodes. For a given feed location, if the patch is loaded with these techniques, the field and current distributions for various modes will be disturbed and therefore their characteristics will change. This change will depend on the amount of the load. If used properly, the loading effect can be used to obtain a desirable change in antenna characteristics. First we focused on the applications of loaded antennas to realize the increasing the impedance bandwidth and radiation pattern control (Kaya & Yüksel, 2004). The performance parameters of the designed microstrip antenna with and without loaded network are compared. The simulation results show that the loading network can control the resonant frequency and obtain better matching level.

3.3.1 Multiport Network Model (MNM) for Loaded RMSA

In MNM, the edge admittance network (EAN) represents the fields external to the patch, namely the fringing and radiating fields as shown in Figure 2.6. The radiation conductance associated with an edge of the microstrip patch is defined as conductance, which will dissipate power equal to that radiated by the edge. If the

edge is of width W_i and the power radiated for uniform voltage distribution is P_{rad} , then the radiation conductance per unit length of the edge is given by $G_r=2P_{rad}/W_i$ the closed-form expression for radiation conductance G_r is given by (Lier & Jakopsen, 1983).

$$G_r = \frac{w^2}{6\pi^2(60+w^2)} \quad \text{Eq. (3.42)}$$

where $w = k_0 W_e$, $k_0 = 2\pi / \lambda_0$, $W_e = W + \Delta W$

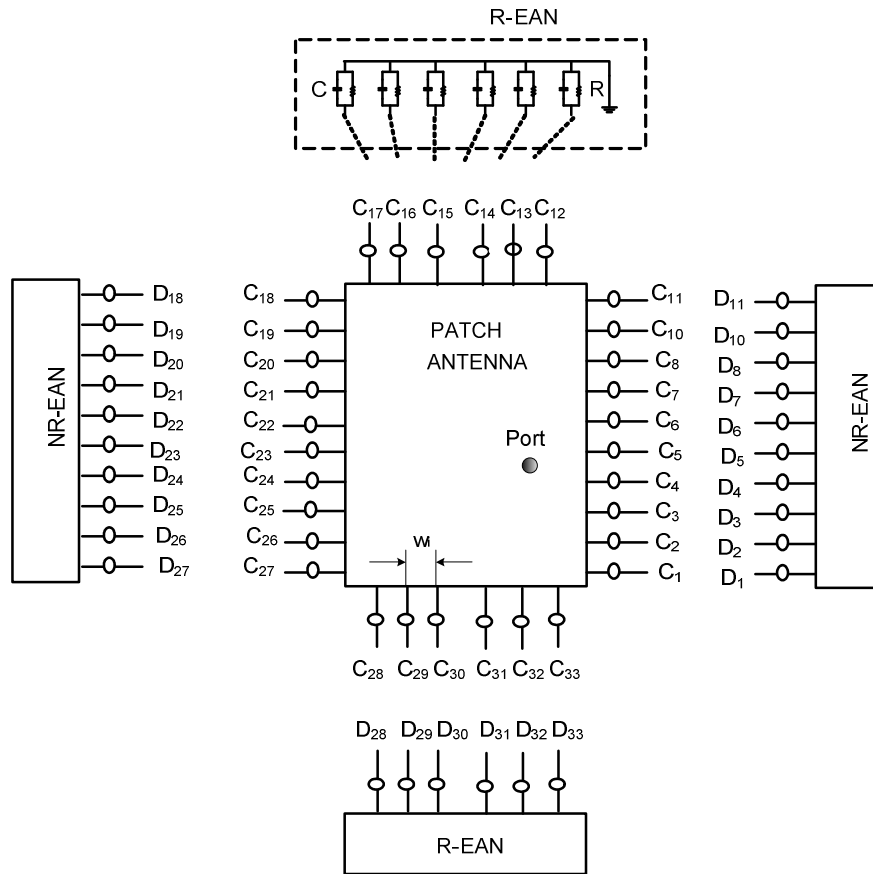


Figure 3.21 Segmentation of an RMSA with its EAN

The susceptance B_s is given by (Chuang, et al., 1980).

$$B_s = 0.01668 \frac{\Delta l}{h} \frac{W_e}{\lambda_0} \epsilon_{re} \quad \text{Eq. (3.43.a)}$$

where

$$\frac{\Delta l}{h} = \frac{0.95}{1+0.85k_0h} - \frac{0.075(\epsilon_{re} - 2.45)}{1+10k_0h} \quad \text{Eq. (3.43.b)}$$

The segmented network for the four-slot model of RMSA is shown in Figure 3.21. For the radiating edge, the physical port W_i is typically chosen to be about $\lambda/10$, while for the non radiating edge (NRA), the port width is decreased to be about $\lambda/20$, because of the rapid field variation. The connected peripheral and external ports are represented by C and D, respectively. For a RMSA, R-EAN and NR-EAN represents the external network. The Z - matrix of the patch and the EAN are combined using the segmentation method (Chadra & Gupta, 1981) which is given by

$$\begin{bmatrix} V_p \\ V_c \\ V_d \end{bmatrix} = \begin{bmatrix} Z_{pp} & Z_{pc} & Z_{pd} \\ Z_{cp} & Z_{cc} & Z_{cd} \\ Z_{dp} & Z_{dc} & Z_{dd} \end{bmatrix} \begin{bmatrix} I_p \\ I_c \\ I_d \end{bmatrix} \quad \text{Eq. (3.44)}$$

Where V_p , V_c and V_d and I_p , I_c and I_d are the port voltages and currents, respectively. The number of C ports are the same as number of D ports, so the boundary conditions at these interconnections are $V_c=V_d$ and $I_c=-I_d$. The input impedance and the voltage distribution around the periphery of the patch are obtained by applying the segmentation method as:

$$Z_{in} = \frac{V_p}{I_p} = Z_{pp} + (Z_{pc} - Z_{pd}) Z_1^{-1} (Z_{dp} - Z_{cp}) \quad \text{Eq. (3.45.a)}$$

where

$$Z_1 = (Z_{cc} + Z_{dd} - Z_{cd} - Z_{dc}) \quad \text{Eq. (3.45.b)}$$

and

$$V_c = Z_{cp} + (Z_{cc} - Z_{cd}) Z_1^{-1} (Z_{dp} - Z_{cp}) I_p \quad \text{Eq. (3.46)}$$

The matrixes Z_{pp} , Z_{pc} , Z_{cp} and Z_{cc} are obtained from the Z -matrix of the rectangular patch using Green's function. Z_{pp} is $N_p \times N_p$ matrix, where N_p is the number of external ports and for a single feed, $N_p=1$. Z_{pc} and Z_{pd} are $N_p \times N_c$ matrixes, where N_c is the total number of ports along the periphery of the patch. The Z_{dd} is the loading matrix, which is obtained by taking the inverse of the EAN. This matrix has only diagonal elements and its size is $N_c \times N_c$ (Benalla & Gupta, 1988).

3.3.2 Bandwidth Enhancement of a Rectangular Microstrip Antenna by Integrated Reactive Loading

The problem of achieving a wide impedance bandwidth (e.g., greater than or about 10% suitable for present-day communication systems) for an integrated-compact microstrip antenna is becoming an important topic in microstrip antenna design. Recently, for a compact design using a shorted patch with a thick substrate, the obtained impedance bandwidth (-10dB return loss) has been reported to be 10% or much greater. There are a lot of studies on the loaded microstrip antennas such as chip resistor loaded, reactive loaded, and shorting pin loaded antennas (Khan, Richards & Long, 1989; Lu & Wong, 1998; Srinivasan, Malhotra, & Kumar, 2000). Microstrip antennas loaded with shorting pin for compact operation are well known. Recently, it has been proposed that, by replacing the shorting pin with a chip resistor of low resistance, the required antenna size can be significantly reduced for operating at a fixed frequency; moreover, the antenna bandwidth can be enhanced. With chip resistor loading, direct matching of the antenna using 50 Ω microstrip line feed has been described (Wong & Lin, 1997). Reactive loading methods are important due to the problems caused by the feeding and impedance characteristic. In this section, a new loading method that consists of a negative capacitor circuit is employed.

3.3.2.1 Negative Capacitance Circuit with Two FET

The negative capacitance circuit with two FET (Kolev & Gautier, 2001) is based on a negative impedance converter, designed with two same type common-source transistors and loaded with an inductor as shown in Figure 3.21 (a). The negative capacitance circuit designed using the Fujitsu FSX017X GaAs FET having $C_{gs} = 0.64$ pF, $g_m = 54$ mS, $C_{gd} = 0.023$ pF, $C_{ds} = 0.096$ pF, $R = 4.8$ Ω , $R_s = 1.3$ Ω , $R_{ds} = 538$ Ω in operating condition $V_{DS} = 8$ V, $I_{DS} = 35$ mA. The negative capacitance loaded circuit having two same type of and the cut-off frequency f_T of FET's is $f_T \approx g_m / (2\pi C_{gs})$ of 10.5 GHz at $I_{DSS} / 2$. When the influence of the parallel elements is negligible in Figure 3.21 (b), the simplified equivalent circuit can be modeled as series *RLC* circuit as shown in Figure 3.22 (c).

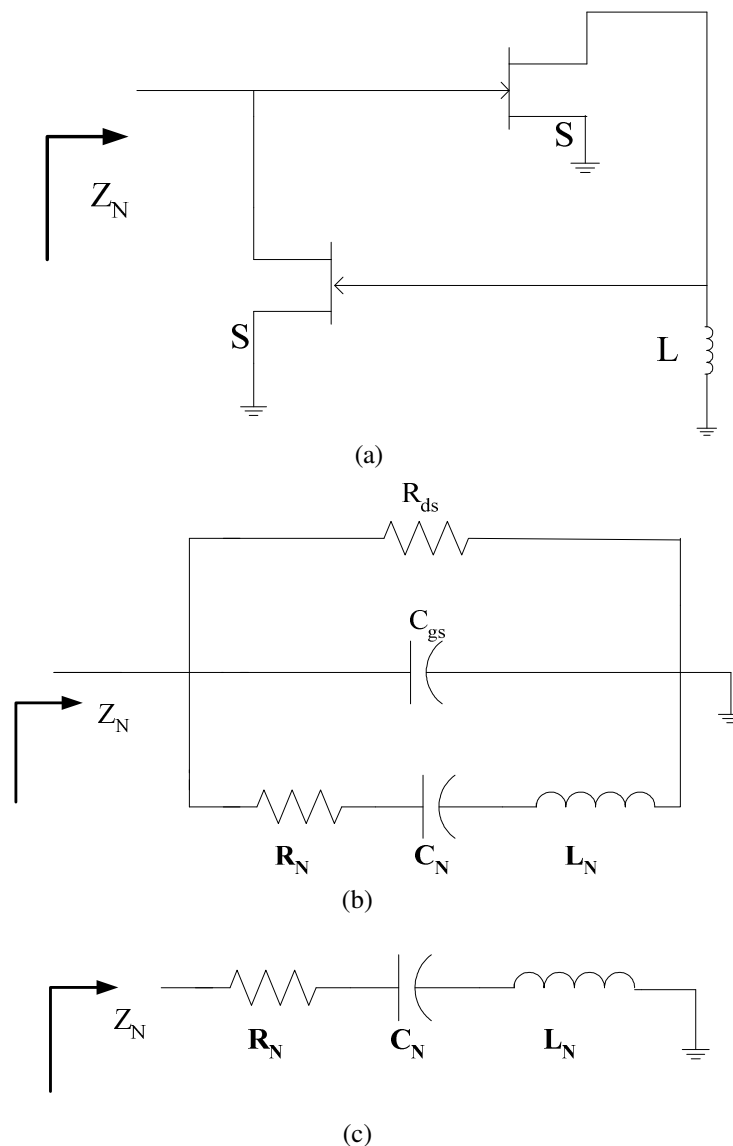


Figure 3.22 (a) Principle scheme of the negative capacitance circuit
 (b) Equivalent circuit of the negative capacitance circuit (c)
 Simplified equivalent circuit of the negative capacitance circuit

When FET is assumed to be the combination of only the transconductance, g_m , drain-source resistance R_{ds} and gate-source capacitance, C_{gs} , the impedance matrix, Z_N , of this negative capacitor is

$$Z_N = -\frac{1}{g_m^2 R_{ds}} - \frac{1}{jLg_m^2} - j\frac{C_{gs}}{g_m^2} \quad \text{Eq. (3.47)}$$

Two same type of FETs with identical transconductance ($g_{m1} = g_{m2} = g_m$) and gate-source capacitance parameters ($C_{gs1} = C_{gs2} = C_{gs}$) are chosen and the capacitance and inductance values in the equivalent RLC circuit can be represented as

$$\begin{aligned} R_N &= -\frac{1}{g_m^2 R_{ds}} \\ L_N &= -\frac{C_{gs}}{g_m^2} \\ C_N &= -g_m^2 L \end{aligned} \quad \text{Eq. (3.48)}$$

The element values in the equivalent circuit can be estimated as $R_N = -0.6374 \Omega$, $L_N = -0.219 \text{ nH}$, $C_N = -277.78 \text{ pF}$ for the Fujitsu FSX017X GaAs FETs.

3.3.3 Simulation and Theoretical Results of the Reactive Loaded Antenna

In this section the design sample of a rectangular patch antenna integrated with a negative capacitor is first discussed. When the negative capacitor circuit is connected to the rectangular microstrip patch antenna, the resulting equivalent circuit of the compensated system can be obtained as shown in Figure 3.23 (a). In this simulation, a substrate material TLC-32 which has a relative permittivity of 3.20 and thickness of 0.78 mm defined by the manufacture firm Taconic is utilized. As an antenna, a simple microstrip patch antenna operating at 10.5 GHz is designed.

The negative capacitor is considered as an additional port and is loaded by its impedance value (Kaya & Yüksel, 2004). The patch itself is analyzed as a two dimensional planar network, with multiple number of ports located all around the edges. The characteristics of loading a microstrip antenna with capacitor provide some advantages. The resonant frequency can be change by varying the loading position. With reactive loading technique, better radiation pattern can be obtain and lower cross-polarization radiation (Lu, Tang & Wong, 1998).

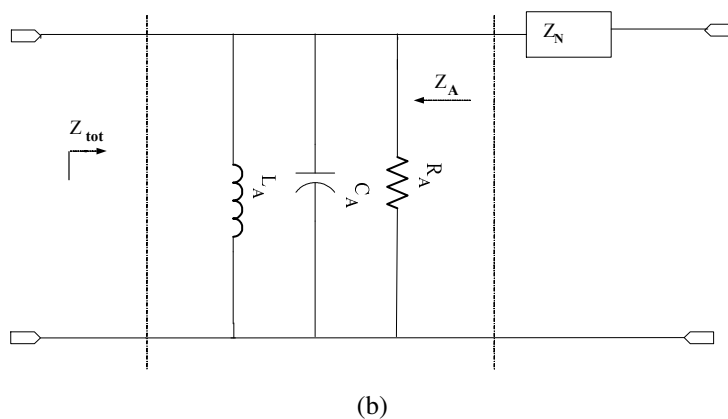
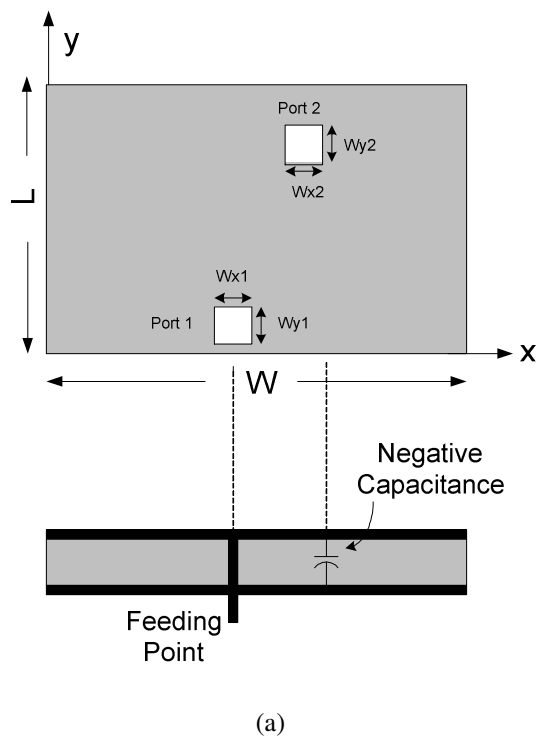


Figure 3.23 (a) Original circuit configuration; $(x_p, y_p) = (8, 0.2)$ mm, $(x_2, y_2) = (7.25, 8.25)$ mm (b) Equivalent circuit of the compensated patch antenna with negative capacitance.

The patch dimensions of width $W=16$ mm and length $L=9$ mm are selected along with the ground plane dimensions of 50×50 mm as shown in Figure 3.23 (a). Second port was selected near the non radiating edge and opposite the feeding port on the patch geometry. The negative capacitor loading port is located at $(x_2, y_2; 7.25$ mm, 8.25 mm). The probe feed is located at $(x_p, y_p; 8$ mm, 0.2 mm).

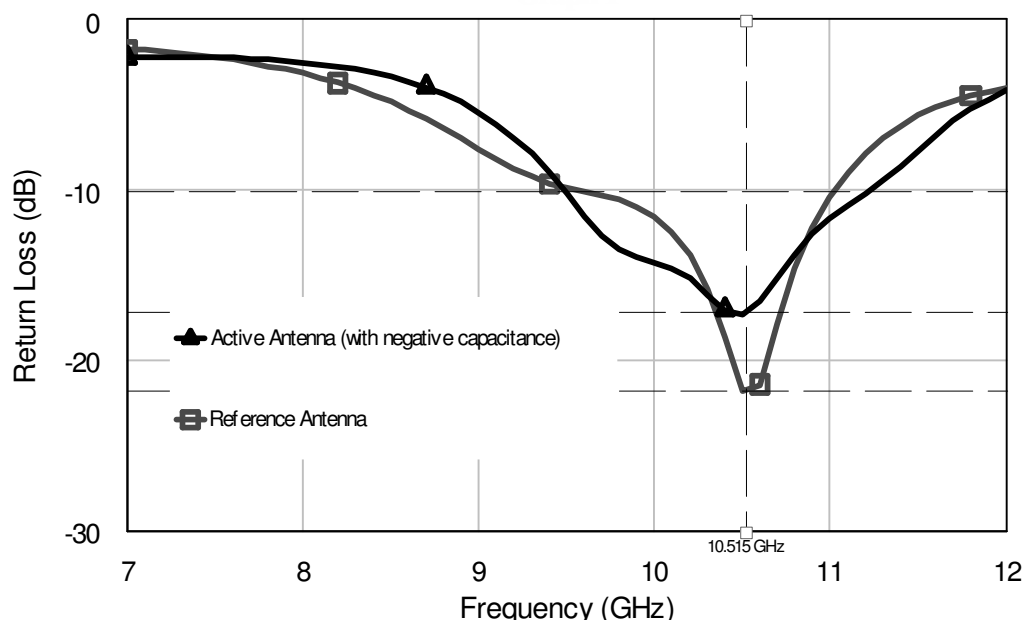
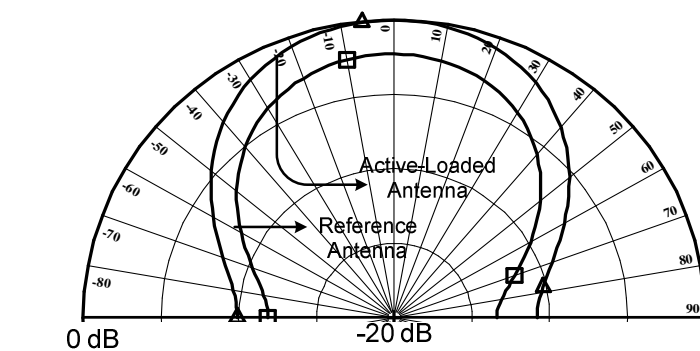
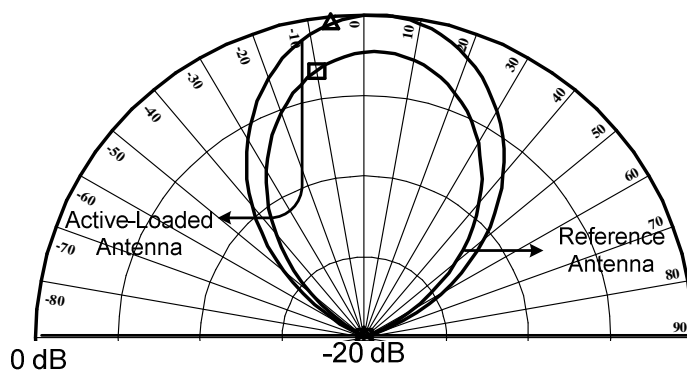


Figure 3.24 Return Loss plot of the compact antenna



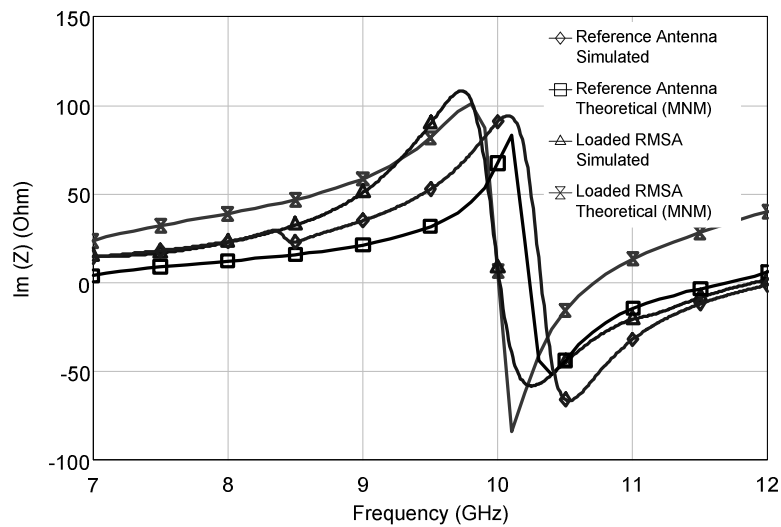
(a)



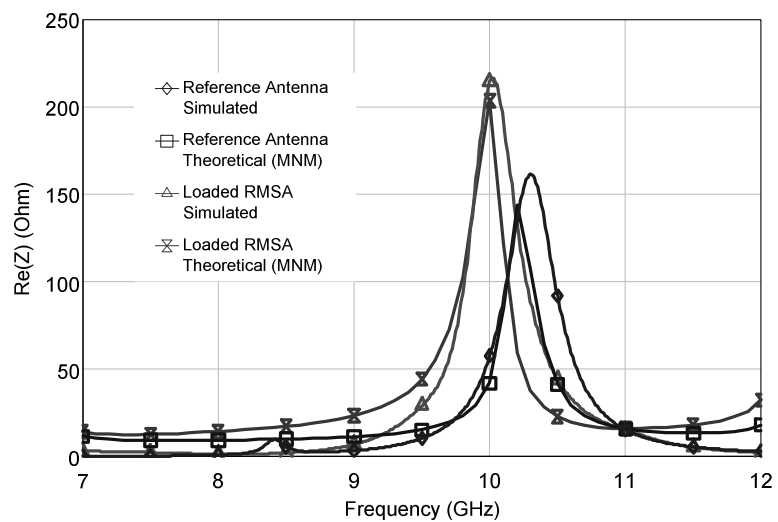
(b)

Figure 3.25 Radiation pattern of the RMSA (a) E-Plane (b) H-Plane ($f=10.5$ GHz, $L=1$ nH)

The return loss a characteristic shows that 10 dB return loss bandwidth is increased compared to that of the reference antenna as depicted in Figure 3.24. The simulated radiation patterns for the loaded and conventional microstrip antennas are plotted in Figure 3.25. It is observed that the component of co-polarization radiation is increased due to negative capacitance loading, especially for H plane (y-z plane) radiation. It is seen that the antenna gain increased as shown in Figure 3.25 when the negative capacitor is used as a loading. This reactive loading technique is similar the short circuit, resistive and capacitor loading RMSA technique.



(a)



(b)

Figure 3.26 Variation of the (a) imaginary parts (b) real part of the reference and active loaded antenna impedances

Both theoretical and simulated results of the imaginary and real impedance variations versus frequency are shown in Figure 3.26 for the reference and loaded antenna. When the loading position is considered or the other loading techniques are used with the negative capacitor, better results in terms of the impedance bandwidth, matching level or co-polarization radiation levels are obtained. Theoretical analysis has been done by using multiport network model which is placed 10 ports peripheral of the patch antenna. The impedance matrix and the radiation conductance network are then combined by the segmentation method (Benalla, et al., 1988) to obtain input impedance of the RMSA. The antenna impedance at the resonant frequency is a complex number having both real and imaginary parts. Thus Figure 3.26 has been obtained. It is clearly seen that the theoretical and simulation results are in well agreement.

3.3.3.1 Negative-Capacitor and Chip-Resistor-Loaded RMSA

Broadband matching techniques suitable for applications for compact microstrip antennas with a thin dielectric substrate are available in literature. One of these compact broadband techniques uses a chip resistor of low resistance (usually on the order of 1Ω) connected between the antenna's radiating patch and ground plane (Srinivasan, Malhotra & Kumar, 2000). In this case, with the chip-resistor loading technique, similar antenna size reduction to the compact design using shorting-pin loading can be obtained. Moreover, owing to the introduced small ohmic loss of the chip resistor, the quality factor of the microstrip antenna is greatly lowered. The characteristics of loading a circular microstrip antenna with chip resistors and chip capacitors have also been studied (Lu, et al., 1998). Results show that, by incorporating the loading of a chip capacitor to a chip-resistor-loaded microstrip antenna, a much greater decrease in the antenna's fundamental resonant frequency can be obtained at a given operating frequency. In this section, effects of the negative capacitor and chip resistor loadings on the microstrip-fed rectangular microstrip antenna are analyzed. Figure 3.27 shows the geometry of chip resistor and negative capacitor loaded rectangular microstrip antenna with a 50Ω microstrip line feed. This design is achieved simply by loading negative capacitor over the feeding point

and 1Ω chip resistor near the radiating edge of the antenna and the equivalent circuit diagram is shown in Figure 3.27.

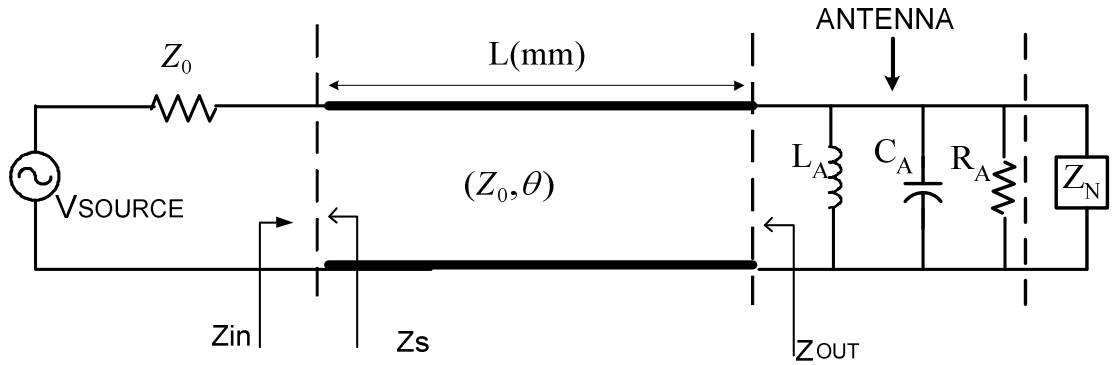


Figure 3.27 The equivalent circuit of the compensated patch antenna

The total input impedance can be given by

$$Z_{in} = Z_0 \left(\frac{\left(\left((-jR_{ant} + X_{ant})(-j\omega L + R_{ds}(-1 + \omega^2 C_{gs} L)) \right) \cos(\beta l) \right. \right.}{\left. \left. \begin{aligned} &+ Z_0(-R_{ds} + jL(-1 + g_m^2 \omega(R_{ant} + jX_{ant})R_{ds})) \\ &+ \omega^2 C_{gs} L \sin(\beta l) R_{ds} \end{aligned} \right)} \right) \quad \text{Eq. (3.49)}$$

$$\left(\frac{\begin{aligned} &Z_0(-j\omega L + R_{ds}(j + \omega L(g_m^2(R_{ant} + jX_{ant}) - j\omega C_{gs}))) \\ &\cos(\beta l) + (R_{ant} + jX_{ant}) \\ &(-j\omega L + R_{ds}(-1 + \omega^2 C_{gs} L)) \sin(\beta l) \end{aligned} \right)$$

where L is the value of load inductor, and R_{ant} real part of the rectangular microstrip antenna, X_{ant} imaginary part of the rectangular microstrip antenna. The antenna has been analyzed using multiport network model. This technique is used previously to predict the electrical behavior of both loaded and unloaded microstrip radiators.

The layout configuration of the designed microstrip patch antenna is shown in Figure 3.28. TLC-30 substrate material manufactured by Taconic, which has a relative permittivity (ϵ_r) of 3.00 and a thickness (h) of 0.51 mm, is used in this design. The patch dimensions of $W=10$ mm and $L=8$ mm, are selected along with the ground plane dimensions of 40 x 40 mm. When this substrate is used, chip-resistor-loaded microstrip antenna can have an impedance bandwidth of 10% or greater. For

the chosen dimensions, the designed antenna operates at 10.57 GHz, having $|S_{11}|$ of -13.27 dB at resonant frequency. The chip resistor has a cross section of 2.0×1.2 mm² and is connected to the ground plane at (x_3, y_3) .

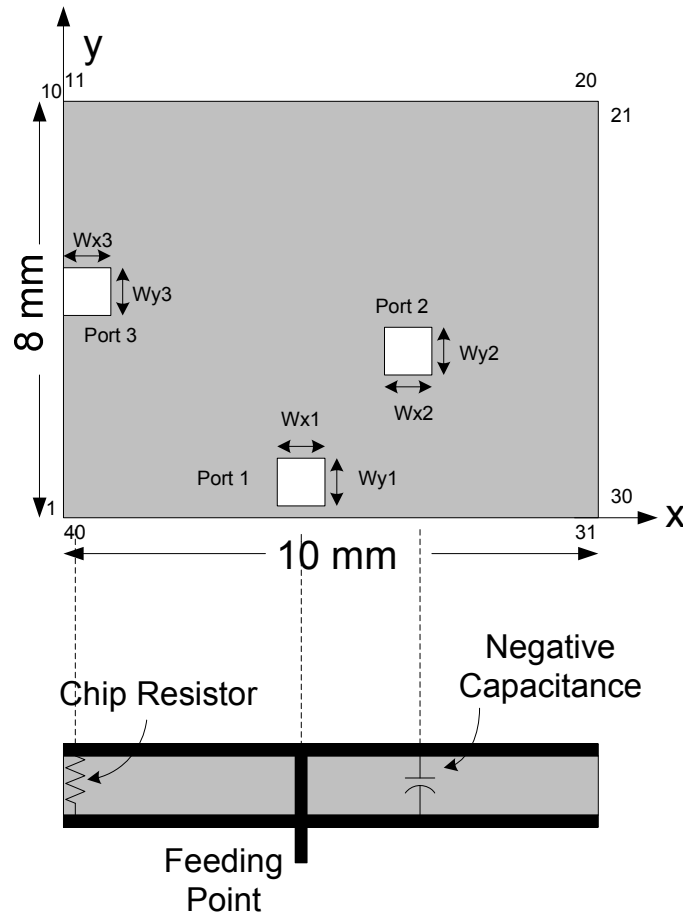


Figure 3.28 Microstrip antenna configuration with chip resistor and negative capacitor

The negative capacitor has a cross section of 2.0×1.2 mm² and is loaded at (x_2, y_2) . The feed is point symmetrically located and the microstrip line feed is denoted (x_1, y_1) .

Performances of the reference passive antenna and the loaded active antenna are compared using Microwave Office simulation (*MoM*) program. Figure 3.29 shows the simulated reflection coefficient parameter of the antenna loaded with various negative capacitors (L values). It is clearly seen that fundamental resonant frequency is shifted by changing L values.

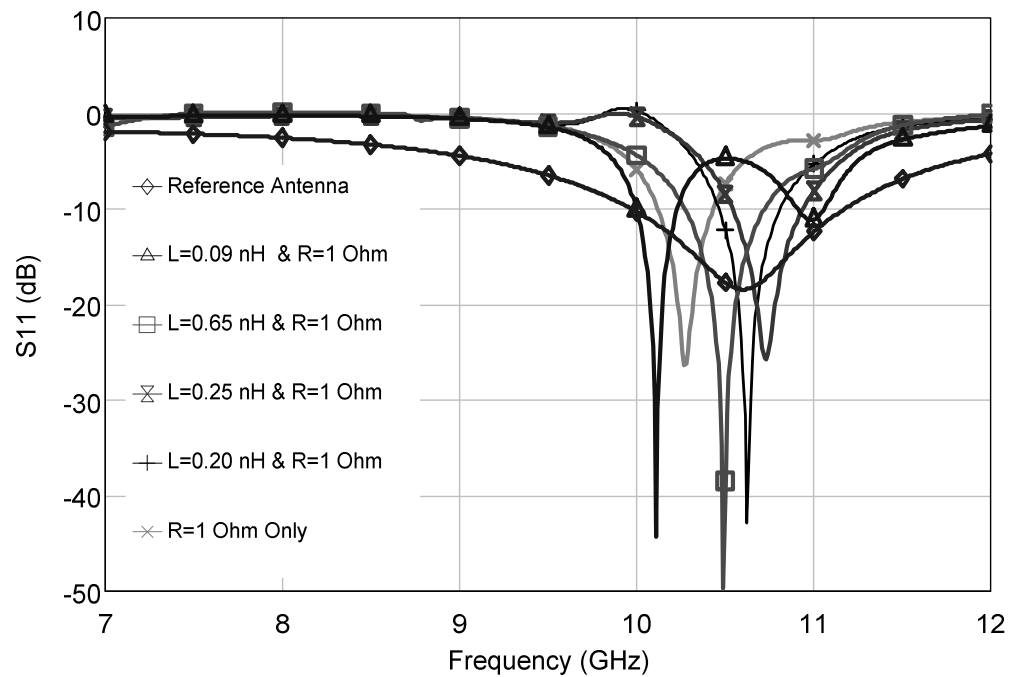


Figure 3.29 Return loss characteristics of the reference and loaded antennas versus frequency ($\epsilon_r = 3.0$, $h = 0.51$ mm, L (length) = 2 mm, $R = 1 \Omega$, $(x_1, y_1) = (5.5, 0.5)$ mm, $(x_3, y_3) = (0, 4)$ mm, and $(x_2, y_2) = (3, 5.5)$ mm).

To investigate the combined effect of loading both a chip resistor and a chip capacitor, the optimal loading positions for the loads are selected. The maximum resonant frequency reduction was occurred for L is 0.009 nH. The feed position is selected for optimal impedance matching for the case of centre of the edge; that is, the chip resistor and chip capacitor are placed on opposite side of the patch. However, by varying the L values changes the impedance matching level is slightly.

As for the resonant frequency, it is found that the case with $L = 0.09$ nH has the lowest resonant frequency, 10.20 GHz, which have the bandwidth of 3.7 %. The imaginary part of the antenna impedance around the resonant frequency is minimized using the negative capacitor loaded circuit with chip resistor as shown in Figure 3.30.

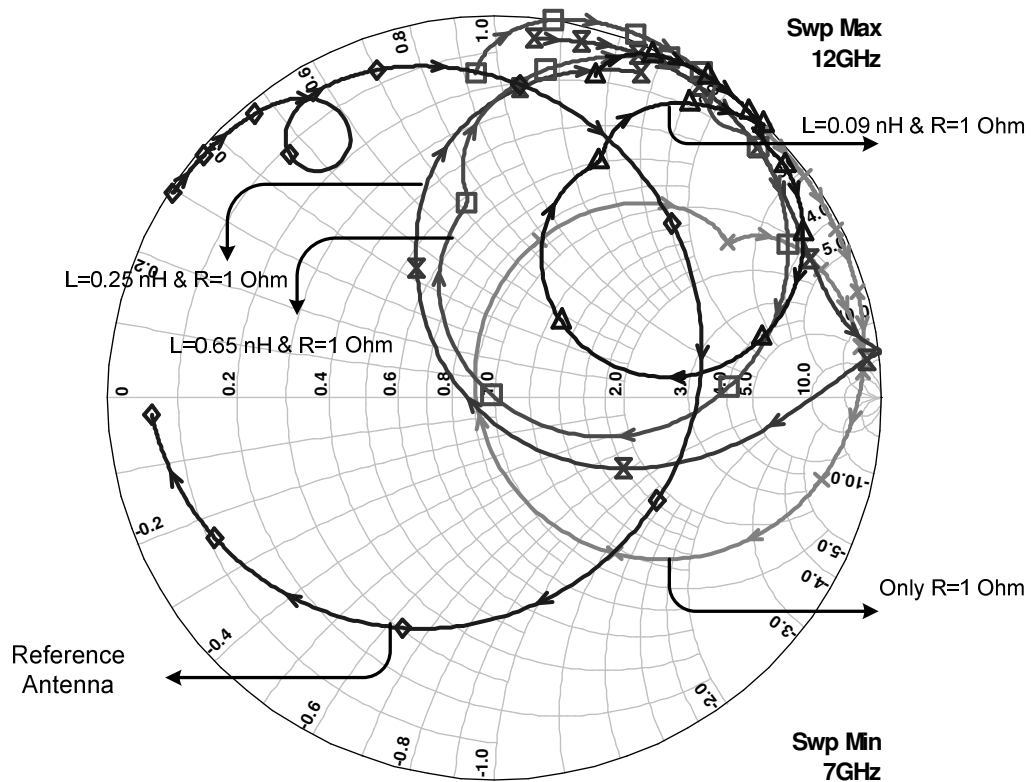


Figure 3.30 Input Impedance characteristics of the reference and loaded antennas versus frequency

For the impedance bandwidth, a significant increase is observed with the loading L values for the loaded antenna. By comparing the results in Figures 3.28 the enhancement in the return loss level is seen to be more effective for the RMSA patch, especially, where the loading of a L 0.20 nH . Also, by combining chip-resistor and negative chip-capacitor loadings, the resonant frequency of the microstrip patch antenna can be affected on the loading position. The impedance bandwidth increased from 9 MHz to 145 MHz when the value of the negative capacitor is increased. The radiation pattern remains in broadside direction for all cases. E-Plane and H-Plane pattern is improved for the active reactive loading antenna. Note that, the radiation pattern is normalized 0 dB for all cases as shown in Figure 3.31. In summary, the loaded antenna matching level is very high as comparing the reference antenna. The antenna gain is slightly increased for some loading combinations in Figure 3.31.

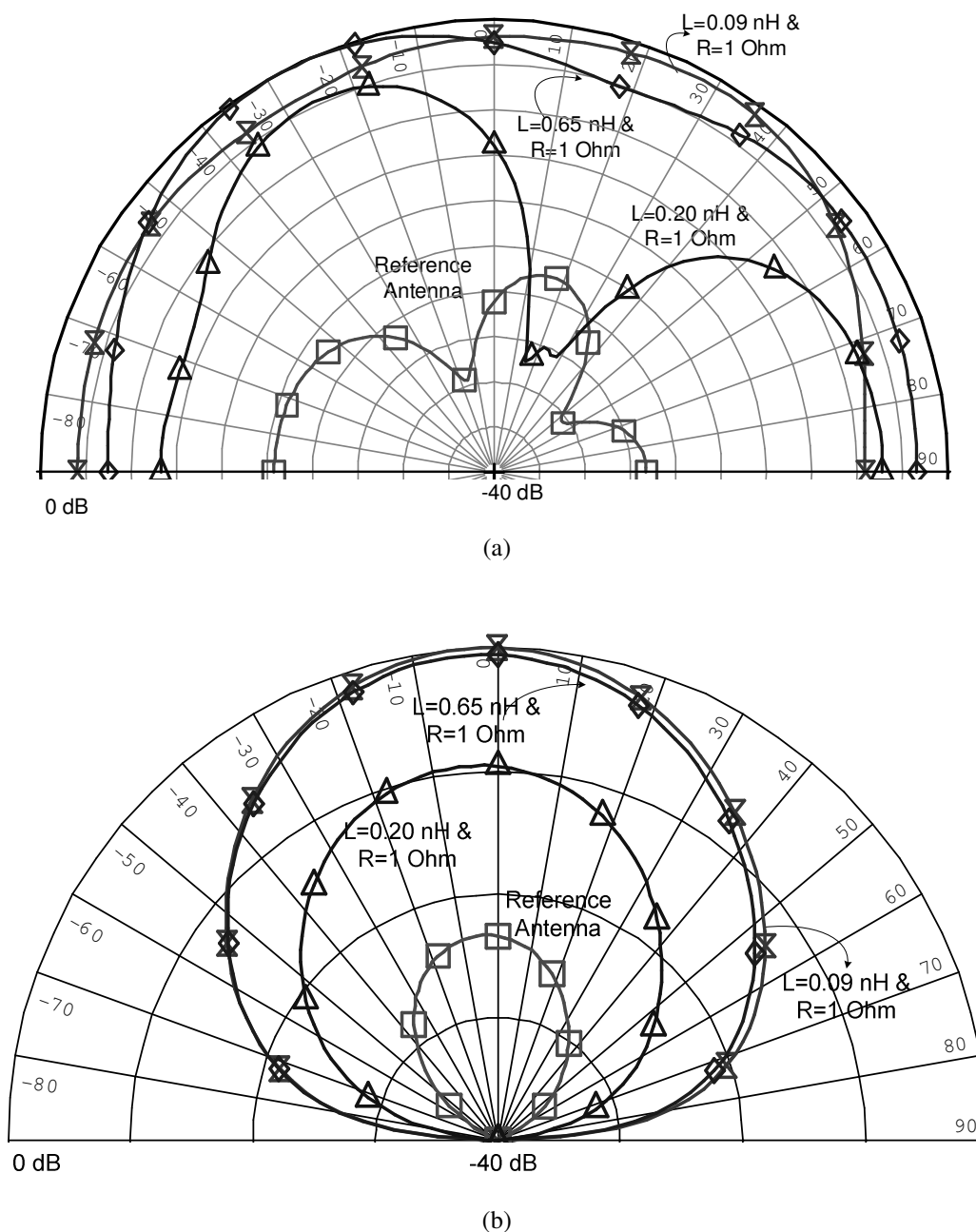


Figure 3.31 E and H-plane patterns of the reference and loaded antennas

The simulation results show that the loaded network can improve the return loss from -26.35 dB to -46.26 dB for (L 0.65 nH). Therefore, the most important finding of our study is that matching level is increased near the resonant frequency of the reference antenna by using negative capacitance together with the chip resistor. The performance of the antenna for different values of the negative capacitor values is summarized in Table 3.3.

Table 3.3 Performance comparison for the reference and the loaded-active (compact) antenna

| <i>Performance Parameter</i> | <i>Loaded-Active Antenna</i> | | | | | <i>Reference Antenna</i> |
|------------------------------|------------------------------|--------|--------|--------|--------------|--------------------------|
| L (nH) & R= 1Ω | 0.09 | 0.20 | 0.25 | 0.65 | 0 & (R only) | 0 |
| Frequency (GHz) | 10.20 | 10.62 | 10.73 | 10.5 | 10.27 | 10.57 |
| S_{11} deep point (dB) | -33.55 | -42.58 | -25.56 | -46.26 | -26.35 | -18 |
| Bandwidth (%) | 2.87 | 3.3 | 3.77 | 4.23 | 3.0 | 11.22 |
| Re (Z_{in}) (Ω) | 51.5 | 46.77 | 46.122 | 49.12 | 43.0 | 64.76 |
| Im (Z_{in}) (Ω) | -2.66 | -0.68 | -3.11 | 0.199 | 3.0 | -64.72 |

3.4 Comparison with Other Techniques

The single stub matching method basically works to overcome the fundamental bandwidth limitation. For the evaluation and comparison purpose, the stub matching technique has been also applied to the reference patch antenna. An impedance matching single stub connected to the feed line of the reference microstrip patch antenna is depicted in Figure 3.32.

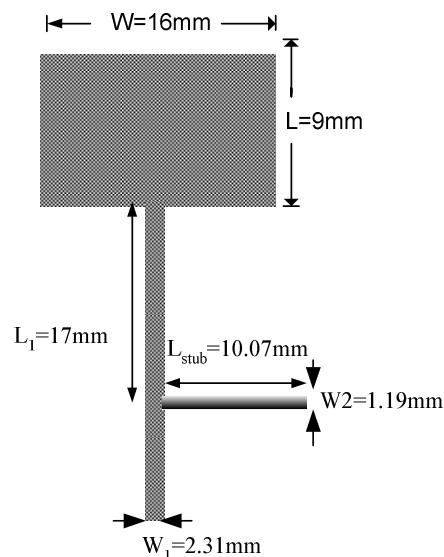


Figure 3.32 Stub matching

The reference antenna, the stub matched antenna, and the active compensated antennas have been simulated. The results for the antenna impedances, bandwidth,

return loss and the gain parameters have been evaluated using the simulation data. Variations of the real and imaginary parts of the antenna impedances as a function of frequency are presented in Figure 3.33 and 3.34, respectively.

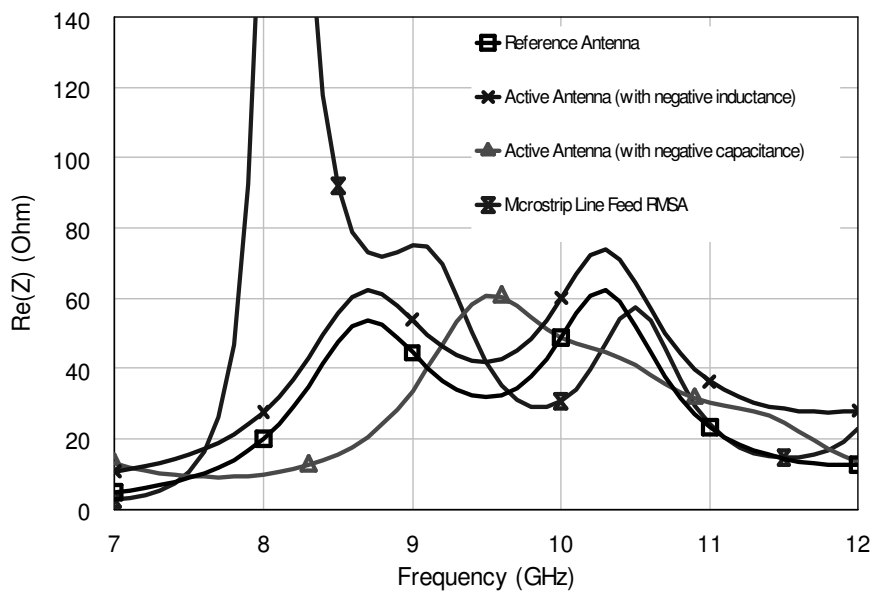


Figure 3.33 Variation of the real parts of the antenna impedances for all configurations

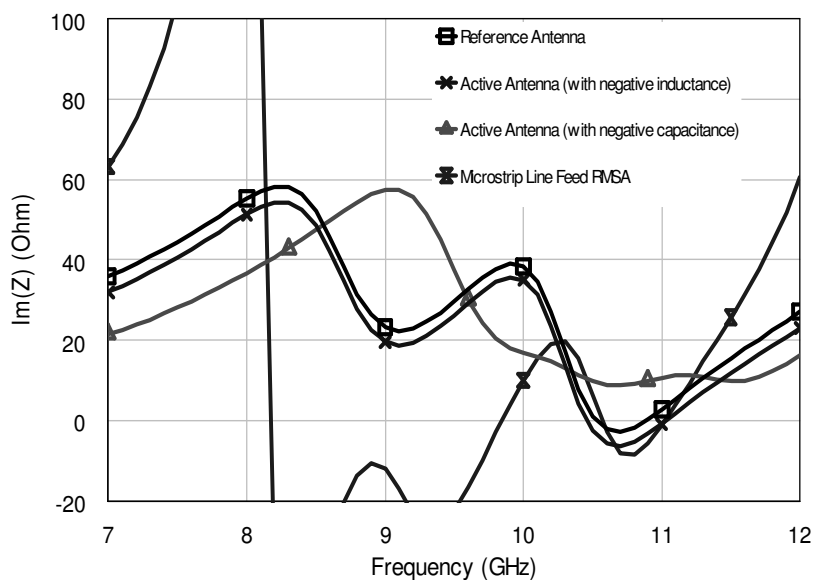


Figure 3.34 Variation of the imaginary parts of the antenna impedances for all configurations

In these comparisons the compensated systems with the active negative floating inductor shown in Figure 3.16 and the negative capacitance circuit shown in Figure 3.22 have been examined. The return loss characteristics $|S_{11}|$ for both reference and active antennas are shown in Figure 3.36. The reference antenna has the return loss better than -10 dB within the bandwidth of 12.21 %. This value is increased to 24.50 % by utilizing the negative inductor circuit at the input port of the reference antenna.

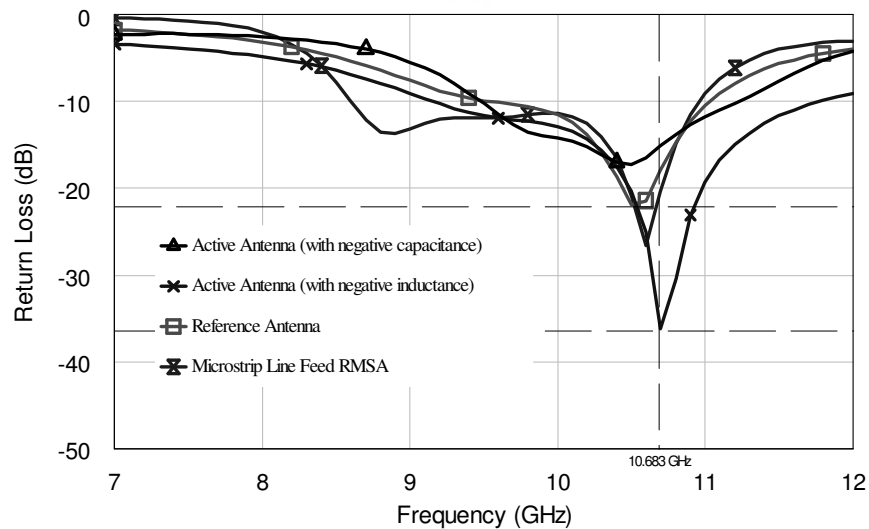
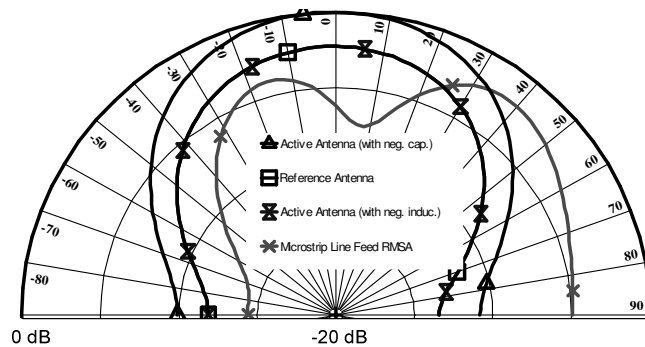


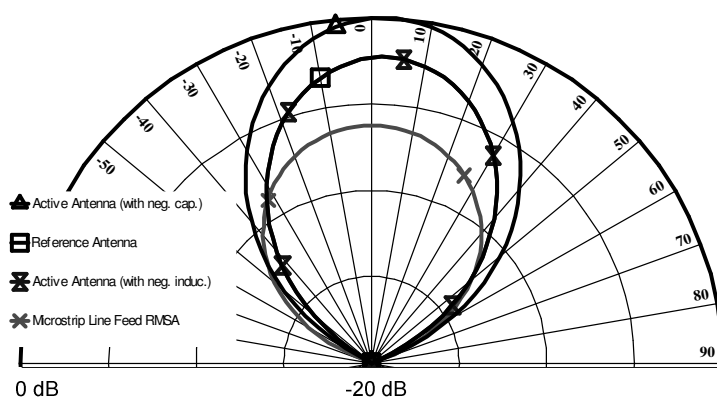
Figure 3.36 Return Loss plot of the designed antenna for all configurations

This improvement of the bandwidth does not cause a shift in the resonant frequency. In addition to these, the minimum return loss value is -36.33 dB. This technique not only improves the bandwidth but also takes the lowers deep point of the return loss characteristics at the resonant frequency. However, the antenna gain is the same of the reference antenna because the antenna structure remaining same.

It can be seen that the resonant frequency shifts (Figure 3.36) and the radiation pattern is disturbed (Figure 3.37) when the common stub compensation technique is used. All this circumstances are occurred due to unwanted radiation that exists in discontinuous structures in passive stub technique. This is not the case for the proposed active compensation circuit, which is an obvious advantage of the suggested technique.



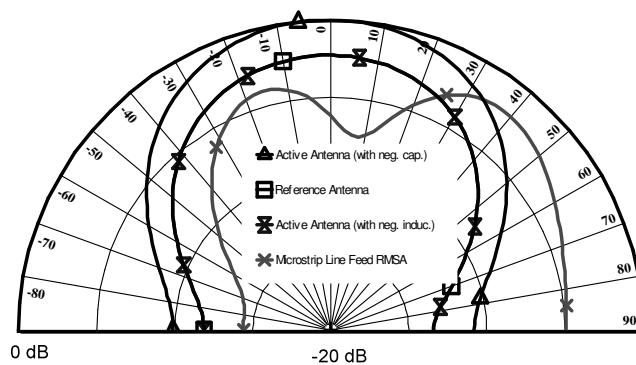
(a)



(b)

Figure 3.37 Radiation pattern at 10.5 GHz (a) E Plane (b) H Plane

The resonant frequency for both the negative capacitance loaded and the reference antenna are the same but the radiation pattern is improved. The antenna gain is increased to 9.27 dBi value for the reactive loading case.



(a)

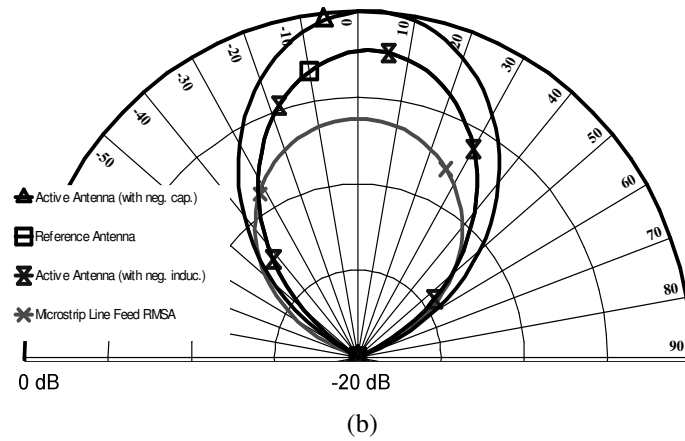


Figure 3.38 Radiation pattern at 10.7 GHz (a) E Plane (b) H Plane

The E and H plane patterns have been investigated for two different frequencies in impedance bandwidth with respect to -20 dB. It is clearly seen that the reference antenna pattern is approximately similar to the active antenna with negative inductance, because it has been placed in front of the antenna. But more power transfer can be succeeded to the antenna and further distance communication can be possible for this technique.

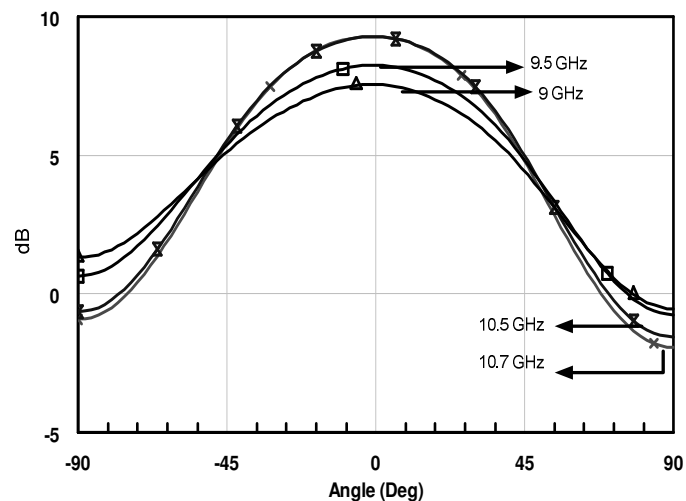


Figure 3.39 E-Plane pattern (with negative capacitor loading RMSA) for 9-10.7 GHz frequencies

The best results have been obtained with the compensated active antennas in terms of $|S_{11}|$ and radiation pattern. When the negative capacitance is used as a reactive load, the bandwidth of 16.96% and maximum gain of 9.273 dBi have been

obtained with a small amount of shift in the resonant frequency. The simulation results are summarized in Table 3.4 for the bandwidth, the return loss and the radiation pattern parameters for various configurations. When the radiation patterns are examined, there is no significant difference in the H-plane and the E-plane patterns for all the antennas as seen in Figure 3.37 and Figure 3.38. The E plane radiation pattern with negative capacitor loading antenna is shown in Figure 3.39 for 9-10.7 GHz.

Especially, good gain and beam shape results have been obtained in negative capacitor loading condition in E-plane pattern which is near the resonance frequency (in Figures 3.35-3.39). The maximum of the radiation pattern is in the broadside direction for all cases.

Table 3.4 Performance comparisons for the active antennas, reference antenna and stub technique

| Configuration | <i>Antenna Characteristics</i> | | | |
|--|--------------------------------|--------|-------------|------------|
| | S_{11} (dB) | BW (%) | f_r (GHz) | Gain (dBi) |
| Reference Antenna | -21.5 | 12.22 | 10.5 | 6.608 |
| Microstrip Line Feed RMSA (with single stub) | -26.59 | 22.28 | 10.59 | 7.978 |
| Active Antenna (with negative inductance) | -36.33 | 24.50 | 10.7 | 6.608 |
| Active Antenna (with negative capacitance) | -17.22 | 16.96 | 10.5 | 9.273 |

The resonance frequency of the negative capacitance loaded RMSA is 10.5 GHz. The impedance bandwidth of the proposed antenna is about 2.0 and 1.38 times larger than that of the reference microstrip antenna. The E-plane pattern has been dramatically improved for the active loading antenna. Note that the radiation power is normalized in broadside direction. The relatively large peak in the pattern of the reference patch has been obtained near the 0° . The asymmetry probably occurs due to the surface

wave effects in the stub situation.

Finally, the simulation results show that the compensation network with the negative inductor can improve the bandwidth from 12.21% to 24.50% with a minimum deep point of -36.33 dB. Utilizing the negative capacitor as the compensation circuit, bandwidth has been increased to 16.96% and the best radiation pattern in (E and H planes) has been obtained. These pattern shapes are similar to the reference antenna but results show that the radiation patterns of the active antenna with reactive loading case are significantly improved compared to conventional stub matching technique.

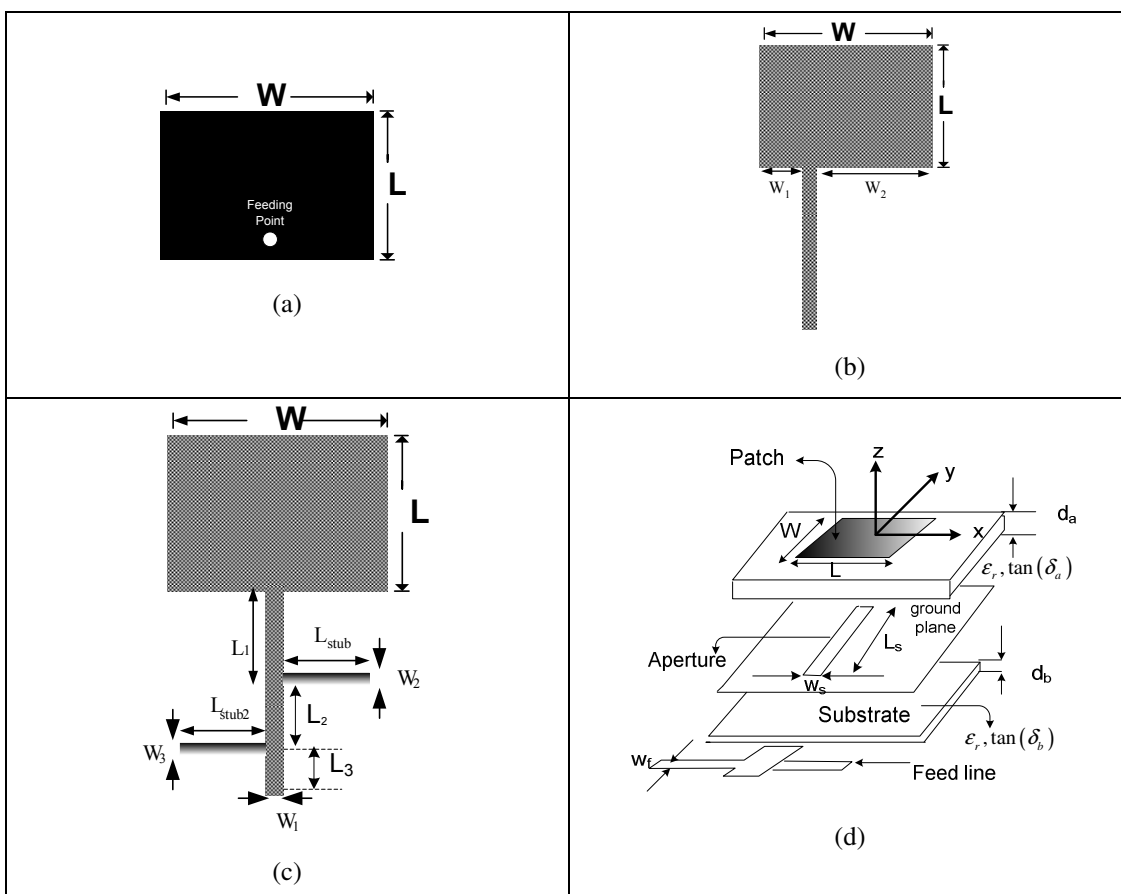


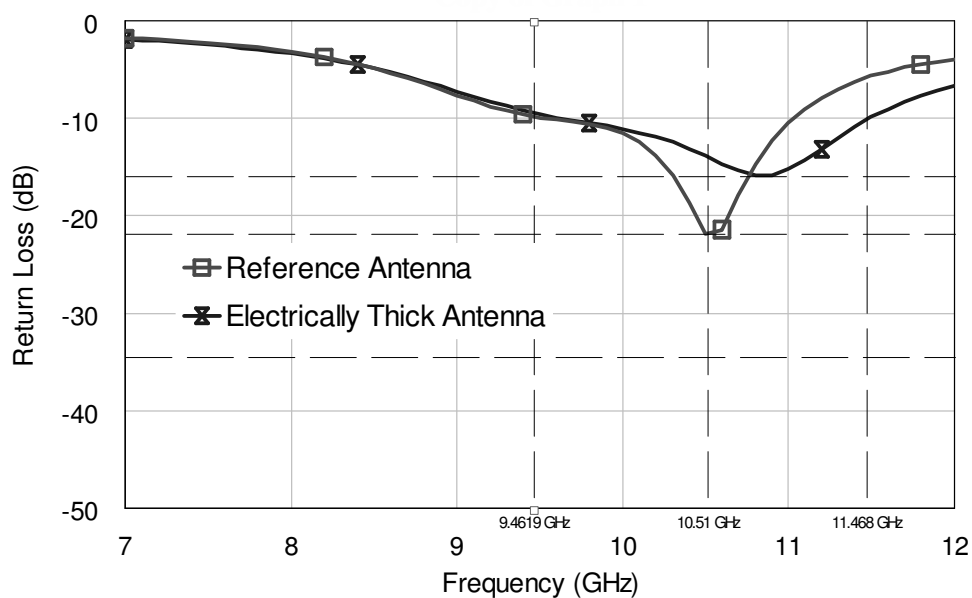
Figure 3.40 Different geometry of the RMSA (a) Thick antenna ($h=1.2$ mm) (b) Microstrip line feed RMSA (with double stub) (c) Feed-point RMSA (d) Geometry of aperture couple RMSA

There are some different classical well known techniques such as aperture couple RMSA, depending on the feeding point and symmetric or double stub techniques as shown in Figure 3.40. These techniques have been investigated for the comparison of

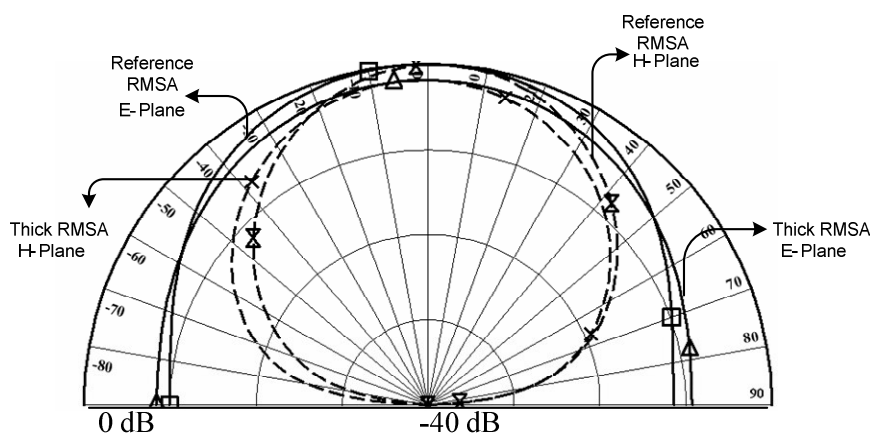
the new proposed methods. One of the well known classical techniques is electrically thick antenna. Electrically thick antenna can be obtain large bandwidth but this method when using the coaxially fed large inductance is added to the system ($h=1.2\text{mm}$). Therefore return loss level is decreased but the BW is increased as shown in Figure 3.41. The probe reactance is (Dearnley & Barel, 1989)

$$X_p = 120\pi \frac{h}{\lambda_0} \left(-\gamma + \ln \frac{2\lambda_0}{\pi d \sqrt{\epsilon_r}} \right) \quad \text{Eq. (3.50)}$$

where d is the probe diameter and $\gamma=0.5772$ is Euler's constant.



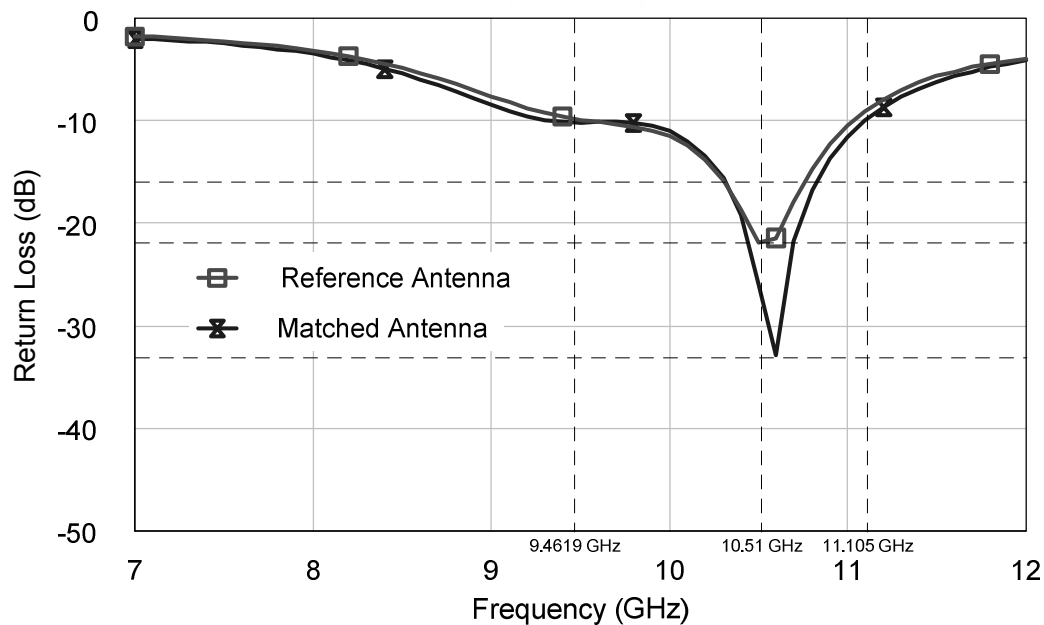
(a)



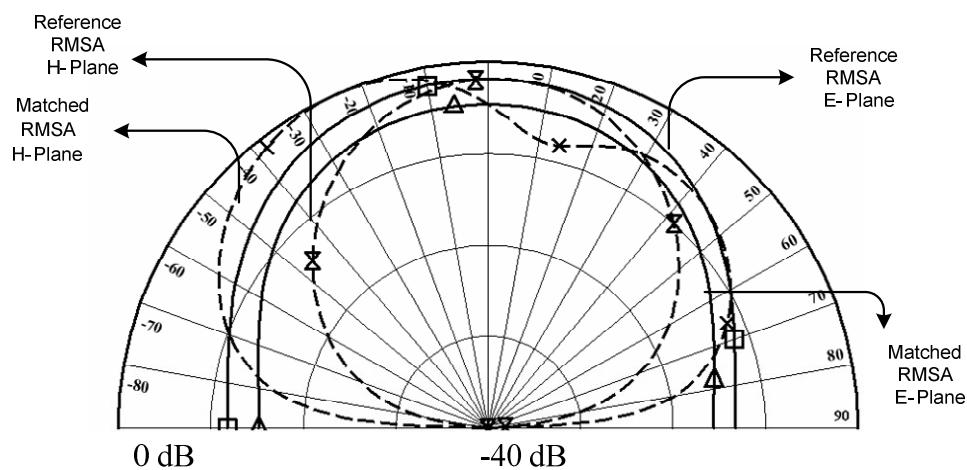
(b)

Figure 3.41 Thick RMSA ($\epsilon_r=3.2$, $h=1.2$ mm): (a) Return Loss plot versus frequency
(b) Radiation pattern 10.55 GHz, $W \times L = 16 \times 9$ mm

Changing the Feed-Point position as a different technique can be proposed for the increasing BW but it generates the unwanted surface waves and disturbed the radiation pattern and it is demonstrated in Fig 3.40 (b). The values of W_1 and W_2 are selected as 6mm and 12 mm. The results are shown in Figure 3.42.



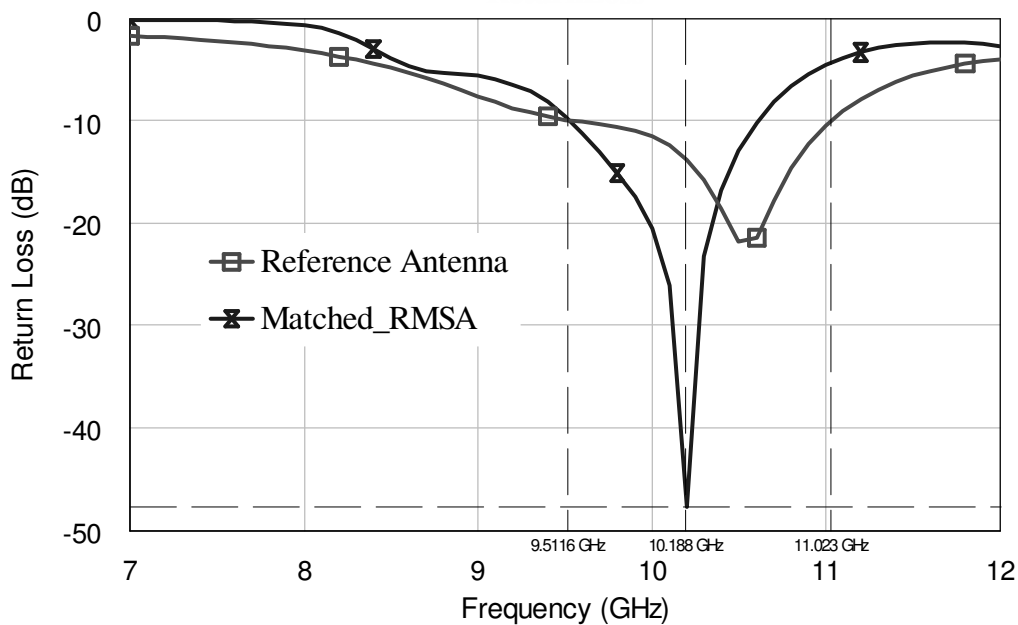
(a)



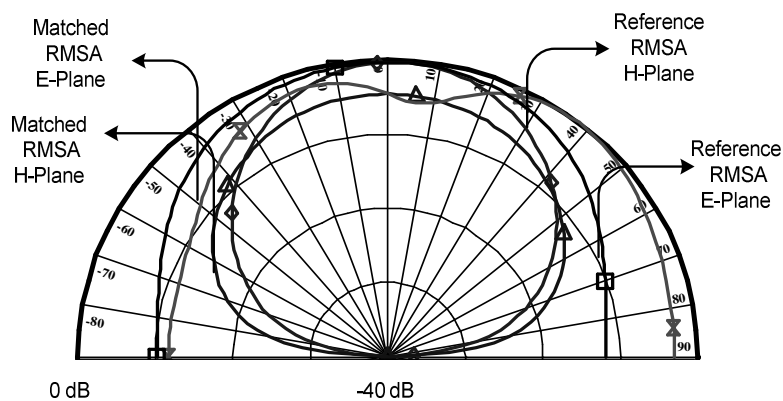
(b)

Figure 3.42 Microstrip Line Feed RMSA ($h=0.78$ mm, $\epsilon_r=3.2$:TLC-32): (a) Return Loss plot versus frequency (b) Radiation pattern 10.55 GHz, $W \times L = 16 \times 9$ mm

Double stub matching method basically works to overcome the matching problem (in Fig 3.40.(c)). With an impedance matching double stub connected to the feed line increased matching level was achieved and its dimensions are $W=16$ mm and $L=9$ mm. $W_1=1.8$ mm, $L_1=6.25$ mm, $W_2=1.8$ mm, $L_{stub1}=7.5$ mm, $W_3=1.8$ mm, $L_{stub2}=11$ mm, $L_2=10$ mm, $L_3=10$ mm. The results for the double stub technique are shown in Figure 3.43.



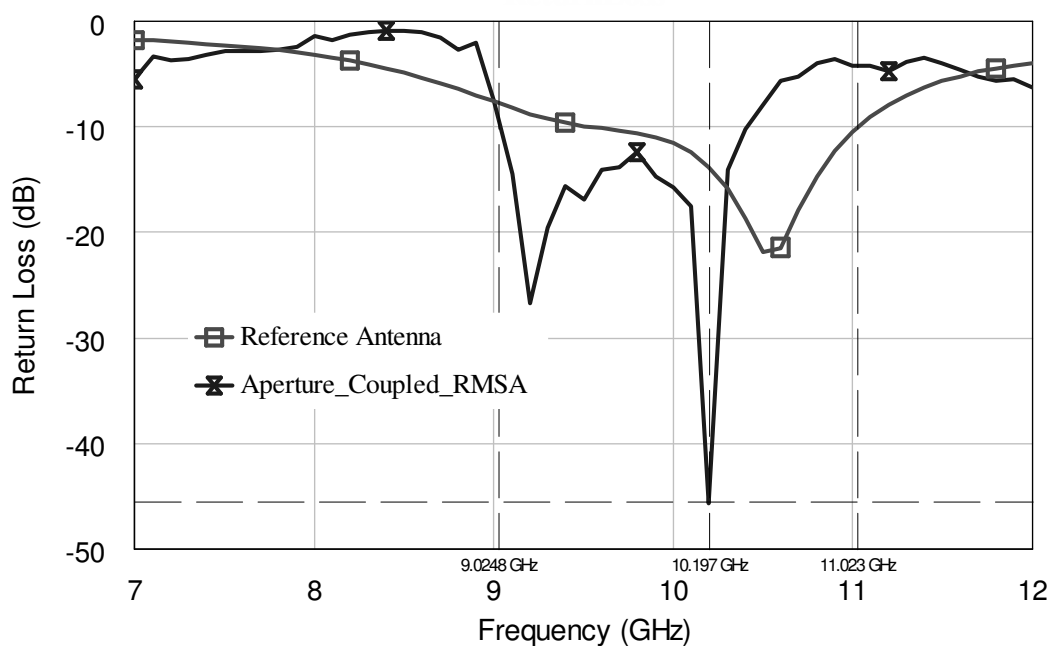
(a)



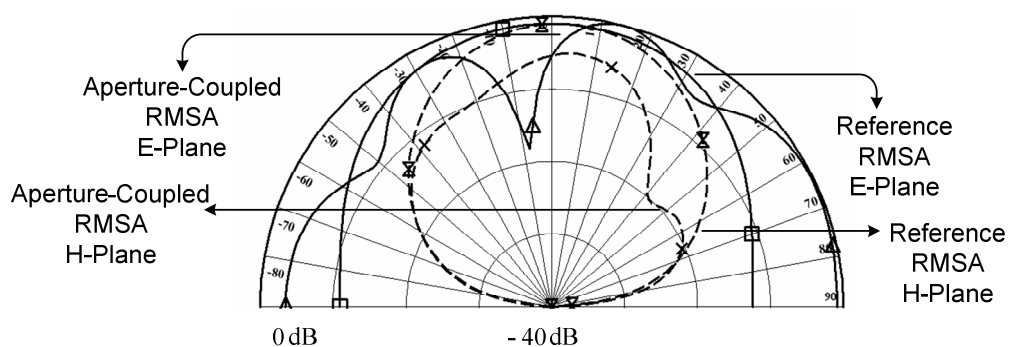
(b)

Figure 3.43 Double stub matched antenna ($h=0.78$ mm, $\epsilon_r=3.2$, $\tan(\delta)=0.0010$): (a) Return Loss plot versus frequency (b) Radiation pattern at 10.55 GHz Substrate type: TLC-32 by Taconic, $W \times L = 16 \times 9$ mm.

The aperture couple rectangular microstrip antenna (Shin & Kim, 2002) is shown in Figure 3.40(d). Both the microstrip line feed and probe feed causes inherent asymmetries which generate higher order modes which produce cross-polarized radiation. To overcome these problems, noncontacting aperture coupling feeds can be used. The aperture coupling is the most difficult to fabricate and it also has narrow bandwidth. The feed mechanism and radiating patch are independent. The simulation results for the aperture couple antenna and reference antenna are shown in Figure 3.44.



(a)



(b)

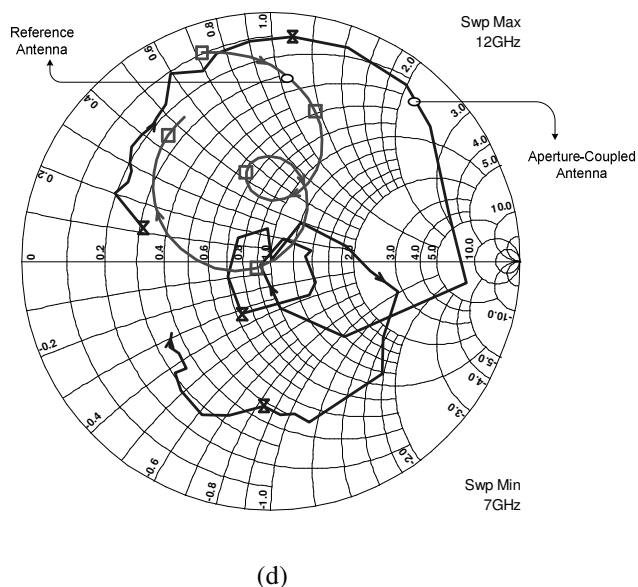
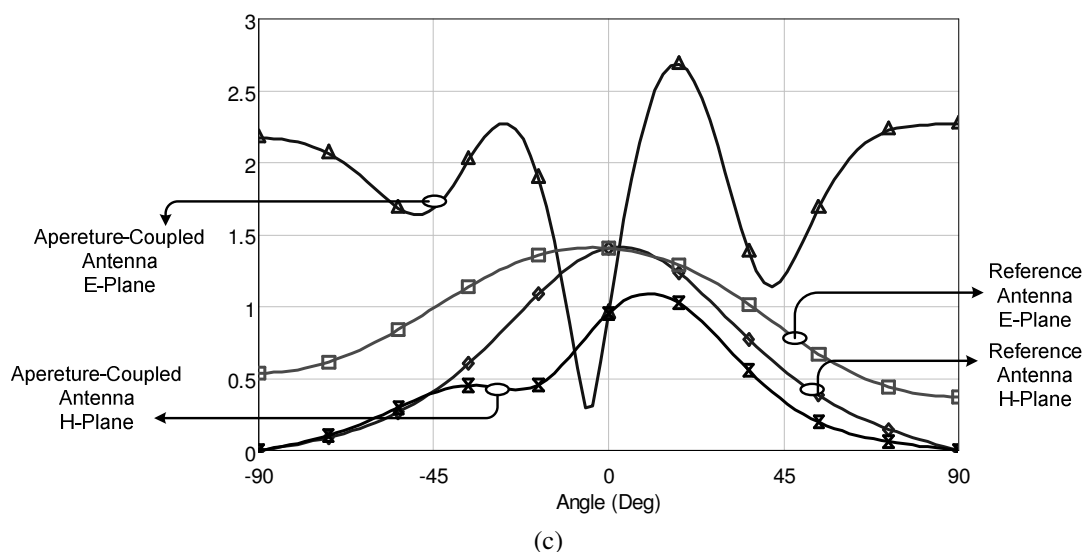


Figure 3.44 Aperture coupled RMSA (a) Return Loss plot versus frequency (b) Radiation pattern at 10.55 GHz (c) Radiation pattern at 10.19 GHz (d) Input impedance loci for various values of frequency, $W \times L = 16 \times 9$ mm.

The patch resonator now appears as a series RLC network with a shunt inductance representing the coupling slot. Maximum coupling occurs when the aperture is centered below the patch ($s=L/2$). This network allows the possibility of increased the bandwidth. Aperture couple antenna is designed on substrate thickness (h) 0.78 mm, dielectric constant 3.2. The precise dimension of the antenna are: feed line width 1 mm reference plane 2.86 mm from the edge of patch, feed line height 0.78 mm, slot dimensions are $W_s=5.5$ mm $L_s=1$ mm patch antenna dimension. In addition

the other dimensions are $W \times L = 16 \times 9 \text{ mm}$, stub length = 17 mm, $\epsilon_{ra} = 1$, $\tan(\delta_a) = 0.0$ (Foam), $d_a = 2 \text{ mm}$, $\epsilon_{rb} = 3.2$, $\tan(\delta_b) = 0.0009$, $d_b = 0.78 \text{ mm}$.

By using a reactance in the form of negative inductance and capacitance along the feeding point and end point it is possible to achieve an increase up to 24.50% and 16.96% in the operational bandwidth in the 'S' band. The most direct method of increasing the bandwidth of microstrip antenna is to be use a thick substrate but as discussed above, this inevitably leads to unacceptable spurious feed radiation (in Figure 3.38(a)), surface wave generation, or feed inductance. Therefore, the impedance matching level is obtained lower values than other techniques. It is seen that the impedance bandwidth is generally the limiting factor. As the surface wave explanation predicts there is no difference between the shapes of the H-plane patterns for the active compensated antennas. The E-plane pattern is dramatically improved at the active loading antenna in Figure 3.38 and 3.39. If double stub technique was used as matching network, matching level has increased but impedance bandwidth is a little decreased as shown in Figure 3.42.(a). Note that the radiation powers are normalized to 0 dB in broadside direction in all circumferences.

The radiation pattern for double stub matching is distorted between -90° and 0° and the gain is decreased in this region. But it is seen that the gain is increased in the other part of the region around 2 dB. The undesired radiation may increase the sidelobe level and the cross-polar amplitude of the radiation pattern. Minimization of spurious radiation and its effect on the radiation pattern is one of the important factors for the evaluation of the feed. Similar implementation can be accepted for the aperture coupled antenna. The entire region except 0° - 20° , the gain is higher approximately 3-4 dB than the reference antenna but still, the radiation pattern is distorted and this technique having some disadvantages such as very complex and fabricated is very hard.

The design of microstrip antenna by a combination of active device with radiating patch to obtain broad bandwidth can be realized. The performance parameters of the designed microstrip antenna with and without compensation

network are compared. The simulation results show that the compensation network with the negative inductance can improve the bandwidth from 12.21% to 24.50%. The antenna gain improved from 6.6 dB to the 9.3 dB for the negative capacitance loaded antenna. The all results are summarized in Table 3.5 for all of the above techniques.

Table 3.5 Performance comparison for different techniques

| | $Z_{in} \text{ at } f_r \text{ (Ohm)}$ | $S_{11} \text{ (dB)}$ | $BW \%$ | $f_r \text{ (GHz)}$ | $HPBW \text{ Beamwidth}$ | Computed Gain (dB) |
|--|--|-----------------------|---------|---------------------|--------------------------|--------------------|
| Reference Antenna | 45.565+7.57j | -21.5 | 12.22 | 10.55 | 76.6° | 6.608 |
| Microstrip Line Feed RMSA (with double stub) | 57.423+6.412j | -46.55 | 5.49 | 10.203 | 55.4° | 7.608 |
| Active Antenna (with negative inductance) | 51.467-0.5678j | -36.33 | 24.50 | 10.7 | 77.1° | 6.608 |
| Active Antenna (with negative capacitance) | 42.363+10.13j | -17.22 | 16.96 | 10.55 | 77.7° | 9.273 |
| Matched-RMSA (Feed – Point) | 47.765+0.006j | -32.32 | 16.90 | 10.6 | 77.3° | 4.338 |
| Aperture-Coupled RMSA | 41.519+3.389j | -44.94 | 12.25 | 10.197 | 23.8° | 8.55 |
| Thick RMSA | 43.15+13.74j | -15.83 | 16.5 | 10.56 | 88.9° | 4.80 |

CHAPTER FOUR

ELECTRONICALLY CONTROLLED IMPEDANCE TUNING NETWORKS

4.1 Impedance Matching Networks

The design of broadband active-compensated antenna system is an important problem in commercial satellite, military, and high-speed communication systems. And so, impedance matching networks are used extensively in radio transmission and receiving systems. As combined with appropriate matching modeling techniques, the patch antenna design is basically a matter of designing impedance-matching networks to obtain the required performance. Much research has been performed to achieve broadband characteristics in the design of microstrip antennas (Pues & Van De Capelle, 1989). Among these studies, matching circuits with lumped elements have been generally introduced. However, a terminating load resistance usually cannot be adjusted to a desired value by this approach. Simplified block diagram is shown in Figure 4.1.

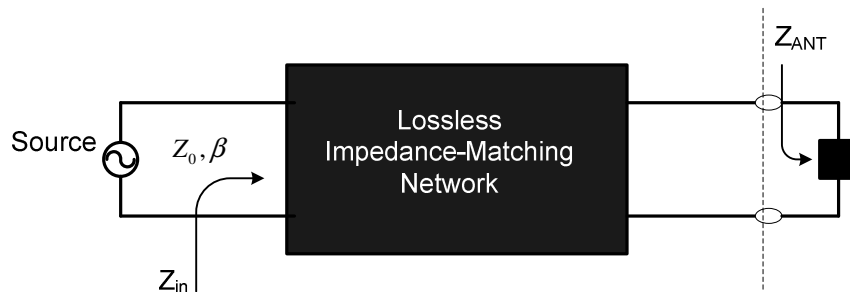


Figure 4.1 Matching network

The design of an antenna element usually involves attempting to provide feed point impedance equal to some known, real, system impedance. A broad band design often results with a large of imaginary part of the antenna impedances. Maximum real power is delivered to the load when the source impedance presented to the load is equal to the complex conjugate of the load impedance. In case of transmitting antennas, the impedance of the load can vary greatly due to changing antenna configuration, environment, and operating frequencies. Each time this occurs, the

transmission system needs to be re-tuned by means of a matching network. The purpose of the impedance matching network therefore, is to ensure that the source impedance seen by the load is equal to its complex conjugate.

Ideally, this matching network would transform the frequency-dependent complex antenna impedance Z_{ANT} to a pure real resistance Z_0 over as large a required bandwidth. However, there appear to exist some theoretical limitations. Bode first showed what the physical limitations were on the broadband impedance matching of the loads consisting of a reactive element and a resistor in series or parallel (Pues, et al., 1989). Later, Fano presented the general limitations on the impedance matching of any load (Fano, 1950). Indeed, it is impossible to realize a perfect match over a continuous band of frequencies by means of a purely reactive (losses, linear, passive, i.e.) network.

Antennas cannot be considered as isolated elements, but as integrated parts of more complex system, that modify its electromagnetic properties, such as radiation pattern, input impedance, directivity, etc. At the usual conditions of the use the antenna is critically affected by the environment and this situation is especially significant in mobile systems because of the electromagnetic variability inherent to the mobile system. Changing electromagnetic condition, developing the complexity of communication systems, interest on matching systems is increased. First, front modules couldn't employ optimum efficiency under the load variation. Radiated power decreases due to reflecting power from load and the equipment has to increase the power to compensate the reduction. As a result, increment energy consumption and deterioration in the transmission quality are occurred and in fact, input module could be damaged because of high reflected power if no isolator is used in transmitter system. In fact, for many practical circuits matching networks are not only designed to meet requirement of minimum power loss but are also based on additional constraints, such as minimizing the noise influence, maximizing the power handling capabilities, and linearizing and controlling the frequency response.

The most frequently used matching networks are the L network, Pi network, and T network (Ludwig & Bretchko, 2000). L network have only two variables, allowing the network to be tuned easily for specified load impedances. The advantage of the L network is that when given an impedance problem, the unique solution may be found. Where greater impedance matching flexibility or where additional criteria are of significance, the Pi or T networks must be used. These networks consist of three component variables allowing greater impedance matching capabilities and allowing greater control over other criteria such as parasitic effects or harmonic rejection. Some possible matching networks are shown in Figure 4.2.

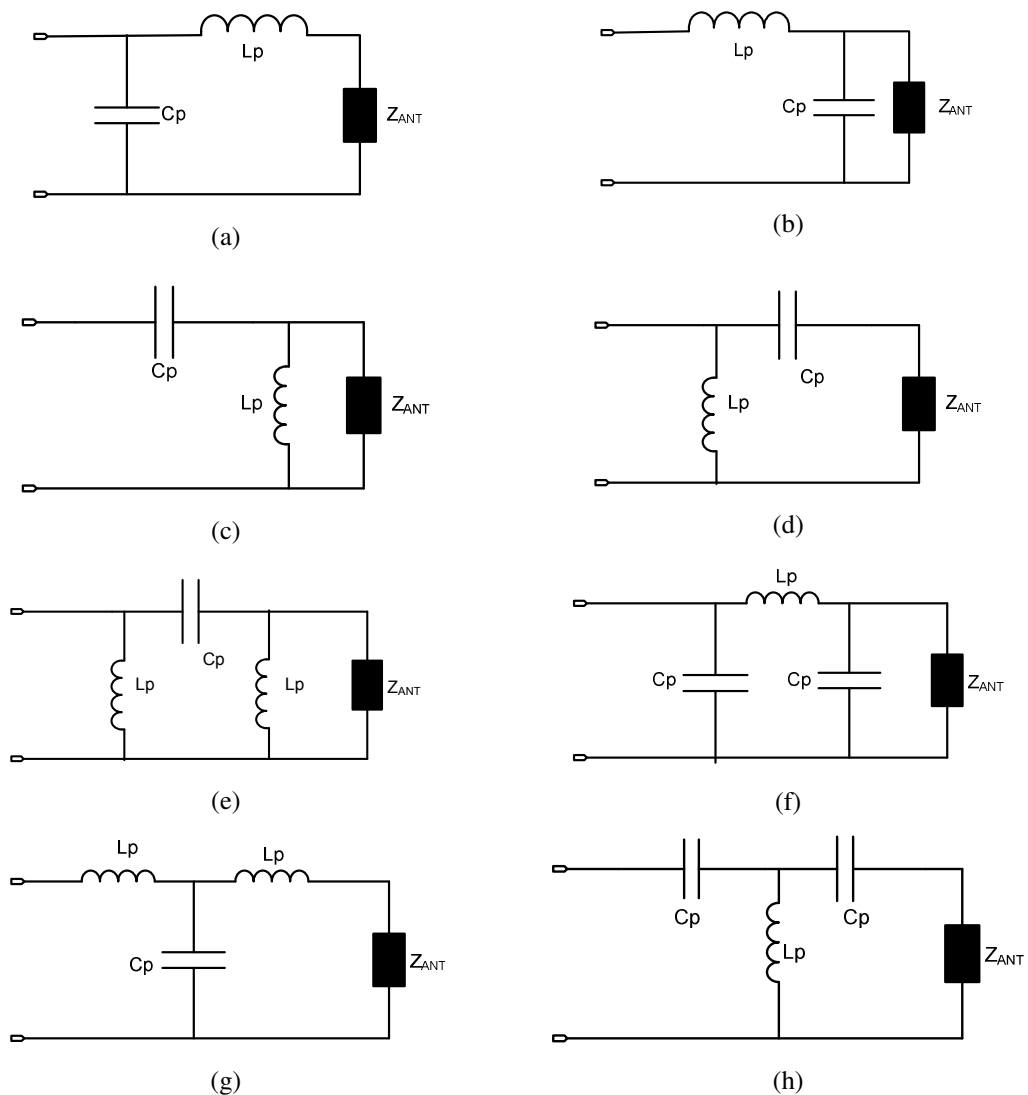


Figure 4.2 Some possible impedance-matching networks with two or three reactive components

There are a lot of possible configurations for matched antenna but it is important that most compatible configuration is selected. Because, some selected configurations can not be produced effective results in contrary it can be distorted system performance. So selection may be important some applications. The research reported here has concentrated on Pi network; however circuit analysis is just as applicable to the T network. Some configurations are shown in Figure 4.2. The overall efficiency and bandwidth performance of the matched antenna is generally best when the network is mounted as close as possible to the radiating element.

Finally, the design of impedance-matching networks which use lumped transformers as shown Figure 4.2 (f) is presented to achieve the good matching level performance of patch antenna. Some theoretical and measurement results are obtained by using configuration of Figure 4.2 (f). This network was selected due to having some advantages such as floating inductor can be easily realized by using J-inverter structures. Other configurations can be also used but the impedance characteristics and sensitivity results will be changed. These impedance matching techniques are powerful techniques to increase the return loss level of the patch antennas. Some circuits may result in more reasonable component values. In addition, sometimes matching these components can be used as dc blocks (capacitors) or to provide bias currents (inductors). At the same time harmonic filtering can be done with a low pass matching network.

4.2 Design of Pi-Matching Network for Compensated Antenna

Impedance tuning networks are also widely used in many electronic applications, such as RF power amplifier designs, impedance-matching devices like antenna tuning units. In this section, a novel technique with pi-matching network is proposed based on lumped and electronically tunable elements. The pi-matching device is used to construct the antenna tuning units, which is only used to match the front module and the antenna. This is interesting application because antennas cannot be considered as alone component with changing electromagnetic properties. When the input impedance varies, there is a mismatch between the front module and the

antenna, with two major effects. First, the front module will not perform at optimal efficiency under load variations, and, second, the radiated power decreases due to the reflected power. The result is an increase in the energy consumption or transmission quality deterioration. In addition, the input module in antenna system could be damaged if reflection of the signal levels is excessively high.

The starting design point is low-pass pi matching topology network shown in Figure 4.3, which is typical in tunable impedance transformers or antenna tuning unit applications (Mingo, et al., 2004). It is well known that a transmission line can be approximated using the simple network illustrated in Figure 4.4. The problem occurs when trying to tune this network but it can be overcome by using simple techniques.

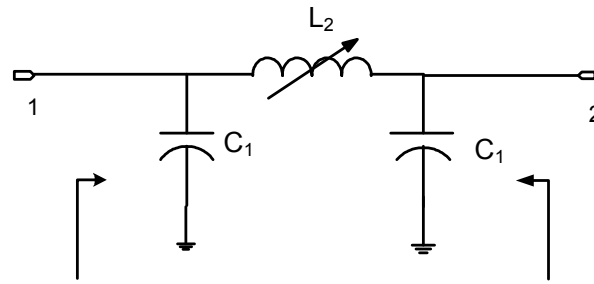


Figure 4.3 Starting matching network

Electronically tunable capacitors are easily obtained but electronically tunable inductors are not easily achieved except MMIC process (Zhang & Gautier, 1993). Unfortunately, tunable inductors have power and band limitations which may be prohibitive some certain applications. In MMIC design, spiral inductor is often used to reduce chip size. However, the area of a spiral inductor is still rather large compared to that of other lumped elements and the inductance values are related to physical structure. It is also difficult to realize a broadband spiral inductor, especially one of high inductance value, because of intersegment fringing capacitance. The inductor can be realized different methods such as J-inverters and capacitors.

4.2.1 Theory

This pi-circuit is a flexible structure that offers many tuning possibilities. For these reasons, the inductor (L_2) is realized by using J-inverter ($\lambda_g/4$) and capacitor as shown

in Figure 4.4.b. The following sections outline a technique for designing electronically tunable transmission lines capable of the performance of a transmission line over a specified bandwidth. This flexibility can be enhanced controlling the input and output capacitor values. When every capacitor can be tuned, controlling complexity is increased but at the same time, matching capacity can be increased.

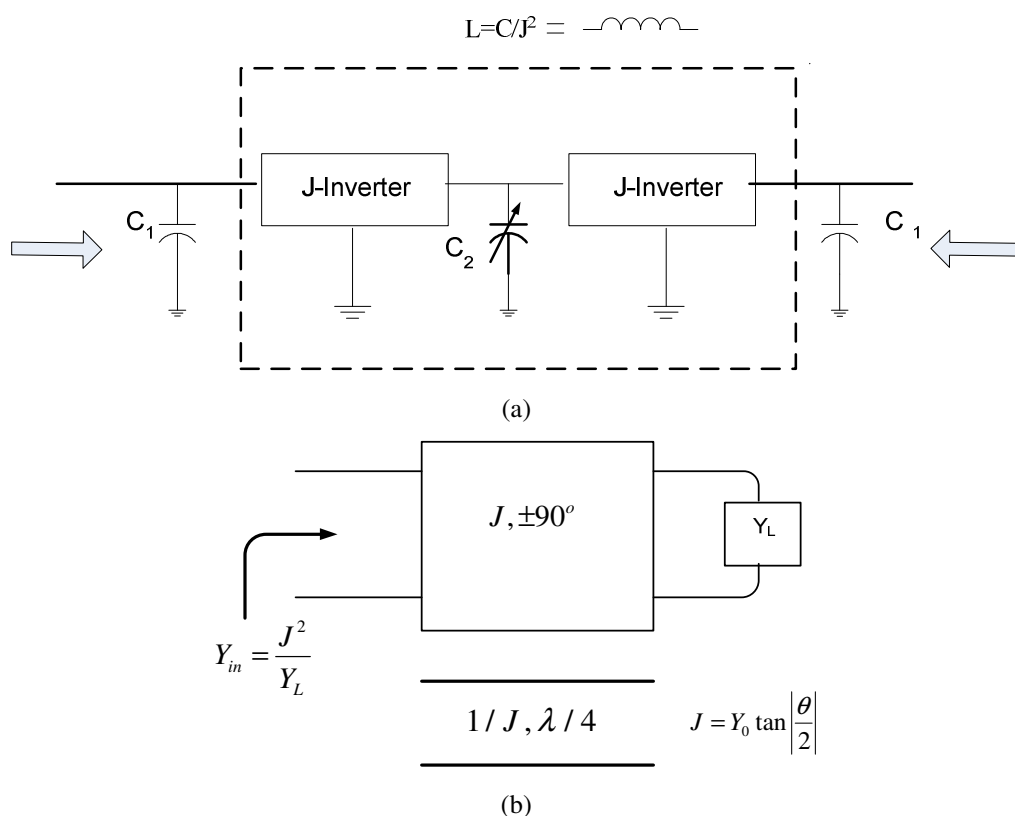


Figure 4.4 (a) Equivalent Pi-circuit topology (b) J-inverter diagram

J-inverters are discussed in great detail by Matthei et al (Matthei & Young, 1980). The Y matrix for ideal transmission line is equated to the Y matrix for the circuit in Figure 4.4 and C_1, C_2, θ values can be obtained by using these equations. The steady state Y parameters for an ideal transmission line are as follows:

$$Y = \begin{pmatrix} -\frac{jCot(\theta)}{Z_0} & \frac{jCsc(\theta)}{Z_0} \\ \frac{jCsc(\theta)}{Z_0} & -\frac{jCot(\theta)}{Z_0} \end{pmatrix} \quad \text{Eq. (4.1)}$$

The steady state Y parameters for the circuit in Figure 4.3 are

$$Y = \begin{pmatrix} j\left(-\frac{1}{\omega L_2} + \omega C_1\right) & \frac{j}{\omega L_2} \\ \frac{j}{\omega L_2} & j\left(-\frac{1}{\omega L_2} + \omega C_1\right) \end{pmatrix}. \quad \text{Eq. (4.2)}$$

Equating terms in the Y matrices of (4.1) and (4.2) the two following unique equations are obtained:

$$j\left(-\frac{1}{\omega L_2} + \omega C_1\right) = j\left(\frac{-\text{Cot}(\theta)}{Z_0}\right) \quad \text{Eq. (4.3.a)}$$

$$j\left(\frac{1}{\omega L_2}\right) = j\left(\frac{\text{Csc}(\theta)}{Z_0}\right) \quad \text{Eq. (4.3.b)}$$

It is simple to solve for C_1, C_2 as follows:

$$C_1 = \frac{-\text{Cot}(\theta) + \text{Csc}(\theta)}{\omega Z_0} \quad \text{Eq. (4.4)}$$

$$C_2 = \frac{J^2 \text{Sin}(\theta) Z_0}{\omega} \quad \text{Eq. (4.5)}$$

Conversely, one can solve for Z_0 and θ in terms of C_1 and C_2 as follows:

$$\theta = 2\text{ArcTan} \left(\frac{-J^2 \sqrt{\frac{C_2}{-2J^2 C_1 + \omega^2 C_1^2 C_2}}}{\omega C_2} + \omega C_1 \sqrt{\frac{C_2}{-2J^2 C_1 + \omega^2 C_1^2 C_2}} \right) \quad \text{Eq. (4.6)}$$

$$+ \sqrt{\frac{J^4}{-2J^2 \omega^2 C_1 C_2 + \omega^4 C_1^2 C_2^2}}$$

$$Z_0 = \sqrt{\frac{C_2}{-\omega^2 C_1^2 C_2 + 2J^2 C_1}} \quad \text{Eq. (4.7)}$$

Eq. (4.6) and Eq. (4.7) are valid under the following circumferences:

$$0 < C_2 < \frac{J^2}{\omega^2 C_1} \quad \& \& J \omega C_2 \neq 0 \quad \& \& C_1 (-2J^2 + \omega^2 C_1 C_2) \neq 0 \quad \text{Eq. (4.8)}$$

It is clear that not all possible values of C_1 and C_2 yield a circuit equivalent to a transmission line. Equations (4.6), (4.7) and (4.8) provide to compute the required

components over any desired range of frequencies and transformation ratios. Pi-network which is used for impedance matching network circuit model is shown in Figure 4.5. In this Figure, it is clear that impedance matching level can be controlled where the values of C_1 and C_2 are changed. But there are some impedance boundary conditions. This network is a slightly more complex because there is transmission line part in front of the antenna module. It can be easily found input impedance and it can be evaluation of the system performance.

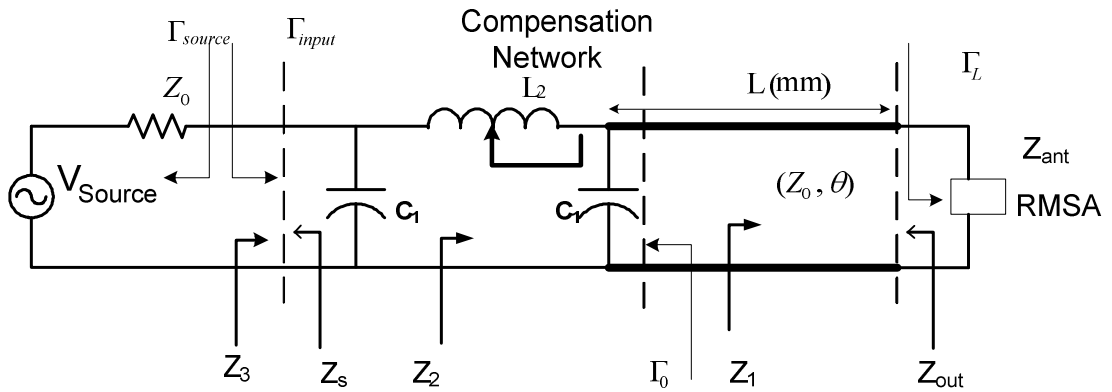


Figure 4.5 Equivalent circuit model both matched to source and the antenna

System input impedance is depended Pi-network components and transmission line characteristics and antenna parameters. Input impedance of this system is obtained $Z_3=Z_{in}$

$$Z_{in} = \frac{\left\{ -j(C_1 L_2 X_L \omega^2 - L_2 \omega - X_L - jR_L (C_1 L_2 \omega^2 - 1)) \cos(\beta l) + \right.}{\left. \left((C_1 L_2 \omega^2 - 1) Z_0^2 + L_2 (X_L - jR_L) \omega \right) \sin(\beta l) \right\}}{\left\{ A \cos(\beta l) + B \sin(\beta l) \right\}}$$

$$A = (Z_0 (C_1^2 L_2 (X_L - jR_L) \omega^3 - C_1 (-2jR_L + 2X_L + L_2 \omega) \omega + 1)) \quad \text{Eq. (4.9)}$$

$$B = (C_1 \omega (C_1 L_2 \omega^2 - 2) Z_0^2 - jR_L (C_1 L_2 \omega^2 - X_L (C_1 L_2 \omega^2 - 1)))$$

where R_L and X_L represent antenna real and imaginary impedances.

It is seen that the impedance matching is achieved a specific impedance domain and the input impedance control is dependent many circuit parameters. From a design point of view, it is essential to know the limits of a matching network, that is,

what impedances can and cannot be conjugate matched at a specific frequency. This is useful of course as an initial investigation can be carried out to evaluate whether certain loads can be matched at certain operating frequencies. If they cannot, then the network must be redesigned and the process will be repeated. When sensitivity analysis is the main consideration, the parametric explanation is more significant.

4.2.2 Analytical solution of compensation network under load condition

Pi-Network used for the impedance matching network, the circuit model is shown in Figure 4.6 (Kaya & Yüksel, 2006; Mingo, Valdovinos, Crespo, Navarro, & Garcia, 2004). Z_L represents the complex load impedance such as antenna. Z_1 , Z_2 , and Z_3 represent the impedance of the network at each stage from the load to the source.

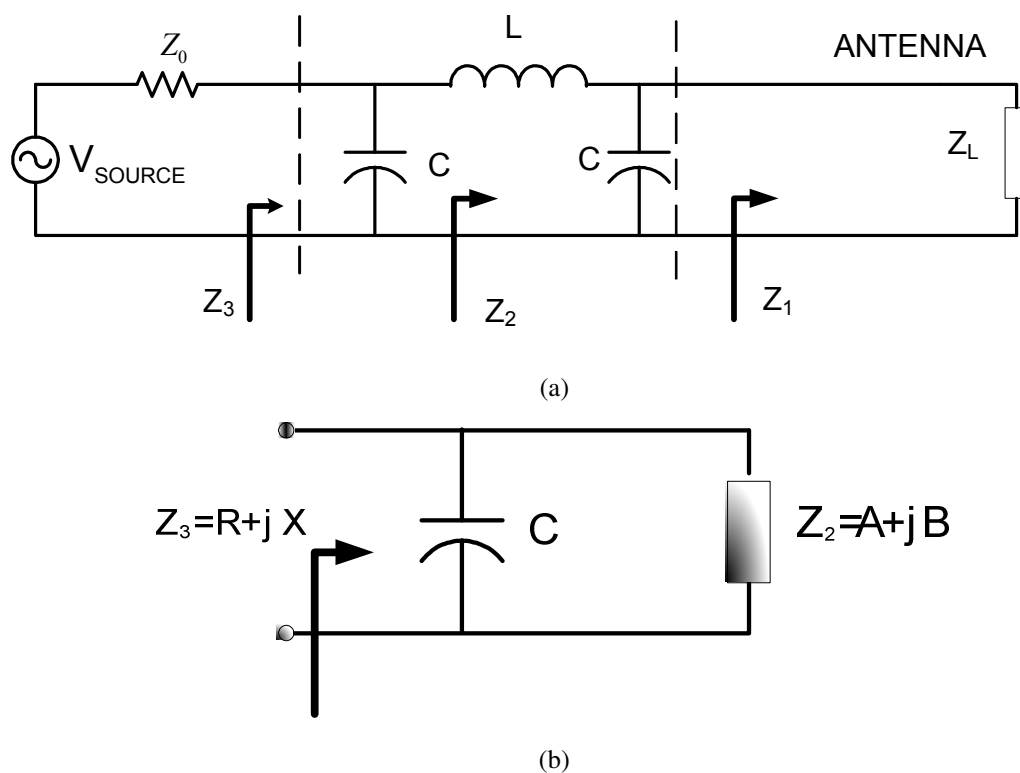


Figure 4.6 Equivalent circuit model both matched to source and antenna

In order to achieve conjugate impedance matching and hence maximum power transfer from the transmitter to the load, Z_3 needs to equal the complex conjugate of

the load impedance Z_L . Input impedance of *Pi*-compensation circuit, is represented as $Z_3=R+jX$, and these equations are given by

$$R = \frac{Z_{ANT}}{1 + \omega^2 C (\omega^2 CL - 2) (\omega^2 C^2 LZ_{ANT}^2 - 2CZ_{ANT}^2 + L)} \quad \text{Eq. (4.10)}$$

$$X = \frac{\omega L - 2\omega CZ_{ANT}^2 - \omega^3 CL^2 + 3\omega^3 C^2 LZ_{ANT}^2 - \omega^5 C^3 L^2 Z_{ANT}^2}{1 + \omega^2 C (\omega^2 CL - 2) (\omega^2 C^2 LZ_{ANT}^2 - 2CZ_{ANT}^2 + L)} \quad \text{Eq. (4.11)}$$

The new equations are needed for investigating the changing in according to one parameter when the input impedance is finding. These parameter limit values can be found by implementation of these new functions. These equations may be useful in design and analysis stage. Z_2 impedance is represented $Z_2=A+jB$. The following impedances may be described for in Figure 4.6 (b).

$$R = \frac{A}{(A\omega C)^2 + (B\omega C - 1)^2} \quad \text{Eq. (4.12)}$$

$$X = \frac{B - \omega C (A^2 + B^2)}{(A\omega C)^2 + (B\omega C - 1)^2} \quad \text{Eq. (4.13)}$$

Dividing (4.13) by (4.12) the following expression for C_2 may be obtained:

$$\omega C = \frac{BR - AX}{R(A^2 + B^2)} \quad \text{Eq. (4.14)}$$

Substitution of (4.14) into (4.12) and (4.13), one can drive

$$\left(R - \frac{A^2 + B^2}{2A} \right)^2 + X^2 = \left(\frac{A^2 + B^2}{2A} \right)^2 \quad \text{Eq. (4.15)}$$

where

$$A = \frac{Z_{ANT}}{1 + (\omega CZ_{ANT})^2}$$

$$B = \frac{(\omega L - \omega CZ_{ANT}^2 + \omega^3 C^2 LZ_{ANT}^2)}{1 + (\omega CZ_{ANT})^2} \quad \text{Eq. (4.16)}$$

It is seen that circle center points and radius are depended loads. At the same time, radian frequency is very important for the circle position. The circle centre and radius can be tuned when the any parameter is selected for controlling. Some approximations can be done for impedance boundary conditions under load, from these equations. The following equations can be derived for determining the geometrical place of impedances as a changing capacitor and inductance values one by one.

$$\frac{X}{R} = \frac{\omega L - 2\omega C Z_{ANT}^2 - \omega^3 C L^2 + 3\omega^3 C^2 L Z_{ANT}^2 - \omega^5 C^3 L^2 Z_{ANT}^2}{Z_{ANT}} \quad \text{Eq. (4.17)}$$

The inductance value can be obtained from (4.17) and is given by

$$\omega L = \frac{R\omega + 3\omega^3 C^2 R Z_{ANT}^2 \pm \omega \sqrt{R \left(R - 4\omega C X Z_{ANT} - 2(\omega C)^2 Z_{ANT} - 4(\omega C)^3 X Z_{ANT}^3 + (\omega C)^4 R Z_{ANT}^4 \right)}}{2R(\omega^2 C + \omega^4 C^3 Z_{ANT}^2)}. \quad \text{Eq. (4.18)}$$

The impedance region created by the Pi network may be plotted simply fixing capacitance (C) value at fix values while allowing the inductance (L) values to vary between its extreme values. This process can be repeated until each of the components has been varied. Substitution of the (4.10) in to (4.11) gives rise to the following equation

$$4Z_{ANT} \left(Z_{ANT} (1 + \omega C X)^2 + R(-1 + \omega^2 C^2 Z_{ANT} (R - Z_{ANT})) \right) = 0. \quad \text{Eq. (4.19)}$$

The impedance arcs obtained when L_2 is varied between its minimum and maximum values while C_1 and Z_{ANT} are held constant maybe expressed as following circular expression:

$$\left(R - \frac{1 + \omega^2 C^2 Z_{ANT}^2}{2\omega^2 C^2 Z_{ANT}} \right)^2 + \left(X - \frac{-1}{\omega C} \right)^2 = \left(\frac{1 + \omega^2 C^2 Z_{ANT}^2}{2\omega^2 C^2 Z_{ANT}} \right)^2 \quad \text{Eq. (4.20)}$$

Center of the circle and radius can be obtained depending on the frequency form the (4.15) equation. Finally, when the total input impedance is expanded complex, the impedance may be derived as (Kaya, Günel & Yüksel, 2005)

$$Z_{in} = \frac{R_L}{\xi} + j \left(\frac{X_L + \frac{\omega L_2}{\xi} - \frac{2\omega C_1 R_L^2}{\xi} - \frac{2\omega C_1 X_L^2}{\xi} - \frac{4\omega^2 C_1 L_2 X_L}{\xi}}{\xi} - \frac{\omega^3 C_1 L_2^2}{\xi} + \frac{3\omega^3 C_1^2 L_2 R_L^2}{\xi} + \frac{3\omega^3 C_1^2 L_2 X_L^2}{\xi} - \frac{\omega^5 C_1^3 L_2^2 R_L^2}{\xi} - \frac{\omega^5 C_1^3 L_2^2 X_L^2}{\xi} \right) \quad \text{Eq. (4.21)}$$

$$\xi = \left(2C_1\omega R_L + C_1^2\omega^3 R_L \right)^2 + \left(1 + C_1^2\omega^3 L_2 X_L - C_1\omega(2X_L + L_2\omega) \right)^2$$

where $Z_{ANT}(\Omega) = R_L + jX_L$ is the impedance of the seen by the antenna input.

The impedance region created by the Pi network may be plotted as shown in Figure 4.7 and 4.8 by fixing C_1 and Z_L component value while allowing the L component vary between its extreme values. It is clearly seen that the return loss levels are very low because the values of R and X remain the same for the Z_L 50 Ω load condition. The input impedance can reach sufficient values when the L inductance value is changed between specific values. The inductance values are determined from the above equations.

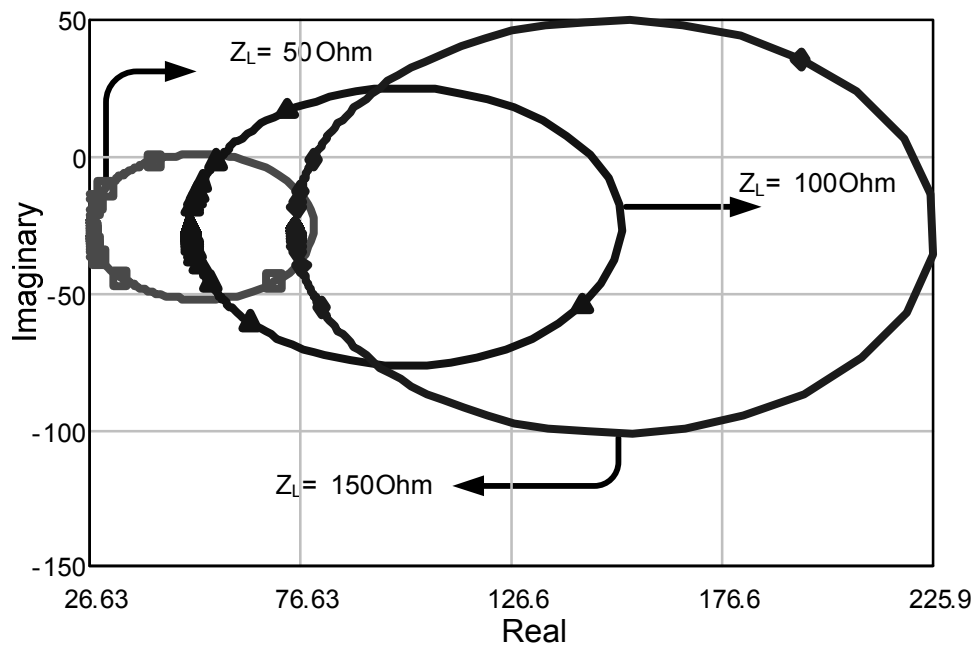


Figure 4.7 Impedance region of the Z_{in} ($f=2.5$ GHz, $C_1=5$ pF and L range between 0.1 nH~20 nH)

The inductance component related to other components is given by

$$L_2 = \frac{2C_1 R_L^2 + C_1^2 R_L^2 X_L \omega + C_1^2 X_L^3 \omega}{2(C_1 X_L \omega - 1)} \quad \text{Eq.(4.22)}$$

In order to illustrate how these equations may be used in the development of the impedance of the Pi-network, consider above examples and as shown in Figure 4.7. The return loss is shown in Figure 4.8 for the different loads.

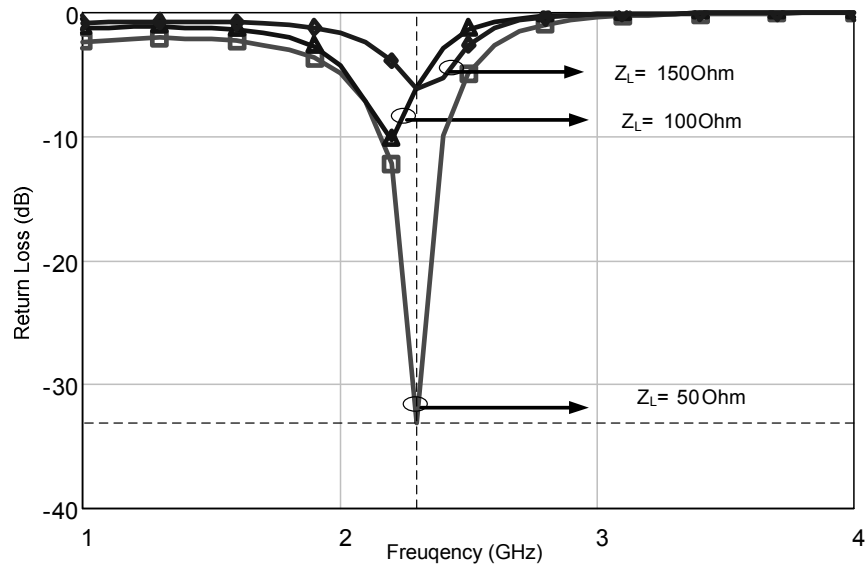


Figure 4.8 Return Loss parameter ($C_1=5$ pF and $L=2$ nH)

Γ_{source} is the source reflection coefficient required to be seen from the antenna system input terminals.

$$\Gamma_{in} = \frac{\left(\begin{aligned} &\omega C_2 (R_L + jX_L) + Z_0 (J^2 Z_0 (j - 2C_1 \omega (R_L + jX_L))) \\ &+ C_2 \omega (1 + C_1 \omega Z_0 (-j + C_1 \omega (R_L + jX_L))) \end{aligned} \right)}{\left(\begin{aligned} &-\omega C_2 (-j + C_1 \omega Z_0) (-jR_L + X_L - jZ_0 + C_1 \omega Z_0 (R_L + jX_L)) \\ &+ J^2 Z_0 (2X_L - 2jR_L - jZ_0 + 2C_1 \omega Z_0 (R_L + jX_L)) \end{aligned} \right)} \quad \text{Eq.(4.23)}$$

where $\Gamma_{opt}(f)$ is the reflection coefficient corresponding to maximum power transfer to the antenna. The resonant frequency and BW can be controlled by using Pi-matching network with tuning L_2 inductance and so the reflection coefficient at

the input antenna terminals which is represented ($\Gamma_{in}(f) = \Gamma_{opt}(f)$) can be controlled.

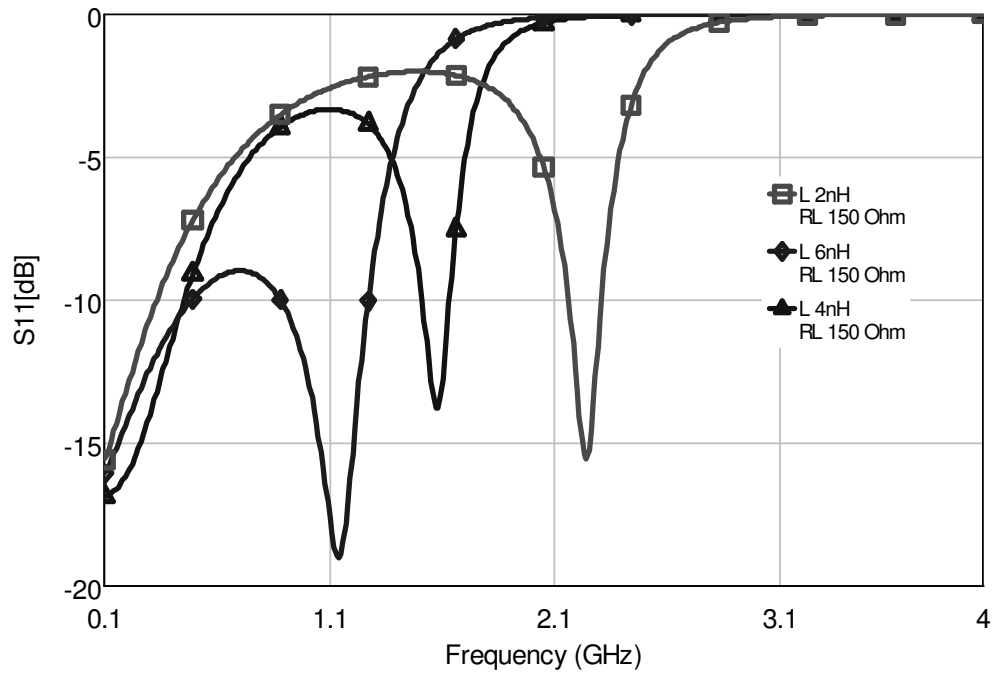


Figure 4.9 Reflection parameter of the antenna for different L_2

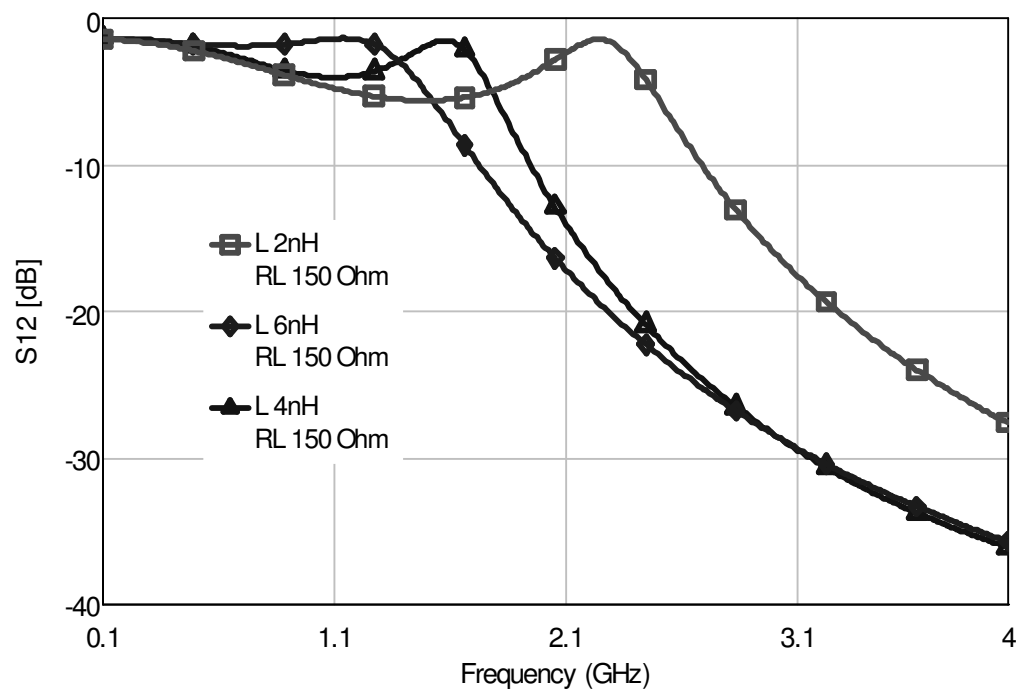
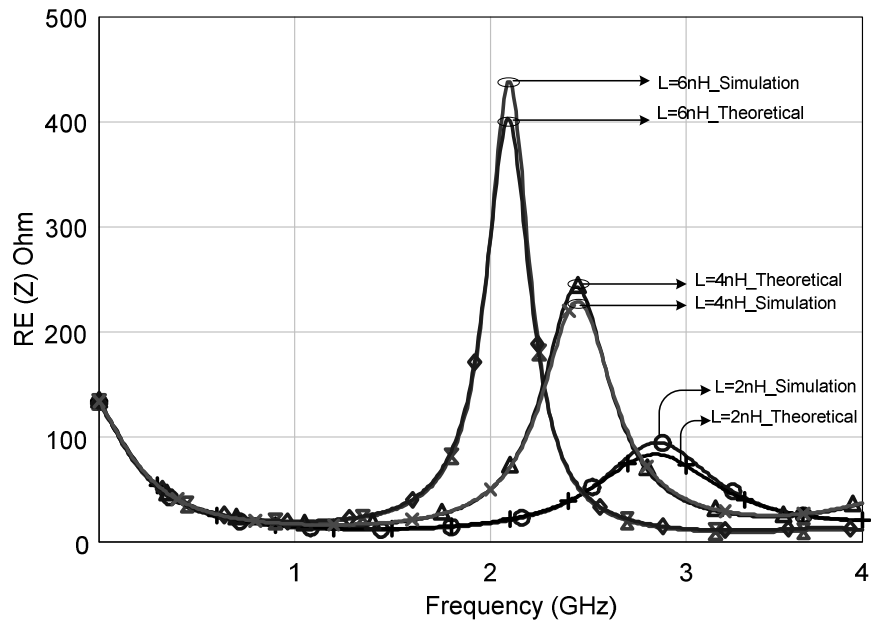
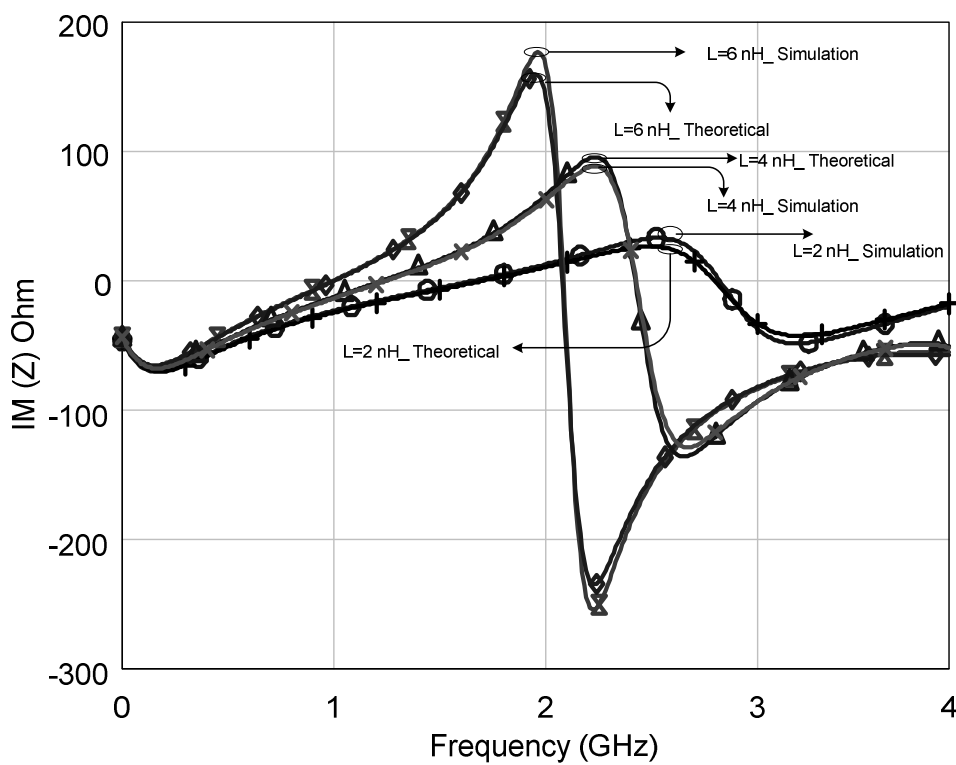


Figure 4.10 Transmission parameter of the antenna for different L_2



(a)



(b)

Figure 4.11 Theoretical and simulation results for the compensated system: (a) Variation of real part of the impedance (b) Variation of imaginary part of the impedance versus frequency ($C_1=5pF$, $l=20\text{ mm}$ & $R_L=150\text{ Ohm}$)

When the circumferences are more complex and close to the application form, the obtained simulation results by using AWR microwave simulation pocket (MoM) and the theoretical results by using (4.9) are shown in Figure 4.8 - Figure 4.11. From the figures, it can be seen that the impedance graphics are well agreed. The system impedance characteristics are changed when the transmission line is added such as in Figure 4.5. When the parametric components of $C_I=5$ pF, $l=20$ mm & $R_I=150$ Ohm are selected, Figure 4.9 and Figure 4.10 are obtained. There is a significant difference between the different inductance values for the return loss parameter and it is predicted that resonance points are shifted under constant loads as shown in Figures 4.8 and 4.11.

A design option for impedance inverters consists on utilizing $\lambda_g/4$ transmission line inverters, which have a normal size at frequencies 2.5 GHz. Pi- circuit layout is shown in Figure 4.12.

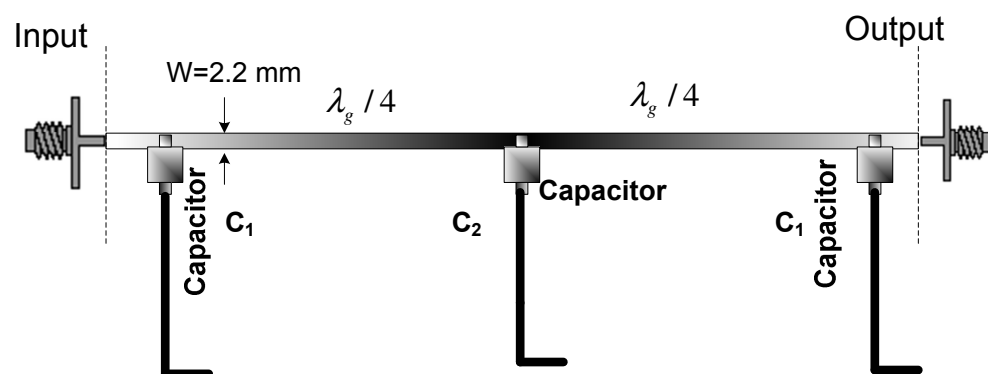


Figure 4.12 Pi-circuit layout

If the rectangular microstrip antenna connected as a load, some of the results obtained are shown in Figure 4.13 and 4.14. The rectangular microstrip antenna designed for this application is printed on TLY-5A substrate material manufactured by Taconic, which has a relative permittivity of 2.17 and a thickness (h) of 0.52 mm. The patch dimensions of $W=40$ mm and $L=40$ mm, are selected along with the ground plane dimensions of 80×80 mm.

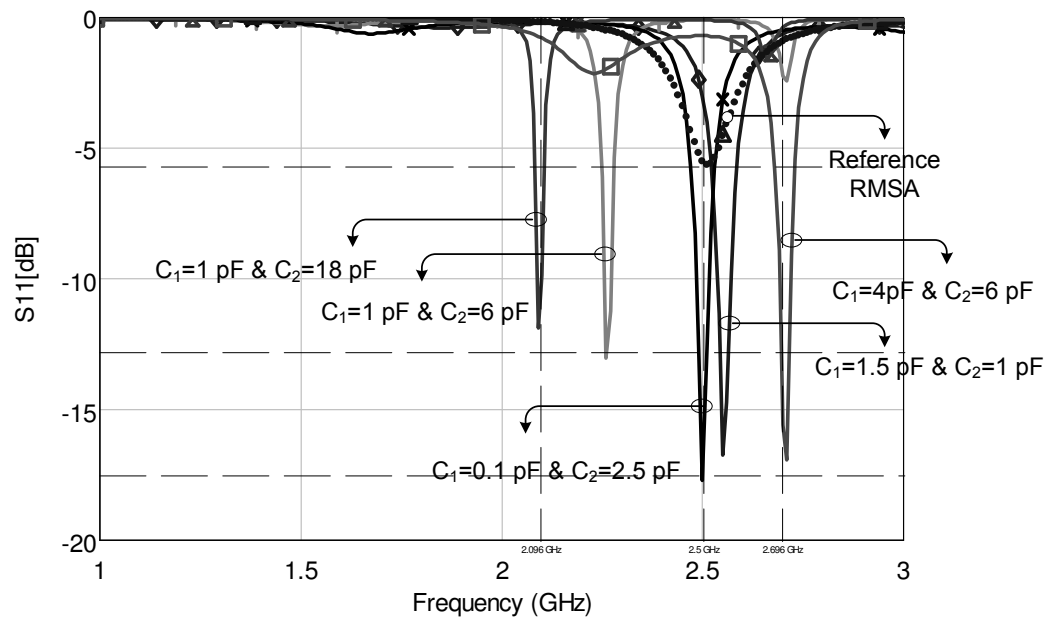


Figure 4.13 Simulation results for the compensated system (only capacitors) RMSA dimensions; $40 \times 40 \times 0.52$ mm and $\epsilon_r = 2.17$

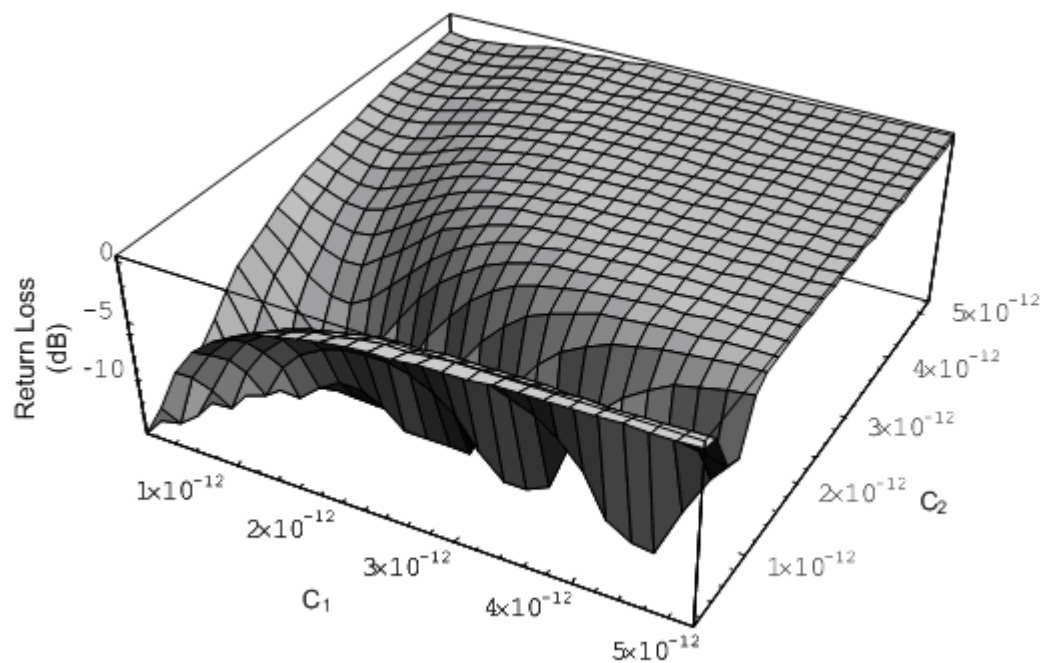


Figure 4.14 3-D Simulation results for the compensated system ($f = 2.5$ GHz) RMSA dimensions; $40 \times 40 \times 0.52$ mm and $\epsilon_r = 2.17$

4.3 Mutators and Generalized Mutators

The mutator is defined for the purpose of transforming one type of network element into another. An R - L mutator will transform a nonlinear resistor into a nonlinear inductor, and vice-versa. An R - C mutator will transform a nonlinear resistor into a nonlinear capacitor, and vice versa. A third type of mutator, the C - L mutator, will transform a nonlinear capacitor into a nonlinear inductor, and vice versa. For example an L - R mutator transforms a resistor characterized by the relation $u = f(i)$ into an inductor characterized by $\varphi = f(i)$.

This section gives brief information of expressed for the purpose of transforming one type of network element into another. R - C type mutator is investigated and two port relations are derived (Goras, 1981). In this section, R - C type mutator is used because the capacitor values can be controlled with resistive components in R - C mutator efficiency.

The symbol for a type R - C mutator is shown in Figure 4.15 and simple realization using controlled sources is shown in Figure 4.16.

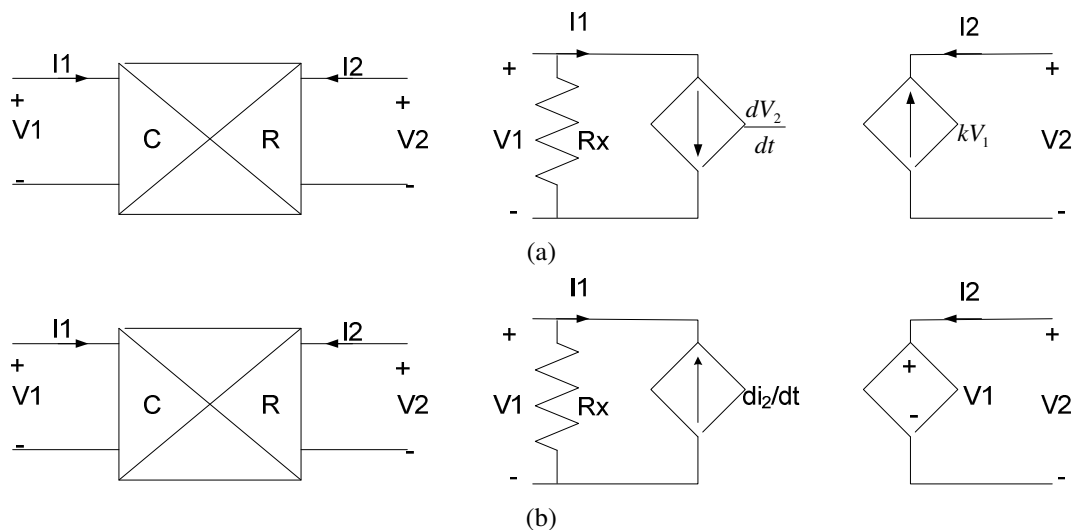


Figure 4.15 Symbolic RC mutator and a controlled source realization (a) Type 1 (b) Type 2

The values R_x , I_2 and C are given as

$$R_x \frac{dV_2(t)}{dt} k = I_2(t) \quad \text{Eq.(4.24)}$$

$$I_2(t) = C \frac{dV_2(t)}{dt} \quad \text{Eq.(4.25)}$$

$$C = kR_x \quad \text{Eq.(4.26)}$$

Hereafter capacitor can be controlled linearly.

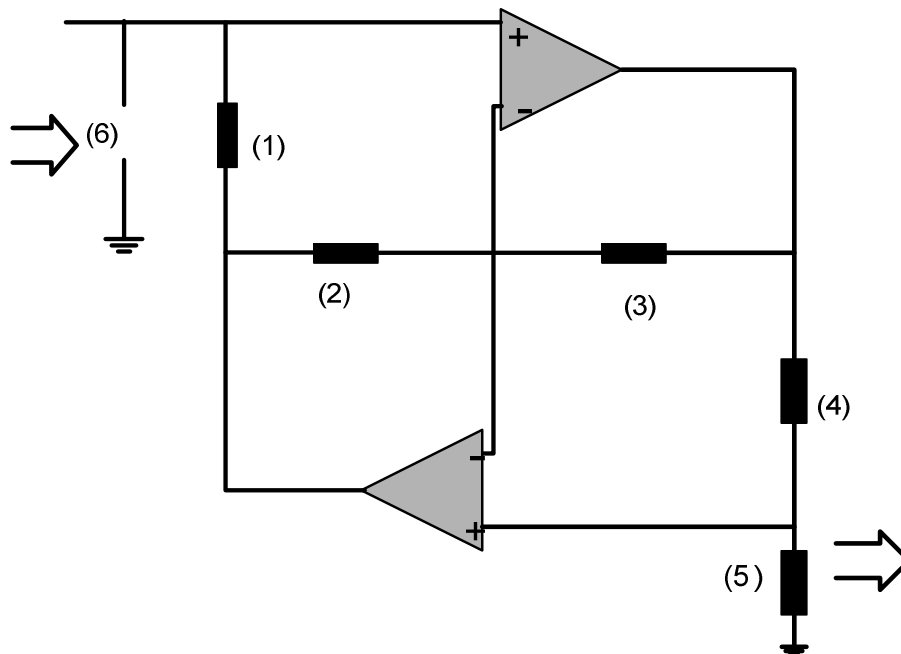


Figure 4.16 Configuration of mutator viewed as a six port

This mutator transforms a type 2 terminal element into other 2 terminal elements. There are many possibilities and a different kind of mutators can be obtained. However, usually the transmission matrix is the same. This mutator has a fundamental role in the system impedance synthesis. Meantime, it reduces from the general nonlinear element realization problem to the synthesis of 2-terminal nonlinear resistors.

The different transmission matrices corresponding to the selection of the output port for linear and nonlinear cases are summarized in Table 4.1 (Goras, 1981). In the following we use the structure of Figure 4.16 with port 6 as the input (grounded), one

of the remaining ports (ungrounded except port 5) as the output of a two-port, the rest of the ports being terminated with linear or nonlinear resistors. The results summarized in Table 4.1 show the possibility of obtaining a large number of mutators (generalized mutators) using the configuration presented in Figure 4.16.

Table 4.1. Configuration of the mutator

| Output port; Inner port with capacitor | Transmission matrix | | Type of Mutator |
|--|---|--|-----------------|
| | Nonlinear Case | Linear Case | |
| 1;5 | $\begin{bmatrix} \frac{1}{C} \int_0^t (i_4 \circ u_3 \circ i_2)(\cdot) dt & 0 \\ 0 & 1 \end{bmatrix}$ | $\begin{bmatrix} \frac{G_4 R_3 G_2}{C_s} & 0 \\ 0 & 1 \end{bmatrix}$ | RL_1 |
| 2;5 | $\begin{bmatrix} 0 & \frac{1}{C} \int_0^t (i_4 \circ u_3) dt \\ i_1(\cdot) & 0 \end{bmatrix}$ | $\begin{bmatrix} 0 & \frac{G_4 R_3}{C_s} \\ G_1 & 0 \end{bmatrix}$ | RC_2 |
| 4;2 | $\begin{bmatrix} 0 & u_5(\cdot) \\ i_1 \circ \frac{1}{C} \int_0^t i_3(\cdot) dt & 0 \end{bmatrix}$ | $\begin{bmatrix} 0 & R_5 \\ \frac{G_1 G_3}{C_s} & 0 \end{bmatrix}$ | RL_2 |
| 5;2 | $\begin{bmatrix} 1 & 0 \\ 0 & i_1 \circ \frac{1}{C} \int_0^t i_3 \circ u_4(\cdot) dt \end{bmatrix}$ | $\begin{bmatrix} 1 & 0 \\ 0 & \frac{G_1 G_3 R_4}{C_s} \end{bmatrix}$ | RC_1 |
| 5;4 | $\begin{bmatrix} 1 & 0 \\ 0 & i_1 \circ u_2 \circ i_3 \frac{1}{C} \int_0^t (\cdot) dt \end{bmatrix}$ | $\begin{bmatrix} 1 & 0 \\ 0 & \frac{G_1 G_3 R_2}{C_s} \end{bmatrix}$ | RC_1 |
| 5;3 | $\begin{bmatrix} 1 & 0 \\ 0 & i_1 \circ u_2 \circ C \frac{\partial u_4(\cdot)}{\partial t} \end{bmatrix}$ | $\begin{bmatrix} 1 & 0 \\ 0 & G_1 R_4 R_2 C_s \end{bmatrix}$ | CR_1 |

Output port = port 6 ; ° denotes functional composition

The linear and nonlinear cases can be derived from each other by means of the correspondence ($u_j \longleftrightarrow R_j$; $i_j \longleftrightarrow G_j$; " \circ " \longleftrightarrow ".") (Goras, 1981).

4.3.1 Single Capacitor R-C Mutator

The R-C mutator can be built using only op amps operating high frequencies and linear passive resistors and capacitors. In the frequency domain, The Figure 4.17's equation is equivalent to the following transmission matrix:

$$ABCD_{mutator} = \begin{pmatrix} 1 & 0 \\ 0 & \frac{G_1 G_3 R_4}{C_x s} \end{pmatrix} \quad \text{Eq.(4.27)}$$

$$ABCD_{R_x} = \begin{pmatrix} 1 & 0 \\ \frac{1}{R_x} & 1 \end{pmatrix} \quad \text{Eq.(4.28)}$$

In here, the RC mutator configuration is selected as shown in Figure 4.17.

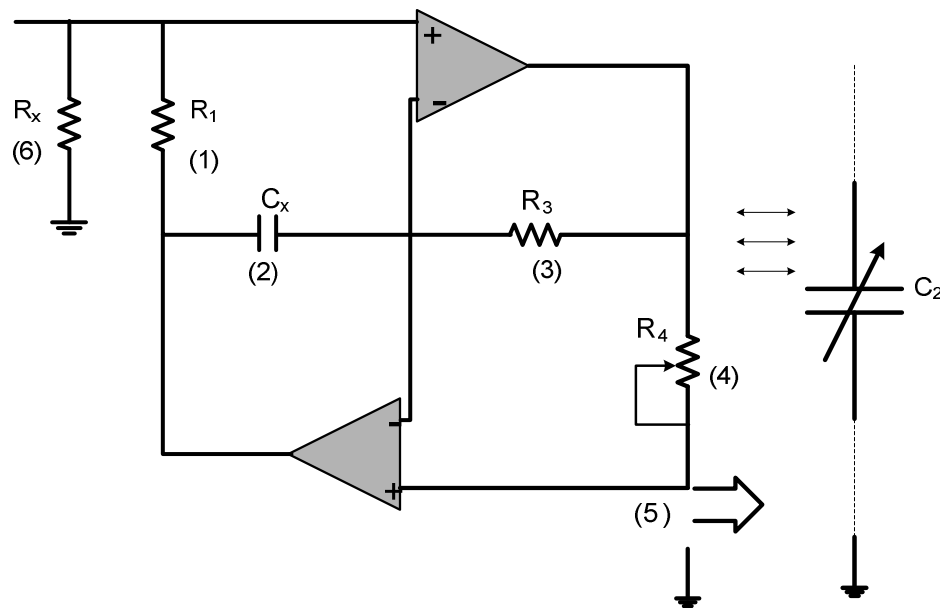


Figure 4.17 Configuration of RC Mutator

If the R_x resistor is connected to the input of the circuit, at the output of the circuit Z_{port} can be written as

$$Z_{port} = \frac{G_1 G_3 R_4 R_x}{s C_x} \quad \text{Eq. (4.29)}$$

Some resistor controlled RC mutator and the only C capacitor values are shown in Figure 4.18. The RC mutator circuit is simulated using the model in Figure 4.17

which has $C_x = 3.3$ pF, $R_l = 10$ Ω , $R_3 = 100$ Ω , $R_x = 10$ Ω , $R_4 =$ controlling parameter Ω . The capacitor results obtained from the mutators are shown in Figure 4.18 for variable R_4 values.

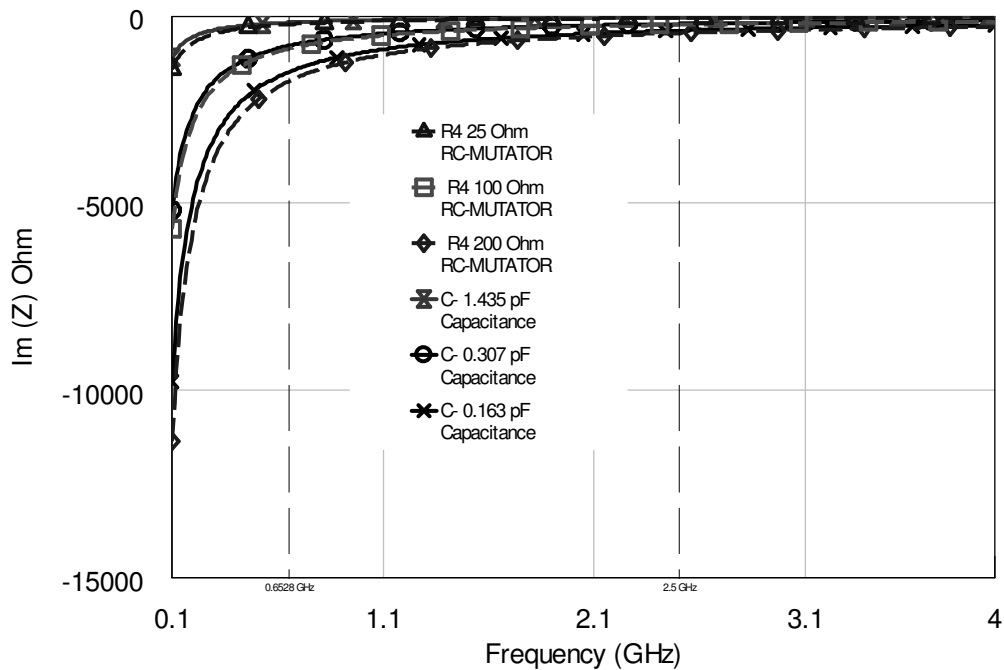


Figure 4.18 Comparison results of the R - C mutator and capacitor

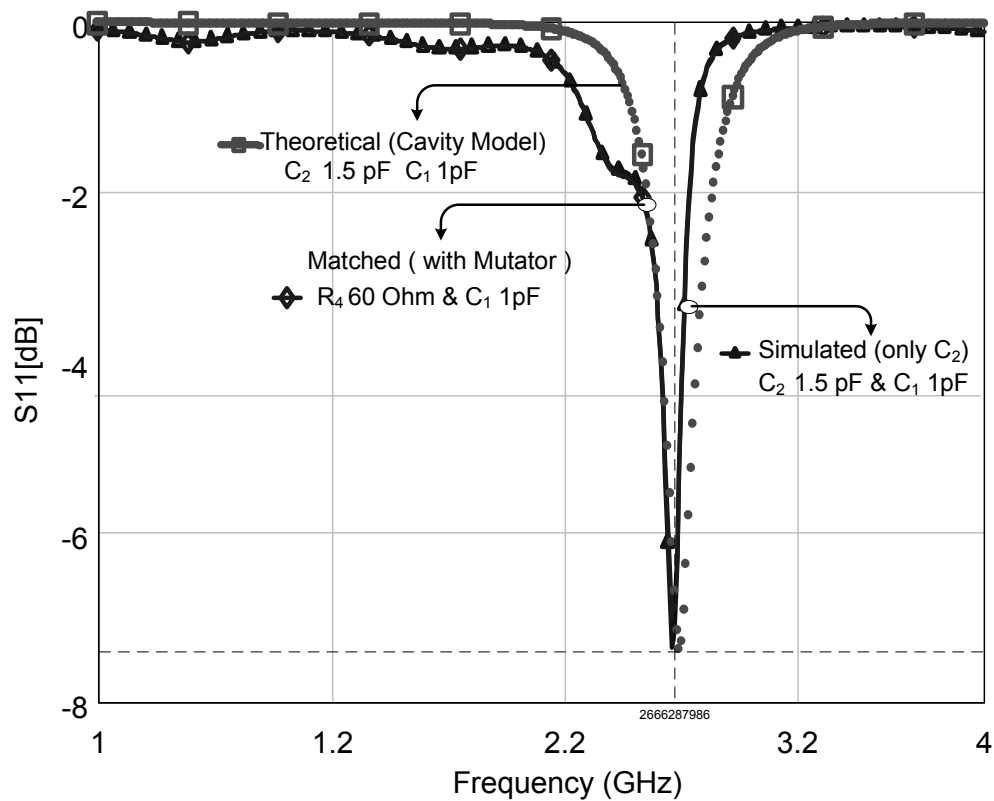
Results indicate that this controllable RC mutator circuit can be utilized in matching systems effectively. The linear mutators can be used to nonlinear capacitor.

4.4 Input Impedance Analysis of Rectangular Microstrip Antenna with Pi Matching Network using RC Mutator

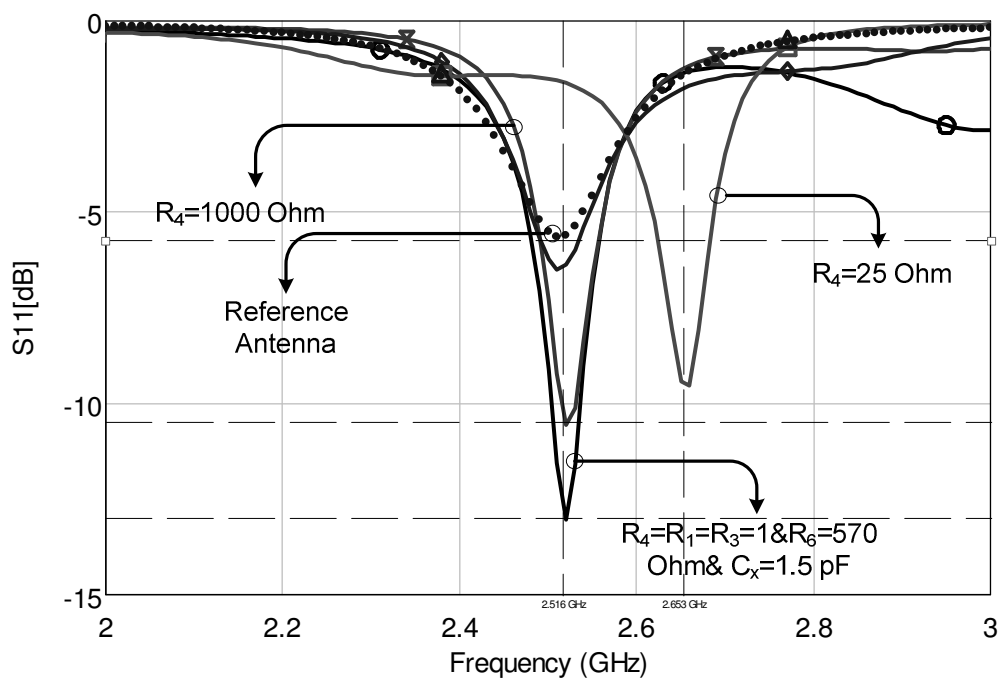
The new proposed method is used RC mutator as a C_2 capacitor as shown in Figure 4.17. The RC mutator has some advantages:

(i) wide microwave frequency band (ii) can be realized with MMIC (monolithic microwave integrated circuit) process (iii) works on the high power application (iv) and C values are controlled only changing R values.

When the rectangular microstrip antenna connected as a load, the obtained results are shown in Figure 4.19. TLY5 substrate fabricated by Taconic firm was selected.



(a)



(b)

Figure 4.19 Simulation results for the compensated system (C_2 Mutator, and $C_1 = 1 \text{ pF}$)
 RMSA dimensions; $40 \times 40 \times 0.52$ & l (length) 20 mm and $\epsilon_r = 2.52$

Table 4.2 RC mutator component values

| C_x | $R_1 \Omega$ | $R_3 \Omega$ | $R_x \Omega$ | $R_4 \Omega$ | $C_2(F)$ |
|-------|--------------|--------------|--------------|--------------|------------------------|
| 3 pF | 7 | 25 | 12 | 1000 | $4.375 \cdot 10^{-14}$ |
| 3 pF | 7 | 25 | 12 | 50 | $8.75 \cdot 10^{-13}$ |
| 3 pF | 7 | 25 | 12 | 25 | $1.75 \cdot 10^{-12}$ |
| 4 pF | 1 | 1 | 570 | 1 | $7.01 \cdot 10^{-15}$ |

The some C_2 values couldn't be obtained practically but with this technique can be possible. The return loss characteristics $|S_{11}|$ for compensated circumferences are shown in Figure 4.19. The reference antenna isn't defined with a return loss better than -10 dB within a percent bandwidth. The reference antenna is become more efficiency with pi-matching circuit. This technique not only improves the bandwidth but also lowers the deep point of the return loss characteristics at the resonant frequency. The simulation results are also summarized in Table 4.3 for the bandwidth and the return loss parameters. These results are very attractive for broadband communications.

Table 4.3 Comparison of the Performances

| Configuration | $ S_{11} $ | BW | f_r (GHz) |
|---------------------------------------|------------|-------|----------------|
| Reference Antenna | -5.58 dB | -- % | 2.5 |
| R_4 1000 Ω | -10.44 | 3.2 % | 2.44 |
| R_4 1 Ω & R_x 570 Ω | -13.01 dB | 3.6 % | 2.46 |
| R_4 25 Ω | -9.48 dB | -- % | 2.66 |

The return loss minimum level is increased from -5.58 dB to -13.01 dB and these levels can be more improved by constitute more compatible conditions. For these variable circumferences, 3-D simulations results are shown in Figure 4.20. However, when the matching level is greater than the -10 dB, resonant frequency points can be a slightly shift but it may be ignored since this does not affect antenna performance.

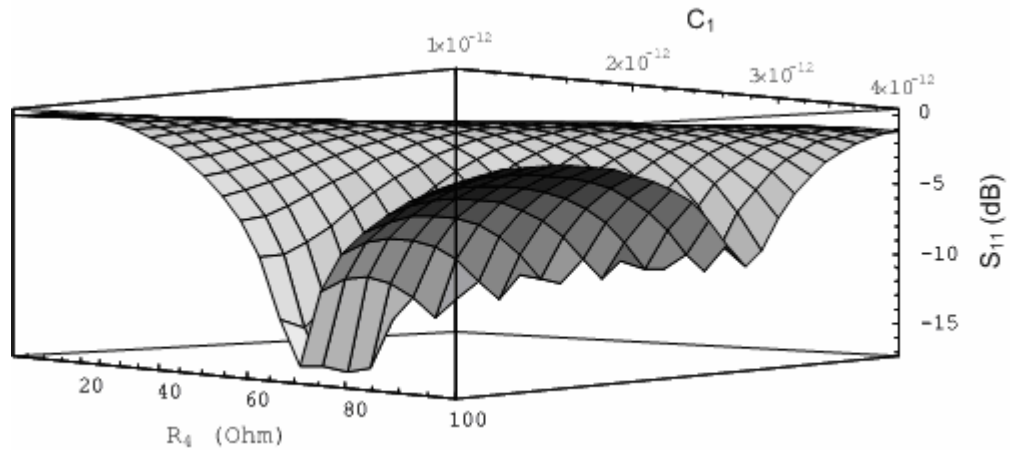


Figure 4.20 3-D Simulation results for the compensated system at $f=2.5$ GHz (C_2 mutator and configurations: $C_x=4$ pF, $R_l=10$ Ω , $R_3=25$ Ω , $R_x=10$ Ω)

The other important parameter is radiation pattern. The antenna has to radiate in defined impedance bandwidth in Table 4.3.

4.5 Analysis of Radiation Pattern from Compensated RMSA

The radiation patterns of the antenna are of prime importance in determining most of its radiation characteristics such as radiated power. The radiation from the patch can be derived from the E_z field across the aperture between the patch and the ground plane (employing the vector magnetic potentials). The radiation mechanism is clearly shown in Figure 4.21. The radiation patterns of the antenna can be determined from the far-zone fields in the air region ($z \gg h$).

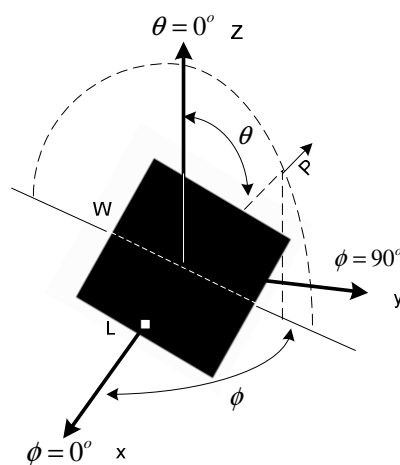


Figure 4.21 Radiation pattern

The phase stationary-phase point (θ, ϕ) is defined as (Garg, et al., 2001)

$$\begin{aligned} k_x &= k_0 \sin(\theta) \cos(\phi) \\ k_y &= k_0 \sin(\theta) \sin(\phi) \\ \beta^2 &= k_x^2 + k_y^2 \\ \beta &= k_0 \sin(\theta) \end{aligned} \quad \text{Eq.(4.30)}$$

The current density expressed in terms of a single entire domain basis function with the current in the x direction can be written as (Perlmutter, Shrikmann & Treves, 1985).

$$J_{nx} = \frac{V_0}{Z_0 W} \sin\left(\frac{n\pi}{L}(x - L/2)\right) \text{for} \begin{cases} -L/2 \leq x \leq L/2 \\ -W/2 \leq y \leq W/2 \end{cases} \quad \text{Eq.(4.31)}$$

where V_0 is the voltage at $x=L/2$ and Z_0 is the characteristic impedance of the microstrip line of which the patch is a segment. The radiation pattern for the TM_{10} mode ($n=1$) then become

$$F(J_{1x}) = \frac{V_0}{Z_0} \frac{(2\pi/L) \cos(\pi k_x / (2k_0 \sqrt{\epsilon_{re}}))}{k_0^2 \epsilon_{re} - k_x^2} \text{Sinc}(k_y W / 2) \quad \text{Eq.(4.32)}$$

The principal plane power patterns are obtained for the $\phi = 0^\circ$ plane or E-plane pattern:

$$E_\theta(r, \theta, \phi) = \frac{\eta_0}{2\pi r} e^{-jk_0 r} F(J_{1x}) \frac{k_0 k_1 \sin(k_1 h)}{T_m} \cos(\theta) \cos(\phi) \quad \text{Eq.(4.33)}$$

For the $\phi = 90^\circ$ plane or H-Plane pattern:

$$E_\phi(r, \theta, \phi) = -\frac{\eta_0}{2\pi r} e^{-jk_0 r} F(J_{1x}) \frac{k_0^2 \sin(k_1 h)}{T_e} \cos(\theta) \sin(\phi) \quad \text{Eq.(4.34)}$$

where

$$T_m = \epsilon_r k_2 \cos(k_1 h) + j k_1 \sin(k_1 h) \quad \text{Eq.(4.35.a)}$$

$$T_e = k_1 \cos(k_1 h) + j k_2 \sin(k_1 h) \quad \text{Eq.(4.35.b)}$$

$$k_1^2 = \epsilon_r k_0^2 - \beta^2 \quad \text{for} \quad 0 < z < h \quad \text{Eq.(4.36.a)}$$

$$k_2^2 = k_0^2 - \beta^2 \quad \text{for } z > h \quad \text{Eq.(4.36.b)}$$

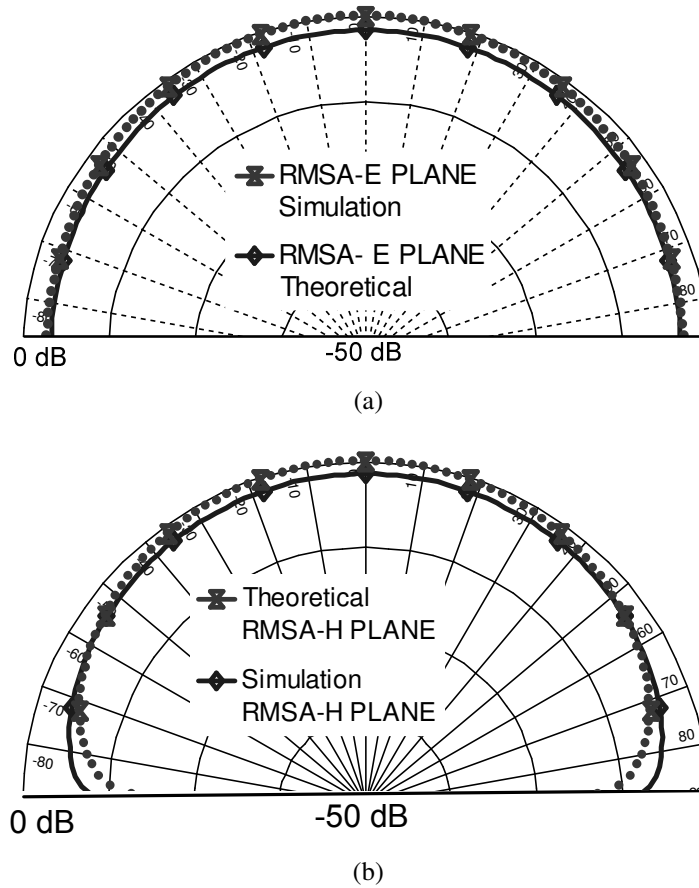


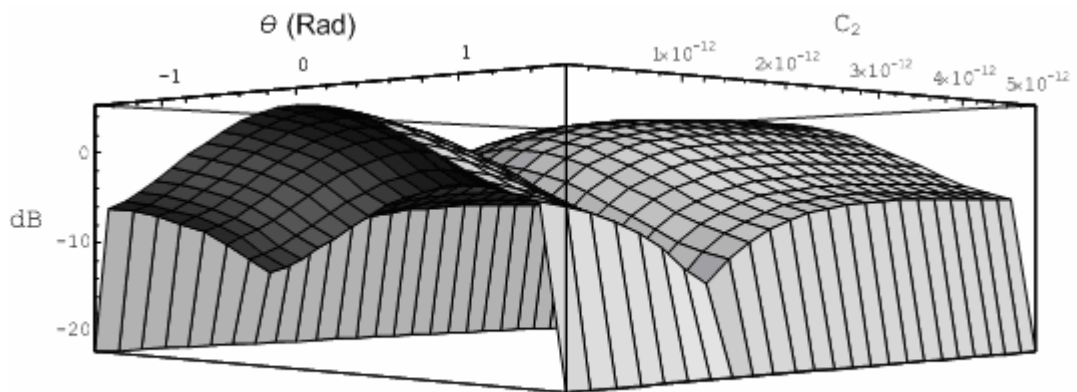
Figure 4.22 Simulated and theoretical radiation pattern of the RMSA (a) E-Plane ($f=2.5$ GHz) (b) H-Plane ($f=2.5$ GHz)

The directivity is a measure of the directional properties of an antenna compared to those of isotropic antenna, and it is defined as the ratio of the maximum power density in the main beam direction to the average power density. The directivity expressed as

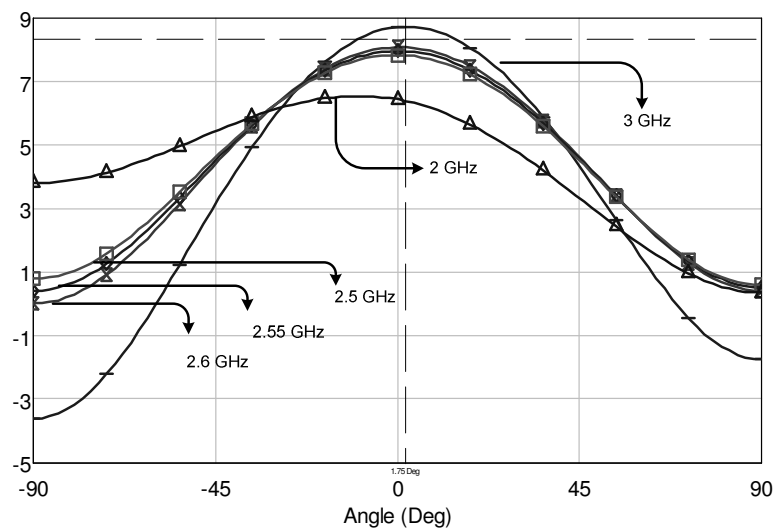
$$D = \frac{\frac{R^2}{2\eta_0} \left(|E_\theta|^2 + |E_\phi|^2 \right) \Big|_{\theta=0}}{P_r / 4\pi} \quad \text{Eq.(4.37.a)}$$

$$G = e_r D \quad \text{Eq.(4.37.b)}$$

where P_r is radiated power, $\eta_0 = 120\pi$ Ohm, and G is the gain, e_r is the radiation efficiency of the antenna. The gain is always less than directivity because e_r lies in the range $0 < e_r < 1$. The directivity increase with increase in substrate thickness and patch width. Conversely, the beamwidth is expected to decrease for higher value of h and W . The simulated and the theoretical radiation patterns are shown in Figure 4.22. As beamwidth increases, antenna gain and directivity decrease.



(a)



(b)

Figure 4.23 (a) Radiation pattern of the 3-D view of compensated system E-Plane ($f=2.5$ GHz)
 (b) E plane pattern for 2-3 GHz frequencies RMSA dimensions; $40 \times 40 \times 0.52$ mm & $\epsilon_r = 2.52$

There are changing in radiation pattern when the C_2 is changing and the 3-D theoretical results are shown in Figure 4.23 (a). The RMSA radiation patterns in different frequencies are shown in Figure 4.23 (b).

4.6 Evaluation of Sensitivities

Sensitivity approach is very useful for determining the behavior of a system due to the first-order effects of parameter variations. It is based on variations in parameter values. The sensitivity of a parameter A with respect to a parameter B is defined as

$$S_B^A = \text{Limit}_{\Delta B \rightarrow 0} \frac{\Delta A / A}{\Delta B / B} \quad \text{Eq.(4.38)}$$

or

$$S_B^A = \frac{B}{A} \frac{\partial A}{\partial B} \quad \text{Eq.(4.39)}$$

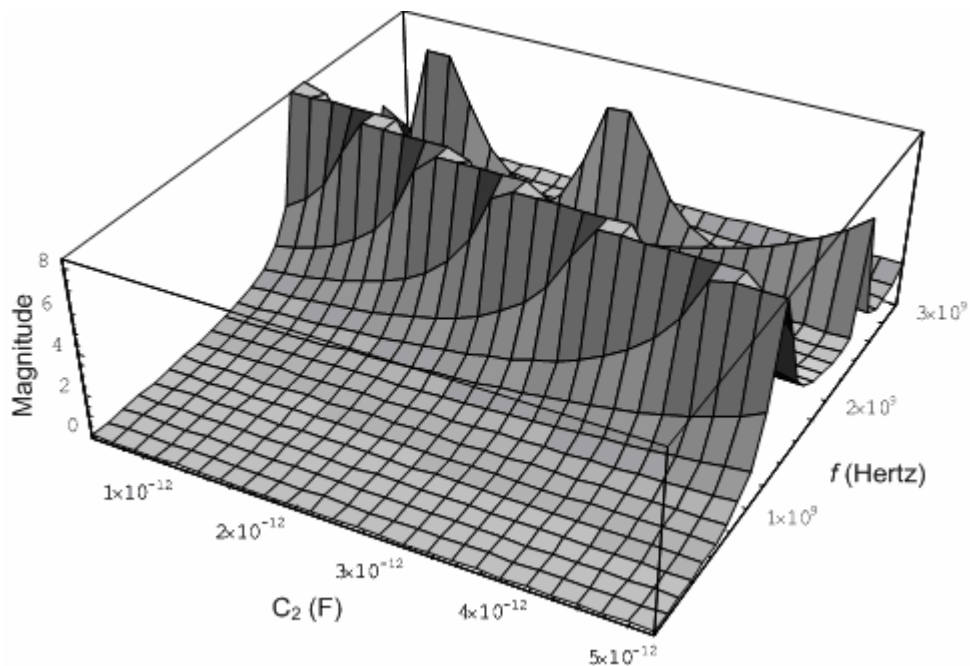


Figure 4.24 Frequency response of sensitivity magnitude for different C_2 and f values.

RMSA dimensions; $40 \times 40 \times 0.52$ mm and $\epsilon_r = 2.52$

The sensitivity, as defined in (4.38) or (4.39), may be utilized to determine the deviation in system characteristics for a given changed in a parameter. The system

characteristics may be, e.g., *VSWR*, insertion loss, isolation. The change in impedance ΔZ of an antenna system is related to the ΔC_2 in parameter C_2 by relation using (4.38)

$$\frac{\Delta Z}{Z_{in}} = \frac{\Delta C_2}{C_2} S_{C_2}^{Z_{in}} \tag{Eq.(4.40)}$$

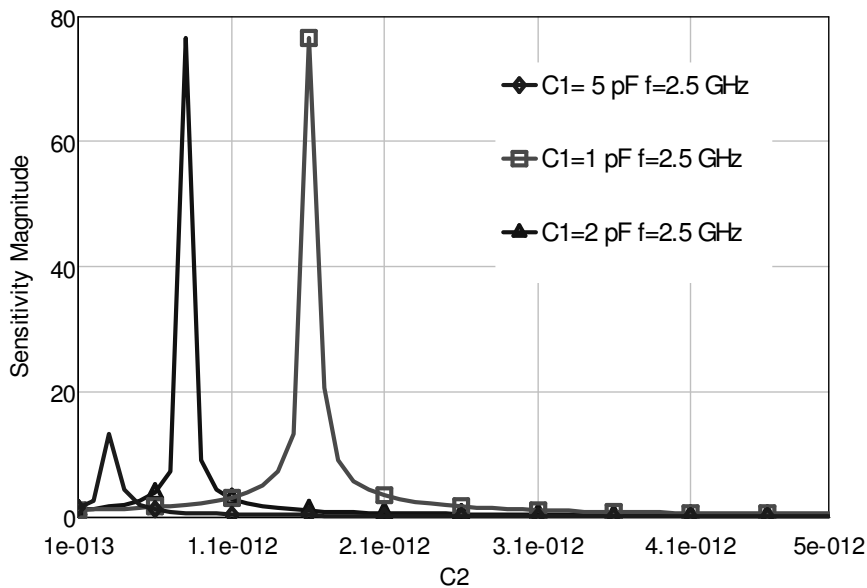


Figure 4.25 Sensitivity of magnitude for different C_2 values. RMSA dimensions; $40 \times 40 \times 0.52$ and $\epsilon_r = 2.52$ & $l=20$ mm

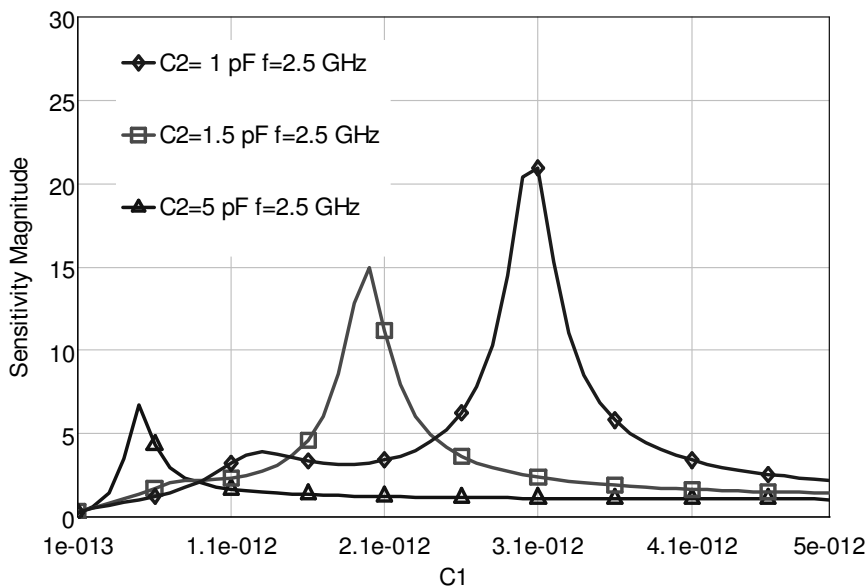


Figure 4.26 Sensitivity of magnitude for different C_1 values. RMSA dimensions; $40 \times 40 \times 0.52$ and $\epsilon_r = 2.52$ & $l=20$ mm

Some magnitude of sensitivity results are shown in Figure 4.24 - 4.26. It is inferred from the figures that some regions are more sensitive than the others.

In addition, deviations in the effective electrical dimensions of the patch antenna from the designed values can lead to differences between the designed and actual resonant frequencies. These deviations may include the variations in the relative permittivity of the substrate material, or nonuniformity in the substrate thickness, or slight variations in the antenna width and length. The effect of fabrication inaccuracies and substrate tolerances on the frequency is considered.

As the statistical nature of the independent variables that determine the resonant frequencies is unknown, a worst-case analysis can be made. If ϕ is a function of independent variables $\phi_1, \phi_2, \dots, \phi_n$ i.e. $\phi = f(v_1, v_2, \dots, v_n)$, which have uncertainties $\Delta v_1, \Delta v_2, \dots, \Delta v_n$ then the uncertainty in the function $\Delta\phi$ is given by

$$\Delta\phi = \sum_{p=1}^n \left[\frac{\partial\phi}{\partial v_p} \right] \Delta v_p \quad \text{Eq.(4.40)}$$

The resonant frequency can be obtained by using tolerance analysis (Garg, 1978) and is given

$$\Delta f_{r_{mn}} = \frac{\partial f_{r_{mn}}}{\partial \epsilon_r} \Delta \epsilon_r + \frac{\partial f_{r_{mn}}}{\partial h} \Delta h + \frac{\partial f_{r_{mn}}}{\partial L} \Delta L + \frac{\partial f_{r_{mn}}}{\partial W} \Delta W \quad \text{Eq.(4.41)}$$

where the partial derivatives are easily determined. Figure 4.27 shows the response of antenna parameters.

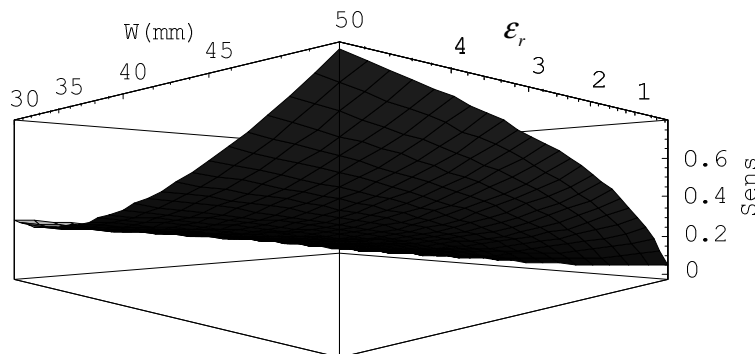


Figure 4.27 Sensitivity magnitude ($C_1 = 1$ pF, $C_2 = 2$ pF).

It is now possible to control the resonant frequency shifted by using Pi matching technique. Finally, it can be say that the input impedance of the rectangular microstrip antenna is more sensitive to values of C_2 , than the values of C_1 ($|S_{C_2}^{Z_{in}}| > |S_{C_1}^{Z_{in}}|$).

4.7 Design Examples, Simulation and Measurement Results

Compact microstrip antennas have recently received much attention due to the increasing demand small antennas for personal communication equipment. The compact antenna is selected as an example due to its complex structures. Much significant progress in the design of compact microstrip antennas with broadband, dual-frequency dual-polarized circularly polarized, and gain-enhanced operations have been reported over the past several years. Compact operation of microstrip antennas can be obtained by meandering the radiating patch (Lu & Wong, 1998). In the following, the compact design combining the techniques of meandering and compensated network with pi matching for a microstrip antenna is demonstrated.

With size reduction at a fixed operating frequency, the impedance bandwidth of a microstrip antenna is usually decreased. To obtain an enhanced impedance bandwidth, one can simply increase the antenna's substrate thickness to compensate for the decreased electrical thickness of the substrate due to lowered operating frequency or one can meandering ground plane or a slotted ground plane. Two type compact rectangular patch antennas shown in Figure 4.28 are analyzed. When the antenna is loaded with the pair of slits and slots, the resonant frequency is changed. The antenna performances are increased, when the pi-circuit is added this antennas.

In the study, TLC-32 substrate material manufactured by Taconic (a relative permittivity of 3.20 and a thickness of 0.80 mm) were used. The Compact_I rectangular patch dimensions of $48 \times 34 \text{ mm}^2$ (W x L), are selected along with the ground plane dimensions of $60 \times 40 \text{ mm}^2$ as shown in Figure 4.28 (a).

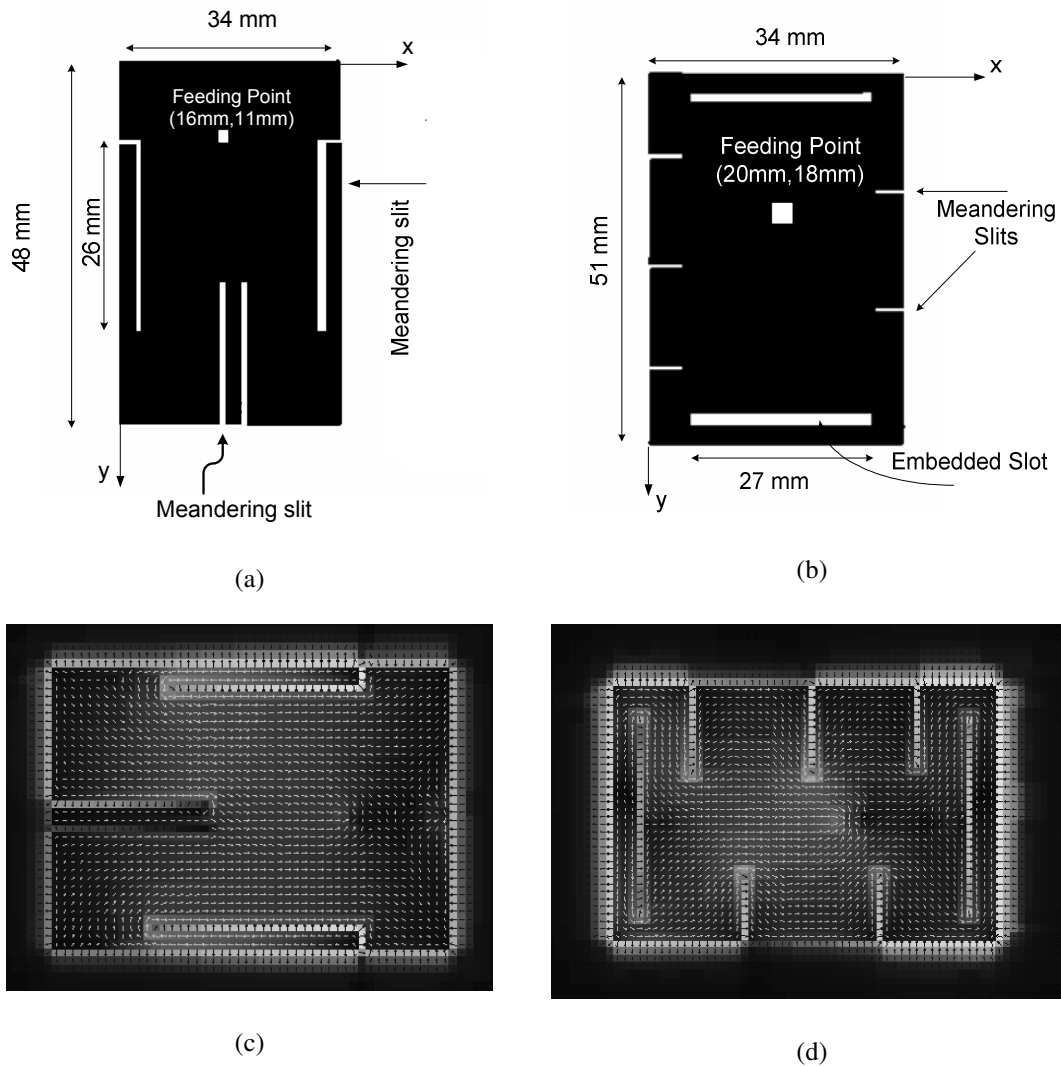


Figure 4.28 (a) Schematic layout of Compact I (b) Schematic layout of Compact II –RMSA with multiple slit ($\epsilon_r=3.0$ & $h=0.78$ mm; TLC-32) (c) and (d) Simulated surface current distributions in radiating patch 1.5 GHz and 2.5 GHz

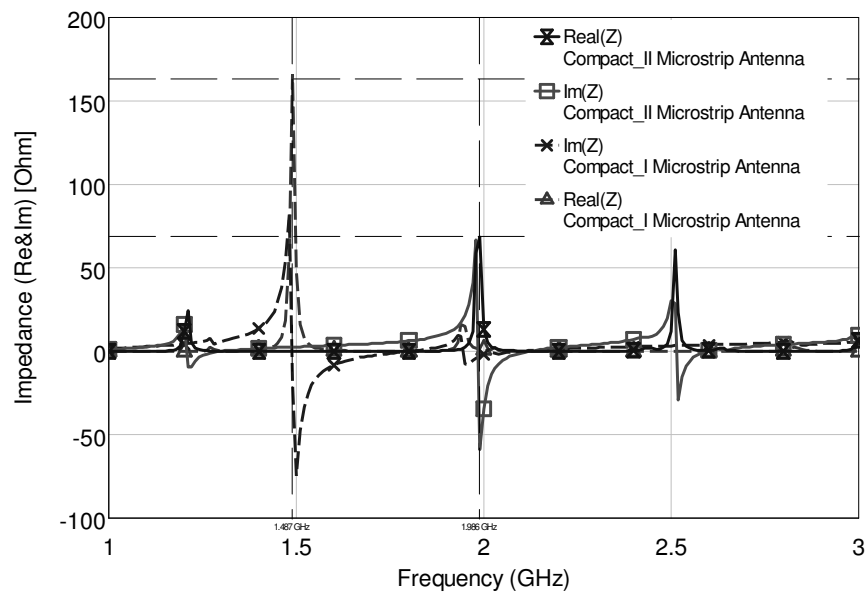
By embedding suitable slot in the radiating patch, compact operation of microstrip antennas can be obtained. Dual frequency operation can be obtained using the compact design of slot loaded rectangular patch antenna or a folded slits as shown in Figure 4.24 (b). This antenna can be considered to consist of two connected resonators. The smaller resonator is encircled by the slit and resonates at a higher resonant frequency; the larger resonator encircles the smaller one and resonates at a lower resonant frequency. This kind of compact dual-frequency design is very suitable for applications in handset antennas of mobile communication units. By loading a pair of narrow slots parallel and close to the radiating edges of a meandered

rectangular, dual frequency operation with tunable frequency-ratio ranges of about 1.8-2.4 and 2.0-3.0, respectively, have been reported (Lu & Wong, 1998). Many designs have been reported for compact dual-frequency operation with orthogonal polarization (Wong & Yang, 1998). These design methods mainly use the loading of suitable slots, such as cross slot, a pair of bent slots, four inserted slits, a square slot, and so on in a rectangular patch.

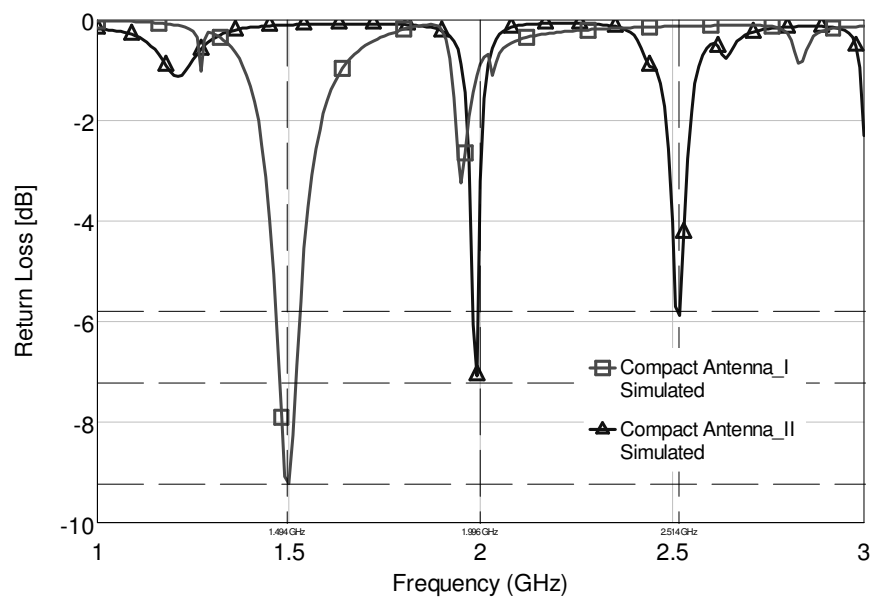
A compact dual-band antenna is realized when multiple slits are cut along the length of the slot loaded RMSA. The geometry looks like a meandered structure as shown in Figure 4.28. With the slits on the nonradiating edges, the surface current path for the two modes TM_{10} and TM_{30} increases, leading to a reduction in the resonance frequency as shown in Figure 4.28 (c-d).

The Compact_II rectangular patch dimensions of $51 \times 34 \text{ mm}^2$ (W x L), are selected along with the ground plane dimensions of $60 \times 40 \text{ mm}^2$. Based on the above designed concept, the matched microstrip antenna with slots was constructed. Compact_I rectangular microstrip patch antenna which the slot length is fixed to be 26 mm is represented in Figure 4.28.a. and the slot length for the Figure 4.28.b which is named Compact_II Antenna is selected 27 mm. The probe-fed compact patch antenna operated at 1.5 GHz and 2.5 GHz. And antennas have meandering slits that is different lengths.

These antennas impedance variations of versus frequency are shown in Figure 4.29. There are two or more frequencies. When the antenna is loaded with the pairs of $27 \times 1 \text{ mm}^2$ slots and pairs of slits $9 \times 1 \text{ mm}^2$, the frequency of operations are 2 and 2.5 GHz as shown in Figure 4.29 (b) but return loss level isn't enough for efficient operations. This problem is overcome by using proposed pi-matching circuit above. When the antenna that it is called Compact_I antenna is loaded with pairs of $24 \times 1 \text{ mm}^2$ slots similar the in Figure 4.28 (a), the resonant frequency of operation decreases to 1.5 GHz, that is, about of 40% reduction in the frequency. Coaxial feed is used for excitations.



(a)



(b)

Figure 4.29 (a) Simulated input impedance and (b) Return loss parameter

First, the antenna return loss parameter is measured using HP 8592B Spectrum Analyzer. Measurements are held using HP 8592B Spectrum Analyzer, HP8350B Sweep Generator via an IEEE 488 interface board attached to a PC and validated by Matlab script runs on this PC (all peripherals are GPIB devices) as shown in Figure 4.30.

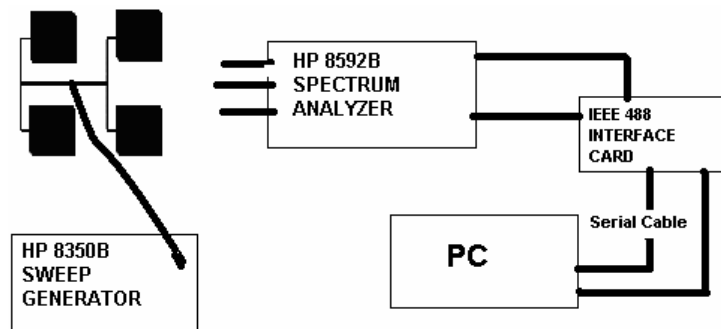


Figure 4.30 Antenna characteristics measurement test environment

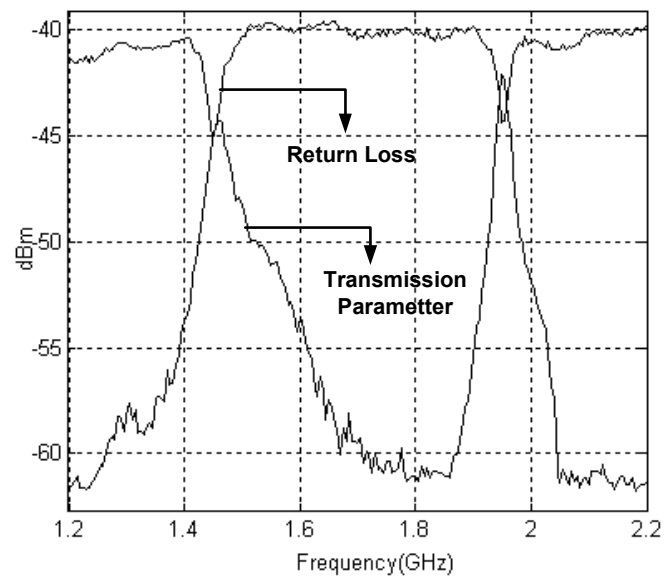


Figure 4.31 Measured return loss and transmission parameter of Compact_I antenna

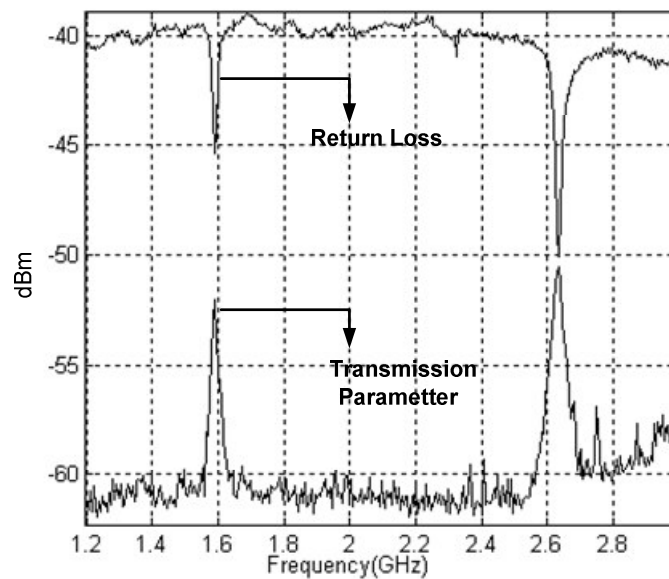


Figure 4.32 Measured return loss and transmission parameter of Compact_II antenna

There are little differences between the simulated and the measurement data as shown in Figures 4.31 and 4.32. This difference occurs due to some circumstances such as laboratory and manufacturing tolerances.

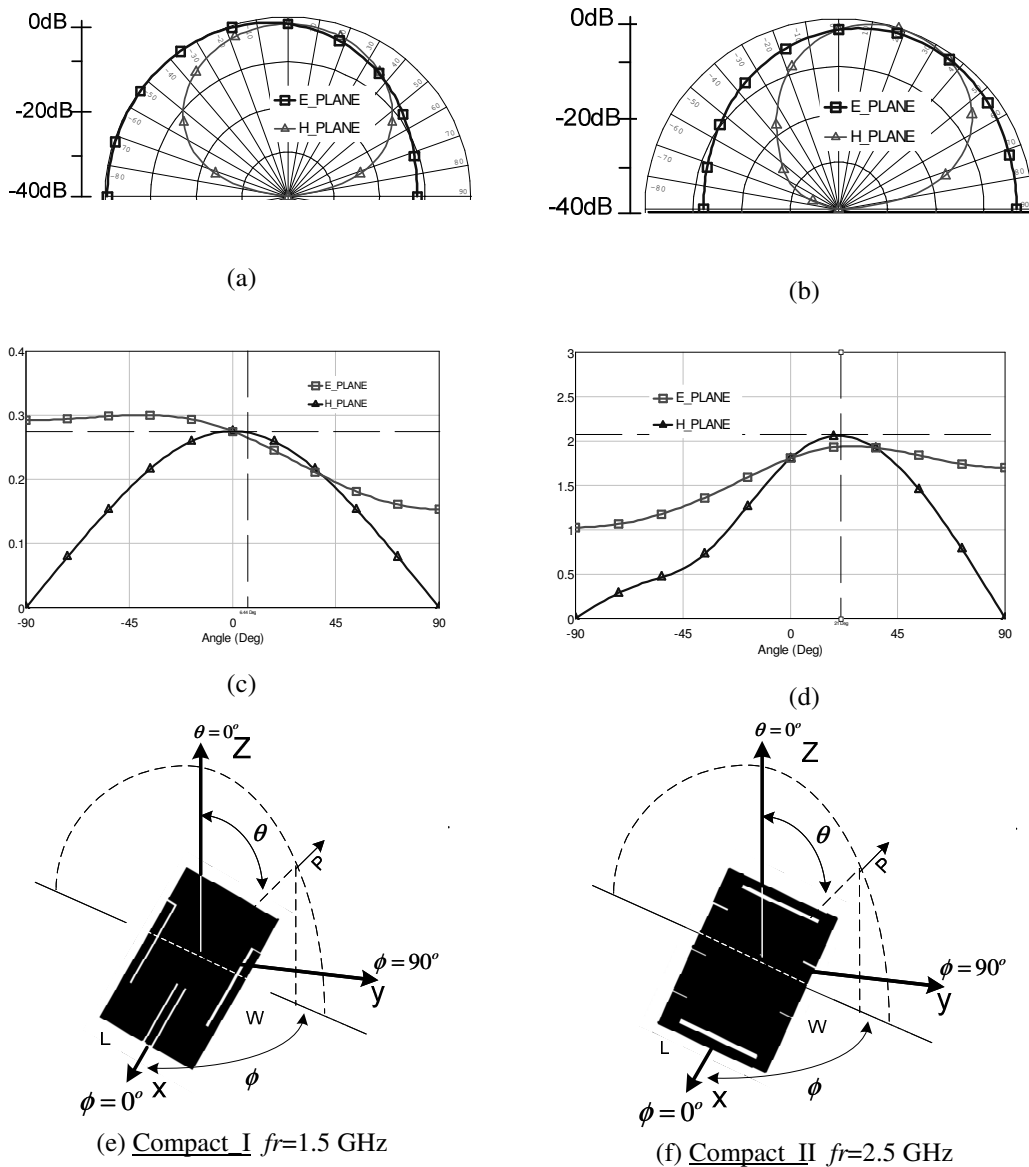


Figure 4.33 E and H plane pattern for 1.5 GHz for Type_I and 2.5 GHz for Type_II

For the simulated radiation pattern, the antenna geometry is mounted on a $80 \times 80 \text{ mm}^2$ metallic plane. From the orientation of the fields in the radiating slot of the antenna the E-plane refers to the xz -plane and the H-plane the yz -plane. The radiation patterns for these planes are plotted in Figure 4.33. It is clearly seen that the radiation patterns aren't symmetric.

When the pi matching circuit is used as a compensated network, the resonant frequency can be controlled. Results clearly indicate that, with increasing R_4 , the resonant frequency of the meandered patch decreases as shown in Figure 4.30. From the results for the case of Compact_I, microstrip antenna has a resonant frequency 1.5 GHz and for the case of Compact_II 2.5 GHz and can be changed by controlling the R_4 value. The slot width has a small effect on the resonant frequency. For a conventional patch antenna (without a meandering slit and slots), the resonant frequency can be higher.

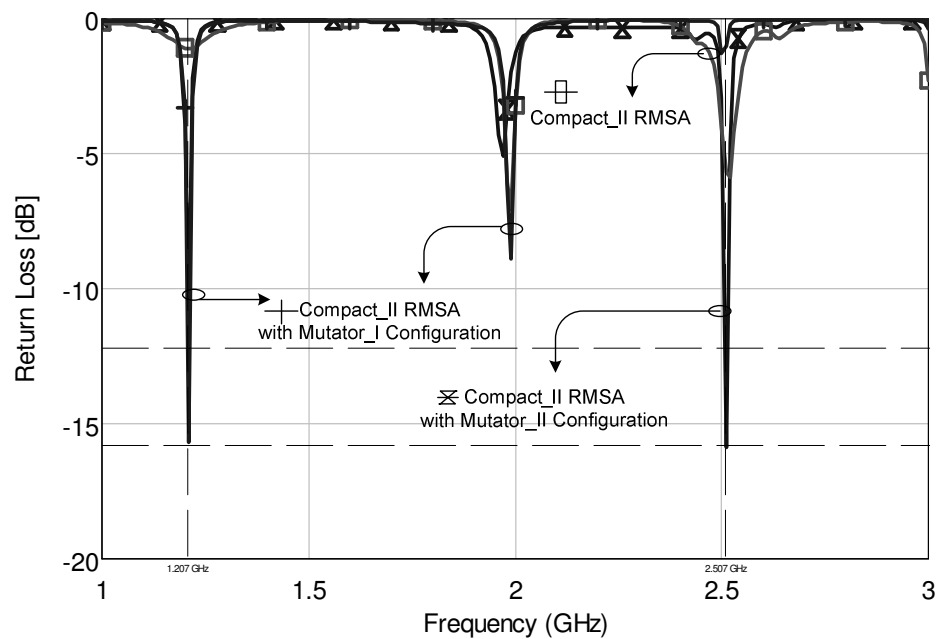


Figure 4.34 Simulation results for the compensated system (C_2 mutator, and $C_1 = 2$ pF) RMSA dimensions; $51 \times 34 \times 0.78$ and $\epsilon_r = 3$; TLC-32

Table 4.4 RC mutator configuration

| Mutator_I Configuration for the Compact_II Antenna ($f=1.21$ GHz & $S_{11}=-15.14$ dB) | | | | | |
|--|----------------|----------------|----------------|----------------|------------------------|
| C_x pF | R_1 Ω | R_3 Ω | R_x Ω | R_4 Ω | C_{eq} F |
| 1.65 | 10 | 25 | 10 | 10 | $4.125 \cdot 10^{-12}$ |
| Mutator_II Configuration for the Compact_II Antenna ($f=2.51$ GHz & $S_{11}= -15.76$ dB) | | | | | |
| 1 | 10 | 25 | 10 | 12 | $2.08 \cdot 10^{-12}$ |

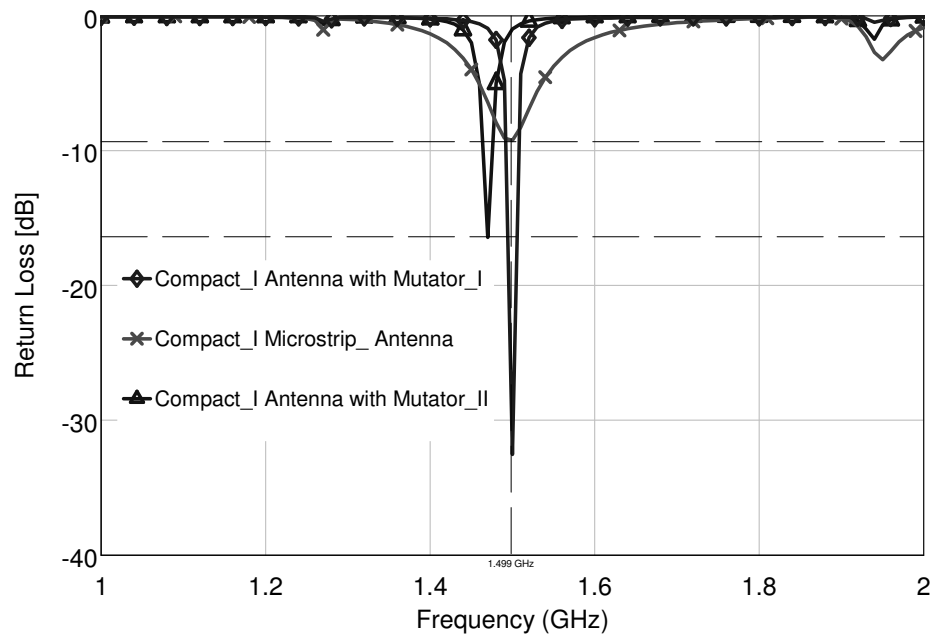


Figure 4.35 Simulation results for the compensated system (C_2 mutator and $C_1 = 2$ pF) RMSA dimensions; $48 \times 34 \times 0.78$ mm and $\epsilon_r = 3$

Table 4.5 RC mutator configuration

| Mutator_I Configuration for the Compact_I Antenna | | | | | |
|---|----------------|----------------|----------------|----------------|-----------------------|
| (f=1.5 GHz & $S_{11} = -32.53$ dB) | | | | | |
| C_x pF | R_1 Ω | R_3 Ω | R_x Ω | R_4 Ω | C_{eq} F |
| 4 | 10 | 25 | 10 | 10 | $10 \cdot 10^{-12}$ |
| Mutator_II Configuration for the Compact_I Antenna | | | | | |
| (f=1.47 GHz & $S_{11} = -16.39$ dB) | | | | | |
| 5 | 10 | 10 | 50 | 110 | $9.09 \cdot 10^{-14}$ |

When the matching circuit connected to the antenna, the results are shown in Figures 4.34 and 4.35, and the results are summarized in Table 4.4 and Table 4.5. These results will be changed when the feeding-point positions are changed. However, slits lengths, slots lengths and meandering slots dimensions are important. Return loss level is increased using compensated system realized by RC mutator.

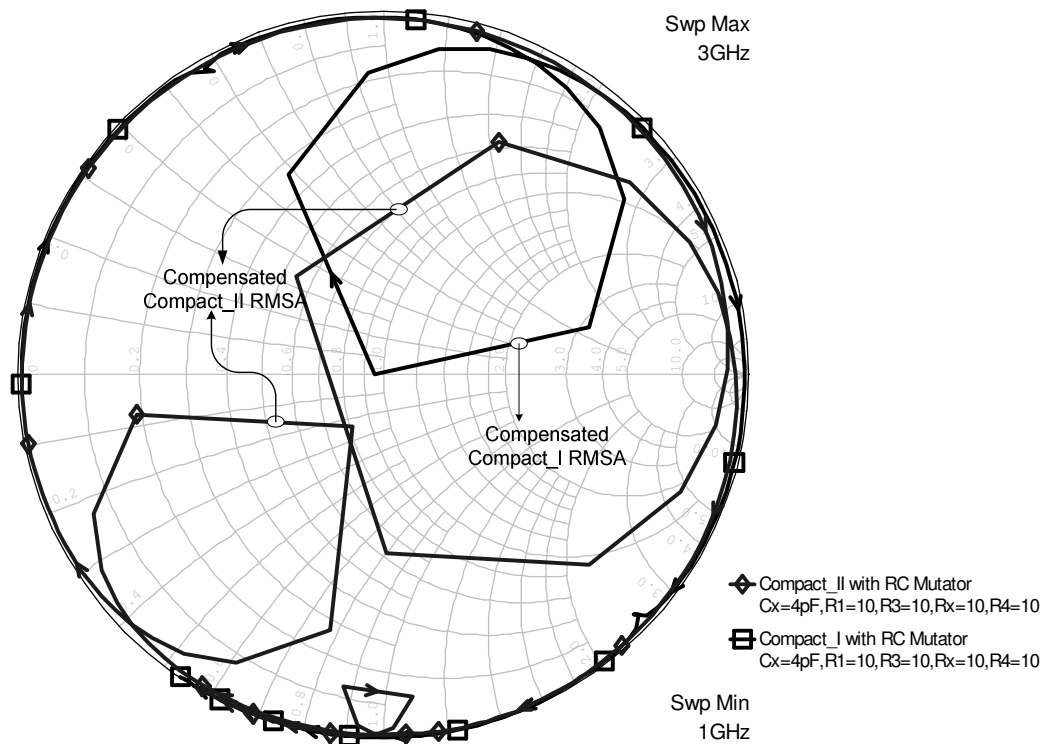


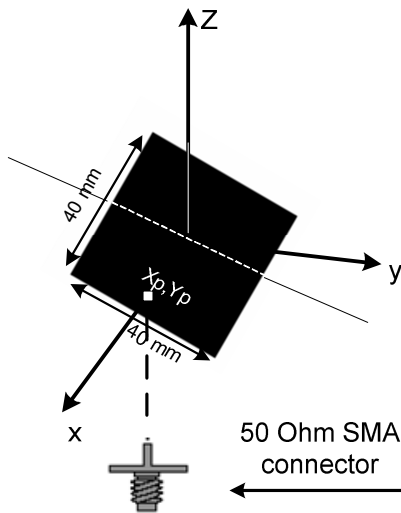
Figure 4.36 Smith chart of input impedance (C_2 mutator, and $C_1 = 2\text{ pF}$)

It is also seen that there are two resonant frequencies in Figure 4.36 for the type II. There are large impedance changing in Compact_I RMSA configuration. The frequency-ratio range is about 1.25 in Compact_II RMSA. It can be noted that the matching network should be carefully chosen in according to the application. Finally, the matching level is increased in compensated compact antenna with RC mutator and the resonant frequency can be controlled with only resistive components.

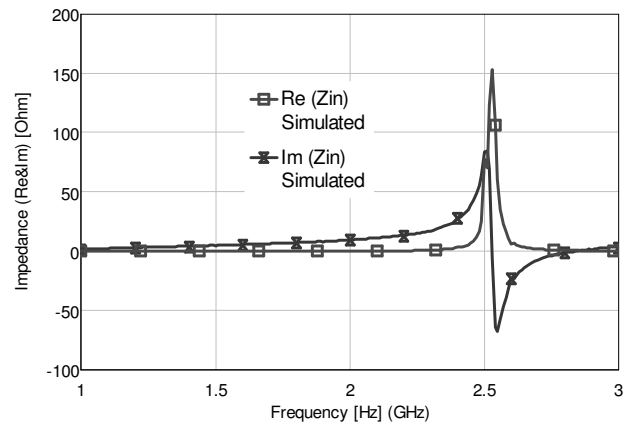
CHAPTER FIVE
DESIGN, FABRICATION AND MEASUREMENT RESULTS OF DIFFERENT
MICROSTRIP PATCH ANTENNAS

5.1 Design Concept of Compensated Microstrip Patch Antennas

A broad band matching design procedure was presented to improve matching level and the bandwidth characteristics of several microstrip antennas. In this chapter, theoretical, simulation and measurement results employing the laboratory tests have compared. Coaxial feed, which has an inner conductor of the coax extended across the dielectric to the radiation patch while the outer conductor is connected to the ground plane, is also widely used. This feed method is easy to fabricate and has low spurious radiation. However, it has narrow bandwidth and the location of the feed point can be determined for the given mode so that the best impedance match is achieved. Figure 5.1 (a) shows a coaxial feed. The variation of the real and imaginary part of the coaxial feed rectangular microstrip antenna impedances are shown in Figure 5.1 (b). The return loss and transmission parameter are shown in Figure 5.2 for the reference antenna.



(a)



(b)

Figure 5.1 (a) The geometry of coaxial coupled RMSA (b) Variation of Real & Imaginary part of the impedance versus frequency. RMSA dimensions; $40 \times 40 \times 0.52$ mm & $\epsilon_r = 2.52$.

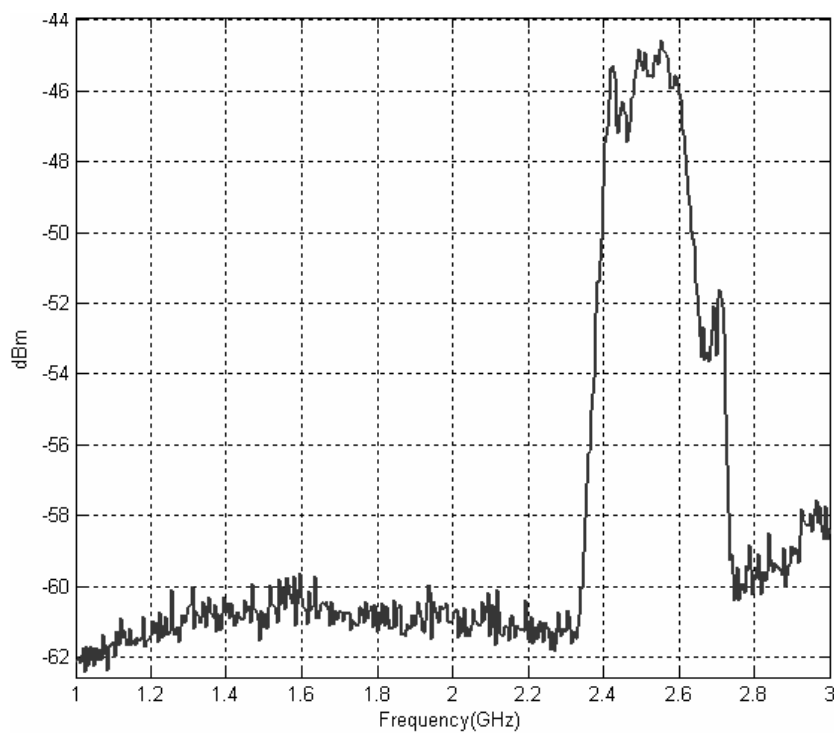
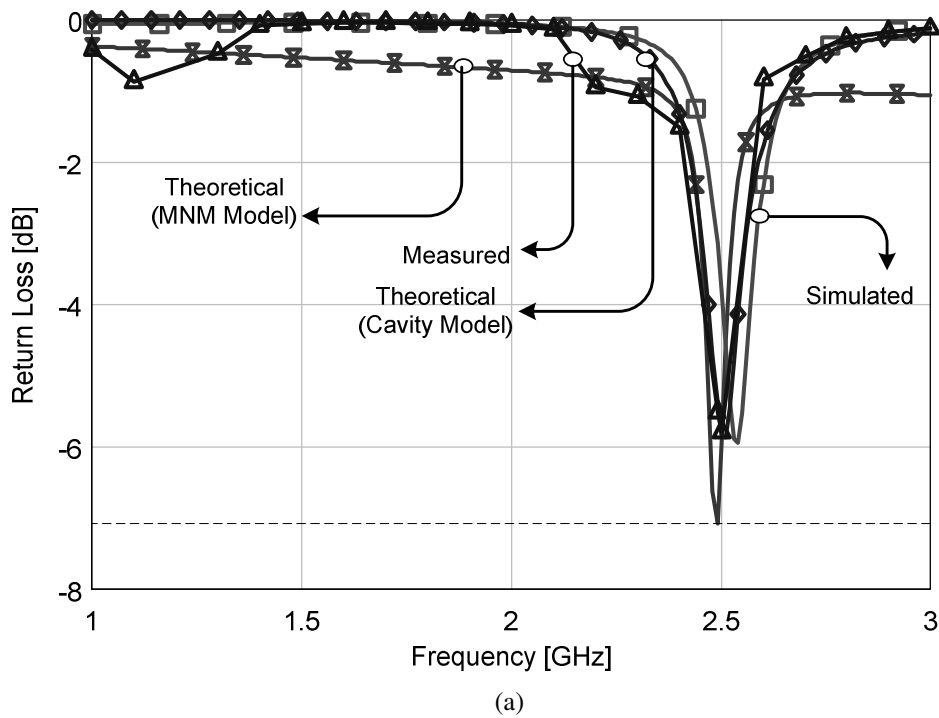


Figure 5.2 (a) Return loss for the reference Coax-RMSA (b) Measured transmission parameter.

A comparison of the simulated and the measured values shows that they are good agreement as shown in Table 5.1. The reference antenna impedance bandwidth characteristic can be improved by using Pi-matching circuits.

Table 5.1 Measured and simulated results

| PATCH Dimension | Computed using MWO | | Measured | | Error between computed and measured values | |
|--------------------|--------------------|---------------|-----------|---------------|--|---------------|
| | f (GHz) | S_{11} (dB) | f (GHz) | S_{11} (dB) | f (GHz) | S_{11} (dB) |
| W=40 mm L=40 mm | 2.52 | -5.9 | 2.4 | -7.2 | %0.79 | %10 |

When the varicap diode is added to the Pi-matching circuit, the matching flexibility can be increased. As an illustration of this new tunable impedance transformer, a hybrid circuit was built using the varactor diode in conjunction with two 50Ω microstrip quarter wave transformer. This circuit was fabricated on TLY-5A substrate, 0.52 mm thick and with a 2.17 dielectric permittivity. MMBV109LT1 was used as a varactor diode. This diode has maximum reverse voltage at 30V (V_{dc}) and forward current 200 mA (I_{dc}). The circuit layout is illustrated in Figure 5.3.

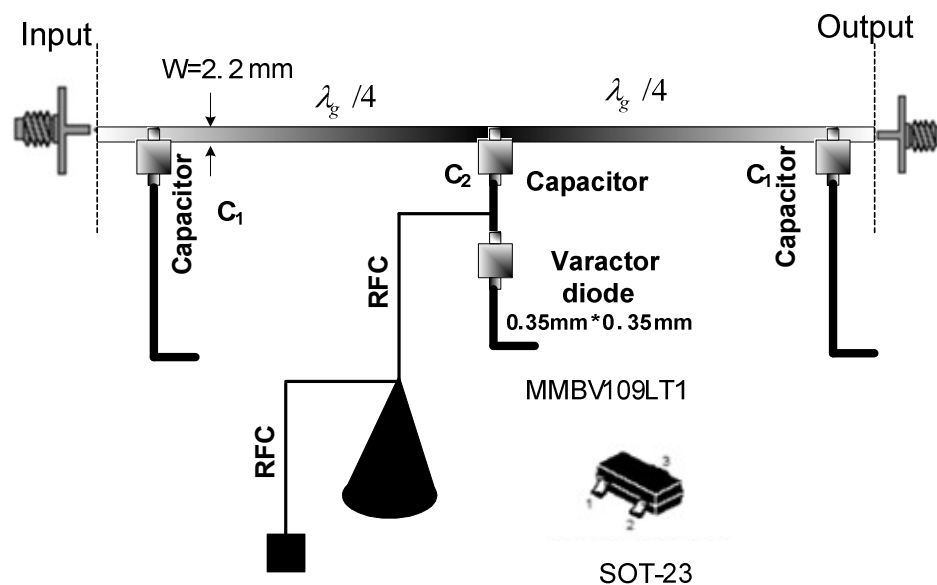


Figure 5.3 Schematic diagram of Pi matching network.

Varactors can be tuned as tunable capacitor, but these components are not usually suitable for high-power applications. Impedance tuning flexibility is increased with varactor diode. If the diode connected to the capacitor is in the direct state (ON), the capacitor adds its own capacity to the global structure capacity.

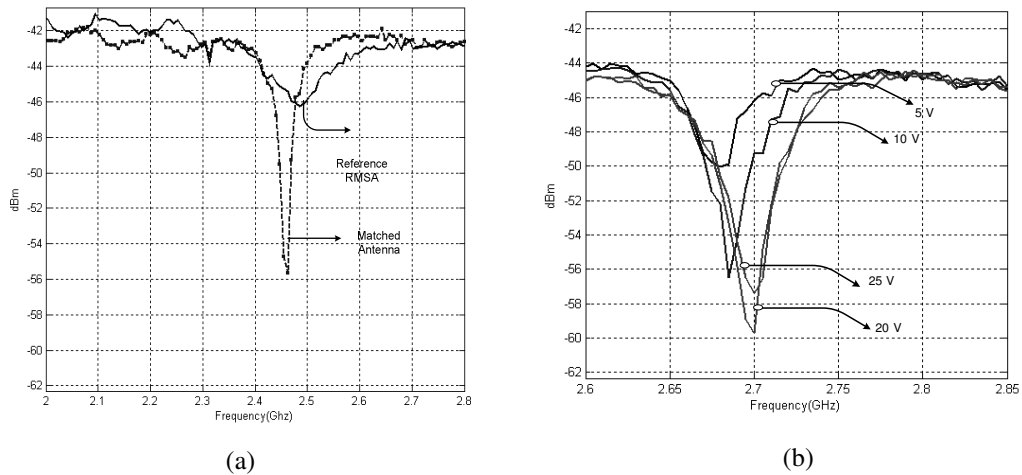


Figure 5.4 (a) Measured return loss for the reference and external pi-matched Coax-RMSA ($C_1=1.5$ pF and $C_2= 2$ pF) (b) Measured return loss for the external matched Coax-RMSA with varicap diode ($C_1=1.5$ pF , $C_2= 1.5$ pF and varicap diode).

It is shown that matching level can be tuned by using voltage levels as shown in Figure 5.4 (b) but resonant frequency shifted to 2.7 GHz and measured return loss $S_{11}=-17$ dB at $f_r = 2.7$ GHz with the bandwidth of 50 MHz. The impedance bandwidth of the antenna increases. A better result can be obtained when the feed point is optimized. This is a flexible structure that offers many tuning possibilities.

5.2 Experimental and Theoretical Analysis for Different Microstrip Patch Antennas

We concentrate on also microstrip transmission line fed rectangular patch antennas. This feeding is suitable for the passive and active matching techniques on same board. The microstrip feed line is the simplest way to feed a microstrip patch. In this feeding method, the microstrip feed line is connected directly to the edge of the patch as shown in Figure 5.5. Microstrip feed line length is important parameter for determining to the input impedance. However, appropriate impedance values can be obtained by using compatible Pi-matching circuit.

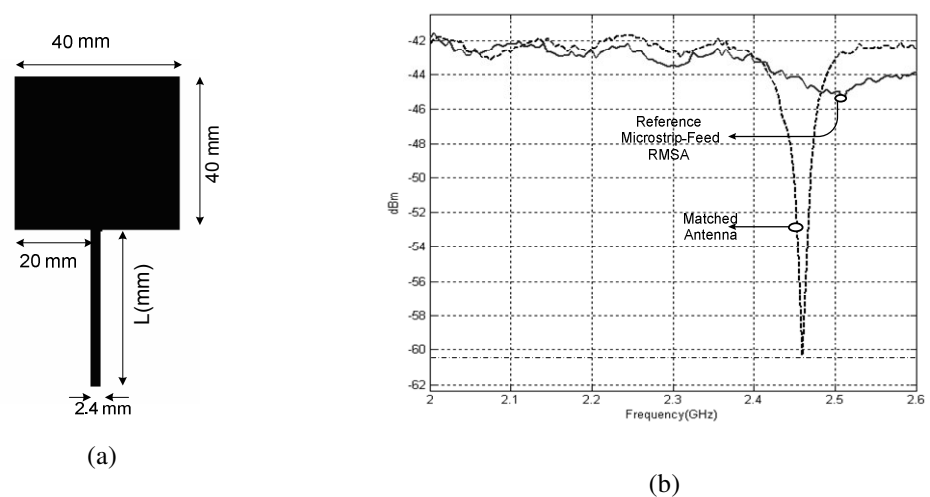


Figure 5.5 (a) The geometry of microstrip feed RMSA (b) Measured return loss for the external matched RMSA with ($C_1=1.5$ pF and $C_2= 1.5$ pF): (RMSA: $\epsilon_r=2.2$ & $h=0.52$ mm: TLY_5)

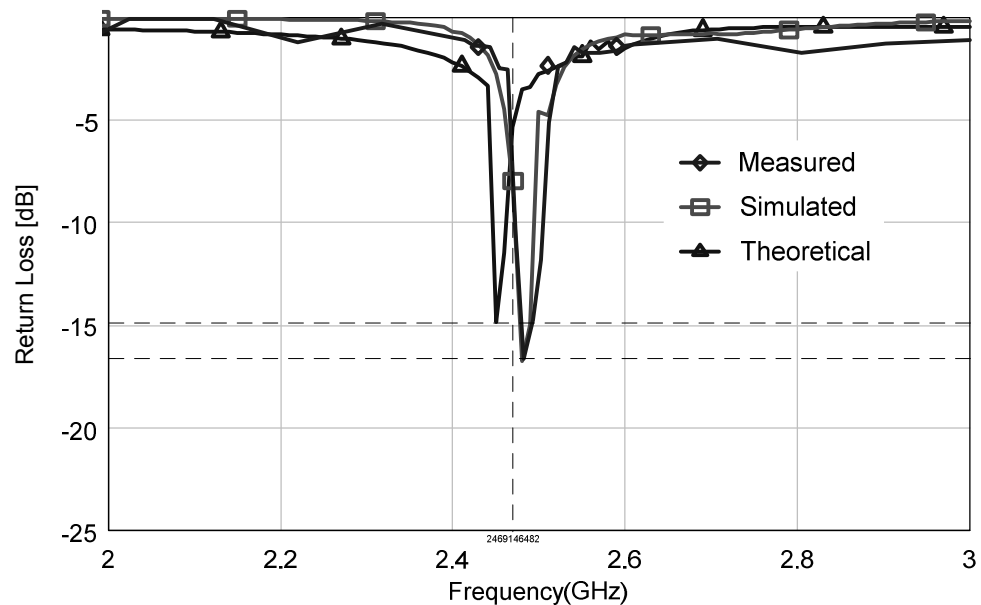


Figure 5.6 Theoretical (Cavity Model), measured and simulated return loss parameter (C_1 and C_2 1.5 pF, $L=20$ mm).

The substrate used for the design has a thickness of 0.52 mm, the relative permittivity of (ϵ_r) 2.52 and $\tan \delta$ of 0.004. The return loss characteristics $|S_{11}|$ for simulated (*MoM*), measured and theoretical results are shown in Figure 5.6. When the pi matching circuit was added in the microstrip fed-antenna, the resonance

frequency shifted approximately 80 MHz. It is important to note that the fixed capacitors should be selected properly. If the system is well matched, return loss level $|S_{11}|$ is very small. C_1 and C_2 have been selected as 1.5 pF and thereafter, return loss level having -16.86 dB has been obtained in Figure 5.6. The resonant frequency of the simulation model was 2.5 GHz, which is close to measured and theoretical results. The results are also summarized in Table 5.2 for the resonant frequency and the return loss parameters. The S_{11} and the input impedance at the resonant frequency are obtained as -15.69 dB and $54 + j6.4$ with the Type I (having discrete capacitor).

Table 5.2 Comparison of the results

| Electromagnetic Simulation (MoM Analysis) MWO | | Theoretical Results (Cavity Model) | | Experimental Results | |
|--|-----------|---------------------------------------|-----------|----------------------|-----------|
| S_{11} [dB] | f_r GHz | S_{11} [dB] | f_r GHz | S_{11} [dB] | f_r GHz |
| -16.67 | 2.519 | -12.5 | 2.509 | -16.04 | 2.501 |

When comparing the results, it is seen that the resonant frequency shifted. The impedance bandwidth is obtained 45 MHz. The 3-D representation of radiation pattern is shown in Figure 5.7.

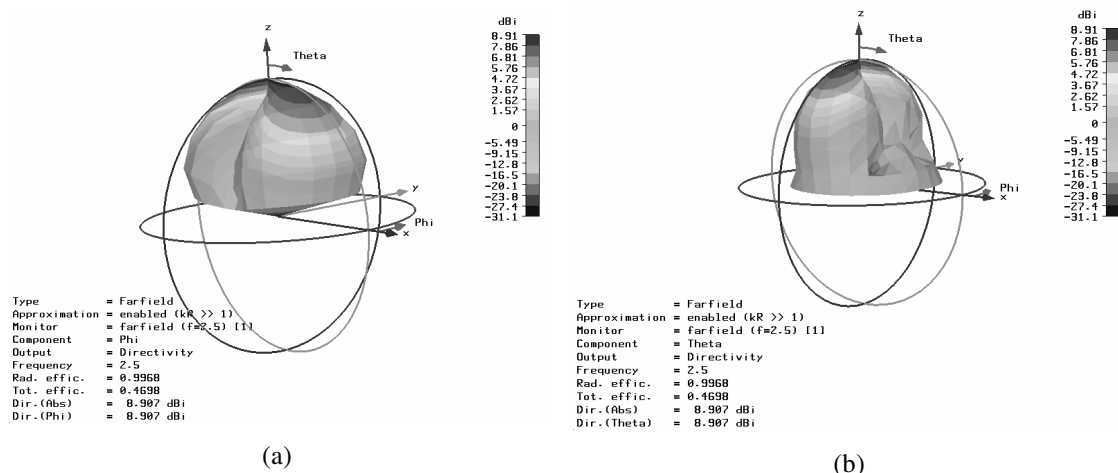


Figure 5.7 3-D representation of the radiation pattern at the 2.5 GHz (a) H-Plane (b) E-Plane.

The simulated (by using CST-microwave studio) 2-D representation of the radiation pattern at 2.5 GHz in E-planes and H-planes are shown in Figure 5.8.

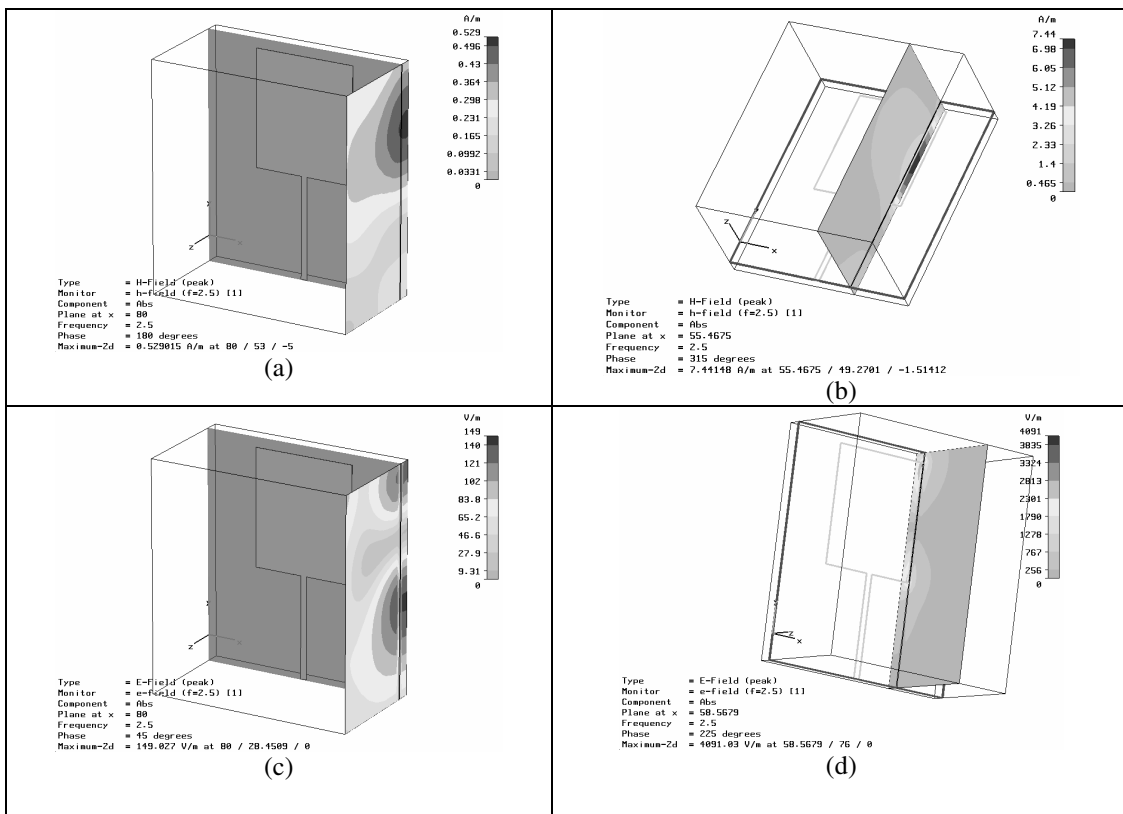


Figure 5.8 2-D representation of the radiation patterns at 2.5 GHz (a) H-Plane –boundary (b) H-Plane –on plane (c) E-Plane–boundary (d) E-Plane–on plane.

The geometry of the compensated RMSA has significant effect on the input impedance, impedance BW, and gain of the antenna. Figure 5.9 shows the simulated radiation pattern (AWR Microwave Office) for the different frequencies.

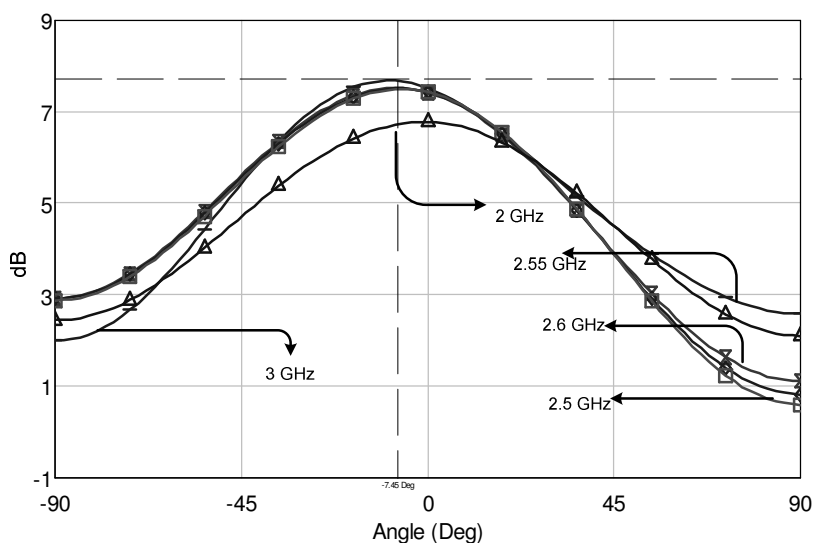


Figure 5.9 E plane patterns for 2-3 GHz frequencies

The resonant frequency shifted to the 2.65 GHz for the compensated antenna with varicap diode as shown in Figure 5.10.

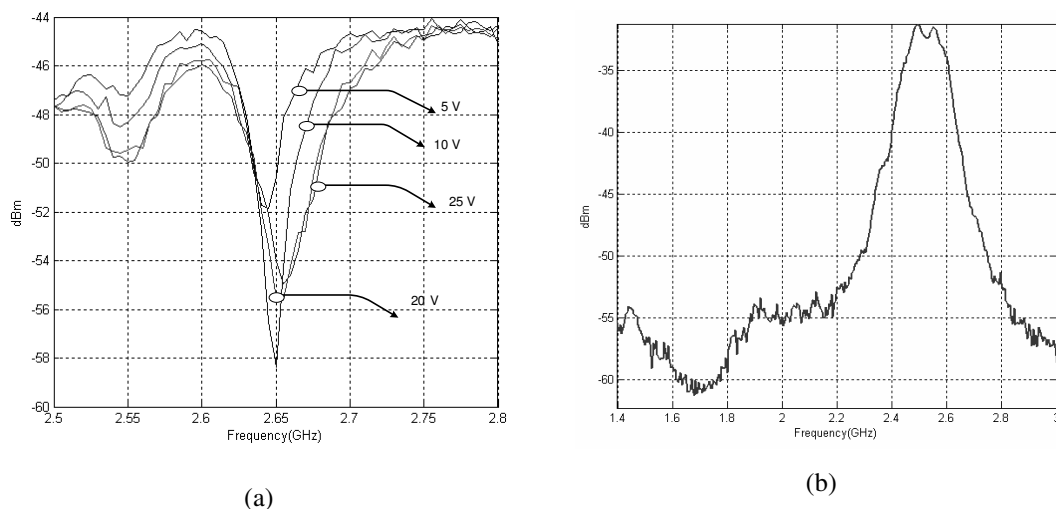


Figure 5.10 (a) Measured return loss for matched with varicap diode type (b) Transmission parameter ($C_1 = C_2 = 1.5$ pF, $L=20$ mm).

The results are summarized in Table 5.2. The BW is increased to 45 MHz. The gains of the RMSA for compensated and reference antennas are the same due to the geometry. When comparing the results between the reference antenna and varicap diode compensated antenna, it is seen that the resonant frequency shifted 1.03%. The radiation pattern symmetry is distorted at 2.65 GHz as shown in Figure 5.10.

Table 5.2 Comparison of the reference and matched microstrip feed line RMSA

| Parameter | Value Reference | Value Matched (C_1 and C_2 1.5 pF) |
|---------------------------------------|-----------------|---|
| Resonant frequency | 2.55 GHz | 2.47 GHz |
| S_{11} at resonant frequency | -5.5 dB | -16.86 dB |
| Z_{in} at resonant frequency | 19.098+j 24.393 | 64.645+j 24.44 |
| Directive co-polarized gain | 7.499 dB | 7.499 dB |
| $S_{11} < -10$ dB impedance bandwidth | ----- | 45 MHz |
| Half-Power Beam width | 86° | 86° |

There is classical method for the matching that is inset RMSA. The purpose of the inset cut is to match the impedance of the feed line to the patch. This is achieved by properly chosen inset position. The input impedance behavior for coaxial probe fed

patch antenna is well studied analytically using cavity model. Experimentally and theoretically it has been found that coaxial probe fed antenna's input impedance exhibits $\cos^2(\pi y_0 / L)$ behavior, where y_0 is the position of the feed from the edge along the direction of the length (L) of the patch. Approximately, a curve fit formula is derived to find the inset length to achieve 50Ω input impedance (Ramesh & Yip, 2003). The simulated and measurement results for the reference inset-RMSA are shown in Figure 5.11.

$$y_0 = 10^{-4} \left\{ \frac{0.001699\epsilon_r^7 + 0.1376\epsilon_r^6 - 6.1783\epsilon_r^5 - 682.69\epsilon_r^3 +}{2561.9\epsilon_r^2 - 40043\epsilon_r + 6697} \right\} \frac{L}{2} \quad \text{Eq. (5.1)}$$

$$2 \leq \epsilon_r \leq 10$$

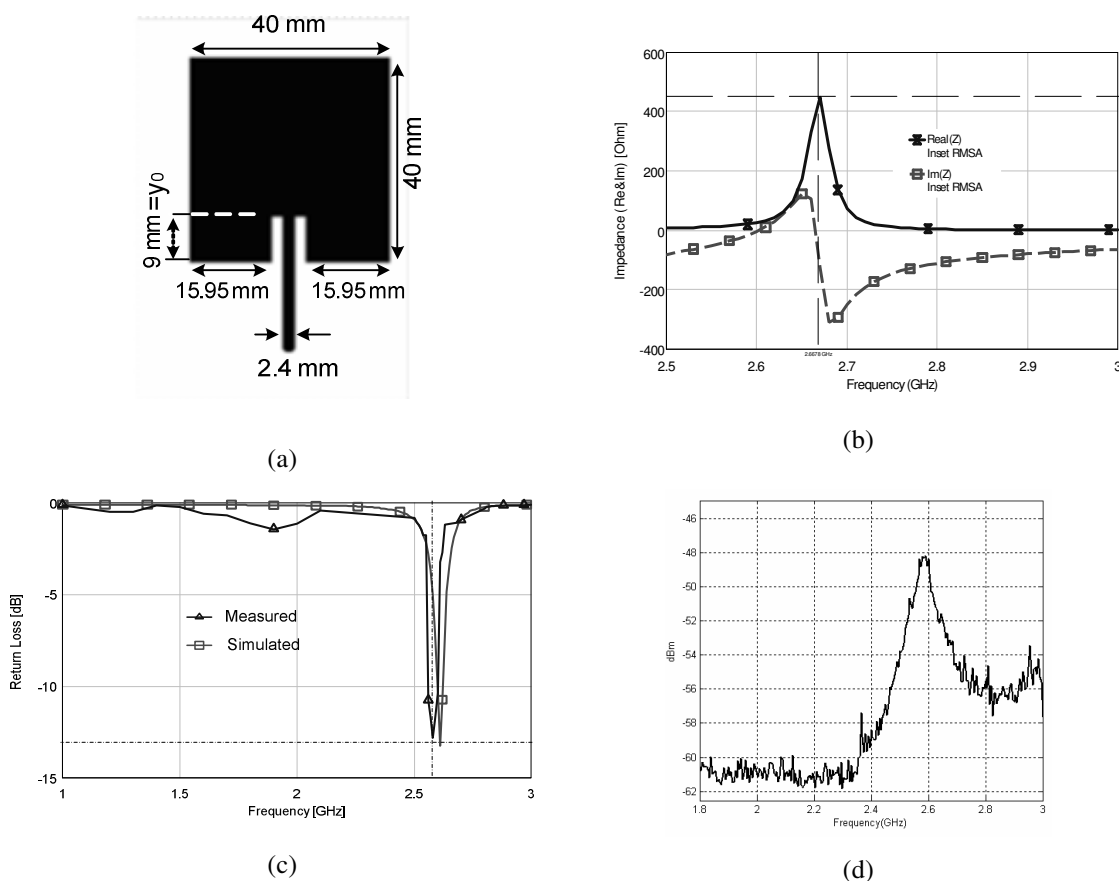


Figure 5.11 (a) The geometry of Inset RMSA measured and simulated return loss for the microstrip inset-RMSA (b) Simulated input impedance (c) Simulated and measured return loss parameter (d) Measured transmission parameter. ($\epsilon_r = 2.2$ & $h = 0.52$ mm)

Input impedance of the inset fed microstrip patch antenna mainly depends on the inset distance y_0 and to some extent on the inset width (spacing between feeding line

and patch conductor). The inset feed has the advantage of simplicity of design through the positioning of the feed point to adjust the input impedance level. Some measurement results are given in Figure 5.12 for the compensated inset antenna.

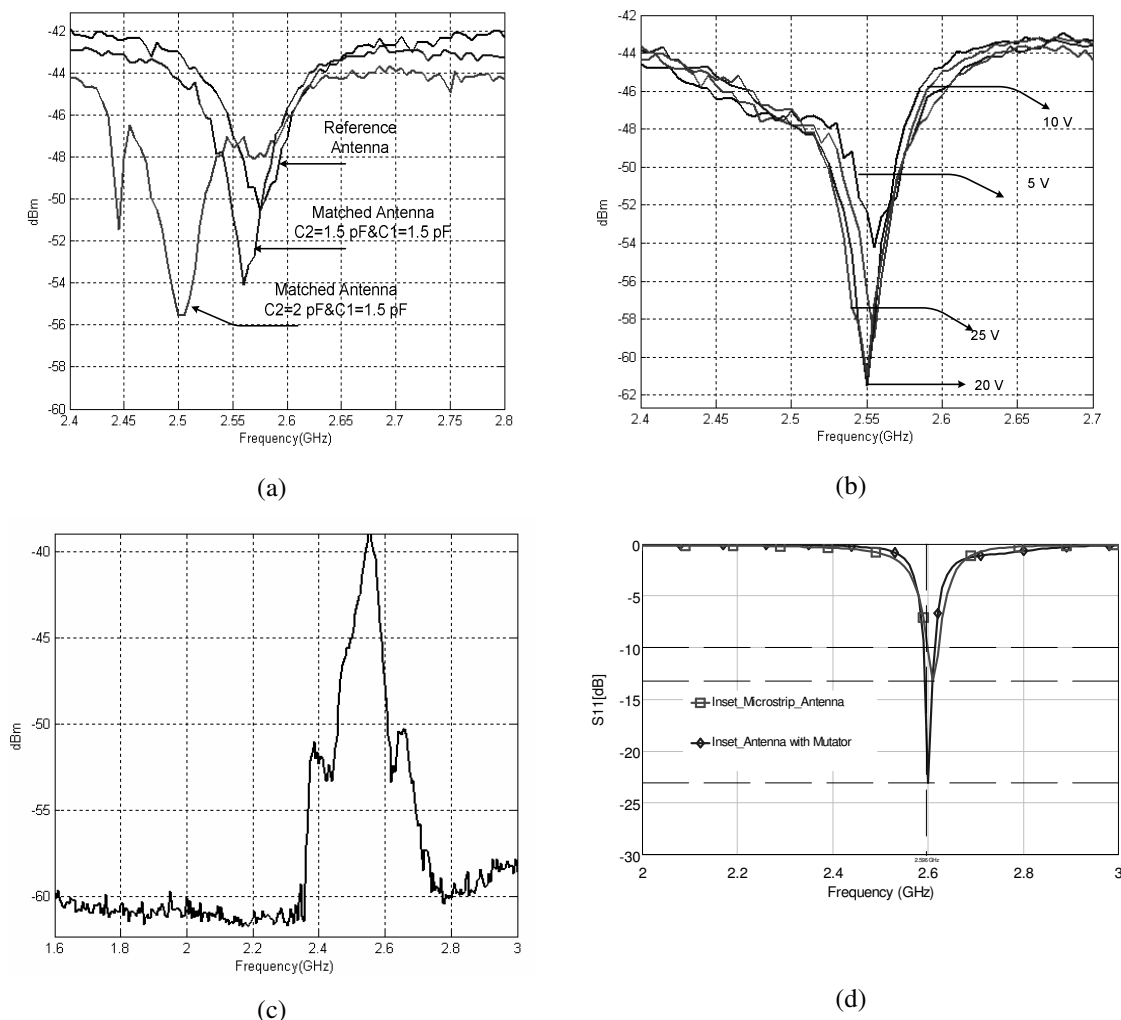


Figure 5.12 (a) Measured return loss for the matched inset antenna with discrete capacitors (b) and with varicap diode matched antenna (c) Measured transmission parameter for matched antenna with varicap diode (d) Return Loss parameter (C_2 mutator and configurations: $C_x=4$ pF, $R_1=10$ Ω , $R_3=25$ Ω , $R_x=10$ Ω , $R_3=80$ Ω)

The return loss level increases from -13.19 dB to -23 dB due to matching circuit with mutator as shown in Figure 5.12(d). The input impedance at resonance increases from 25.74 Ω to 47.437 Ω . The transmission performance is increased but the impedance bandwidth slightly decreased.

The radiation patterns in the E-plane (E_θ in the $\phi = 0^\circ$ plane) and H-plane (E_ϕ in the $\phi = 90^\circ$ plane) of the inset RMSA at 2.55 GHz are shown in Figure 5.13.

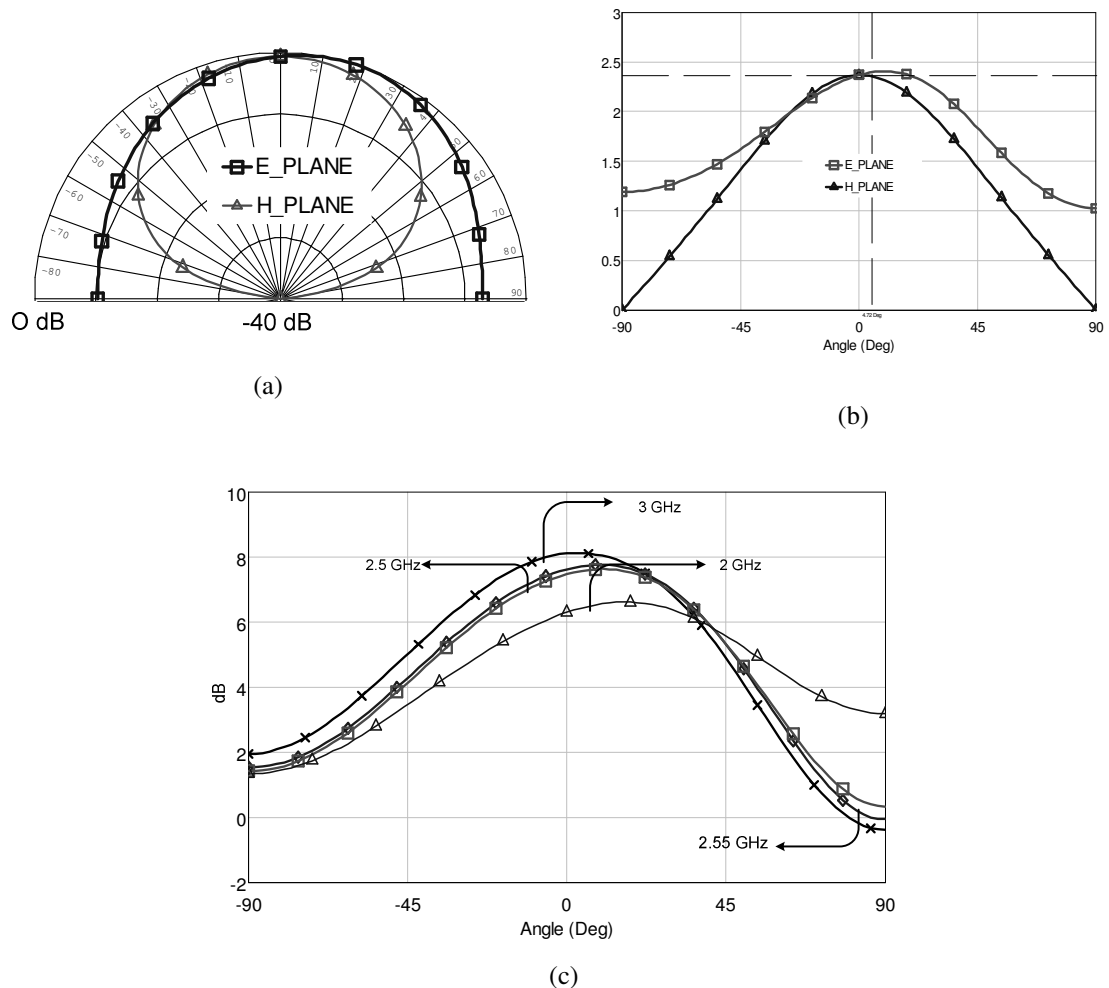


Figure 5.13 Radiation characteristics in the principal planes of the antenna (a) The E and H fields in the xz and yz -plane on polar plane (2.55 GHz) and (b) rectangular plane (2.55 GHz) (c) E plane pattern for 2-3 GHz frequencies

The other application can be given as microstrip array geometry. Microstrip antenna arrays are popular for many application because they are low profile and easy to fabricate. In some wireless applications, such as base station transmission, where maximum directivity and gain of an antenna are of major concern, the use of a single radiating element is insufficient. One approach to improve on this is to use arrays of radiating elements in an antenna. Higher power gain and more flexibility in controlling the shape of the beamwidth and sidelobe levels can be achieved with this

method (Kaya, Çelebi & Yüksel, 2003). The geometry of planar array antenna and measurement results are shown in Figure 5.14.

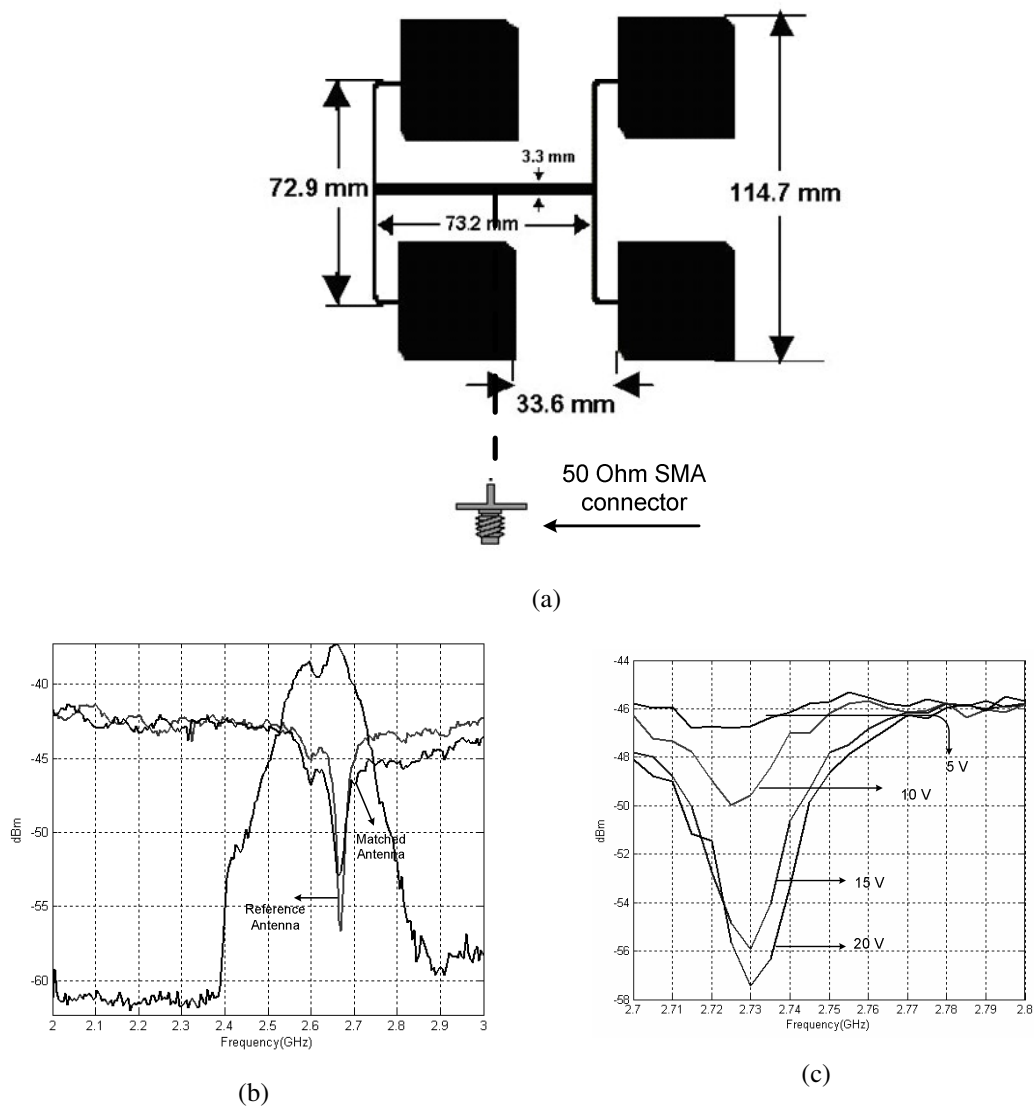


Figure 5.14 (a) The geometry of planar array RMSA (b) Measured return loss and transmission parameter for the matched symmetric array antenna with discrete capacitors (c) and with varicap diode matched antenna

The surface wave effects are important for the array design. The surface waves get excited and travel along the dielectric substrate. When these waves reach the edges of the substrate, they are reflected, scattered, and diffracted causing a reduction gain and an increase in the end fire radiation and cross-polar levels. This also

increases the cross coupling between the array elements (Kaya & Yüksel, 2004). The E-plane radiation pattern is shown in Figure 5.15 between 2 and 3 GHz frequencies.

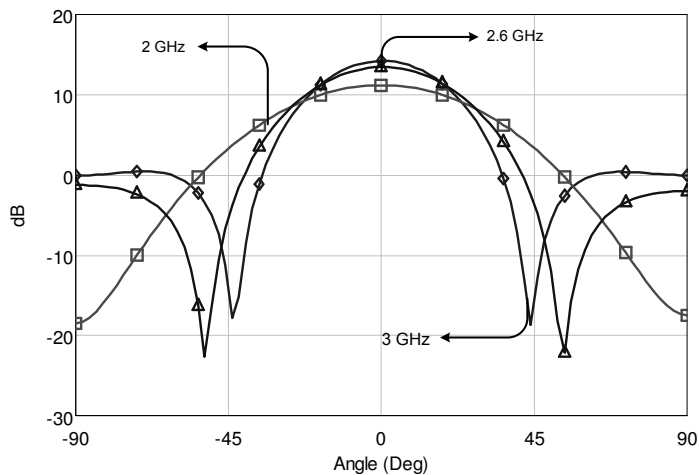


Figure 5.15 E plane pattern for 2-3 GHz frequencies

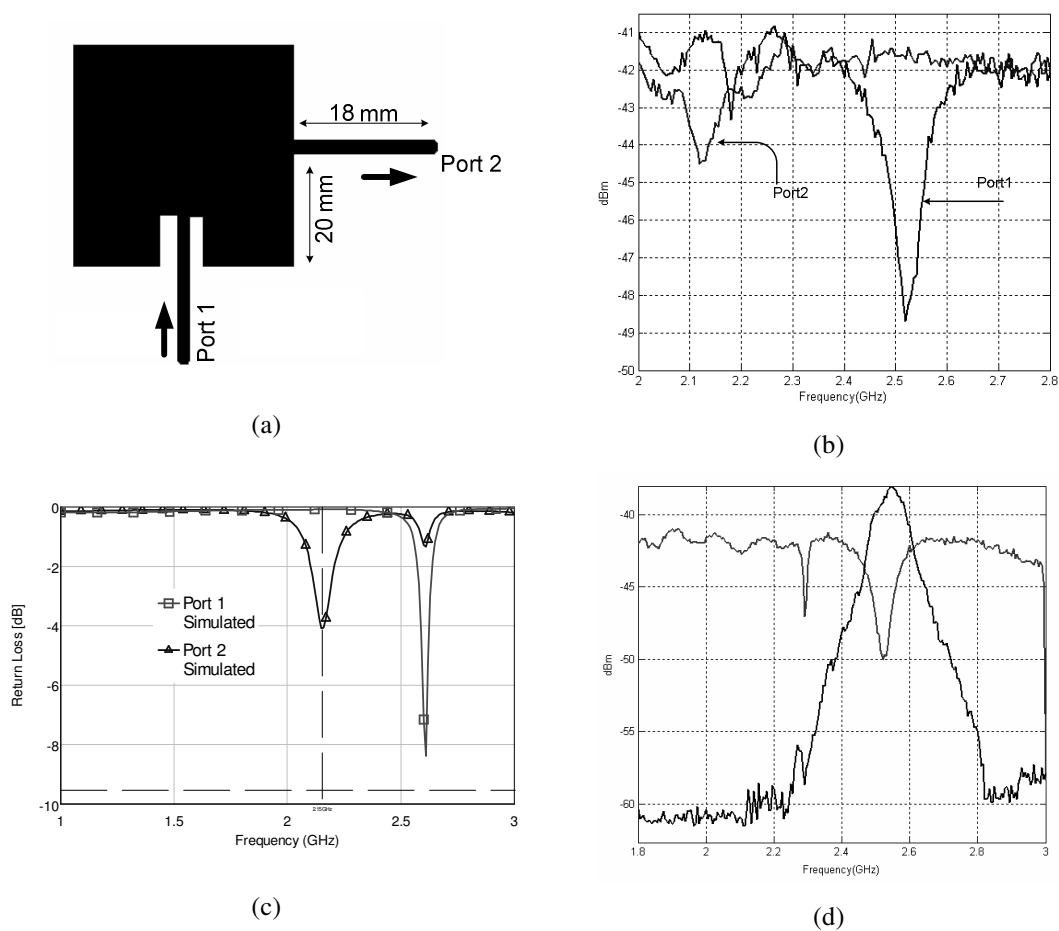


Figure 5.16 (a) The schematic layout of dual band Inset RMSA (b) Measured (c) Simulated return loss for the antenna (d) Transmission parameter

When two or more resonance frequencies of a microstrip antenna are close to each other, a broad BW is obtained. When these are separated, dual-band operation is obtained. RMSA as shown in Figure 5.16 provide a good isolation between the ports and this type of antenna can be used for simultaneous transmit and receive functions. The simulated and measurement results for the reference antenna are shown in Figure.16 (b,c,d).

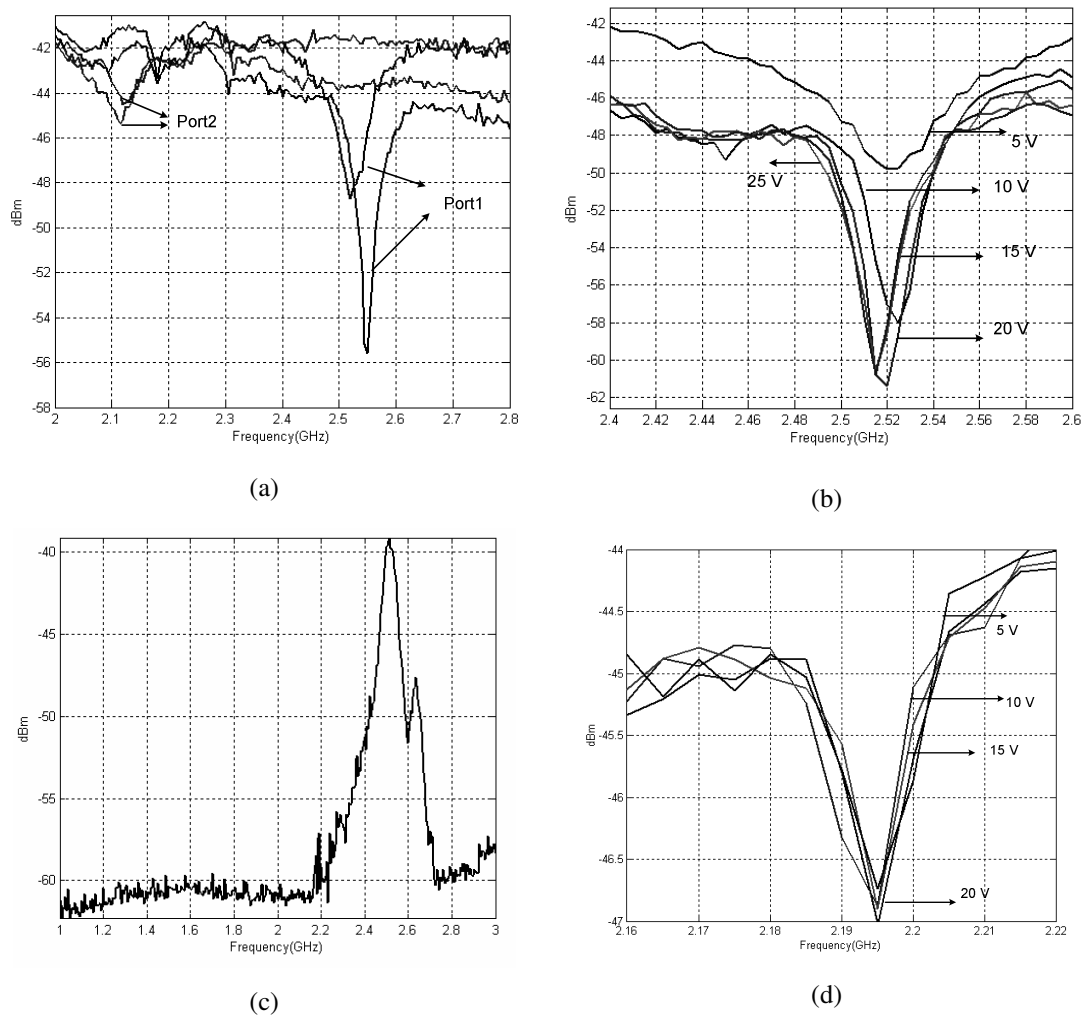


Figure 5.17 (a) Measured matched antenna (C_1 and C_2 1.5 pF) (b) Measured return loss for matched antenna with varicap diode for Port 1 (Transmitter mode) (c) Transmission parameter for Port 1 (TX) (d) Measured return loss for Port 2 with varicap diode (Receiver Mode)

The layout configuration of the compact inset RMSA designed is shown in Figure 5.18 (a) and measurement and simulated results are shown in Figure 5.18 (b)-(d).

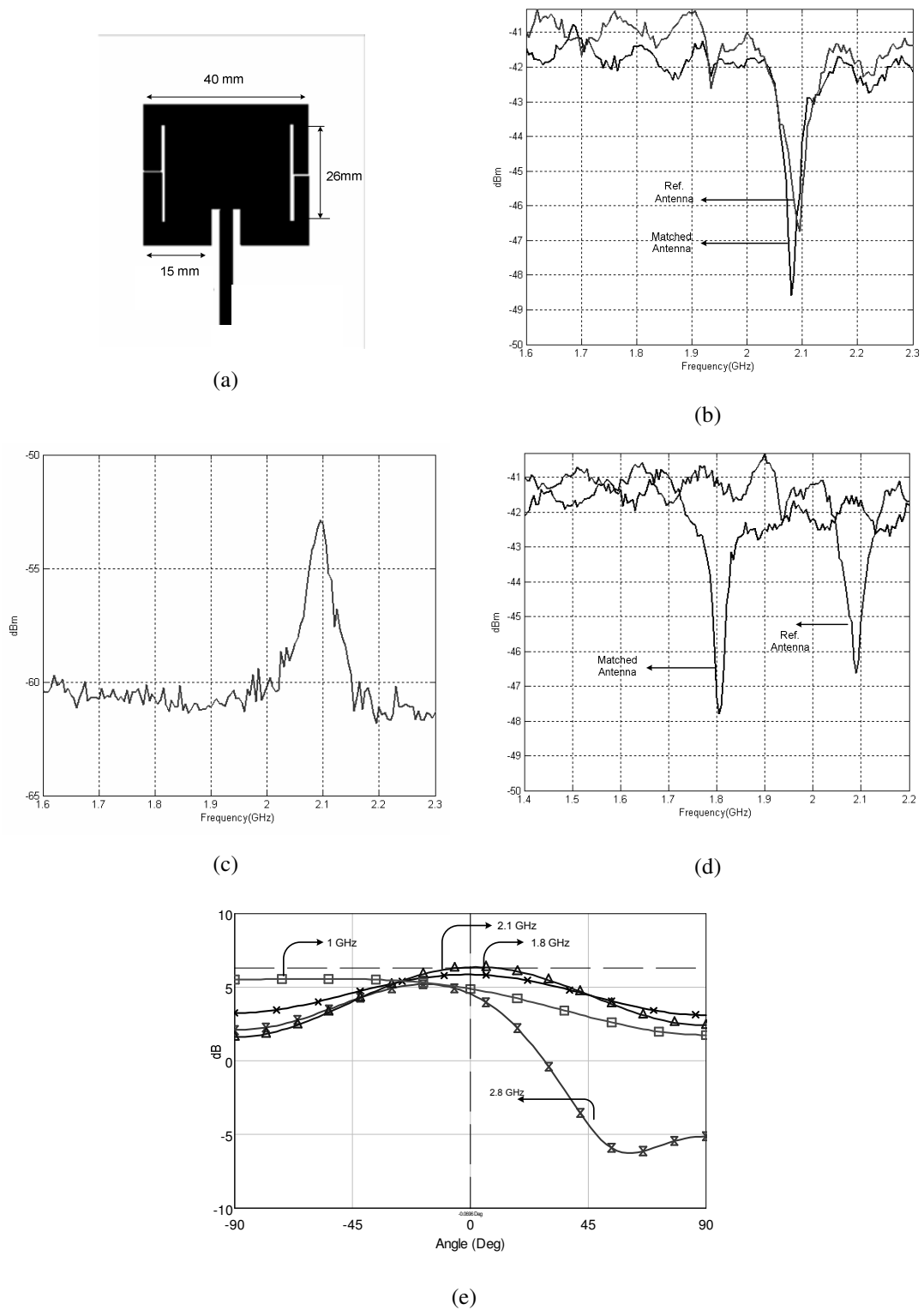


Figure 5.18 (a) Schematic layout of compact inset RMSA (b) Measured matched ($C_1=C_2=1.5$ pF) and reference antenna (c) Transmission parameter (d) Measured matched ($C_1=1.5=C_2$ 2 pF) and reference antenna (e) E plane pattern for 2-3 GHz frequencies.

The material used in above antennas is one of the special materials which is manufactured by Taconic, TLY-5. The thickness of the dielectric substrate is 0.52 mm that is covered by copper sheets with a thickness of 0.035 mm. It has a dielectric constant of 2.2 and a loss tangent of 0.0009. The thickness of the metallic, top conducting strip and conductivity (σ) are generally of much lesser importance and may be often neglected.

Normally, thick substrates with low dielectric constants are often used since they provide better efficiency, larger bandwidth and loosely bound fields for radiation into space. However, it would also result in a larger antenna size.

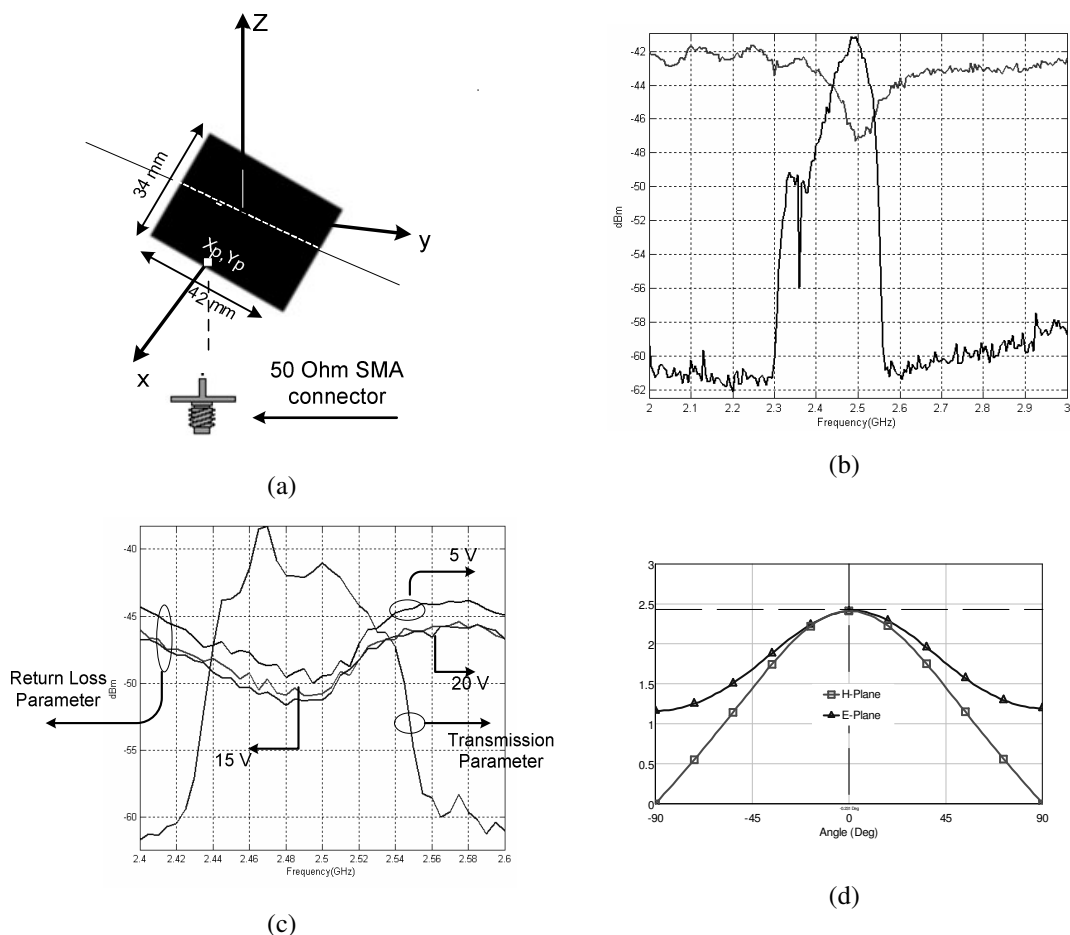


Figure 5.19 (a) Schematic layout of coaxial-coupled RMSA ($\epsilon_r = 3.0$ & $h = 0.78$) (b) Measured return loss and transmission parameter of the reference antenna (c) Measured the return loss and transmission parameter of the matched antenna (e) E plane pattern for 2.5 GHz

On the other hand, using thin substrates with higher dielectric constants would result in smaller antenna size as shown in Figure 5.19 (a). The antenna has relatively smaller bandwidths. The following RMSA antennas were fabricated using TLC_3 manufactured by Taconic. The thickness of the dielectric substrate is 0.78 mm that is covered by copper sheets with a thickness of 0.035 mm. It has a dielectric constant of 3.0 and a loss tangent of 0.003. The simulated and measured results are shown in Figure 5.19.

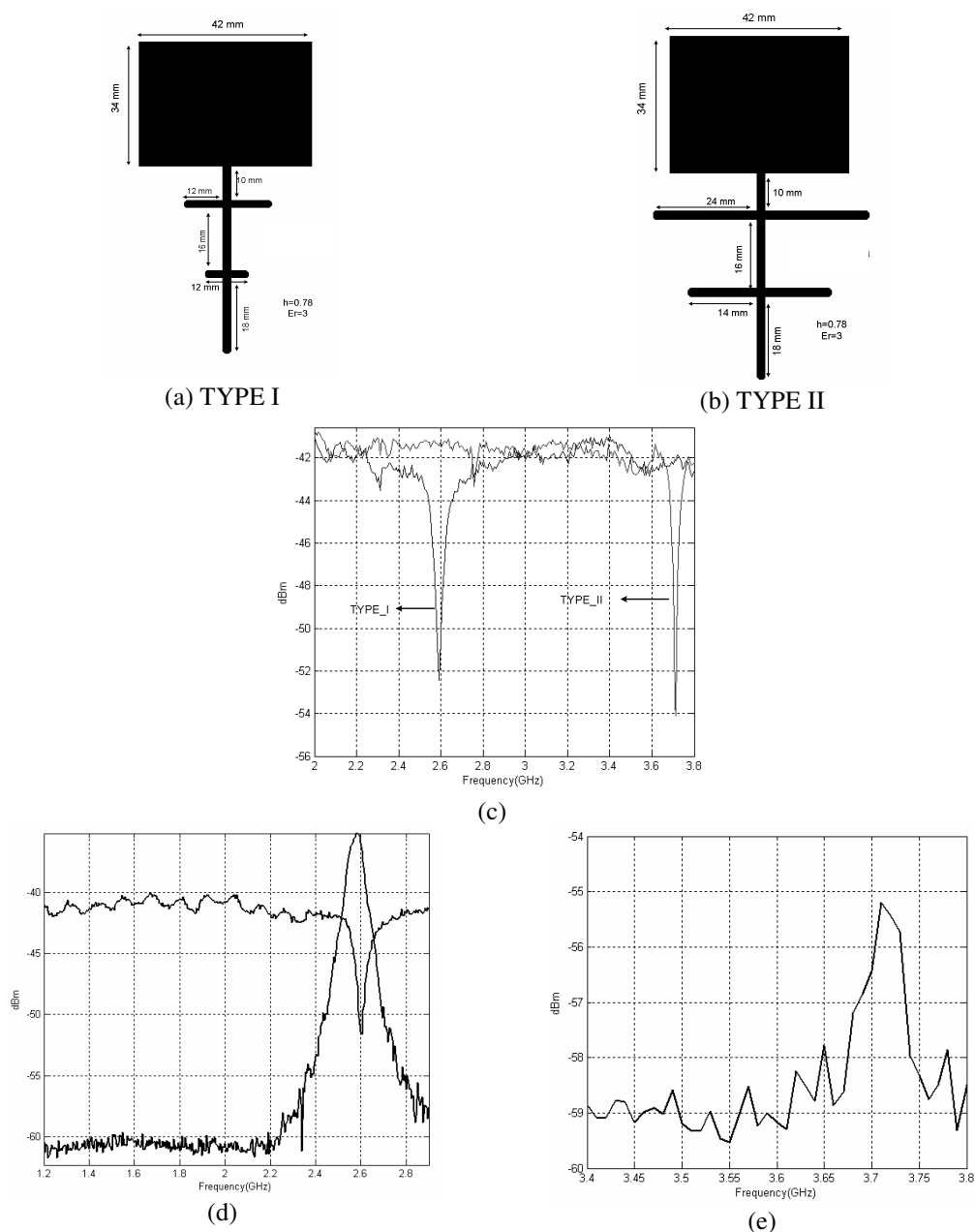
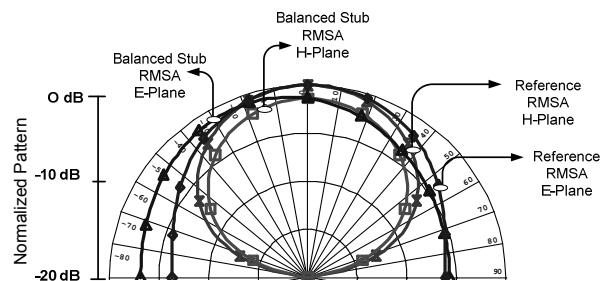


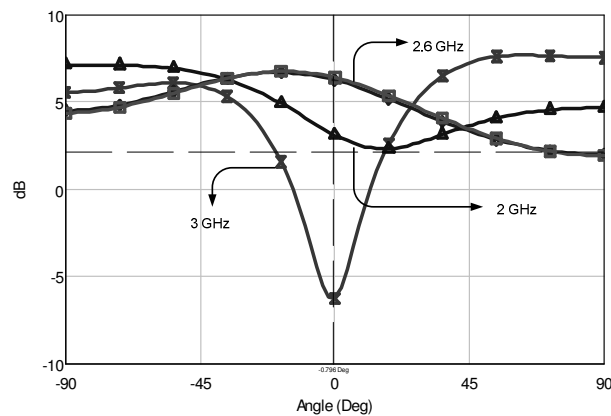
Figure 5.20 Schematic layout of Symmetric balanced stub matched RMSA (a) Type I (b) Type II (c) Return Loss Type I and Type II (d) Transmitter for Type I (e) Transmitter for Type II ($\epsilon_r = 3.0$ & $h = 0.78$ mm; TLC-30-0310-C1)

The impedance matching networks as shown in Figure 5.20 (a) (b) are used to increase the matching level and BW of the microstrip antenna. The measurement results are shown in Figure 5.20 (c) – (e).

Microstrip patches associated with passive feed networks have been previously analyzed (in chapter two) using a magnetic current model of the radiation source distribution. For the patch, the continuous magnetic current at the patch edge is calculated using a cavity patch model which includes the effect of higher-order modes. The feed discontinuities affect the radiation pattern. The radiation from the system is simulated as shown in Figure 5.21. The symmetry is slightly distorted at the resonance frequency.



(a)



(b)

Figure 5.21 (a) Polar plane (2.6 GHz) (b) E plane pattern for 2-3 GHz frequencies

The microstrip antennas mentioned above have been analyzed using AWR Office (Spectral MoM method). The simulated and measured performances of the antennas are summarized in Table 5.3.

Table 5.3 Measured performance for the resonant frequency and the return loss and simulated performance for the beamwidth and the gain results

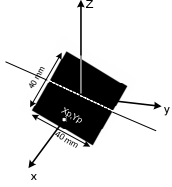
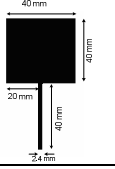
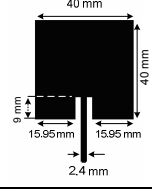
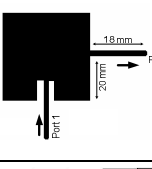
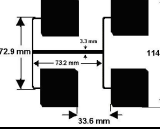
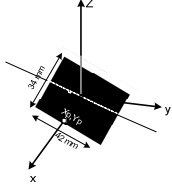
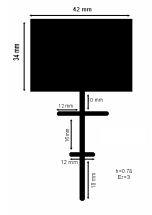
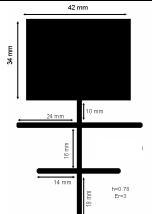
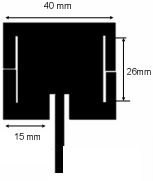
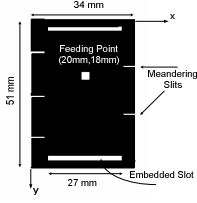
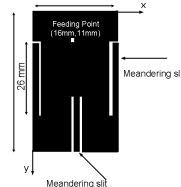
| Configuration | | Measurement | | | | Simulation |
|---|---------------------|-------------|--------------|--------|---------------------------|------------|
| Element Type | $\epsilon_r, h(mm)$ | f_r (GHz) | $S_{11}(dB)$ | | Beamwidth & Gain at f_r | |
|  | 2.52, 0.52 | 2.5 | -5.9 dB | | 84 (7.806 dB) | |
|  | 2.52, 0.52 | 2.55 | -5.5 dB | | 86 (7.499 dB) | |
|  | 2.52, 0.52 | 2.55 | -12.8 dB | | 88 (7.83 dB) | |
|  | 2.52, 0.52 | Port 1 | Port 2 | Port 1 | Port 2 | ---- |
| | | 2.52 | 2.15 | -9 dB | -4 dB | |
|  | 2.52, 0.52 | 2.6 | -15 dB | | 40 13.44 dB | |
|  | 3, 0.78 | 2.5 | -6.1 dB | | 91 (7.646 dB) | |
|  | 3, 0.78 | 2.6 | -12 dB | | 6.738 dB | |
|  | 3, 0.78 | 3.65 | -14 dB | | ----- | |

Table 5.3. Continued

| | | | | |
|---|-----------|--|-------|---------------------------|
|  | 2.52,0.52 | 2.1 | -8 dB | 75 (4.946 dB) |
|  | 3,0.78 | $f_{r1}=1.2$ $f_{r2}=2$ $f_{r3}=2.5$ | -9 dB | 80 (1.2GHz) (5.506 dB) |
|  | 3,0.78 | 1.5 | -8 dB | 85 (1.5GHz) (5.896 dB) |

Depending on the application, matching may be required over a band of frequencies. The bandwidth of the matching network is an important design parameter. In general, matching networks are constructed with reactive components only so that no loss is added to the overall network.

5.3 Amplifying Active Integrated Microstrip Patch Antennas

The integration of a two-port active device with a passive microstrip antenna at the input or output port for the purpose of signal amplification is classified as being of amplifier type. When the antenna is at the input port, it is considered to be source impedance for the device. The integrated active antenna works as a receiver. The low-noise amplifier design technique is usually applied in order to achieve the required noise performance. When the antenna is placed at the output port, it works as device load impedance (Morrow & Hall, 1994). In this case, the active antenna functions as a transmitter. An amplifier design technique for achieving gain bandwidth performance is generally applied (Robert, Razban & Papiernik, 1992).

Experimental setup of the antenna system is shown in Figure 5.22 and examples of transmit active integrated microstrip antennas are shown in Figures 5.23 and 5.25.

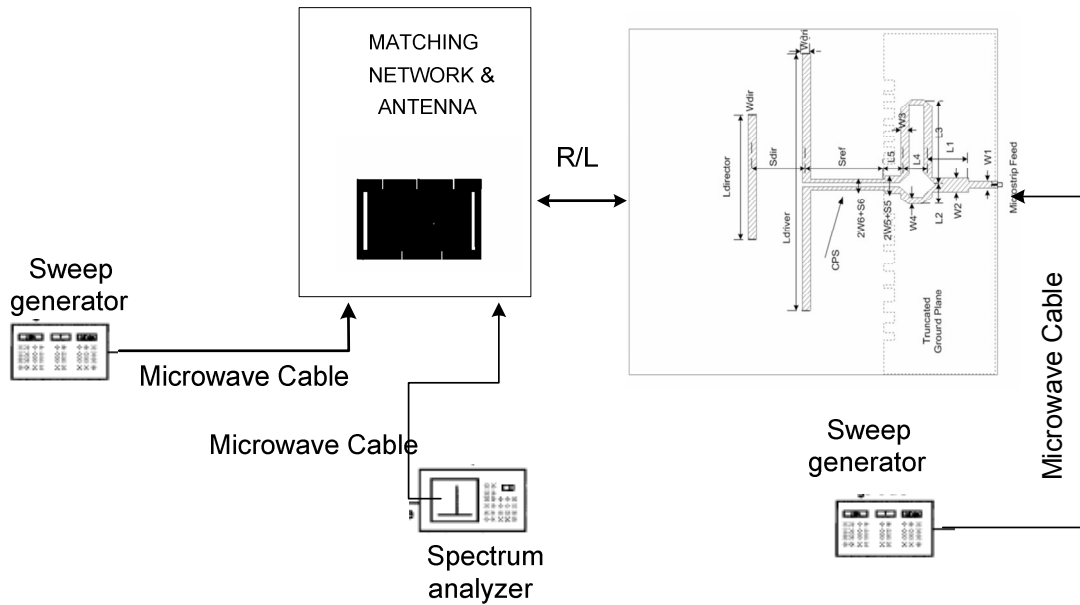


Figure 5.22 Experimental setup of T/R Module

The Quasi-Yagi antenna (Kaneda, Deal, Waterhouse & Itoh, 2002) was used receiver antenna due to having wide impedance bandwidth. The performance results for this antenna were given in Appendix B.

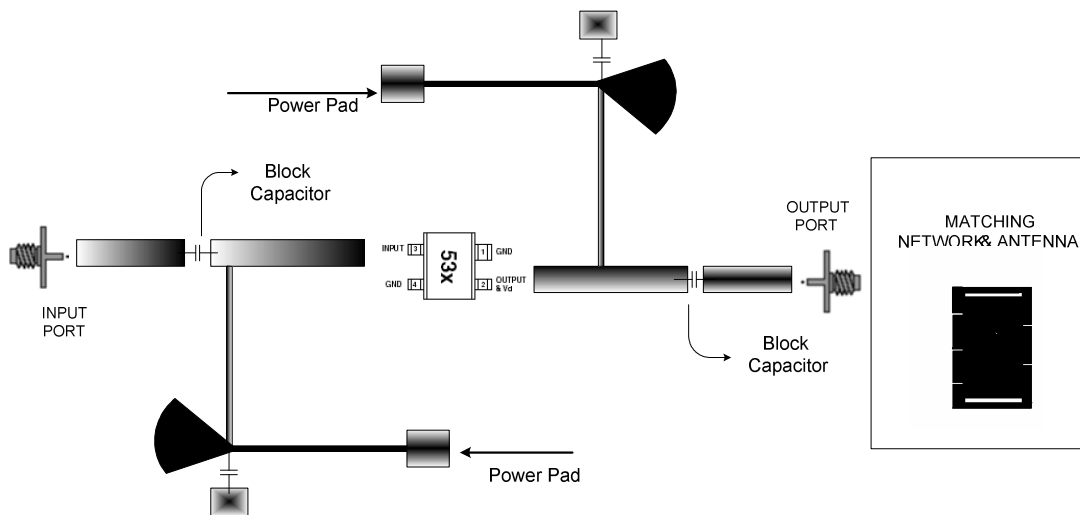
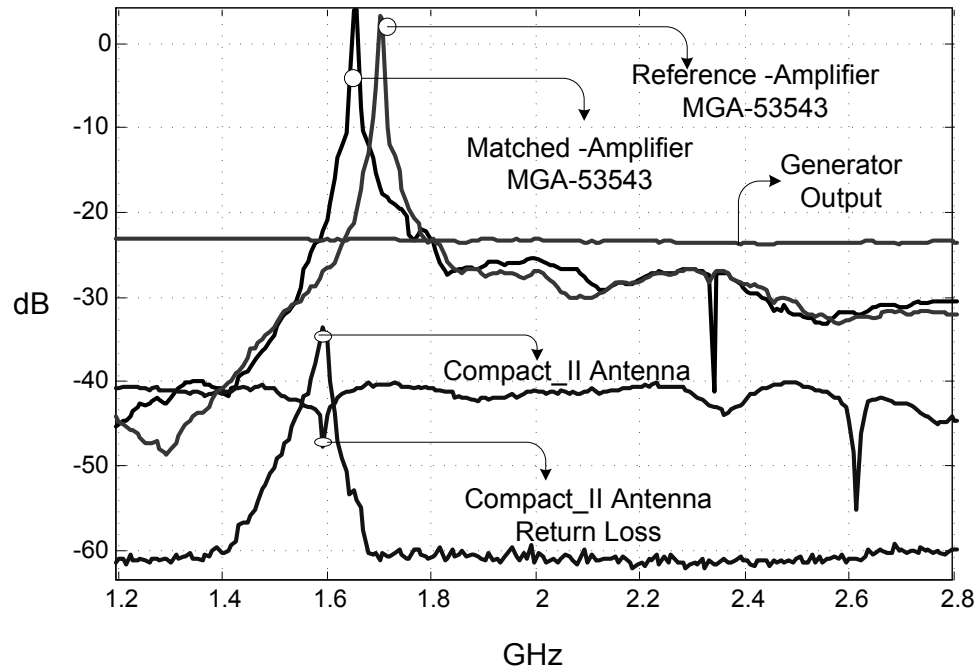
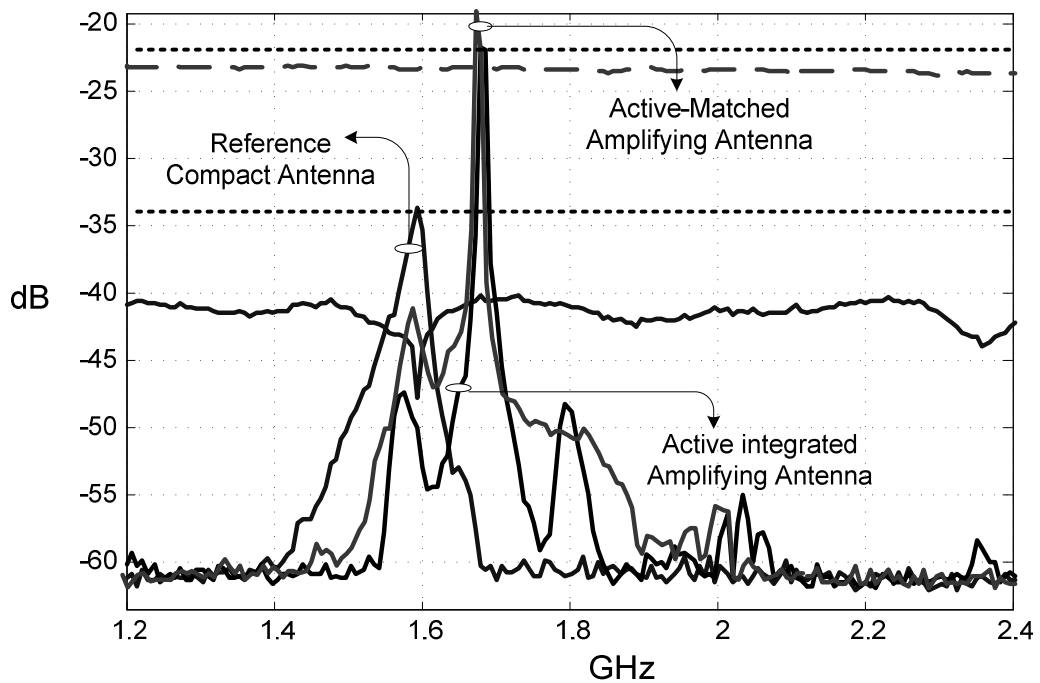


Figure 5.23 The layout of active amplifying antenna

The measured and return loss performances are shown in Figure 5.24 (a) and Figure 5.24 (b).

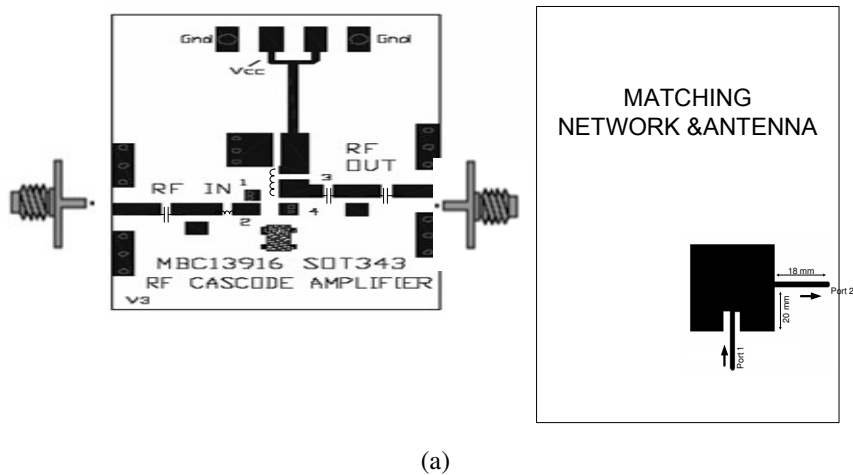


(a)

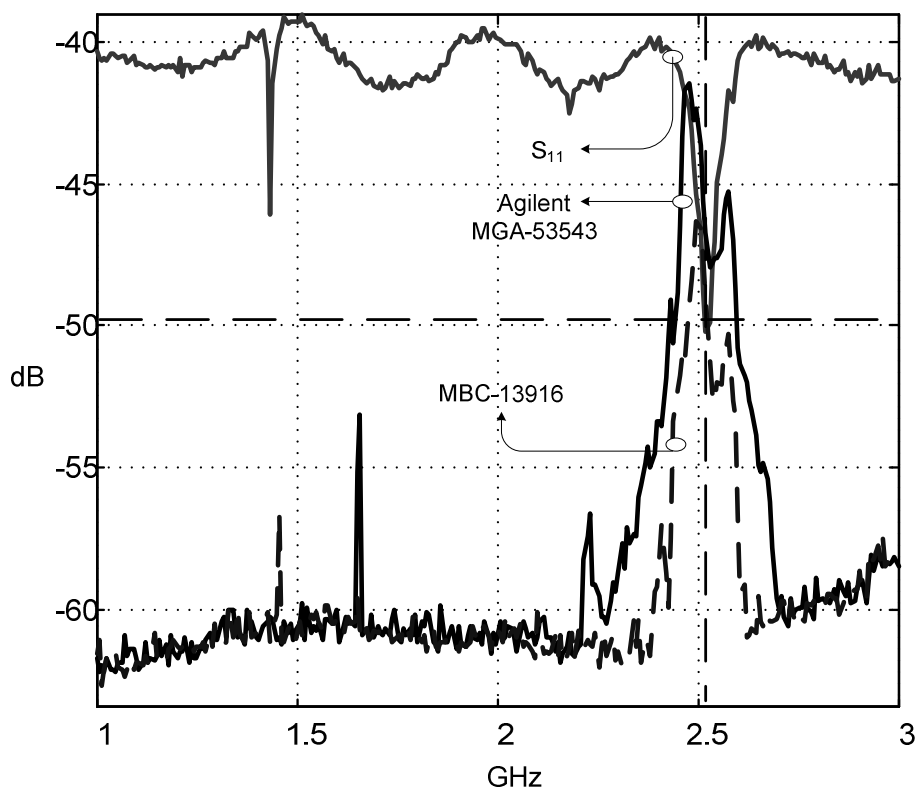


(b)

Figure 5.24 Measured Results (a) Transmission performance of RF amplifier ($\epsilon_r = 2.55$ & $h = 1.52$ mm; TLX) (b) Amplifying active integrated compact microstrip antenna



(a)



(b)

Figure 5.25 (a) The layout of active antenna (2.5 GHz) (b) Transmission performance ($\epsilon_r=2.55$ & $h=1.52$ mm; TLX)

The advantages of incorporating an amplifier with a passive antenna structure include gain and bandwidth enhancement and improvement noise performance.

CHAPTER SIX

CONCLUSION

1.4 Conclusion

The microstrip antennas have been used extensively in microwave systems and wireless communication applications. Although the microstrip antenna suffer from some serious drawbacks like narrow frequency bandwidth and low efficiency, the performance of the microstrip antenna elements has been constantly enhanced through the years. Many different forms of microstrip antennas have been developed over the years and in this thesis, different types of broadband antennas have been analyzed for usage in wide band applications.

Different type rectangular antennas were analyzed both theoretically, experimentally. Simulations were realized with MoM based software Microwave Office. Detailed characteristics of the microstrip antennas are presented, including their advantages, disadvantages and individual radiation properties. In addition, the design procedures for all configurations of planar antennas was also investigated and presented.

The first step in designing an antenna is to choose an appropriate substrate. The antennas were fabricated using substrates with different properties such as *TLY-5A*, *TLY-5*, *TLX-0*, *TLC-30*, *TLC-32*, and *FR4*. Design and analysis of the RMSA, including the simplified formulas, were given. The effects of varying several parameters- such as the feed point location, width of the patch, ϵ_r , h of the substrate and finite ground plane size- on the resonant frequency, input impedance, BW and gain were described in detail.

The adaptive impedance matching is a rather simple and effective technique to compensate the loss due to the antenna impedance mismatch in system. Some typical and new configurations of matching techniques have been presented and considered. In chapter three, improvement of bandwidth by utilizing floating negative inductor

circuit as compensation network has been presented. As an antenna, a simple microstrip patch operating at 10.55 GHz was designed. The active floating inductive compensation circuit (S. El. Khory, 1995) is realized using three FETs or two FETs. Simulation results for both compensated and non-compensated antennas are presented. The reference antenna has a return loss better than -10 dB within a percent bandwidth of 17.21 %. This value is increased to 32.67 % by utilizing the negative inductor circuit together with the reference antenna, which is about two times the inherent bandwidth of the reference antenna. In the meantime, this improvement of the bandwidth does not cause a shift in the resonant frequency. Utilizing the negative capacitor as a compensation circuit, bandwidth has been increased from 12.21% to 16.96% and the best radiation pattern is obtained. These pattern shapes are similar to the reference antenna but results show that the radiation patterns (in E and H planes) of the active antenna with reactive loading case is significantly improved compared to the conventional techniques. The thick antenna, aperture couple microstrip antenna, double symmetric stub RMSA techniques have been used for the comparison of the proposed methods and the conventional methods.

Impedance tuning networks are also widely used in many electronic applications, such as RF power amplifier designs, impedance-matching devices like antenna tuning units. In this thesis, a novel technique with pi-matching network is proposed based on lumped and electronically tunable elements. The pi-matching device is used to construct the antenna tuning units, which is only used to match the front module and the antenna. This is an interesting application since antennas cannot be considered as alone component with changing electromagnetic properties. The research reported here has concentrated on Pi network; however circuit analysis is just as applicable to the other matching networks such as T network.

A new method for designing an electronically tunable microwave impedance transformer (Pi type matching with R - C mutator) has been demonstrated. In the matching network, the system behaviors are examined by using R - C mutator instead of the L_2 inductor. R - C mutator circuit can work on high power applications and the

equivalent capacitance value C can be controlled only by the R value. The tunable microwave impedance transformer is analyzed using microstrip technology. Due to the low insertion loss and wide tunable impedance, transformer has many applications including wireless components. Additionally, this new matching circuit (with R - C mutator) building block can be used in conjunction to provide impedance matching of poorly characterized complex loads such as all different type microstrip antennas. Due to the demonstrated low insertion loss and wide tunable impedance bandwidth, this new type of electronically tunable matching network has many applications including adaptive matching of RF amplifiers, wireless communication. It is seen that the theoretical, simulation and measurement results are in good agreement for Pi compensation circuit. The impedance boundary conditions are examined by using theoretical analysis for circuit's components. The derivation of the boundary equations for the Pi- Network has allowed the development of antenna performances.

The final design and laboratory measurements for the integrated antennas presented in Chapter 5. The measured operating frequencies and bandwidths for the antennas were slightly lower or upper than the design specifications but this is acceptable as a starting for final evaluation and design modifications.

Consequently, this thesis has demonstrated a design process for the active matching networks as front- end modules. In this thesis, some new techniques, and some new circuits have been proposed to overcome the narrow bandwidth, radiation pattern and the gain problem. Conventional design methodologies and commercial software's, Microwave Office and Ansoft – CST were extensively used for circuit and electromagnetic simulations.

6.2 Suggestion for Future Research

The design of impedance-matching networks using lumped and active transformers has been described to achieve broadband performance of microstrip antennas. Promising experimental and simulated data indicated that if the matching

network is implemented in a system with more variable outputs, the overall efficiency of active antenna system can be improved. The interest on the compensated network will be increased when the new matching circuit components are invented for improve the impedance bandwidth and increase the matching level. Thus, with further improvements and researches, these compensated antennas would be very useful in applications like wireless communications systems. In the design of matching circuits more convenient methods should be further studied for the increase controlling parameter and practical development.

In the design and implementation of compensated networks with negative floating inductor or negative capacitor, new circuit configurations should be further studied to adapt to the advanced matching technology. Possible future work for this project could include incorporating new mutator, inductor or capacitor structures for microstrip antenna geometries. Additionally, the integration of a low noise amplifier integrated antenna systems is also an area to investigate.

REFERENCES

- An, H., Nauwelaers, B., & Van De Capelle, A. (1991). Broadband active microstrip array elements. *Electronic Letters*, 27 (25), 2378-2379.
- Anderson, A.P., Davies, W.S, Dawoud, M., & Galanakis, D. E. (1971). Notes on transistor-fed active-array antennas. *IEEE Trans. Antennas Propagation*, 19 ,537-539.
- Balanis, C.A. (1989). *Advanced engineering electromagnetic*, John Wiley & Sons, New York.
- Balanis, C.A. (1997). *Antenna theory analysis and design* (2.Ed.). John Wiley & Sons, New York.
- Benalla, A., & Gupta, C. (1988). Multiport network model and transmission characteristics of two-port rectangular microstrip patch antennas. *IEEE Trans. Antennas and Propagation*, 36 (10), 1337-1342.
- Carver, K. R., & Mink, J. W. (1981). Microstrip antenna technology. *IEEE Trans. Antennas and Propagation*, 29 (1), 2-24
- Chang, K., York, R. A., Hall, P. S., & Itoh, T. (2002). Active integrated antennas. *IEEE Trans. On Microwave Theory and Techniques*, 50 (3), 937-942
- Copeland, J. R., Roberston, W. J., & Verstraete. (1964). Antennafier arrays. *IEEE Trans. Antennas and Propagation*, 12, 227-223.
- Chuang, C. L., Tsang, L., & Chew, W. (1980). The equivalence of the electric and magnetic surface current approaches in microstrip antenna studies. *IEEE Trans. Antennas and Propagation*, 28 (4), 569-571.

- Chadha, R., & Gupta, K. C. (1981). Segmentation method using impedance-matrices for analysis of planar waveguide circuits. *IEEE Microwave Theory Tech.*, 29 (1), 71-74.
- Daniel, J. P., & Terret, C. (1975). Mutual coupling between antennas-optimization of transistor parameters in active design. *IEEE Trans. Antennas Propagation*, 23 (4), 513-516.
- Davidson, S.E., Long, S.A., & Richards, W.F. (1985). Dual-band microstrip antennas with monolithic reactive loading. *Electronics Letters*, 21, 936-937.
- Dearnley, R.W. & Barel, A.R.F. (1989). A Broad-Band Transmission line model for microstrip patches. *IEEE Trans. Antennas and Propagation*, 33 (5), 6-15.
- Derneryd, A.G. (1979). Analysis of the microstrip disk antenna elements, 27, 660-664.
- Descamps, G.A. (1953). Microstrip microwave antennas. *Third USAF Symposium on Antennas*.
- Dubost, G., & Rabbaa, A. (1986). Analysis of a slot microstrip antennas. *IEEE Trans. Antennas Propagation*, 34 (2), 155-163.
- Duffy, M. (2000). An enhanced bandwidth design technique for electromagnetically coupled microstrip antennas. *IEEE Trans. On Antennas and Propagation*, 48 (2), 155-163.
- Fano, R.M. (1950). Theoretical limitations on broadband matching of arbitrary impedances. *J. of the Franklin Institute*, 249, 57-83.
- Garg, R., Bhartia, P., Bahl, I., & Ittipiboon, A. (2001). *Microstrip antenna design handbook*. Boston. London; Artech House.

- Garg, R. (1978). Effect of tolerances on microstrip line and slotline performances. *IEEE Trans. On Microwave Theory and Techniques*, 26 (1), 16-19.
- Goras, L (1981). Linear and nonlinear mutators derived from GIC-type configurations, *IEEE Trans. On Circuits and Systems*, 28 (2), 165-168.
- Gupta, C. & Sharma, P. C (1981). Segmentation and desegmentation techniques for the analysis of two dimensional microstrip antennas. *IEEE AP-S Int. Symp. Digest*, 19-22.
- Harrington, R. F. (1961), *Time-Harmonic Electromagnetic Fields*, McGraw-Hill.
- Hammerstad, E. O. (1975). Equations for microstrip circuit design. *Proc. Fifth European Microwave Conf.*, 268-272.
- Henderson, A., James, J. R., & Hall, C. M. (1986). Bandwidth extension techniques in printed conformal antennas. *Military Microwaves*, 86, 329-334.
- Howell, J. W. (1975). Microstrip antennas. *IEEE Trans. Antennas Propogate*, 23 (1), 90-93.
- Iglesias, E. R., Vargas, S., Vazquez, J. L., Gonzalez, V., & Pascual, C.M. (2001). Bandwidth enhancement in noncentered stacked patches. *Microwave and Optical Technology Letters*. 31 (1), 53-56.
- Jackson, D. R., & Alexopoulos, N. G. (1991). Simple approximate formulas for input resistance, bandwidth, and efficiency of a resonant rectangular patch. *IEEE Trans. On Antennas and Propagation*. 39 (3), 407-410.
- Johnson, R. C. (1993). *Antenna Engineering Handbook* (3rd ed.). New York: McGraw-Hill.

- Kaya, A., Çelebi, A., & Yüksel, E. Y. (2003). Analysis and design of circularly polarized active planar microstrip antenna array. *ISEF 2003 11th International Symposium on Electromagnetic Fields in Electrical Engineering*, 18-20, Maribor, Slovenia.
- Kaya, A., Özmehmet, K., Yüksel E. Y., & Tamer, Ö. (2005). Dört elemanlı dairesel kutuplanmış düzlemsel dizi antende uyartım sisteminin boyutlarını değiştirerek parametrelerdeki değişimlerin incelenmesi. *Fen ve Mühendislik Dergisi*.
- Kaya, A., & Yüksel, E. Y. (2004). Mikroşerit düzlemsel dizi antenlerde empedans bant genişliğinin negatif kapasitans kullanılarak artırılması, Elektrik-Elektronik ve Bilgisayar Mühendisliği Sempozyumu. 153–156, Bursa.
- Kaya, A., Kılınç, S., Yüksel, E. Y., & Cam, U. (2004a). Bandwidth enhancement of a microstrip antenna using negative inductance as impedance matching device. *Microwave and Optical Technology Letters*, 42, 476-478.
- Kaya, A., Kılınç, S., Yüksel, E. Y., & Cam, U. (2004b). Mikroşerit antenlerde bandın artırılması için 2-Fetli negative endüktans kullanarak empedans uyumlandırma tekniğinin incelenmesi. *URSI 2004 Bilkent Sempozyumu*, 438-440, Ankara
- Kaya, A., Kılınç, S., Yüksel, E. Y., & Cam, U. (2004c). Bandwidth enhancement technique using negative inductance with three FET for the rectangular microstrip antenna. The 47th *IEEE International Midwest Symposium on Circuits and Systems*, Hiroshima, Japan.
- Kaya, A., Günel, S., & Yüksel, E. Y. (2005). RC Dönüştürücü ile rf elektronik kontrollü empedans ayarlama devresi kullanılarak, aktif dikdörtgen mikroşerit antenin ışınma örüntüsü ve bant kontrol analizi. *11. Elektrik Elektronik Bilgisayar Mühendisliği Ulusal Kongresi*, 153-156, İstanbul.

- Kaya, A., & Yüksel, E. Y. (2006). Pi uyumlandırma devresi kullanılarak tasarlanan anten sisteminin performans analizi. *IEEE 14. Sinyal İşleme ve İletişim Uygulamaları Kurultayı, Antalya*.
- Kaneda, N., Deal, W. R., Waterhouse, R., & Itoh, T. (2002). A broad-band quasi-yagi antenna. *IEEE Trans. On Antennas and Propagation*, 50 (8), 1158-1160.
- Khan A. A., Richards, W. F., & Long, S.A. (1989). Impedance control of microstrip antennas using reactive loading, *IEEE Trans. Antennas and Propagation*, 37 (2), 247-251.
- Khoury, S. El. (1995). The design of active floating positive and negative inductors in MMIC technology. *IEEE Microwave and Guided Wave Letters*, 5, 321-323.
- Khoury, S. El. (1996). New approach to the design of active floating inductors in MMIC technology. *IEEE Trans. MTT*, 44 (4), 505-511.
- Kolev, S., & Gautier, J. L. (2001). Using a negative capacitance to increase the tuning range of a varactor diode in MMIC technology. *IEEE Trans. On Microwave Theory and Techniques*, 49(12), 2425-2430.
- Lee, R. Q., Lee, K. F., & Bobinchak, J. (1987) Characteristic of a two-layer electromagnetically coupled rectangular patch antenna. *Electron. Letter*, 23, 1070-1072.
- Lin, J., & Itoh, T. (1994). Active integrated antennas. *IEEE Trans. On Microwave Theory and Techniques*, 42 (12), 2186-2194.
- Lier, E., & Jakopsen, K. R. (1983). Rectangular microstrip patch antenna with infinite and finite ground plane dimensions. *IEEE Trans. Antennas and Propagation*, 31 (6), 968-974

- Lo, Y. T., Solomon, D., & Richards, W.F. (1979). Theory and experiment on microstrip antennas. *IEEE Trans. On Antennas and Propagation*, 27 (2), 740-747.
- Ludwig, R., & Bretchko, P. (2000). *RF circuit design theory and applications*. New-Jersey; Prentice-Hall.
- Lu, J. H., Tang, C. L., & Wong, K.L. (1998). Slot-coupled compact broadband circular microstrip antenna with chip-resistor and chip-capacitor loadings. *Microwave and Optical Technology Letters*, 18, 345-349.
- Lu, J. H., & Wong, K. L. (1998). Slot-loaded, meandered rectangular microstrip antenna with compact dual frequency operation. *Electronic Letters*, 34, 1048-1049.
- Maci, S., & Gentili, G. B.(1997). Dual-frequency patch antennas. *IEEE APMagazine*, 39 (6), 13-19.
- Matthei, G., & Young, L. (1980). *Microwave filters, impedance-matching networks, and coupling structures (434-438)*. Artech House.
- Michalski, K. A., & Hsu, C.I. G. (1994). RCS computation of coax-loaded microstrip patch antennas of arbitrary shape. *Electromagnetics*, 14, 33-62.
- Mingo, J., Valdovinos, A., Crespo, A., Navarro, D., & Garcia, P. (2004). An rf electronically controlled impedance tuning network design and its application to an antenna input impedance automatic matching system. *IEEE Trans. On Microwave Theory and Techniques*, 52, 489-491.
- Morrow, I. L., & Hall, P. S. (1994). Analysis of radiation from active microstrip antennas. *IEE Proc. Antennas Propagation*, 141 (5), 359-363.

- Munson, R. E. (1974). Conformal microstrip antennas and microstrip phased arrays. *IEEE Trans. Antennas Propagation*, 23 (1), 74-78.
- Newman, E. H., & Tulyathan, P. (1981). Analysis of microstrip antennas using method of moments. *IEEE Trans. Antennas Propagation* 29 (1), 47-53.
- Parschen, D. A. (1986). Practical examples of integral broadband matching of microstrip antenna elements. *Proceedings of the 1986 Antenna Applications Symp.*, 199-217.
- Perlmutter, P., Shrikmann, S., & Treves, D. (1985). Electric surface current model for the analysis of microstrip antennas with application to rectangular elements. *IEEE Trans. Antennas Propagation*, 33(3), 301-311.
- Pozar, D. M. (1983). Considerations for millimeter wave printed antennas. *IEEE Trans. On Antennas and Propagation*, 31 (5), 740-747.
- Pozar, D. M. (1986). An update on microstrip antenna theory and design including some novel feeding techniques. *IEEE Trans. Antennas Propagat Soc Newsletter*, 28 (5), 5-9.
- Pozar, D. M. & Kaufman, B. (1987). Increasing the bandwidth of a microstrip antenna by proximity coupling. *Electronics Letters*, 23 (8), 368-369.
- Pozar, D. M. (1992). Microstrip antennas. *Proc. IEEE*, 80 (1), 79-81.
- Pues, H. F., & Van de Capelle, A. R. (1989). An impedance matching technique for increasing the bandwidth of microstrip antennas. *IEEE Trans. On Antennas and Propagation*, 37 (11), 1345-1354.
- Ramesh, M & Yip, K. B. (2003). Design formula for inset fed microstrip patch antenna. *Microwaves and Optoelectronics*, 3, 5-7.

- Robert, B., Razban, T., & Papiernik, A. (1992). Compact amplifier integration in square patch antenna. *Electronics Letters*, 28 (19), 1808-1810.
- Richards, W. F., Lo, Y. T., & Harrison, D. D. (1981). An improved theory for microstrip antennas and applications. *IEEE Trans. On Antennas and Propagation*, 27 (1), 38-46.
- Shin, H. S., & Kim, N. (2002). Wideband and high-gain one-patch microstrip antenna coupled with H-shaped aperture. *Electronics Letters*, 38 (19), 1072-1073.
- Srinivasan, V., Malhotra, S., & Kumar, G. (2000). Multiport network model for chip-resistor-loaded rectangular microstrip antennas. *Microwave and Optical Technology Letters*, 24 (1), 11-13.
- Svitak, A. J., Pozar, D. M., & Jackson, R. W. (1992). Optically fed aperture coupled microstrip patch antennas. *IEEE Trans. Antennas and Propagation*, 40 (1), 85-90.
- Thouroude, D., et al. (1990). CAD-oriented cavity model for rectangular patches. *Electron. Lett.*, 26, 842-844
- Wong, K. L., & Lin, Y. F. (1997). Small broadband rectangular microstrip antenna with chip resistor loading. *Electronics Letters*, 33, 1593-1594.
- Wong, K. L., & Yang, K. P. (1998). Compact dual-frequency microstrip antenna with pair of bent slots. *Electronic Letters*, 34, 225-226.
- Wong, K. L., & Kou, J. S. (1999). Bandwidth enhancement of bow-tie microstrip antenna using integrated reactive loading. *Microwave Opt. Technol. Lett.*, 22 (7), 2186-2194.

Zhang, G., & Gautier, J. (1993). Broad-band, lossless monolithic microwave active floating inductor. *IEEE Microwave and Guided Wave Letter*, 3 (4), 99-100.

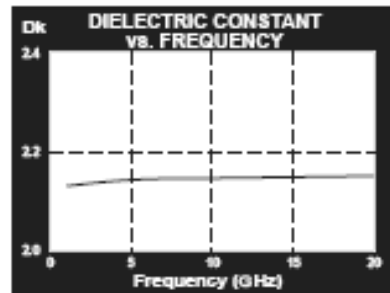
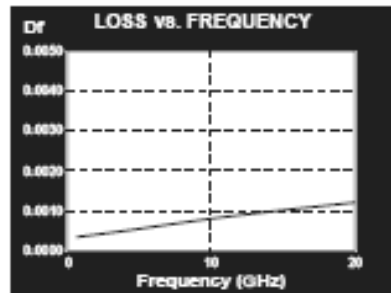
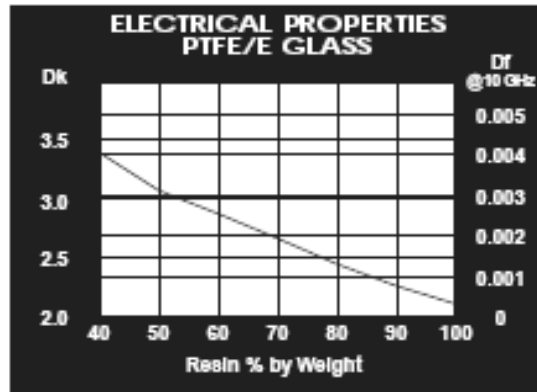
APPENDICES

APPENDIX A. MANUFACTURER DATA

This appendix contains the manufacturer data used to process in the work presented in chapter 3, 4, 5.

| TLY-5 TYPICAL VALUES | | | | | |
|------------------------------|---------------------|-----------------|-----------------|-------------------|-----------------|
| Property | Test Method | Units | Value | Units | Value |
| Dielectric Constant @ 10 GHz | IPC-TM 650 2.5.5.5 | | 2.20 | | 2.20 |
| Dissipation Factor @ 10 GHz | IPC-TM 650 2.5.5.5 | | 0.0009 | | 0.0009 |
| Moisture Absorption | IPC-TM 650 2.6.2.1 | % | <0.02 | % | <0.02 |
| Dielectric Breakdown | IPC-TM 650 2.5.6 | kV | >60 | kV | >60 |
| Volume Resistivity | IPC-TM 650 2.5.17.1 | Mohm/cm | 10 ⁷ | Mohm/cm | 10 ⁷ |
| Surface Resistivity | IPC-TM 650 2.5.17.1 | Mohm | 10 ⁷ | Mohm | 10 ⁷ |
| Arc Resistance | IPC-TM 650 2.5.1 | seconds | >180 | seconds | >180 |
| Flexural Strength Lengthwise | IPC-TM 650 2.4.4 | lbs./in. | >12,000 | N/mm ² | >83 |
| Flexural Strength Crosswise | IPC-TM 650 2.4.4 | lbs./in. | >10,000 | N/mm ² | >69 |
| Peel Strength (1oz copper) | IPC-TM 650 2.4.8 | lbs./linear in. | 12.0 | N/mm | 2.1 |
| Thermal Conductivity | ASTM F 433 | W/mK | 0.22 | W/mK | 0.22 |
| x-y CTE | ASTM D 3396 (TMA) | ppm/°C | 20 | ppm/°C | 20 |
| z CTE | ASTM D 3396 (TMA) | ppm/°C | 280 | ppm/°C | 280 |
| UL-94 Flammability Rating | UL-94 | | V-0 | | V-0 |

| Type | Dk |
|--------|------|
| TLY-5A | 2.17 |
| TLY-5 | 2.20 |
| TLP-5 | 2.33 |
| TLP-0 | 2.45 |
| TLP-9 | 2.50 |
| TLP-8 | 2.55 |
| TLP-7 | 2.60 |
| TLP-6 | 2.65 |
| TLE-95 | 2.95 |
| TLC-27 | 2.75 |
| TLC-30 | 3.00 |
| TLC-32 | 3.20 |
| RF-30 | 3.00 |
| RF-35 | 3.50 |
| RF-50 | 6.15 |
| CER-10 | 10 |



2/02

Figure B.1 Substrate material (Taconic)

fsx017x.s2p 12/96

! FSX017X

! @8V-35mA

! 1GHZ 20GHZ 20

! S-parameters include bonding wires:

! gate : total 1 wire, 1 per bond pad, 0.1mm long each wire.

! drain : total 1 wire, 1 per bond pad, 0.1mm long each wire.

! source: total 4 wires, 2 per side, 0.2mm long each wire.

! wire : 25u dia., gold.

GHZ S MA R 50

| | | | | | | | | |
|--------|------|--------|-------|-------|------|-------|------|-------|
| 1.000 | .989 | -24.0 | 4.538 | 162.3 | .013 | 76.7 | .837 | -6.1 |
| 2.000 | .960 | -46.5 | 4.260 | 145.7 | .025 | 65.4 | .820 | -11.9 |
| 3.000 | .925 | -66.6 | 3.890 | 130.9 | .035 | 55.1 | .801 | -16.9 |
| 4.000 | .890 | -84.0 | 3.493 | 117.7 | .042 | 46.0 | .782 | -21.6 |
| 5.000 | .860 | -99.0 | 3.132 | 106.3 | .048 | 38.6 | .764 | -25.9 |
| 6.000 | .833 | -111.8 | 2.814 | 95.9 | .052 | 32.5 | .751 | -29.9 |
| 7.000 | .814 | -122.6 | 2.525 | 86.5 | .054 | 27.4 | .740 | -33.8 |
| 8.000 | .799 | -132.1 | 2.294 | 78.2 | .057 | 23.2 | .733 | -37.8 |
| 9.000 | .788 | -140.6 | 2.095 | 70.2 | .060 | 18.6 | .726 | -41.7 |
| 10.000 | .780 | -148.1 | 1.931 | 62.8 | .061 | 15.1 | .720 | -45.7 |
| 11.000 | .773 | -154.7 | 1.782 | 55.5 | .063 | 12.0 | .716 | -49.7 |
| 12.000 | .768 | -160.9 | 1.646 | 48.7 | .064 | 9.1 | .710 | -53.6 |
| 13.000 | .762 | -166.3 | 1.536 | 42.5 | .065 | 5.9 | .704 | -57.6 |
| 14.000 | .759 | -171.4 | 1.442 | 36.4 | .065 | 2.6 | .702 | -61.4 |
| 15.000 | .759 | -176.0 | 1.343 | 29.7 | .065 | 2.1 | .699 | -65.4 |
| 16.000 | .759 | 179.6 | 1.269 | 25.1 | .068 | -.2 | .699 | -69.5 |
| 17.000 | .764 | 175.6 | 1.215 | 18.1 | .066 | -3.1 | .697 | -73.4 |
| 18.000 | .766 | 171.6 | 1.137 | 12.7 | .069 | -3.6 | .695 | -77.7 |
| 19.000 | .771 | 167.7 | 1.087 | 7.5 | .071 | -6.6 | .694 | -81.8 |
| 20.000 | .778 | 164.1 | 1.042 | 1.2 | .070 | -10.1 | .691 | -85.4 |

! fhx35x.s2p 4/90

! FHX35X

! @3V-10mA

! .1GHZ 22GHZ 24

! S-parameters and Noise parameters include bonding wires

! gate : total 2 wires, 1 per bond pad, 0.3mm long each wire.

! drain : total 2 wires, 1 per bond pad, 0.3mm long each wire.

! source: total 4 wires, 1 per side, 0.3mm long each wire.

! wire : 20u dia., gold.

GHZ S MA R 50

| | | | | | | | | |
|--------|-------|--------|-------|-------|------|------|------|-------|
| .100 | 1.000 | 1.3 | 4.235 | 178.9 | .002 | 89.4 | .506 | -.7 |
| .500 | .998 | -6.7 | 4.227 | 174.7 | .009 | 86.8 | .505 | -3.3 |
| 1.000 | .993 | -13.3 | 4.200 | 169.2 | .017 | 83.6 | .503 | -6.7 |
| 2.000 | .973 | -26.3 | 4.097 | 159.2 | .033 | 77.5 | .493 | -13.1 |
| 3.000 | .943 | -38.8 | 3.941 | 149.4 | .048 | 71.9 | .478 | -19.2 |
| 4.000 | .907 | -50.6 | 3.752 | 140.3 | .060 | 67.0 | .460 | -24.8 |
| 5.000 | .869 | -61.8 | 3.546 | 131.8 | .071 | 62.8 | .441 | -29.9 |
| 6.000 | .831 | -72.2 | 3.337 | 123.9 | .080 | 59.4 | .422 | -34.6 |
| 7.000 | .795 | -81.9 | 3.134 | 116.7 | .087 | 56.7 | .403 | -38.8 |
| 8.000 | .763 | -91.0 | 2.943 | 110.1 | .093 | 54.6 | .386 | -42.8 |
| 9.000 | .734 | -99.5 | 2.766 | 103.9 | .097 | 53.2 | .371 | -46.5 |
| 10.000 | .709 | -107.5 | 2.604 | 98.2 | .102 | 52.3 | .357 | -50.1 |
| 11.000 | .688 | -115.0 | 2.457 | 92.8 | .105 | 51.8 | .344 | -53.6 |
| 12.000 | .670 | -122.0 | 2.323 | 87.8 | .109 | 51.8 | .333 | -57.1 |
| 13.000 | .655 | -128.7 | 2.202 | 83.1 | .112 | 52.2 | .323 | -60.7 |
| 14.000 | .644 | -135.0 | 2.093 | 78.6 | .116 | 52.8 | .314 | -64.3 |
| 15.000 | .634 | -141.0 | 1.993 | 74.3 | .119 | 53.7 | .306 | -68.0 |
| 16.000 | .627 | -146.7 | 1.903 | 70.2 | .124 | 54.7 | .300 | -71.8 |
| 17.000 | .622 | -152.1 | 1.820 | 66.3 | .128 | 55.8 | .294 | -75.8 |
| 18.000 | .619 | -157.3 | 1.744 | 62.6 | .134 | 56.9 | .289 | -80.0 |
| 19.000 | .618 | -162.2 | 1.675 | 59.0 | .140 | 58.0 | .285 | -84.3 |
| 20.000 | .617 | -167.0 | 1.610 | 55.5 | .146 | 59.0 | .282 | -88.8 |
| 21.000 | .618 | -171.5 | 1.551 | 52.1 | .154 | 59.9 | .280 | -93.5 |
| 22.000 | .621 | -175.8 | 1.495 | 48.8 | .162 | 60.6 | .279 | -98.3 |

! NOISE DATA 4/90

| | | | | |
|----|------|-----|-----|-----|
| 2 | 0.40 | .81 | 20 | .67 |
| 4 | 0.50 | .77 | 39 | .56 |
| 6 | 0.68 | .74 | 57 | .46 |
| 8 | 0.86 | .71 | 78 | .37 |
| 10 | 1.03 | .69 | 92 | .29 |
| 12 | 1.20 | .67 | 109 | .22 |
| 14 | 1.38 | .65 | 124 | .17 |
| 16 | 1.54 | .64 | 139 | .13 |
| 18 | 1.70 | .63 | 153 | .10 |

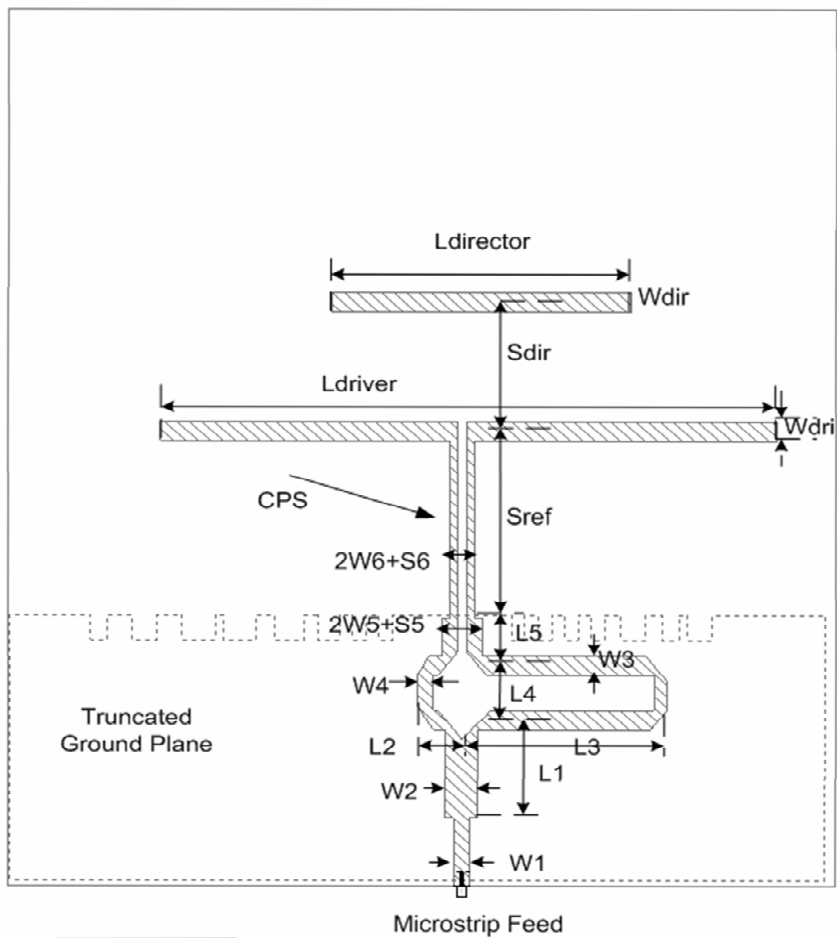
APPENDICES

APPENDIX B. RECEIVER ANTENNA AND ALGORITHM

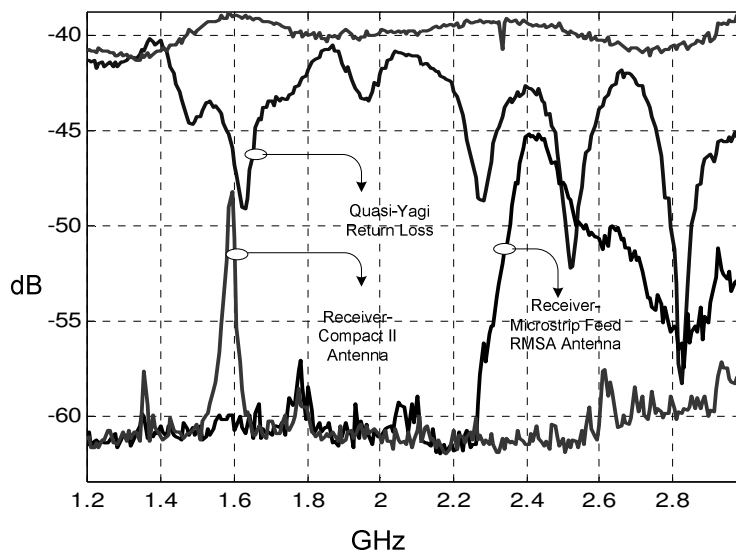
Uniplanar quasi Yagi antenna has gained considerable attention recently as a method of producing a broad bandwidth antenna with a well defined end-fire radiation pattern.

The quasi yagi antenna consists of two elements. One of them is the CPS transition and the other is the microstrip-to CPS (Coplanar strip) transition is shown in Figure B.1 (a). The microstrip-to-CPS balun is also essential part of the transition. The baluns phase shifter creates 180° phase difference between the coupled microstrip lines around 2.5 GHz, and offers a good impedance matching. The optimization of the balun is also done with the full-wave simulation. We have used 50 Ohm lines for the phase shifter and coupled line. The CPS line is connected to the printed dipole antenna that has length of approximately $\lambda_g/2$ where $\lambda_g = \lambda_0 / (\sqrt{\epsilon_r} + 1)$ and positions approximately $\lambda_g/4$ away from the reflector (Defected truncated ground plane).

The X-band prototypes have been designed using TLC substrate material manufactured by Taconic, which has a relative permittivity of 3.20 and a thickness of 0.78 mm, is used in this design. With the classic Yagi-Uda antenna, proper design requires careful optimization of the driver, director and reflector parameters, which include element spacing, length, and width. As detailed dimensions are (unit: millimeters): $W_1=W_3=W_4=W_5=2$ mm, $W_2=4$ mm, $W_{dir}=W_{dri}=2$ mm $W_6 = S_5 = S_6 = 1$ mm $L_1=10$ mm $L_2=5.4$ mm $L_3=24.2$ mm $L_4=6$ mm $L_5=5$ mm $S_{ref}=20$ mm $S_{dir}=13.5$ mm $L_{dri}=74$ mm and $L_{dir}=36$ mm.



(a)



(b)

Figure B.1 Quasi-Yagi antenna (a) Layout view (b) Performances

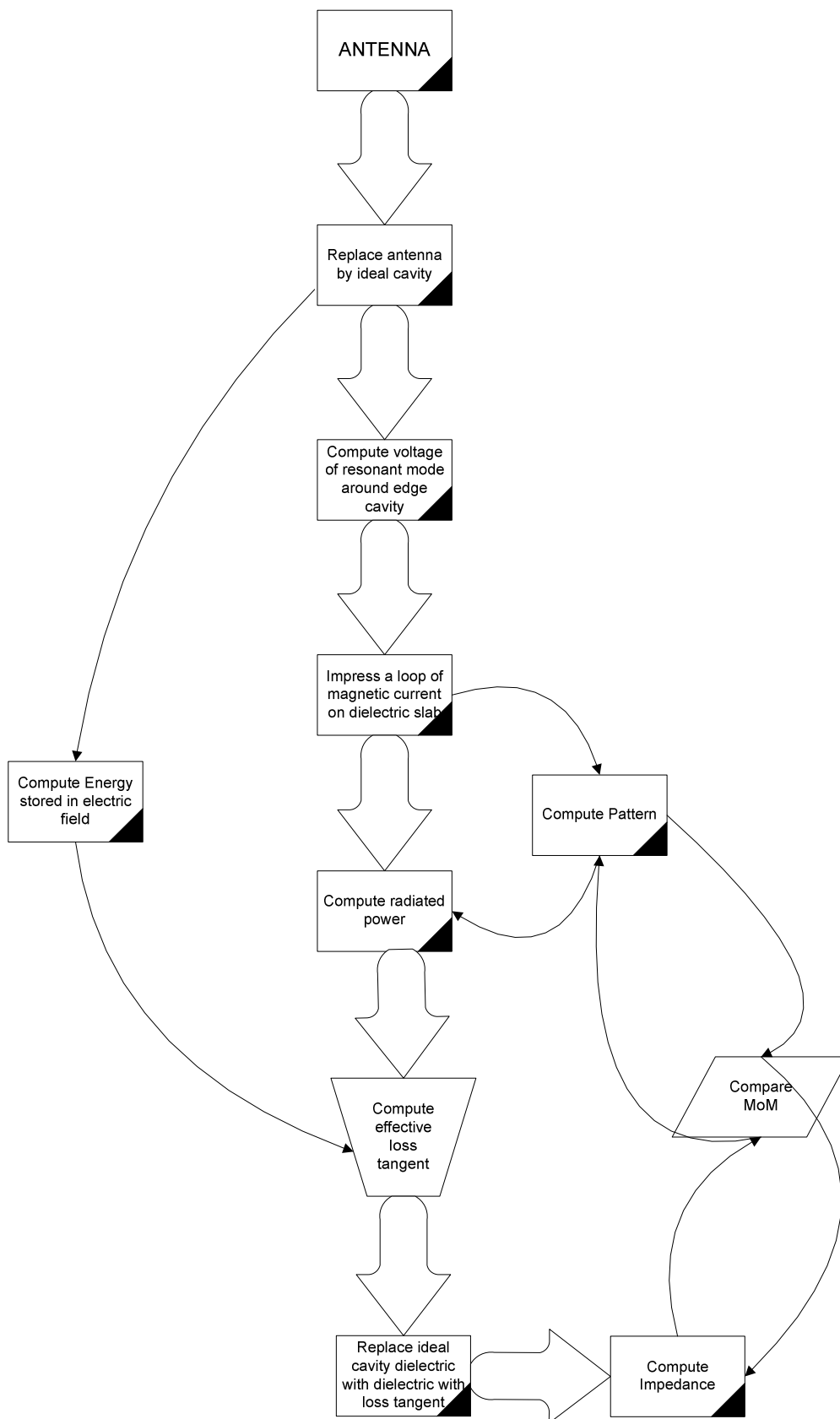


Figure B.2 Cavity model programming algorithm